

**Characterization of Clays and Clay Minerals  
for Industrial Applications:  
Substitution non-Natural Additives by Clays  
in UV Protection**

**DISSERTATION**

in fulfilment of the academic grade  
doctor rerum naturalium (Dr. rer. nat.)

at the Faculty of Mathematics and Natural Sciences  
Ernst-Moritz-Arndt-University Greifswald



**HOANG-MINH THAO**  
(Hoàng Thị Minh Thảo)

born on 01.6.1979 in Quang Ninh, Vietnam

Greifswald, Germany - 2006

Dekan: Prof. Dr. Klaus Fesser

1. Gutachter: PD. Dr. habil. Jörn Kasbohm

2. Gutachter: Prof. Roland Pusch

Tag der Promotion: 17.11.2006

# CONTENTS

LIST OF TABLES .....	VI
LIST OF FIGURES.....	VII
ABBREVIATIONS .....	X
STATEMENT OF ORIGINAL AUTHORSHIP (ERKLÄRUNG).....	XI
ACKNOWLEDGMENTS .....	XII
<b>1 INTRODUCTION .....</b>	<b>1</b>
<b>2 POSSIBLE FUNCTIONS OF CLAYS, CLAY MINERALS IN UV PROTECTION .....</b>	<b>2</b>
2.1 Clays, clay minerals and sustainability in geosciences.....	2
2.2 Ultraviolet radiation and human skin .....	2
2.3 Actual substances as UV protection factor and their problems.....	5
2.4 Pharmacy requirement in suncreams.....	9
2.5 Clays, clay minerals and their application for human health.....	11
2.6 Possible functions of clays, clay minerals in UV protection cream.....	13
<b>3 METHODOLOGY .....</b>	<b>15</b>
3.1 Clays and clay minerals analyses.....	15
3.1.1 X-Ray diffraction.....	17
3.1.2 TEM-EDX.....	19
3.1.3 X-Ray fluorescence.....	22
3.1.4 Mössbauer spectroscopy.....	23
3.1.5 Atterberg sedimentation.....	23
3.1.6 Dithionite treatment.....	24
3.2 Non-clay samples analyses.....	24
3.2.1 UV-measurement.....	25
3.2.2 Light microscopy.....	27
3.2.3 Skin model test by mouse-ear <i>in vivo</i> .....	27
3.2.4 Lactate DeHydrogenase test <i>in vitro</i> .....	28

<b>4</b>	<b>MINERALOGICAL CHARACTERIZATION OF USED CLAYS AND CLAY MINERALS</b>	29
<b>4.1</b>	<b>Kaolins</b>	29
4.1.1	German reference kaolins	29
4.1.2	Kaolin samples originated from Greifswald clay collection	36
4.1.3	CMS reference kaolins	38
<b>4.2</b>	<b>Bentonites</b>	40
4.2.1	Bentonite samples originated from Greifswald clay collection	41
4.2.2	CMS reference bentonites	50
<b>4.3</b>	<b>Mixed-layer dominated clay</b>	59
4.3.1	Friedland Clay	59
<b>4.4</b>	<b>Mica dominated clays</b>	71
4.4.1	German reference clays	71
<b>4.5</b>	<b>Treated clays</b>	79
4.5.1	Acid treated series	79
4.5.2	Dithionite treated clays	84
<b>5</b>	<b>CHARACTERIZATION OF CREAM SAMPLES/UV-MEASUREMENTS</b>	87
<b>5.1</b>	<b>Pure-clay cream samples – overview</b>	87
5.1.1	Clay concentration	87
5.1.2	Kaolins	88
5.1.3	Bentonites	91
5.1.4	Mixed-layer dominated clay	93
5.1.5	Mica dominated clays	94
<b>5.2</b>	<b>Clay samples with different particle parameters</b>	95
5.2.1	Particle sizes	97
5.2.2	Particle shapes	98
<b>5.3</b>	<b>Iron-reduced samples</b>	99
<b>5.4</b>	<b>Acid treated samples</b>	100
<b>5.5</b>	<b>Clay-fungi cream samples - combination with <i>Ganoderma pfeifferi</i></b>	102



<b>6</b>	<b>RESULTS OF BIO-EXPERIMENTS IN CREAM SAMPLES.</b>	107
<b>6.1</b>	<b>Changes in skin flora after UV-irradiation with different clays</b>	107
<b>6.2</b>	<b>Influences on skin infection of different clays.</b>	109
<b>6.3</b>	<b>Improving the protection ability of skin cream.</b>	110
<b>6.4</b>	<b>Changes in skin flora after UV-irradiation with different mixtures of clay and fungi.</b>	111
<b>7</b>	<b>DISCUSSION.</b>	113
<b>7.1</b>	<b>General UV protection behaviour of clays and clay minerals.</b>	113
7.1.1	UV protection potential of clays and clay minerals in pure-clay creams	113
7.1.2	UV protection potential of clays and clay minerals in clay-fungi creams.	114
7.1.3	Effects of clays media towards skin flora and skin infection.	115
<b>7.2</b>	<b>Structure of clay particles in cream.</b>	116
7.2.1	Structure of clay particles and wool-wax-alcohol ointment in pure-clay creams	116
7.2.2	Structure of clay particles and fungi capsules in clay-fungi creams.	118
<b>7.3</b>	<b>Iron effect on UV-absorption ability of clays and clay minerals</b>	121
7.3.1	Presence of iron effect of clays and clay minerals in ointment.	121
7.3.2	Role of iron in mixture with nanosuspension of fungi <i>G. pfeifferi</i> .	130
<b>7.4</b>	<b>Acid treatment and changing of UV protection ability.</b>	131
<b>7.5</b>	<b>Increasing of UV-absorption potential in clay-fungi combination and meaning of clay charge.</b>	133
7.5.1	Increasing of UV-absorption potential in combination of clays and nanosuspension fungi <i>G. pfeifferi</i> .	133
7.5.2	Influence of charge of clay: non-expandable clay and expandable clay.	134
<b>7.6</b>	<b>Influences of particle parameters on UV protection ability of clay minerals</b>	139
7.6.1	Influence of particle size observed from different grain size distributions.	139
7.6.2	Influence of different particle shapes concerning ability of covering	141
<b>7.7</b>	<b>Interaction between clay creams with skin flora and skin infection.</b>	143
7.7.1	Charges of clay minerals affect growth of skin flora and infectious bacteria.	143
7.7.2	Clay-fungi combination as an opportunity concerning safety to human skin.	146
	SUMMARY.	147
	REFERENCES.	151
	APPENDIX.	159

## LIST OF TABLES

<i>Table 1.</i> Comparative SPF categories (labelling).....	11
<i>Table 2.</i> Untreated kaolin samples involved in UV-measurements .....	15
<i>Table 3.</i> Untreated clay samples involved in UV-measurements .....	16
<i>Table 4.</i> Equipment and technical parameters of XRD measurements.....	18
<i>Table 5.</i> Quantitative Roentgen diffraction of German reference kaolins by “Autoquan” program (Rietveld method) .....	30
<i>Table 6.</i> Chemical composition (main components, oxide form) of Garfield, Chambers and Wyoming bentonites from X-Ray Fluorescence analyses, indicated in mass % .....	43
<i>Table 7.</i> Mineral formulae $[O_{10}(OH)_2]$ of Garfield nontronite, Chambers and Wyoming montmorillonite, based on TEM-EDX analyses .....	46
<i>Table 8.</i> Mineral formulae $[O_{10}(OH)_2]$ of montmorillonite and hectorite from CMS bentonites, based on TEM-EDX analyses .....	56
<i>Table 9.</i> The positions of reflections for estimating proportion of illitic layer in illite/EG- smectite .....	60
<i>Table 10.</i> Chemical composition (main components, oxide form) of bulk and $<2\ \mu\text{m}$ Friedland Clay samples from X-Ray Fluorescence analyses in comparison with literature, indicated in mass %.....	61
<i>Table 11.</i> Mineral formulae $[O_{10}(OH)_2]$ of illite/smectite and dioctahedral vermiculite mixed- layer series from original Friedland Clay samples, based on TEM-EDX analyses .....	67
<i>Table 12.</i> Mineral formulae $[O_{10}(OH)_2]$ of diVerm., diVS-ml, IS-ml and smectite from German clays, based on TEM-EDX analyses .....	75
<i>Table 13.</i> Chemical composition (main components, oxide form) of HCl acid treated series of Friedland Clay in comparison with untreated sample from X-Ray Fluorescence analyses, indicated in mass % .....	79
<i>Table 14.</i> Mineral formulae $[O_{10}(OH)_2]$ of illite/smectite and dioctahedral vermiculite mixed- layer series from some acid treated FRDL samples in comparison with untreated FRDL, based on TEM-EDX analyses .....	82
<i>Table 15.</i> Chemical composition (main components, oxide form) of untreated and dithionite treated Teistungen and Thierfeld from X-Ray Fluorescence analyses, indicated in mass % .....	84
<i>Table 16.</i> UV-transmission at three selected points of 20% pure-clay cream samples.....	90
<i>Table 17.</i> UV-transmission at three selected points of 10% pure-clay cream samples and 10% clay-fungi ( <i>Ganoderma pfeifferi</i> ) cream samples .....	105
<i>Table 18.</i> 001-spacing d-values of clay minerals from XRD patterns of clay samples, pure-clay cream samples and clay-fungi cream samples .....	117

## LIST OF FIGURES

<i>Figure 1.</i> Spectral power distribution of terrestrial ultraviolet radiation .....	3
<i>Figure 2.</i> Action spectra for selected UV-related effects.....	4
<i>Figure 3.</i> One common damaging type on DNA molecule is harmed by ultraviolet photons .....	5
<i>Figure 4.</i> Superficial spreading malignant melanoma .....	5
<i>Figure 5.</i> Electron configuration of outermost orbital shell of Ti and O and their ionic states .....	6
<i>Figure 6.</i> Relationship between accumulation sunburning dose (minimum erythral dose, or MED) and duration of sun exposure - SPF .....	10
<i>Figure 7.</i> Spectral effectiveness of ultraviolet radiation .....	10
<i>Figure 8.</i> Electron diffraction by convergent beam mode .....	19
<i>Figure 9.</i> XRD patterns of German reference kaolins from randomly oriented powder mount, $^{\circ}2\Theta$ CuK $_{\alpha}$ position.....	29
<i>Figure 10.</i> XRD patterns of Wolfka and Spergau kaolins from oriented specimens, $^{\circ}2\Theta$ CoK $_{\alpha}$ position .....	31
<i>Figure 11.</i> TEM images of Spergau sample .....	33
<i>Figure 12.</i> Examples of Spergau kaolin by TEM .....	34
<i>Figure 13.</i> Element distribution in kaolinite aggregate by TEM-EDX-mapping of Spergau kaolin .....	35
<i>Figure 14.</i> XRD patterns of Michalovce halloysite from powder mount, $^{\circ}2\Theta$ CuK $_{\alpha}$ position .....	37
<i>Figure 15.</i> XRD patterns of Michalovce halloysite from oriented specimens, $^{\circ}2\Theta$ CoK $_{\alpha}$ position ..	37
<i>Figure 16.</i> TEM images of halloysite Michalovce.....	38
<i>Figure 17.</i> TEM images of Georgia kaolins: low defect (KGa-1b) and high defect (KGa-2) .....	39
<i>Figure 18.</i> XRD patterns of Greifswald collection betonites from powder mount, $^{\circ}2\Theta$ CuK $_{\alpha}$ position .....	41
<i>Figure 19.</i> XRD patterns of Greifswald collection betonites from oriented specimens, $^{\circ}2\Theta$ CoK $_{\alpha}$ position.....	42
<i>Figure 20.</i> Mössbauer spectrum of nontronite Garfield (bulk sample) at room temperature.....	44
<i>Figure 21.</i> TEM images of nontronite Garfield sample .....	45
<i>Figure 22.</i> TEM images of montmorillonite Chambers sample.....	47
<i>Figure 23.</i> TEM images of montmorillonite Wyoming sample.....	49
<i>Figure 24.</i> TEM images of SHCa-1 (California hectorite) sample .....	51
<i>Figure 25.</i> TEM images of STx-1 (Texas montmorillonite) sample.....	52
<i>Figure 26.</i> TEM images of SAz-1 (Cheto, Arizona montmorillonite) sample .....	54
<i>Figure 27.</i> TEM images of SWy-2 (Wyoming montmorillonite) sample.....	55
<i>Figure 28.</i> X-Ray Diffraction patterns of Friedland Clay samples from randomly oriented powder mount, $^{\circ}2\Theta$ CuK $_{\alpha}$ position.....	59
<i>Figure 29.</i> XRD patterns of Friedland Clay samples from oriented specimens, $^{\circ}2\Theta$ CoK $_{\alpha}$ position .....	60

<i>Figure 30.</i> Grain size distribution of Friedland Clay by Atterberg sedimentation.....	61
<i>Figure 31.</i> TEM images of FRDL - <2 $\mu\text{m}$ , short-term .....	63
<i>Figure 32.</i> TEM images of FRDL - <2 $\mu\text{m}$ , long-term .....	64
<i>Figure 33.</i> Tendency of illite- and dioctahedral vermiculite-components distribution in mixed-layer series from Friedland Clay samples, based on TEM-EDX analyses .....	65
<i>Figure 34.</i> Ternary charge diagrams of end-member particles and mixed-layer particles from Friedland Clay samples, based on TEM-EDX analyses .....	66
<i>Figure 35.</i> Ternary octahedral Al-Fe-Mg diagrams of end-member and mixed-layer particles from Friedland Clay samples, based on TEM-EDX analyses .....	66
<i>Figure 36.</i> Mössbauer spectra of bulk and <2 $\mu\text{m}$ Friedland Clay samples at room temperature...	69
<i>Figure 37.</i> XRD patterns of German clays from powder mount, $^{\circ}2\theta$ $\text{CuK}_{\alpha}$ position .....	71
<i>Figure 38.</i> XRD patterns of German clays from oriented specimens, $^{\circ}2\theta$ $\text{CoK}_{\alpha}$ position.....	72
<i>Figure 39.</i> TEM images of Plessa and Gorrenberg samples .....	74
<i>Figure 40.</i> TEM images of Teistungen and Thierfeld samples.....	77
<i>Figure 41.</i> Proportions of identified mica-like and mixed-layer particles of German clays.....	78
<i>Figure 42.</i> TEM images of some acid treated FRDL clay samples .....	80
<i>Figure 43.</i> Tendency of illite- and dioctahedral vermiculite-components distribution in mixed-layer series from some acid treated FRDL samples in comparison with untreated FRDL, based on TEM-EDX analyses.....	81
<i>Figure 44.</i> Ternary charge diagrams of end-member particles and mixed-layer particles from some acid treated FRDL samples in comparison with untreated FRDL, based on TEM-EDX analyses.....	81
<i>Figure 45.</i> Octahedral $\text{Fe}^{3+}$ component of mixed-layer particles from some acid treated FRDL samples in comparison with untreated FRDL, based on TEM-EDX analyses .....	83
<i>Figure 46.</i> Mössbauer spectra of original and dithionite treated samples of Teistungen and Thierfeld at room temperature .....	85
<i>Figure 47.</i> XRD patterns of original and dithionite treated samples of Teistungen and Thierfeld from powder mount, $^{\circ}2\theta$ $\text{CuK}_{\alpha}$ position .....	86
<i>Figure 48.</i> UV-measurement in comparison clay concentration: 10%-clay and 20%-clay cream samples .....	87
<i>Figure 49.</i> UV-measurement of 20%-clay cream samples of kaolins.....	88
<i>Figure 50.</i> Light microscopy images of 20%-clay cream samples of kaolins .....	89
<i>Figure 51.</i> UV-measurement of 20%-clay cream samples of bentonites.....	91
<i>Figure 52.</i> Light microscopy images of 20%-clay samples of bentonites .....	92
<i>Figure 53.</i> UV-measurement of 10%- and 20%-clay cream sample of mixed-layer dominated clay.....	93
<i>Figure 54.</i> UV-measurement 20%-clay cream samples of mica dominated clays.....	94
<i>Figure 55.</i> Light microscopy images of 20%-clay cream samples of clays.....	95
<i>Figure 56.</i> UV-measurement of 20%-clay cream samples of Wolfka and Michalovce.....	97
<i>Figure 57.</i> UV-measurement of 10%-clay cream samples of untreated Thierfeld and its dithionite treated sample .....	99
<i>Figure 58.</i> UV-measurement of 20%-clay cream samples of untreated Friedland Clay and its acid treated series.....	100

Figure 59. Light microscopy images of 20%-clay cream samples of Friedland Clay series .....	101
Figure 60. UV-measurement of clay-fungi cream samples .....	102
Figure 61. Light microscopy images of clay-fungi cream samples .....	103
Figure 62. Changes in skin flora <i>E. coli</i> after UV-irradiation with different clays (20%-clay pure-clay cream samples) .....	107
Figure 63. Influences on skin infection <i>S. aureus</i> of different clays (20%-clay pure-clay cream samples) .....	109
Figure 64. LDH release from HaCaT cells after irradiation with UV-B band under the influences of suspension of TiO <sub>2</sub> (0.5%) and <i>Ganoderma pfeifferi</i> .....	110
Figure 65. Changes in skin flora <i>E. coli</i> after UV-irradiation with different mixtures of clay and nanosuspension of <i>G. pfeifferi</i> (10%-clay clay-fungi cream samples) .....	111
Figure 66. Light microscopy image (left) and ESEM image (right) from <63 µm bulk Wolfka kaolin cream (20% of clay) .....	114
Figure 67. XRD patterns of selected clay samples and their cream samples, °2θ CoK <sub>α</sub> position .....	117
Figure 68. Plantacare-bearing fungi capsules in interlayer of clay particles .....	118
Figure 69. Plantacare-bearing fungi capsules in voids of clay particles .....	118
Figure 70. Clay-fungi cream matrix of selected clays dominated by swelling clay minerals .....	119
Figure 71. UV-behaviour vs. iron amount: untreated Thierfeld, Teistungen, their dithionite treated samples and pharmacy products .....	122
Figure 72. Relationship between Fe <sub>2</sub> O <sub>3</sub> -amount and UV-transmission of kaolins .....	124
Figure 73. Relationship between Fe <sub>2</sub> O <sub>3</sub> -amount and UV-transmission of clays .....	124
Figure 74. Relationship between Fe <sub>2</sub> O <sub>3</sub> -amount and UV-transmission of bentonites and mixed-layer dominated clay .....	126
Figure 75. Bentonites versus clays and kaolins in the aspect of relationship between Fe <sub>2</sub> O <sub>3</sub> -amount and UV-transmission .....	127
Figure 76. Electron configuration of outermost orbital shell of Fe and O and their ionic states ..	128
Figure 77. UV-behaviour vs. iron amount: iron-rich Garfield and iron-poor Wyoming .....	129
Figure 78. HCl acid treated Friedland Clay series versus untreated samples in the aspect of relationship between Fe <sub>2</sub> O <sub>3</sub> -amount and UV-transmission .....	131
Figure 79. Changes of UV-measurements in combination clays with nanosuspension of <i>Ganoderma pfeifferi</i> : Garfield and Friedland Clay .....	133
Figure 80. Changes of UV-measurements in combination clays with nanosuspension of <i>Ganoderma pfeifferi</i> : Garfield and Wyoming .....	134
Figure 81. UV-behaviour vs. particle distribution in the clay-fungi creams' system .....	135
Figure 82. UV-behaviour vs. particle size: Wolfka – <63 µm and Wolfka - <2 µm .....	140
Figure 83. TEM images of kaolinite and halloysite .....	141
Figure 84. UV-transmission versus bacteria growth .....	143
Figure 85. Bonding mechanism of organic molecules and clay minerals. ....	145
Figure 86. Bacteria are affected by charge of clay mineral .....	145
Figure 87. UV-transmission versus bacteria growth .....	146

## ABBREVIATIONS

Abbreviations	Full names
CM	Clay mineral
CMs	Clay minerals
CMS	The Clay Minerals Society
TS	Clay collection (German: “Ton Sammlung”)
UV	Ultraviolet
XRD	X-ray diffraction
TEM	Transmission electron microscopy
EDX	Energy dispersive X-ray
XRF	X-ray fluorescence
LDH	Lactate dehydrogenase
<i>E. coli</i>	<i>Escherichia coli</i>
<i>S. aureus</i>	<i>Staphylococcus aureus</i>
<i>G. pfeifferi</i>	<i>Ganoderma pfeifferi</i>
<i>Gano.</i>	<i>Ganoderma</i>
DNA	deoxyribonucleic acid
IS-ml	Illite/smectite mixed-layer
diVS-ml	dioctahedral vermiculite/smectite mixed-layer
diVerm.	dioctahedral vermiculite
diCM	dioctahedral clay mineral
Montm.	Montmorillonite
Kao.	Kaolinite
FWHM	Full width at half maximum
CSD	Coherent scatter domain
WW	Wool-wax-alcohol (German: “Wollwachsalkohole”)

LSF	Sun protection factor (German: “Lichtschutzfaktor”)
FOF	Ferrum Oxydatum Flavum ( $\text{Fe}(\text{OH})_3$ )
FOR	Ferrum Oxydatum Rubrum ( $\text{Fe}_2\text{O}_3$ )
LOI	Loss on ignition
MBS	Mössbauer spectroscopy
MB	Mössbauer
API	American Petroleum Institute Clay Mineral Standards
meq/100g	milliequivalents per 100 grams
ect.	etcetera (and so on)
i.e.	id est (that is)
e.g.	exempli gratia (for instance/ for example)
<i>et al.</i>	et aliae (and others)
<i>in vivo</i>	within a living organism/ in the living organism
<i>in vitro</i>	in an artificial environment outside the living organism

## ERKLÄRUNG

*Hiermit erkläre ich, HOANG-MINH Thao, dass diese Arbeit bisher von mir weder an der Mathematisch- Naturwissenschaftlichen Fakultät der Ernst-Moritz-Arndt-Universität Greifswald noch einer anderen wissenschaftlichen Einrichtung zum Zwecke der Promotion eingereicht wurde.*

*Ferner erkläre ich, dass ich diese Arbeit selbständig verfasst und keine anderen als die darin angegebenen Hilfsmittel benutzt habe.*

HOANG-MINH Thao

(Hoàng Thị Minh Thảo)

---

## STATEMENT OF ORIGINAL AUTHORSHIP

*I, HOANG-MINH Thao, hereby state that the work contained in this assignment has not previously been submitted for assessment, either in whole or in part, by either myself or any other student at either Faculty of Mathematics and Sciences, Ernst-Moritz-Arndt-University of Greifswald or at any other tertiary institution except where explicitly acknowledged.*

*To the best of my knowledge and belief, the assignment contains no material which has been previously published or written by another person except where due reference is made.*

---



## ACKNOWLEDGMENTS

I wish to express my deeply thanks to my supervisor, PD. Dr. habil. Jörn Kasbohm. I thank him for the construction of ideas, the expertise of advice and the kind of guidance that made this dissertation possible. My thanks go to him also because of the knowledge brought by him not only in the laboratories but also in many conferences. In addition, I acknowledge him for his kindly helps during my time in Germany.

I would like to thank to my vice supervisor, Dr. Le Thi Lai. Her support and encouragement help me to elaborate this study.

For the financial supporting to do this Ph.D. work, I am highly appreciated the Ministry of Education and Training of Vietnam (MOET) with “Project on Training Scientific and Technical Cadres in educational institutions abroad by the State budget” (322 Project) as well as the German Academic Exchange Service (DAAD) and German Federal Ministry of Education and Research (BMBF).

I am very grateful to the organization of my Ph.D study by “Joint Educational Training Center Hanoi-Greifswald” (JETC), especially Prof. Dr. Maria-Theresia Schafmeister, Prof. Le Tran Binh, Dr. Luu Lan Huong and Dr. Henry Witt.

I would like to thank all of the members of the Institute of Geography & Geology, Ernst-Moritz-Arndt-University of Greifswald, especially Department of Economic Geology. My special thanks to Manfred Zander, Monika Schäfer, Marianne Siebrand, Gisela Liebenow and PD. Dr. habil. Heiko Hüneke because of their support and help on getting TEM-EDX, XRD, XRF and light microscopy works done.

I would like to acknowledge Prof. Dr. Ulrike Lindequist, Doz. Dr. habil. Wolf-Dieter Jülich, Dr. Sabine Mundt, Dr. Gerold Lukowski and other members in Institute of Pharmacy, University of Greifswald for allowing and instructing to use the UV-photometer and the materials. I also would like to thank Dr. Sabine Witt (Biometec GmbH, Greifswald), Dr. Sofia Lessovaia (Department of Soil Science and Soil Ecology, St-Petersburg State University, Russia), Dr. Christian Knoblauch (Uni. of Hamburg) and Frau Katharina Kasbohm for experimental and informational issues involved.

I would like to thank my institution, Faculty of Geology, Hanoi University of Science (Hanoi National University, Vietnam), for the facilitation.

For the day, I also remember to thank my former teachers, who led me on my way with continuously warm-care.

Because of beautiful time in Greifswald and around, I appreciate all my German and Vietnamese friends for sharing their thoughts and fun with me. A thank is to Frank Rohde for such a friendship. I thank N. T. M. Ngoc about the discussing in life and science for long a while. I thank P. K. Huy for his kindly help with the computer. A special thank I would give Steffen Grothe because of the unforgettable and nice collision, the generous help, and especially the improving English for my writing.

Finally, I would bring my warmest thanks to my great family. Their endless love and unconditional support are always available there. Their belief in me has energized me to fulfill the work during far from home. My thanks are also for my dearest friends because of their heartfelt thoughts intended for me that make all my trouble away.

*Luận án và thành công, con xin dành tặng Bà, Bố-Mẹ và gia đình thương yêu!*

*HOANG-MINH, Thao*  
*(Hoàng Thị Minh Thảo)*

# 1 INTRODUCTION

As it is well-known, ultraviolet radiation is a real problem to human health. It can harm human skin and can even lead to the extreme case of skin cancer. That is the reason why UV protection agent is concerned. Day by day, some new UV protection skin creams are introduced into market. However, the topical non-natural substances in these suncreams, for instance  $\text{TiO}_2$  as main organic UV protection factor, are known to produce an unexpected photocatalytic effect. Very photocatalytic effect probably arise serious problems to human health when being applied directly to skin. Therefore, it is promoted to find the natural material, which can substitute for artificial/synthetical agent. Therefore, finding the natural material, which can substitute for artificial/synthetical agent, is strongly promoted. The expected optimal material should not only satisfy pharmacy safety requirement but also can prevent UV-radiation very effectively.

Clays and clay minerals as natural materials, with many benefits towards human health, are used in traditional and industrial applications including pharmacy and cosmetic products. Some common clays and clay minerals which have been applied as skin-care products are kaolinite, talc and smectite. They are popular in the cosmetic industry because of their natural specific properties as well as their remarkable high specific area and adsorption capacity.

From these points of view, this study expects to reveal the characteristics of clays and clays minerals, and to examine which of their advantages are to apply in UV protection cream.

The mineral composition and chemical composition of clay matter as well as the specific properties of clay mineral such as charge and expandable behaviour are considered. Not only the individual property but also the influence of the interaction is discussed to exploit the role on UV protection ability.

Properties which support for UV-absorption ability of clay itself and/or clay in combination with biomass are determined and discussed based on several different. We can expect to discover some optimal clay to block UV radiation effectively.

## **2 POSSIBLE FUNCTIONS OF CLAYS, CLAY MINERALS IN UV PROTECTION**

### **2.1 Clays, clay minerals and sustainability in geosciences**

Integration of the concept of sustainable development, which was developed for industry, also affects the usage of raw material from geosphere. Discussing about this concept and a hierarchy of natural resources, Wellmer & Kosinowski (2005) suggested the rule: “lower value resources should always replace higher value resources”. Related to application of the hierarchy, the authors also showed the improvement of resource efficiency of various commodities, in which kaolin - one kind of clay, has the highest change among others with nearly 250% of increasing from 1978 to 2001.

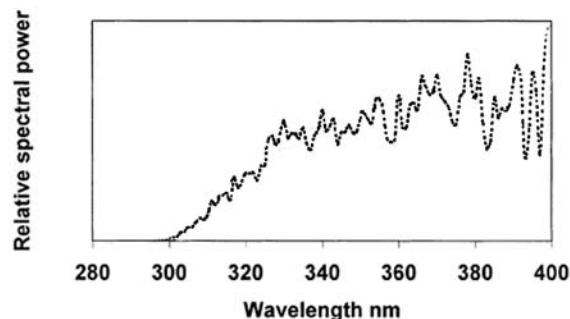
With respect to application of clay as one natural resource, Murray (2005) reviewed that, in the last decade, many new industrial applications of clays have been developed. Currently, clays are used in wide extent, such as paper filling and coating, paint, ceramic raw material, catalysts, food additives, absorbents and carriers, pharmaceuticals, cosmetics and many others (Murray, 1997). The growth in the use of clays and clay minerals will continue in the future. Especially, new techniques to modify clay minerals or new applications can make clays more valuable. For example, in paint industry, calcined kaolins can be used as an extender for titanium dioxide because of economical benefit. Currently, TiO<sub>2</sub> costs over 1 dollar per pound whereas calcined kaolin costs only about 15 cents per pound (Murray, 2005).

Therefore, to contribute to the sustainable development, clays and clay minerals are expected to be more value-added products and be substituted for expensive materials. With this aim, searching for new possible applications of clays and clay minerals should be concerned in geosciences.

### **2.2 Ultraviolet radiation and human skin**

Ultraviolet radiation is broadly noticed with the awareness of harmful effect. With waveband from 100 to 400 nm, which is shorter than waveband 400 – 700 nm of visible light, UV rays have strong thrust ability. UV band includes three parts of UV-C, UV-B and UV-A with the wavelength of <280 nm, 280 - 320 nm and 320 - 400 nm, respectively. This division refers generally to division by Commission Internationale de l'Eclairage (CIE) (Coblentz, 1932), however, the border between UV-A and UV-B is placed at 315 nm by CIE seems to be rarely cited but is defined at 320 nm (Allen, 2001; Setlow, 1974; Young, 1998; Baadsgaard, 1991; Lim *et al.*, 2005). Sunlight that reaches the Earth surface is in the wavelength between 280 and 3000 nm. That means the UV-radiation reaches the Earth surface at 280 - 400 nm, which includes UV-B and UV-A band.

The quality by spectrum and quantity by intensity of terrestrial UV-radiation vary with the time of day, the day of year and geographical latitude and longitude (Diffey, 2002) (one example was shown in figure 1). In this contribution, the UV- measurement focused on UV-absorption abilities of materials with full range of terrestrial UV-radiation in the same conditions. Therefore, the term “ultraviolet” (or “UV” as abbreviation) in the other parts of this contribution mentions to terrestrial ultraviolet radiation which belongs to wavelength 280 - 400 nm.



**Figure 1. Spectral power distribution of terrestrial ultraviolet radiation**

Note: measured in clear sky condition, at around noon in summer at a latitude of 38 °S (adapted to Diffey, 2002)

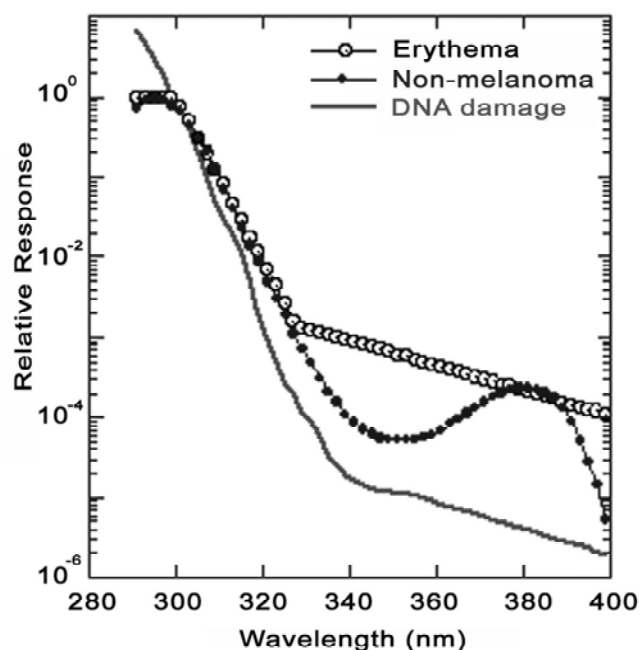
With regard to dermatology, UV-radiation can cause erythema (or sunburn), tanning, DNA-damage (e.g. protein crosslinks, protein breaks), skin cancer (e.g. non-melanoma, malignant melanoma, basal cell carcinoma, squamous cell carcinoma, curaneous melanoma), pigmentation, photoaging as well as produce vitamin D<sub>3</sub> (Setlow, 1974; MacLaughlin *et al.*, 1982; Bissett *et al.*, 1989; Diffey, 1991; Baadsgaard, 1991; de Gruijl *et al.*, 1993; de Gruijl & van der Leun, 1994; Longstreth *et al.*, 1994; MacKie, 2000). The UV-radiation effects on skin depend upon the ray energy and skin sensitivity. There is widespread agreement that, by physical theoretical idea, the shorter is the wavelength, the more energetic is the radiation. An individual's response to UV-radiation is also dependent on skin phototype (Lim *et al.*, 2005). In addition, of course, human skin is not equally sensitive to all wavelength of UV area.

UV-C ray, which is normally absorbed by the ozone layer, hence, does not present an immediate threat. In general, UV-B is well-known as the radiation that can lead the damage to DNA and cause skin cancer because of such high energetic rays (Setlow, 1974; Young, 1998). Besides, UV-B also play helpful role in formation of vitamin D<sub>3</sub> by the skin (MacLaughlin *et al.*, 1982; Diffey, 1991; Chel *et al.*, 1998; Lim *et al.*, 2005). Effective wavelengths in the production of erythema also have a peak in the UV-B range (Setlow, 1974; Lim *et al.*, 2005). However, the symptom of erythema or sunburn might be caused by UV-A radiation because erythematous action spectrum has a high response level in UV-A range (as comparable model by Stratospheric Ozone and Human Health Project and presented in figure 2 (reviewed by SEDAC)). Besides, UV-A has a larger contribution in the spectral distribution than UV-B (Bissett *et al.*, 1998; Diffey, 2002 and figure 1). In other words, UV-A plays a harmful role in that it causes typically sunburn on human skin. But, UV-A has low potential of causing skin cancer.

Diffey (2002) suggested that UV-B contributes about 80% toward most of the harmful effects and UV-A contributing the remaining 20%. Recently it is a general accepted position that solar UV-radiation range of 300 – 320 nm is more damaging than other ranges and in which 300 nm is most effective wavelength (reviewed by Young *et al.*, 1998).

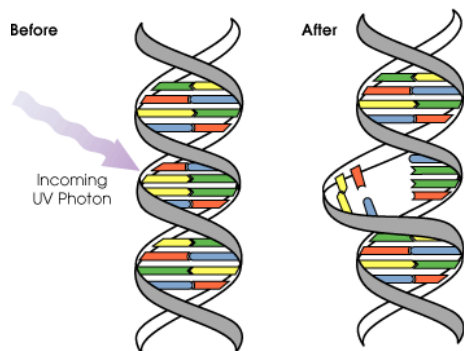
The biological effects of UV-radiation may be classified into three categories: on cell, on tissue and on the whole body (Wong, 1998). At the level of UV-induced cell, the most important effect is the DNA-

damage; for example DNA-to-protein crosslinks and single-strand breaks (Moan & Peak 1989; Peak & Peak, 1991). Figure 3 below is a model of common DNA-damage elucidated by Herring (reviewed by Allen, 2001). With respect to UV-induced tissue, there is induction of sunburn and skin aging (McKinlay and Diffey, 1987; Bissett *et al.*, 1989). “Standard erythema dose” (SED), which is a measure of the erythema effectiveness of UV-exposure, and “minimal erythema dose” (MED), which is a threshold for skin redness or burning, are common terms related to sunburn or erythema problem. In degree of effect on the whole body, UV damage can lead to serious problems include skin cancer (figure 4) and immune suppression (de Fabo *et al.*, 1990; Baadsgaard, 1991; Longstreth *et al.*, 1994). The magnitude of the problem is evident from the fact that in 1988, 1019 people died of skin cancer in Australia (Gies *et al.*, 1998). Unions New South Wales also reported that about 66% Australian people treated for skin cancer at some stage in their life (Unions NSW, 2005).



**Figure 2. Action spectra for selected UV-related effects**

Several action spectra: the erythema action spectrum given by McKinlay and Diffey (1987), the mammalian non-melanoma skin cancer action spectrum of de Gruijl and van der Leun (1994); and the DNA-damage action spectrum of Setlow (1974) (reviewed by SEDAC)



**Figure 3. One common damaging type on DNA molecule is harmed by ultraviolet photons**  
(Illustration by David Herring, reviewed by Allen, 2001)



**Figure 4. Superficial spreading malignant melanoma**  
Note: the irregular outer edge and irregular color within the lesion  
(Health Protection Agency (NRPB, 2002))

In conclusion, with respect to dermatology, ultraviolet radiation has a considerable potential for causing harmful effects to the human health with many kinds of symptom at different levels. UV-B radiation, with waveband of 280 – 320 nm, generally, has the higher damaging potential than UV-A radiation with longer waveband of 320 - 400 nm. Significantly, wavelengths from 300 – 320 nm, especially wavelength of 300 nm, have strong effects, therefore, should be concerned. Nevertheless, most of UV-A radiation amount must be prevented because of its high contribution to solar UV-radiation.

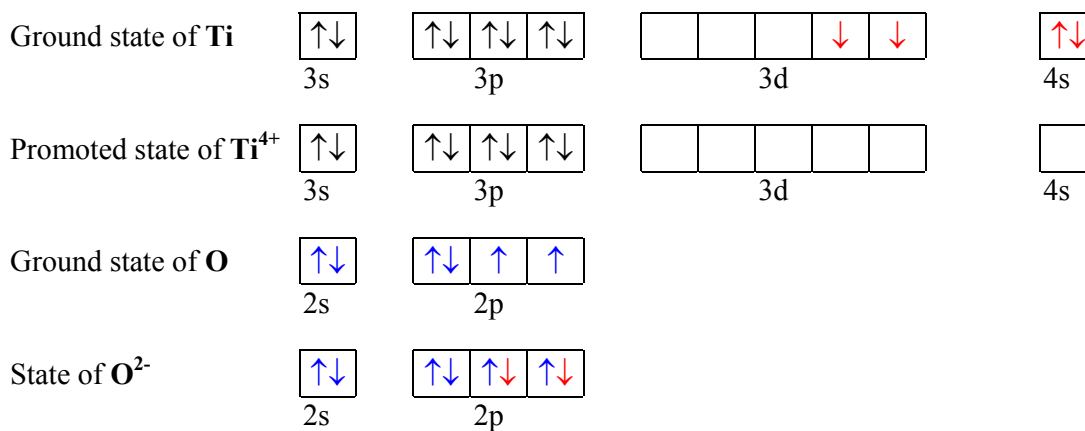
### 2.3 Actual substances as UV protection factor and their problems

As mentioned previously, it is obvious that UV-radiation has potential harmful effects; therefore, researching for ways to control skin exposing under solar radiation is an urgent need. To shield skin from UV, beside wearing protective clothes or staying indoor, which is not always applicable, UV protection cream can be used as the filter.

So far, topical sunscreens contain organic filters, which prevent from either mainly UV-B (e.g. octyl methoxycinnamate) or UV-A (e.g. avobenzone), and inorganic filter such as  $\text{TiO}_2$  and  $\text{ZnO}$  (an example is some of Ladival®'s ingredients in appendix 9) (NRPB, 2002). List of sunscreen active agents allowed in sunscreen products with their maximal quantity was published by U.S. Food and Drug Administration (FDA, 1999). Organic filters as chemical filters are chosen carefully because of photoinstability and possible unfavorable synergistic interactions, therefore, they can cause many seriously problems. Some examples are Padimate-A (or Escalol 506), one commercial organic sunscreen, was withdrawn from European market in the late 1980s and Padimate-O (or Escalol 507) which induces mutations and attacks DNA directly. Therefore, trend of using inorganic UV protectors as physical sunscreens has been increasing (reviewed by one group, published in Knowland *et al.*, 1993; Serpone *et al.*, 2002; Hidaka *et al.*, 1997).

Titanium Dioxide ( $\text{TiO}_2$ ) is the most commonly utilized inorganic protector because of its highly distinctive properties: long-term durability, non-combustible, odorless, color neutrality (white or opaque) and discoloration resistance. Furthermore, U.S. Food and Drug Administration noted (US Federal Register, 43FR38206, 25 August 1978) that  $\text{TiO}_2$  is biologically inert, chemical inert, resistant as well as safe and effective as “physical sunscreen” (FDA, 1999). This advantage, physical sunscreen, was found because of its very high refractive index ( $n = 2.5 - 2.7$ ) (Judin, 1993).  $\text{TiO}_2$  has also a safety card number ICSC 0338 (CAS No: 13463-67-7, March 2002) by International Occupational Safety and Health Information Centre (CIS). In other words,  $\text{TiO}_2$  is expected only to scatter and reflect UV-radiation. Therefore, it has been becoming commercial and popular additive in cosmetic and especially sun-care products as UV protector as well as pigment and thickener.

Actually, due to their applied nano- and micro- particle size in cosmetics,  $\text{TiO}_2$  probably does not reflect and scatter UV-radiation intensively but is capable to express its photocatalysis ability significantly (reviewed by Hidaka *et al.*, 1997).  $\text{TiO}_2$  prevents UV-radiation from going into human skin by absorbing about 70% incident radiation (Dunford *et al.*, 1997). Pure fine  $\text{TiO}_2$  does not occur in nature but can be manufactured from ilmenite or leucosene ores as well as rutile beach sand. To understand this effective absorption of  $\text{TiO}_2$ , ones have learnt about its native characteristics.



**Figure 5. Electron configuration of outermost orbital shell of Ti and O and their ionic states**  
 $\text{Ti}^{4+}$  ( $Z_{\text{Ti}} = 22$ ) and two of  $\text{O}^{2-}$  ( $Z_{\text{O}} = 8$ ) are associated by ionic bond to form  $\text{TiO}_2$ . At promoted state, all of 3d orbitals and 4s orbital of  $\text{Ti}^{4+}$  are empty.  $\text{Ti}^{4+}$  and  $\text{O}^{2-}$  have no single electron.

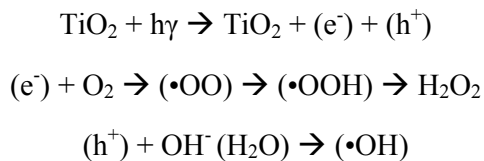


TiO<sub>2</sub> is bonded from Ti<sup>4+</sup> and two O<sup>2-</sup>, which have electron configuration like in figure 5, by electronic valence. Crystalline forms of TiO<sub>2</sub> as anatase and rutile are well known as semiconductor<sup>1</sup> materials. Valence band<sup>2</sup> of TiO<sub>2</sub> is comprised of the 2p orbital of oxygen, while the conduction band<sup>3</sup> is made up of the empty 3d orbital of titanium. Bandgap<sup>4</sup> energies of anatase and rutile are approximately 3.23 eV and 3.06 eV, respectively, corresponding to wavelength of about 390 nm and 405 nm (Judin, 1993).

The UV-radiation, 280 – 400 nm, has enough energy to promote semiconducting property of TiO<sub>2</sub>. TiO<sub>2</sub> absorbs photons resulting in electrons from the valence band being pushed up into conduction band. In this excited state, a number of single electron (e<sup>-</sup>) and electron hole (h<sup>+</sup>) in the valence band (where the electron left) are created. Normally, this photo-excited state is not stable and can break down to become normal state with recombination of (e<sup>-</sup>) and (h<sup>+</sup>). Conversely, photo-excited state of TiO<sub>2</sub> remains stable. Accordingly, TiO<sub>2</sub> is a powerful UV-absorption material as well as an excellent photocatalyst.

TiO<sub>2</sub> was evaluated as a safe chemical material (IARC, 1989) that cannot cause mutagenic and cannot damage DNA, consequently; but the paper did not research on the effect of sun illumination. In the darkness, TiO<sub>2</sub>, even as ultrafine particle, is chemically inert. This characteristic manifests its stability in box-closed trade-ware creams. However, to apply TiO<sub>2</sub> as cosmetics additive, its effectivity must be acknowledged also under illumination condition.

Illuminated TiO<sub>2</sub> is really not safety. Its products of (e<sup>-</sup>) and (h<sup>+</sup>) by photocatalytic process, as described above, can interact with surrounding environment. In the air, (e<sup>-</sup>) can react with oxygen, which has 2 empty orbital in the molecule, into peroxy radical (•OOH). In aqueous environment, (e<sup>-</sup>) react with “dissolved O<sub>2</sub>” and especially, (h<sup>+</sup>) can alter OH<sup>-</sup> into hydroxyl radical (•OH) (Clechet *et al.*, 1979; Jaeger and Bard, 1979; Goswami, 2003). These processes are similar to photosynthesis<sup>5</sup>.




---

<sup>1</sup> The semiconductor, at “absolute zero” temperature, has the outermost electron energy band is fully filled, that is different from a conductor (which is partly electron filled) and the bandgap is small enough for there to be appreciable thermal electrons in its conduction band at room temperature.

<sup>2</sup> Valence band, among the bands filled with electrons, is the one with the highest energy level or the electron orbit farthest from the nucleus.

<sup>3</sup> Conduction band is the range of electron energy, higher than that or “outside” of the valence band.

<sup>4</sup> The bandgap is energy width of the forbidden band between the valence band and the conduction band.

<sup>5</sup> Chlorophyll captures sunlight to turn water and carbon dioxide into oxygen and glucose.

Jaeger and Bard (1979) did detect the radical intermediates in the photodecomposition of water at TiO<sub>2</sub> particulate systems includes (•OO) and (•OH) by using spin trapping and electron spin resonance. Clechet *et al.* (1979) demonstrated that the formation of these radicals with the present of TiO<sub>2</sub> is a real photosynthesis reaction of UV-illumination. Dunford *et al.* (1997) reviewed that both anatase and rutile have this property, whilst anatase is more active than rutile. Burgeth & Kisch (2002) had the same conclusion. Dunford *et al.* (1997) and Goswami (1999) also demonstrated that ZnO (bandgap of 3.3 eV), which is also UV inorganic filter in cosmetics, has similar photosynthesis process but less effective. Dunford and coworkers (1997) concluded that TiO<sub>2</sub> extracted from a sunscreen is photoactive, as well.

(•OO) is not considered to be so reactive and is further reduced slowly to H<sub>2</sub>O<sub>2</sub> (Cai *et al.*, 1992a). The formation from electron hole, (•OH), is probably the most unstable with an *in vivo* half-life of approximately 10<sup>-9</sup> sec (Pryor, 1986). Therefore, (•OH) is highly reactive and is a very dangerous compound to the organism.

(•OH) can oxidize and decompose organic compounds effectively into simpler component of water, carbonic and mineral acids, consequently. In fact, people apply the photocatalytic property of TiO<sub>2</sub> forming (•OH) in detoxification and disinfection of water and air: water treatment, self-cleaning glass and paint, killing bacteria material, killing fungi material (Goswami, 1999; Desrosiers, 2005). Study of Goswami and his coworkers showed that several common bacteria (*E. coli* and *S. aureus*) were killed after just a few minutes under solar exposure in the presence of TiO<sub>2</sub>, meanwhile without TiO<sub>2</sub>, it took over two hours to destroy these bacteria.

Hidaka and coworkers (1997) demonstrated that *in vitro* serious damages to DNA and RNA by (•OH) can be ensured in the presence of nanoparticles of titania (TiO<sub>2</sub>) under exposing to UV-radiation. Knowland and coworkers (1993) concluded that variety of bimolecular including DNA are attacked directly by (•OH) (but in the study, (•OH) is formed from photocatalytic Padimate-O). By *in vitro* and *in vivo* (cultures human fibroblasts) study, Dunford and coworkers (1997) proved that (•OH) inflict direct strand breaks in DNA. In additions, nanoparticles of TiO<sub>2</sub> not only can yield harmful (•OH) but also can pass through human skin (Tan *et al.*, 1996).

In conclusion, with respect to UV protection skin creams of applying to skin directly, TiO<sub>2</sub> is expected to scatter and reflex as physical sunscreen. However, TiO<sub>2</sub> is proved to be an unexpectedly harmful chemical sunscreen because of their inimical effects to human health. It is proved that TiO<sub>2</sub> can cause serious effects to human health. These effects might be comparable with the UV-induced problems.

## 2.4 Pharmacy requirement in suncreams

Sun protection products and products with a Sun Protection Factor (SPF) are regulated as cosmetics<sup>6</sup> (subject to positive lists) in the EU and Japan, as functional cosmetics in Korea, as over-the-counter (OTC) drugs in the USA, as non-prescription drug in Canada and as OTC products in Australia if the SPF is greater than 4 (RPA, 2004). Therefore, depending on the specific market, sun protection products have to obey requirement for accordingly kind of product in category.

The EU Cosmetics Directive (76/768/EEC) was adopted on 27 July 1976. The Directive aims to guarantee the safety of cosmetic products for human use while encouraging commercial exchange and eliminating barriers to trade (EC, 1999). The European Commission has overall responsibility for cosmetics legislation within the EU. Each Member State designates a competent authority that enforces the legislation (RPA, 2004).

In the EU, skin care products as a whole account for 23% of the total cosmetics and toiletries market and are the fastest growing segment (Colipa, 2003). Sun protection products are still expected to a development associated with the introduction of new and more effective UV filters. Until now, titanium dioxide is in the list of UV filters which sunscreens may contain with maximum authorized concentration of 25%. It takes about 2 - 3 years of preparation of the file for approval of new UV filters and afterwards Scientific Advisory Committee, the SCCNFP, need approximately 1 year to issue the expected new one. Data requirements and timescales for approval of new UV filters are considerably different between markets (RPA, 2004).

The main difference of suncream from normal cream is its sun protection ability. To measure the amount of protection against UV-radiation provided by a sunscreen, SPF is applied. An SPF rating of 15 would only allow 1/15<sup>th</sup> of UV-radiation falling on its surface to pass through it. In other words, this suncream would transmit about 7% of UV-radiation.

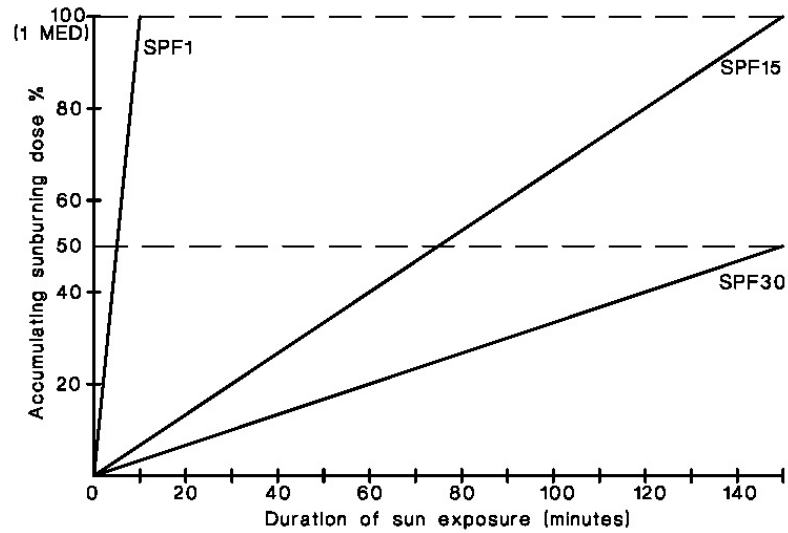
In definition, SPF is arithmetical mean of individual SPF<sub>i</sub> (1 decimal point):

$$SPF_i = \frac{\text{protected MED}_i}{\text{unprotected MED}_i} \quad (\text{see also in figure 6})$$

---

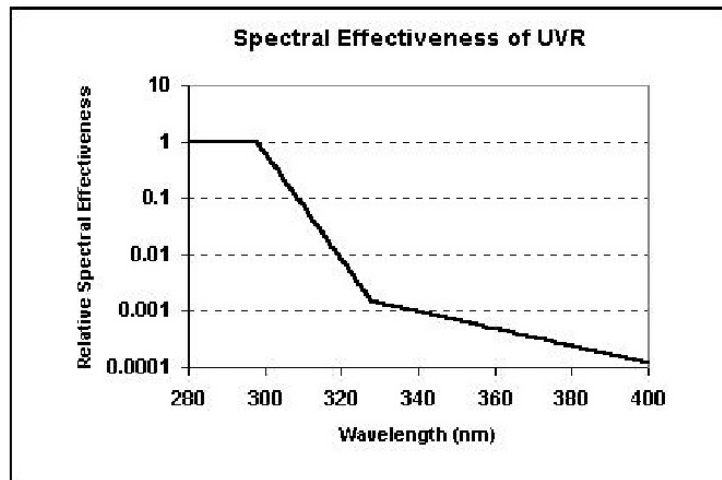
<sup>6</sup> The EU Cosmetics Directive defines a cosmetic product as:

*'any substance or preparation intended to be placed in contact with the various external parts of the human body (epidermis, hair system, nails, lips and external genital organs) or with the teeth and the mucous membranes of the oral cavity with a view exclusively or mainly to cleaning them, perfuming them, changing their appearance and or/correcting body odours and/or protecting them or keeping them in good condition'.*



**Figure 6.** Relationship between accumulation sunburning dose (minimum erythral dose, or MED) and duration of sun exposure - SPF  
(AS/NZS, 1998)

There is an important note that the biological effectiveness of UV-radiation increases by a factor of over 1000 as the wavelength changes from UV-A to UV-B because UV-B exposure causes 1000 times as much of skin damage as the same amount of UV-A exposure (figure 7). However, as showing in the formula, SPF is based solely on prevention of erythema.



**Figure 7.** Spectral effectiveness of ultraviolet radiation  
(ARPANSA, 2003)

SPF ratings are determined by testing sunscreens on the skin of human volunteers in accordance with updated standard for sunscreen.

Australia published as first country a standard for sunscreen products in 1983. The present joint Australian and New Zealand standard is AS/NZS 2604: 1998 “Sunscreen Products Evaluation and Classification”. An international SPF is also published in 2003 by Colipa (European Cosmetic, Toiletry and Perfumery Association) written in collaboration with CTFA-SA (Cosmetic, Toiletry and Fragrance Association of South Africa) and JCIA (Japan Cosmetic Industry Association). Both of updated SPF categories listed a high-SPF level with minimal side of SPF 15 (table 1) (AS/NZS, 1998; ARPANSA, 2003 and CTFA, 2004).

According to the previous discussion,  $\text{TiO}_2$  can cause problem to human health. Therefore, it is preferred to develop new safety UV filters or new series of Sun protection products, which can satisfy the requirement of AS/NZS 2604: 1998 standard, Colipa standard or some updated one. Therein, new cosmetic creams with an  $\text{SPF} \geq 15$  are expected sunscreens. In addition, the new sunscreens are expected to prevent also skin cancer which is caused mainly by UV-B radiation.

**Table 1. Comparative SPF categories (labelling)**

*(According to CTFA, 2004)*

<b>Australia &amp; New Zealand, 1998 (AS/NZS 2604: 1998)</b>	<b>International SPF, 2003 (Colipa, CTFA-SA, JCIA)</b>
<p>Labelled SPF: SPF rounded down to nearest integer or &lt;mean SPF in same category</p> <p>Very Low: 2 - &lt;4</p> <p>Low: 4 - &lt;8</p> <p>Moderate: 8 - &lt;15</p> <p>High: 15 - &lt;30</p> <p>Very High: <math>\geq 30</math></p> <p>SPF <math>\geq 15</math> products should be “Broad spectrum”</p>	<p>Mean value from the test rounded down to the nearest whole number in the SPF classification table summarised below</p> <p>Low: 2-4-6</p> <p>Medium: 8-10-12</p> <p>High: 15-20-25</p> <p>Very High: 30-40-50</p> <p>Very High: 30-40-50</p> <p>Ultra: 50+</p>

## 2.5 Clays, clay minerals and their application for human health

Application of clays and clay minerals in pharmaceutical products and cosmetics is very widespread in daily life. The applied abilities are based on the typical properties of clay minerals: high specific area and adsorption capacity, rheological properties as well as chemical inertness and low or null toxicity. In addition, because of clay’s character as natural material, it is possible to control its active principal and chemical process.

Carretero (2002) reviewed in detail the applications and beneficial effects upon human health of clays and clay minerals. Following is a short introduction about those applications.

Minerals which are utilized for pharmaceutical purpose are mainly natural clay minerals (eg. smectites, kaolinite, palygoskite...) except hectorite "Laponite S". Use of clays and clay minerals for health protection and treatment is already as old as mankind. The ancients used mud to cure wounds and to soothe irritation. Nowadays, people use clays and clay minerals in pharmaceutical formulations, in spas and in aesthetic.

Using clays as bulk material, spas and aesthetic medicine are two popular fields of application. In spas, clay is applied in geotherapy as cataplasms or mud baths, in pelotherapy and in paramuds. Clays are mixed with water then matured in pelotherapy or mixed with paraffin in paramuds. For example in geotherapy spas, the mixture of clays and water can be direct applied upon the skin as cataplasm to treat boils, acne, ulcers, abscess, seborrhoea, etc.; or cool-muds can be used as anti-inflammatory agent and hot-muds can be used for chronic articulatory treating. In aesthetic medicine application, cold clay mud is commonly used in facial treatments. Clays are also used to treat blackheads, spots, acne and seborrhoea as well as to retard the development process of cellulite.

The using of clay minerals in pharmaceutical formulations fall into one of two main categories: excipient<sup>7</sup> and active substance.

As excipient, clay minerals improve organoleptic characteristics such as taste, smell, color and improve physical-chemical properties such as viscosity. They facilitate the preparation and promote the disintegration of pharmaceutical formulation. The clay minerals familiar in this category are palygorskite, smectites, kaolinite and talc. Some examples of the using of these materials are emulsifying agents, thickening agents, lubricants, agents to aid disintegration, dispersion of fibres, inert bases and to avoid the segregation of the pharmaceutical formulation. However, it is noticed that clay minerals can have influence on liberation and stability of bioavailability of the main drug.

Especially in case of excipient, concerning sunscreen, sepiolite and smectites were researched on their abilities to form complexes with organic compounds which absorb UV-radiation (del Hoyo *et al.*, 1998, 2001; Vicente *et al.*, 1989)

---

<sup>7</sup> An excipient is an inert substance used as a diluent or vehicle for a drug. (<http://medical-dictionary.thefreedictionary.com/>)

As active substance, the application is more limited, some should be listed are gastrointestinal protectors, osmotic oral laxatives, dermatological protectors and cosmetics. One familiar is “Beidelix” which is used as a stomach buffer from Na-beidellite. In pharmacy, clay minerals are utilized to produce powders, creams and ointments for protecting skin against external agents and agents exuded by skin itself or excreted liquids. For cosmetic purposes, clay minerals are utilized for inflammatory processes to treat for example boils, acne, ulcers and are produced in creams, powders, emulsions. Kaolinite, smectites, talc and palygorskite are the common used clay minerals.

In conclusion, clays and clay minerals are various and familiar in pharmaceutical and cosmetic application. Because special properties of clay minerals which are different from other minerals, they have many beneficial effects upon human health.

## **2.6 Possible functions of clays, clay minerals in UV protection cream**

Because of problems with UV-radiation as well as the non-natural additives used in suncreams, clay minerals and clays are object of this study with expectation to open some clay characterization which has function in UV protection.

As above mention, clays and clay minerals are applied in many industrial fields including application in pharmaceutical and cosmetic fields. They are used in the health care productions because, besides of specific properties, clays and clay minerals have high surface area and absorption capacity, rheological characterization, chemical inertness and low or null toxicity. However, there is still limitation in the pharmaceutical and cosmetic application of such kind of material. Almost of all application in these fields is using clays and clay minerals as excipient, only few is using as active substance (Carretero, 2002). With the aspect in sunscreen, some former researches of del Hoyo *et al.* (1998, 2001) and Vicente *et al.* (1989) intended for clays but as only excipient and related in UV-C area. Because clays and clay minerals have many possible functions in UV protection, this contribution concerns substitution clays as active substance for non-natural additives in suncreams.

Clay minerals are phyllosilicate minerals, so that they can create conditional feeling on the skin with high rheological property. That is why they are used as cosmetic materials. Some commonly used clay minerals in cosmetic application are talc and montmorillonite. Clays are also characterized as the materials having high absorbency level. Therefore, they are also supportive for skin to absorb greases and toxins. This characterization is advantage for application in cosmetic field.

Because of such the “phyllo-“property, clays have high surface area. Kaolin has the surface area of about 10 – 20 m<sup>2</sup>/g and bentonite has the number around 700 - 800 m<sup>2</sup>/g of total surface area. With such high surface areas, clays can cover effectively a zone of human skin. Therefore, on this applied clay-bearing suncreams, clays are expected that they can support a UV-absorption ability or UV-reflection ability.

With respect to the possible UV-reflection function, the specific surface area of clay should be an important factor. Therefore, particle parameters are concerned. Different grain size distributions of same clay are studied to compare the influence of surface area in the similar chemical composition. Clay minerals in different groups such as kaolinite and smectites are also considered because they are in different surface area levels.

With respect to the possible UV-absorption function, the chemical composition of clays is considered. Hence, clays characterized with different chemical compositions are used in this study. Moreover, different phases of the same chemical element in clay samples can have different influence, so that the clays are studied in detail for all of mineral phases especially main clay mineral phases.

Besides, cream samples are mixture of clays and organic components. Therefore, some properties of clay such as surface charge, which can affect the interaction between clay and organic component, are considered.

Conclusively, besides of many positive properties towards human health and human skin, clay minerals and clays are reasonably expected to support for UV protection substituting non-natural additives.



### 3 METHODOLOGY

#### 3.1 Clays and clay minerals analyses

Used clays and clay minerals for UV experiments were divided into four different groups: kaolin, bentonite, mica dominated clay and mixed-layer dominated clay (table 2, table 3). These categories were identified based on corresponding clay minerals group: kaolinite and halloysite (kaolin); montmorillonite, beidellite and nontronite (bentonite); illite and dioctahedral vermiculite (mica dominated clay); and illite/smectite mixed layer series and dioctahedral vermiculite/smectite mixed layer series (mixed-layer dominated clay).

In this project, XRD, TEM-EDX, XRF, SEM, dithionite treatment and Atterberg sedimentation were performed in the laboratories of Institute of Geography and Geology, E-M-A-University of Greifswald.

<b>Table 2. Untreated kaolin samples involved in UV-measurements</b>			
<b>Sample</b>	<b>Locality</b>	<b>Note and literature</b>	<b>Source</b>
Caminau	Caminau, Lausitz near Bautzen, Saxony, Germany	Granodiorite kaolin by weathering; German reference kaolin; ASMW, 1988	Institute of Geography and Geology, EMAU, Greifswald
Wolfka	Kemmlitz, near Leipzig Saxony, Germany	Porphyry kaolin by weathering; German reference kaolin; ASMW, 1988	Institute of Geography and Geology, EMAU, Greifswald
Spergau	Spergau, Merseburg, Saxony-Anhalt, Germany	weathered New-red Sandstone arkoses; German reference kaolin; ASMW, 1988	Institute of Geography and Geology, EMAU, Greifswald
Seilitz	near Meissen, Saxony, Germany	Pitchstone kaolin by weathering; German reference kaolin; ASMW, 1988	Institute of Geography and Geology, EMAU, Greifswald
KGa-1b	Washington, Georgia, USA	weathered Tuscaloosa Formation sandstone; CMS low defect kaolin; van Olphen & Fripiat, 1979	The Clay Minerals Society (CMS)
KGa-2	Warren, Georgia, USA	probably lower Tertiary sedimentation; CMS high defect kaolin; van Olphen & Fripiat, 1979	The Clay Minerals Society (CMS)
Michalovce	Michalovce, Slovakia	hydrothermal alteration of rhyodacite halloysite (TS-41); Kužvart, 1969	Institute of Geography and Geology, EMAU, Greifswald (TS-41)

**Table 3. Untreated clay samples involved in UV-measurements**

<i>Sample</i>	<i>Locality</i>	<i>Note and literature</i>	<i>Source</i>
Plessa	Bad Liebenwerda, Brandenburg, Germany	German reference clay; Kranz, Ruchholz and Marx, 1990	Institute of Geography and Geology, EMAU, Greifswald
Gorrenberg	Traustein, Thuringia, Germany	German reference clay; Kranz, Ruchholz and Marx, 1990	Institute of Geography and Geology, EMAU, Greifswald
Teistungen	Worbis, Thuringia, Germany	German reference clay; Kranz, Ruchholz and Marx, 1990	Institute of Geography and Geology, EMAU, Greifswald
Thierfeld	Zwickau, Saxony, Germany	German reference clays; Kranz, Ruchholz and Marx, 1990	Institute of Geography and Geology, EMAU, Greifswald
Friedland Clay	Friedland near by Anklam, Mecklenburg-Western Pomerania, Germany	Eocene marine sedimentation; IS-mixed layer rich (30% illite : 70% smectite); Henning, 1971	Pilot Vegetable Oil Technology Magdeburg e.V. (PPM e.V.), Magdeburg, Germany
Garfield	Garfield area, near Spokane, Washington, USA	formed from basalt by weathering; nontronite, API/H-33a; Kerr, 1951	Institute of Geography and Geology, EMAU, Greifswald (TS-1803)
Chambers	Chambers, Arizona, United State	altered volcanic ash; montmorillonite, API/H-23; Kerr, 1951	Institute of Geography and Geology, EMAU, Greifswald (TS-569)
Wyoming	Upton area, near Newcastle, Wyoming, USA	interbedded in Mowry shale; montmorillonite, API/H-25; Kerr, 1951	Institute of Geography and Geology, EMAU, Greifswald (TS-874)
SHCa-1	San Bernardino, California, USA	altered Red Mountain andesite; hectorite, CMS bentonite van Olphen & Fripiat, 1979	The Clay Minerals Society (CMS)
STx-1	Gonzales, Texas, USA	altered rhyolitic, Manning Formation montmorillonite, CMS bentonite van Olphen & Fripiat, 1979	The Clay Minerals Society (CMS)
SAz-1	Cheto Mine, Apache, Arizona, USA	altered vitric tuff, Biodhochi Formation montmorillonite, CMS bentonite van Olphen & Fripiat, 1979	The Clay Minerals Society (CMS)
SWy-2	Crook, Wyoming, USA	volcanic ash, Newcastle Formation montmorillonite, CMS bentonite van Olphen & Fripiat, 1979	The Clay Minerals Society (CMS)

### 3.1.1 X-Ray diffraction

XRD-investigations were carried out to determine the mineral composition of the samples and their semiquantitative distribution. Additionally, some individual parameters have been measured like particle size distribution (coherent scatter domains / CSD). Normally, the used samples were milled and sieved to particle size of  $<63\ \mu\text{m}$  before diffraction measurements.

With randomly oriented powder samples, a Siemens D5000 X-ray diffractometer with a Cu tube,  $K\alpha_{1,2}$  radiation of  $1.54\ \text{\AA}$  was used at 30 mA of current and 40 kV of voltage (table 4). Besides, soller collimator is 0.5/25, measurement step size & time:  $0.02\ ^\circ 2\theta$  for 3 seconds. The data were collected from  $4$  to  $68\ ^\circ 2\theta$ . Some samples with high Fe-proportion were re-investigated by Co tube of  $1.79\ \text{\AA}$  with Fe-filter. XRD measurements with randomly oriented powder could bring out all of diffraction with hkl-spacing. These d-values were compared with the basis of ICDD/JCPDS database to identify the main mineral matter (appendix 1).

XRD analyses were carried out also on oriented mounts including air-dried, ethylene-glycolated and  $550^\circ\text{C}$ -heated (during 4 hours) specimens by means of a Freiberg Praezitronic diffractometry HZG 4A-2 equipped with a Seifert C3000 control unit (Co tube,  $K\alpha_{1,2}$  radiation, 30 kV, 30 mA; fixed slits:  $1.09\ \text{mm} / 6.0\ \text{mm}$ , soller: 0.5/25, detector slit:  $0.35\ \text{mm}$ , see table 4). Data recording was started at  $4$  and ended at  $34\ ^\circ 2\theta$  with a step size of  $0.02\ ^\circ 2\theta$  and a count time of 2 seconds per step. XRD analyzing of oriented specimens checked the 001-spacing and the changing of this spacing that is caused after interlayer space saturation or thermal treatment. Based on different minerals modification (Starkey *et al.*, 1984), the minerals which were presented in oriented mount were identified.

For analyzing the line-profile of clay minerals with broad and heavily overlapping X-ray refraction, specialized WinFit program was used (Krumm, 1994). This program helped to decompose complex or noisy pattern by fitting profile shape functions that can be fixed to Gaussian. The refined profiles were used for determination of positions. Besides, intensity and area of the peak could be taken to quantify phases relatively. Furthermore, by WinFit program, the refined profiles, which include FWHM and peak shape, with Fourier transformation implement were used for the determination of CSD as approximation to the particle thickness distribution.

In this research, dominated clay minerals are divided into 4 groups: kaolin-group with kaolinite and halloysite; smectite-group with montmorillonite, beidellite and nontronite; miscellaneous series with illite, dioctahedral vermiculite and illite/smectite mixed layer (IS-ml) and dioctahedral vermiculite/smectite mixed layer (diVS-ml) phases.

#### *Kaolinite and halloysite*

Although having same formula, XRD pattern of kaolinite is different from this one of halloysite. Kaolinite has  $7.18\ \text{\AA}$  001-spacing and  $3.58\ \text{\AA}$  002-spacing peaks. Otherwise, halloysite has  $7.4\ \text{\AA}$  001-spacing and  $3.63\ \text{\AA}$  002-spacing peaks.

*Montmorillonite, beidellite and nontronite*

Montmorillonite, beidellite and nontronite allow water or other molecules to enter between the layers, so that the expansion is very clear with ethylene-glycol treatment. It is difficult to distinguish between beidellite and montmorillonite, by applying Heller-Kallai test using  $\text{Li}^+$  saturation with suitable material proportion, (Malla & Douglas, 1987; Klopogge *et al.*, 1990), so that beidellite is recognized with TEM analyzing.

*Illite and dioctahedral vermiculite*

In XRD result parts, “illite” is referred to illite, dioctahedral vermiculite and illite/smectite mixed-layer or dioctahedral vermiculite/smectite mixed-layer with very low proportion (smaller than 10%) of smectitic layer.

*IS-ml and diVS-ml*

“IS-ml”, mentioned in XRD results, is referred to illite/smectite mixed-layer and/or dioctahedral vermiculite/smectite mixed-layer.

All these phases occur together mostly as mixture and the resulting overlapping interferences are not to separate clearly, because of their similar behaviour. They have been listed and distinguished in detail by mineral formula in TEM-EDX results.

Especially, according to Moore and Reynolds (1997), it is possible to estimate proportion of illitic layer in ethylene-glycol saturation profile with IS-ml 001/002 and 002/003 peaks by Newmode-modelling.

**Table 4. Equipment and technical parameters of XRD measurements**

<i>Equipment</i>	<i>Siemens D5000 X-ray diffractometer</i> <i>(for randomly oriented mounts)</i>	<i>Praezitronic Freiberg HZG 4 / Seifert C3000</i> <i>(for oriented mounts)</i>
X-ray tube	<b>CuK<math>\alpha</math></b>	<b>CoK<math>\alpha</math></b>
Wavelength	1.54 Å	1.79 Å
Voltage	40 kV	30 kV
Current	30 mA	30 mA
Step	0.02 °2 $\theta$ /3s	0.03 °2 $\theta$ /2s
2 Soller-slits	0.5/25	0.5/25
Divergence-slit	20 mm	1.09 mm
Scatter-slit	2.0 mm	6.0 mm
Receiving-slit	0.06 mm	0.35 mm
Counter	Scintillation counter	Proportional Counter
Other	Graphite secondary-monochromator	Fe-filter

In conclusion, line-profiles from XRD measurement can be interpreted for analyzing phase and individual mineral. Therefore, almost all clay samples, which were used in this research, were analyzed by XRD with both randomly oriented powder mount for hkl-spacing and oriented specimens for 00l-spacing.

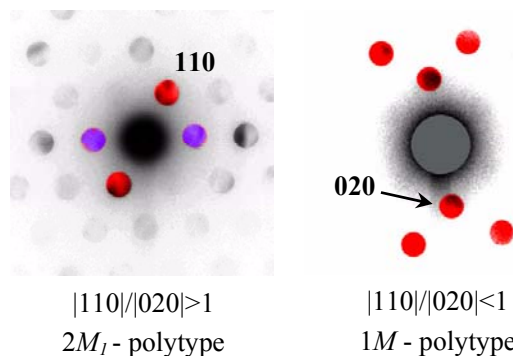
### 3.1.2 TEM-EDX

The selected clay samples were characterized by means of morphology, crystal habit, size, electron diffraction and element distribution by transmission electron microscopy (TEM). Normally, from the bulk sample,  $<2\ \mu\text{m}$  fraction was separated by sedimentation. The sample suspension was prepared by dilution in distilled water and dispersed by shaking in an ultrasonic bath during about 10 minus then air-fried on carbon covered micro Cu-grids.

In this research, TEM investigations were carried out by a transmission electron microscope Jeol JEM-1210 (120 kV, LaB<sub>6</sub>-cathode or CeB<sub>6</sub>-cathode) linked with ISIS LINK-OXFORD EDX-system and a GATAN MULTISCAN camera.

Semiquantitative chemical analyses were performed on selected particles by energy dispersive X-ray (EDX) examines using X-rays. By moving electron beam across the material, an image of each element in sample, not on surface, can be acquired. Therefore, electron diffraction also allows an evaluation of the stack order. Ring-like structures of the electron spots indicate for clay minerals a constructing of reciprocal layers (so called turbostratic orientation of the layers).

Morphology of particles was described according to Henning & Störr (1986). Mineral formulas were calculated from EDX chemical semiquantitative analyses with software toolkit, which was presented by Kasbohm *et al.* (2002). And the  $2M_1$ -polytype and  $1M$ -polytype for 2:1 sheet silicates were demonstrated by Zöller (1993), this author based on intensities of interferences of (110) and (020) in convergent beam system, in which  $|110|/|020| > 1$  is characterized as  $2M_1$ -polytype and  $|110|/|020| < 1$  is characterized as  $1M$ -polytype. Taken together, the particles were identified into mineral species.



**Figure 8. Electron diffraction by convergent beam mode**

*Kaolinite and halloysite*

Kaolinite and halloysite have the same theoretical formula of  $\text{Al}_2\text{Si}_2\text{O}_5(\text{OH})_4 \cdot n\text{H}_2\text{O}$  ( $n = 0$  or 4). However, some substitution of Al by Fe and Mg should be considered. Kaolinite and halloysite were distinguished by variation in morphology: kaolinite is pseudo-hexagonal platy particle, whereas halloysite shows a tube-like shape.

*Montmorillonite, beidellite and nontronite*

Both montmorillonite and beidellite are Al-bearing dioctahedral smectite whereas nontronite is iron-rich dioctahedral smectite. Montmorillonite and beidellite can be distinguished by the site of negative charge on the layers. In montmorillonite, the charge increases in octahedral layer, however, in beidellite, the charge arises in tetrahedral layer (Newman, 1987). According to Newman (1987) and Moore & Reynolds (1997), ideal structural formulae of montmorillonite, beidellite and nontronite are as following:

Montmorillonite:  $\text{M}^{+}_{0.33-0.43} (\text{Al}_{1.67-1.57}, \text{Mg}_{0.33-0.43})_2 \text{Si}_4\text{O}_{10} (\text{OH})_2 \cdot n\text{H}_2\text{O}$

Beidellite:  $\text{M}^{+}_{0.33-0.43} \text{Al}_2 (\text{Si}_{3.67-3.57}, \text{Al}_{0.33-0.43})\text{O}_{10} (\text{OH})_2 \cdot n\text{H}_2\text{O}$

Nontronite:  $\text{M}^{+}_x \text{Fe}^{3+}_2 (\text{Si}_{(4-x)}, \text{Al}_x)\text{O}_{10} (\text{OH})_2 \cdot n\text{H}_2\text{O}$

M is exchangeable cation in the interlayer space.

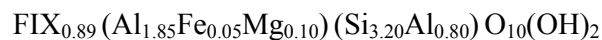
In calculation process of mineral formulae, the indexes of each element can be accepted with larger range of variation corresponding to empirical formulae.

*Illite and dioctahedral vermiculite*

The name “illite” has been used relatively vaguely in the literature. Commonly, muscovite is defined as end-member of the illite series (Rosenberg, 2002; Meunier and Velde, 2004). But IMA (Rieder *et al.*, 1998) reported on the nomenclature of mica defined that illite is a series name with potassium in interlayer of 0.6 - 0.85 and muscovite is another series name in the mica group with potassium in interlayer from 0.7 - 1.0 per  $\text{O}_{10}(\text{OH})_2$  (interlayer  $\geq 0.85$ ). The substitutions causing interlayer charge are found in octahedral and tetrahedral layer.

The Subcommittee of IMA report (Rieder *et al.*, 1998) was unable to find any hydromica that has an excess of water over the equivalent of  $(\text{OH}, \text{F})_2$  and could not be interpreted as a mixed-layer structure (such as biotite-vermiculite, illite-smectite). At the same time, all micas described as hydromicas exhibit a deficiency in the interlayer cation position. Accordingly, the Subcommittee voted to abandon the subgroup name hydromicas and replace it with interlayer-cation-deficient micas or, in an abbreviated form, interlayer-deficient micas.

Illite, recognized in TEM investigation, is referred in this contribution to illite in the sense of Środoń *et al.* (1992). According to these authors, structure formula of illite in the stricto sensu is:

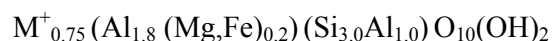


For example, concerning illite formula above, the sum of octahedral layer charge (of -0.1) and tetrahedral layer charge (of -0.8) -0.9 is almost exactly balanced by the +0.89 charge of interlayer cations.

Further K deficient dioctahedral micas (with tetrahedral Si < 3.3 per  $\text{O}_{10}(\text{OH})_2$ ) are called in this contribution as dioctahedral vermiculite offering additional possibilities to distinguish between different genetic signals.

1M and 2M<sub>1</sub> staking are the most frequently encountered in illite particles and were described by Meunier and Velde (2004).

According to Meunier *et al.* (2000, 2004), example of vermiculitization of smectite interfaces was studied. The authors mentioned that montmorillonite can be substituted in tetrahedral and then octahedral sites and addition of exchangeable interlayer cations, in the case without saturation of K<sup>+</sup> or NH<sup>4+</sup>, then montmorillonite transform into vermiculite. When saturated with K<sup>+</sup>, the high charge interlayer is collapsed to construct illite. Moore and Reynolds (1997) also mentioned the process: from muscovite to dioctahedral vermiculite. Vicente (1997) reported some empirical formulae of Al-vermiculite, which were very dioctahedral vermiculite. Taken together, this research concerned in dioctahedral vermiculite as clay mineral which is distinguished from illite by K<sup>+</sup> in interlayer. Based on formulae from Moore & Reynolds (1997), Bailey and Chairmen (1980), the ideal formula of dioctahedral vermiculite is:



In which, M<sup>+</sup> include monovalent and bivalent cations. The charge per  $\text{O}_{10}(\text{OH})_2$  unit of dioctahedral vermiculite is about 0.6 – 0.9 (Bailey and Chairman, 1980).

#### *IS-ml and diVS-ml*

“IS-ml” and “diVS-ml” terms are synonymous for clay series formed of illite/smectite and dioctahedral vermiculite/smectite mixed layers phases. Środoń *et al.* (1992) introduced a system to calculate mineralogical formula allowing for proportion of illitic and smectitic layers. The basic of calculation is relationship of “fixed” cations interlayer with expandability of particles (equa.1). Combined many lines of evidence, the authors proposed an interlayer charge of 0.4 for smectite and 0.89 for illite (per  $\text{O}_{10}(\text{OH})_2$ ) with an accuracy of ± 1% for smectite and ± 0.01% for illite components (equa. 2). Kasbohm

(2002), based on works above, developed indicative system to identify and calculate chemical formulae of those IS-ml or diVS- ml particles with following equations:

$$\%S_{MAX} = (95.6 - 105.75 \times \text{FIX}) \quad (\text{eq. 1})$$

$$\text{XII}_{\text{theoretic}} = [0.89 \times (100 - \%S) + 0.4 \times \%S] / 100 \quad (\text{eq. 2})$$

$$\%S = 100.38 \times (\text{IVAl})^2 - 213 \times (\text{IVAl}) + 109.4 \quad (\text{eq. 3})$$

$$\%I = 100 - \%S \quad (\text{eq. 4})$$

$\%S_{MAX}$  is defined as maximal proportion of smectite layers in the calculating mixed layer phases. FIX is introduced as fixed K+Na cations in interlayer.  $\text{XII}_{\text{theoretic}}$  is the theoretic interlayer charge considering IS-ratio and 0.4 as charge for smectitic layer and 0.89 for illitic layer. The variable  $\%S$  is defined as proportion of smectite layer based on Al in tetrahedral layer. And finally,  $\%I$  is defined as proportion of illitic layer (for example particle with  $\%I$  of 90 is illite/smectite mixed-layer particle with 90% of illitic layers). In fact, the system calculated with  $\%I$  according to  $\%S$  and  $\%S_{MAX}$  equations.

Kasbohm (2002) has introduced two linked controlling parameters distinguishing between IS-ml and diVS-ml - comparison between  $\text{XII}_{\text{theoretic}}$  to  $\text{XII}_{\text{measured}}$  and  $\text{FIX}_{\text{minimum}}$  to  $\text{K+Na}_{\text{measured}}$ .  $\text{FIX}_{\text{minimum}}$  is calculated by equation 1 defining  $\%S_{\text{max}} = \%S$ . It should describe the minimum requested sum of K+Na in the interlayer space of illitic layers to fulfil the postulations of Środoń *et al.* (1992) for illite in stricto sensu. In fact IS-ml phases are valid  $\text{XII}_{\text{theoretic}} \sim \text{XII}_{\text{measured}}$  and  $\text{FIX}_{\text{minimum}} \leq \text{K+Na}_{\text{measured}}$ . Otherwise diVS-ml could be expected.

### 3.1.3 X-Ray fluorescence

Some selected samples, which are untreated and dithionite treated samples, were measured by X-ray fluorescence (XRF) method. It is the only method that can be used to analyze routinely for almost any element including major-elements and trace elements as well as metals and non-metals. Samples were milled to  $<63 \mu\text{m}$  before XRF measurement.

Analysis was carried out using a wavelength dispersive Philips PW 2404 X-ray spectrometer with 10 mA of current and 20 kV of voltage. Mixture of approximately 0.800 gram of bulk sample and 2.000 gram of lithium tetraborate ( $\text{Li}_2\text{B}_4\text{O}_7$ ) and 1.932 gram of lithium metaborate ( $\text{LiBO}_2$ ) were anhydrous dense molten fluxed to assure homogeneity. In the progress, it was using non wetting agent (NWA) or/and oxidizer. Loss on ignition (LOI) at about  $1000^\circ\text{C}$  also served as an approximate measure of volatile  $\text{H}_2\text{O}$ .

Detail of XRF method has been report by Couture & Dymek (1996).



### 3.1.4 Mössbauer spectroscopy

Mössbauer spectroscopy is a method for defining valence and structure state of Fe-ions that could not be done by XRF method. This kind of analysis were presented elsewhere by Menil (1985), Rancourt (1998) and Stucki (2005) and, in this research, were carried out at St-Petersburg State University, Department of Chemistry, Laboratory of MBS, St-Petersburg, Russia (Prof. Dr. Eduard Goilo, Dr. Sofia Lessovaia).

Mössbauer spectra of selected samples were recorded on Ms-1104Em Mössbauer spectrometer at room temperature, using Doppler-velocity and  $^{57}\text{Co}$  isotopes resource. Because of recoil-free of gamma emission, which can be resonantly absorbed by stationary atoms,  $^{57}\text{Fe}$  in the solid samples absorbed 14.41 keV gamma photons and affected equipment probe. Univem MS program was applied to fit the obtained spectra for receiving series of sub-spectra.

Obtained parameters of the sub-spectra, such as isomer shift  $\delta$  (or center shift), quadrupole splitting  $\Delta$  (caused by electric field gradient), line-width  $\Gamma$  (or FWHM) and magnetic hyperfine field  $H_i$ , were collected to characterize the Fe-ion phases in the samples. According to isomer shift values, which were collected by Menil (1985) (appendix 6), the oxidation states Fe atom were identified. The iron oxides or hydroxides can be identified by sextet (component peaks of six-line pattern) and the silicate iron can be identified from doublet with isomer shift at about 0.3 mm/s (Stucki, 2005). The exact silicate site in which Fe-ion is located (e.g. *cis*-octahedral, *trans*-octahedral, tetrahedral or interlayer) could be identified according to the different quadrupole splittings, which depend (1) only on the local cation arrangements around a central  $\text{Fe}^{3+}$  or (2) significantly on mutual disposition of OH groups for spectroscopic characteristic of dioctahedral 2:1 layer silicates (*cis* or *trans*) (Drits *et al.*, 2002).

In combination with mineral identification by other methods, minerals which contain Fe-ion phases, Fe oxidation states and Fe-ion sites were pointed out by MBS analyses.

### 3.1.5 Atterberg sedimentation

The fractions  $<2\ \mu\text{m}$  and  $<6.3\ \mu\text{m}$  were separated from some bulk samples by Atterberg sedimentation in order to investigate also the influence of grain size.

According to Gessner (1931), collected sample was dispersed in distilled water, subsequent the suspension was shaken during one day-night and was filled in the glass container with water level controlling. The  $> 63\ \mu\text{m}$  fractions were a result of wet-sieving first. The falling time for each smaller fraction for the Atterberg sedimentation was determined by STOKES' law:

$$t = \frac{9 \cdot h \cdot \eta}{2 \cdot g \cdot r^2 \cdot (\rho - \rho')} \quad (\text{eq. 5})$$

Where h is height of falling (m);  $\eta$  is viscosity of fluid (kg/m×s); g is acceleration due to gravity (m/s<sup>2</sup>); r is radius of particle (m);  $\rho$  is density of particle and  $\rho'$  is density of fluid (kg/m<sup>3</sup>). Using the g = 9.81 m/s<sup>2</sup>;  $\eta$  = 0.001 kg/m×s (for water at 20°C);  $\rho$  = 2650 kg/m<sup>3</sup> (density for quartz);  $\rho'$  = 998 kg/m<sup>3</sup> (20°C) and h = 30 cm, for <2  $\mu$ m, it was took 23 h 11' 08'' and for <6.3  $\mu$ m 2 h 20' 12''.

After Atterberg sediment process was completely, determined by clear-looked water column, the suspension was condensed by centrifuge, warm dried or by vacuum-filter and then freezing dried in the case of <2  $\mu$ m particle size.

### 3.1.6 Dithionite treatment

For removing free iron phases (oxides and/or hydroxides) in the samples, dithionite method based on the procedure of Mehra and Jackson (1960) was applied. The method used sodium dithionite<sup>8</sup> as reducing agent in citrate<sup>9</sup>-bicarbonate<sup>10</sup> buffered suspension. An amount of approximately 10 gram of each selected samples was placed in 45 ml of an 8 volume of 0.3 Na-citrate: 1 volume of 1 M NaHCO<sub>3</sub> solution in a tube. Afterwards, the suspension was heated to about 70°C by water. Na-dithionite was added as the solid phase, and stirred for 1 minute (dissolving time of hematite) and then for 15 minutes (dissolving time of goethite). It took four hours for the reaction. Subsequently, the suspension was cooled and washed by distilled water to remove excess dithionite. Finally, the treated clay samples were dried at 40°C and milled slightly to get the powder and estimate the reduction.

## 3.2 Non-clay samples analyses

Apart from clay, some pharmaceutical or trade-ware materials as following list were utilized:

#### Suncream trade ware:

- Ladival® allerg 20: trade-ware, STADA GmbH, Bad Vilbel, Germany
- L'Oreal (LSF 15): trade-ware, L'Oreal Paris, Karlsruhe, Germany

---

<sup>8</sup> Dithionite: NaO<sub>2</sub>SSO<sub>2</sub>Na

<sup>9</sup> Na-citrate: HOC(COONa)(CH<sub>2</sub>COONa)<sub>2</sub>·2H<sub>2</sub>O

<sup>10</sup> Sodium bicarbonate: NaHCO<sub>3</sub>

Pharmaceutical substances:

- Ferrum Oxydatum Flavum: C.I.Nr.77492, Caesar & Lorentz GmbH, Hilden, Germany
- Ferrum Oxydatum Rubrum: C.I.Nr.77491, Caesar & Lorentz GmbH, Hilden, Germany
- Titandioxid: Eu Rho ® Ph.Eur.4, Euro OTC Pharma GmbH, Bönen, Germany

Cream matrix and cream admixtures:

- Wool-wax-alcohol cream: SR 90, Bombastus Werke AG, Dresden, Germany
- Plantacare® 2000: Decyl Glucoside, Merck, Darmstadt, Germany
- Glycerol: Merck, Darmstadt, Germany

Nanoparticles (lipids):

- *Ganoderma pfeifferi*: harvested in laboratories at Institute Pharmacy, E-M-A-University of Greifswald

Wool-wax-alcohol cream (“Wollwachsalkoholesalbe” by German) includes wool-wax-alcohol, sorbitanum trioleinicum GOT and mainly vaseline. Wool-wax-alcohol has also the name “Lanolin Alcohol” as International Nomenclature of Cosmetic Ingredients (INCI) (Parmentier, 2004).

*Ganoderma pfeifferi* was characterized that its extracts can inhibit the growth of microorganisms responsible for skin problems (Lindequist *et al.*, 2005). Especially, according to Julich *et al.* (2004), *Ganoderma pfeifferi* extracts are suitable for pharmaceutical and cosmetic preparation as well as controlling infection. The authors also indicated that extracts of some *Ganoderma* species have a scavenging effect on free radicals so that they exhibit an anti-oxidative effect and cause a delay toward aging process.

**3.2.1 UV-measurement**

UV-measurement was used to characterize reduction potential to reduce the transmission abilities of cream samples. Before measurements of UV-transmission could carry out, cream samples were mixed with clay samples, which are also characterized in this research (chapter 4). For the measurement, each cream sample was prepared with 0.003 mm of thickness based on one layer of sticking-plaster. A couple of special quartz cuvette has guaranteed this thickness and kept the cream sample during the measuring process.

All of cream samples were UV-measured using an AnalytikJenaAG SPECORD 50 photometer at the Institute of Pharmacy, University of Greifswald (UV lamp as light source electric potential of 483 V, current of 0.3 A, and frequency of 200 Hz). The samples were kept as far as 10 cm away from the light-source. Measurement interval of wavelength was chosen from 250 nm to 400 nm.

*Pure-clay cream sample*

First of all, normally, clay samples were milled slightly to get the particle size smaller than 63  $\mu\text{m}$  and to homogenize the powder. In some specific samples, clay samples were used with particle size <2  $\mu\text{m}$ . Two mixing ratios between wool-wax alcohol and clay were tested (10% clay; 20% clay). The 10% clay - cream samples were made from clay sample and wool-wax-alcohol cream by 0.1 g clay per 1 g wool-wax-alcohol cream. However, clay sample was mixed primarily with 0.2 gram of glycerol. The cases of 20% clay-creams are completely similar. Every mixture should be milled to become homogeneous one.

*Clay-fungi cream sample*

Involving of UV-active organic compounds in the experiments, fungi nanosuspensions will be prepared, too. The warmed fine powder terrestrial fungi *Ganoderma pfeifferi* and warmed emulsifier Plantacare 2000 with the ratio of approximately 5.00 gram and 45 ml are united at around 50°C. Subsequently, with the help of an agitator (rotor stator principle or ultrasonic) working on 45,000 rpm, a pre-suspension was manufactured. The pre-suspension is homogenized about 4 times thereafter with a support of highly pressure homogenizer, whereby the organic solvent was also removed by evaporation. In one end, precipitation active substance containing biomass was the form of stable particles. In other words, expected nanosuspension of fungi was obtained. This process was presented in detail by Julich *et al.* (2004). Each 1 ml of the received nanosuspension was blended with 1 gram of wool-wax-alcohol cream and afterward with 0.1 gram of clay. At the end, clay-fungi cream samples of 10% clay were prepared to measure UV-transmission.

In this project, for every cream sample, the measurement was repeated 20 times or more to get the average value. The data are showed by transmission:

$$T = (I \times 100) / I_0 (\%) \quad (\text{eq. 6})$$

In which,  $I_0$  is intensity of incident UV ray;  $I$  is intensity of penetrate ray, which is remains of incident UV ray after passing the cream-bearing cuvettes into the target.

The results will be drawn from completely 280 to 400 nm of wavelength.

### 3.2.2 Light microscopy

A light microscopy, ZEISS - AXIOSKOP linked with Carl Zeiss AxiCam HR system, was used to observe and to take typical images of selected clay-pure and clay-fungi cream samples. The cream samples with about 0.003 mm of thickness were prepared between two glass pieces. From obtained images, the structures of cream samples were described. Consequently, the homogeneities of cream matrix were estimated by STDV parameter with Adobe Photoshop 7.0 software supporting. With samples originated from the same clay (e.g. untreated Friedland Clay and acid treated Friedland Clay), the lower STDV could present the more homogeneity of matrix.

### 3.2.3 Skin model test by mouse-ear *in vivo*

Selected clay cream samples, both types of pure-clay creams and clay-fungi creams, were investigated on their behaviours towards human skin based on skin model test with skin flora *Escherichia coli* and infectious bacteria *Staphylococcus aureus*. The experiments were performed by Biometec GmbH, Greifswald.

*E. coli*, usually harmless, is frequently studied in life sciences because of its ubiquity and its clear structure. The bacteria species is a germ of normal skin flora, so that, in this research, it is used as indicator a safety of clay cream for human skin under UV-exposure condition. Mouse-ears were prepared at pistils disinfected with ethanol and then infected with *E. coli* (strain 25922, MF 0.125, dilution 1:20). After 1.5 hours of incubation at 30°C, the mouse-ears were coated with the clay creams and consequently were irradiated under UV-radiation (30 cm of distance to the lamp) during 30 seconds. The control sample was not coated with any clay cream. After exposure under UV-radiation, the Germ-colonies of the mouse-ears were plated on Müller-Hinton Agar plates. The plates were incubated during 24 hours at about 37°C. At the end, number of growing colonies *E. coli* was counted.

*S. aureus*, a germ of many skin infections, was also used in this study to identify behaviours of clays with skin. *S. aureus* (strain ATCC 6538, MF\* 0.125, dilution 1:20) was infected with ethanol disinfected mouse-ears which were prepared at pistils. After incubating at 30°C during 1.5 hours, except the control sample, all of the mouse-ears were coated with clay creams and then incubated for 24 hours at 37°C. Subsequently, the Germ-colonies of these mouse-ears were plated on Müller-Hinton Agar plates and incubated for 24 hours at 37°C. Number of growing colonies should be counted after the experiments.

### 3.2.4 Lactate DeHydrogenase test *in vitro*

The enzyme lactate dehydrogenase (or lactic dehydrogenase or LDH) is found in the cells of many body tissues. As cell die, its LDH is released. Therefore, LDH test is used to measure an alteration of cells. In this research, toxicities of  $\text{TiO}_2$  in comparison with fungi *Ganoderma pfeifferi* and control samples were identified by LDH test using HaCaT cell, which is a spontaneous transformed human skin keratinocyte cell line. The experiments were analysed in Biometec GmbH, Greifswald

The immortalized HaCaT cells were incubated in Roswell Park Memorial Institute medium supplemented with 8% fetal calf serum,  $37^\circ\text{C}$ , 95% humidity and 5%  $\text{CO}_2$  in plastic culture dishes. In the parallel experiments, the cells were pretreated by coating on the clean quartz plates as control samples, or on the quartz plates with mixture of clay and biomass or suspension of  $\text{TiO}_2$ . Until HaCaT cells grown reaching confluence of 50% in the  $60\text{ mm}^2$  area dishes, the medium was replaced by 2 ml phosphate-buffered saline. Subsequently, the cells were illuminated with UV light (medical UV-B, broad band, maximum 311 nm) using a dose of  $20\text{ mJ/cm}^2$ .

During irradiation process, the LDH releases were determined corresponding to optical density (OD) at 550 nm at different selected time points. The higher toxicity is expressed as the higher OD value or the higher concentration of LDH release.

## 4 MINERALOGICAL CHARACTERIZATION OF USED CLAYS AND CLAY MINERALS

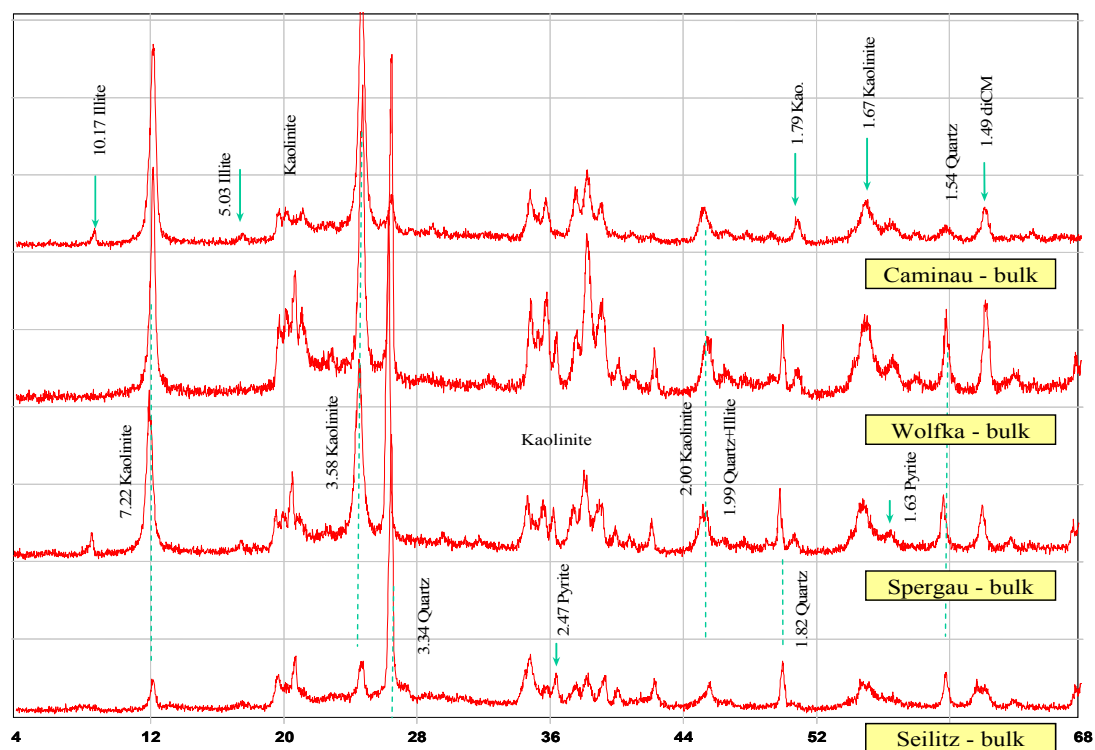
Experiments with different untreated clay and clay mineral samples are divided in 4 groups: kaolin, bentonite, mixed-layer dominated clay and mica dominated clay. Furthermore some clay samples were treated under different technical viewpoints.

### 4.1 Kaolins

The used kaolin samples include German reference kaolins like Caminau, Wolfka, Spergau and Seilitz as well as Georgia kaolins (KGa-1b and KGa-2) from US and Michalovce halloysite from Slovakia.

#### 4.1.1 German reference kaolins

XRD-results from randomly oriented powder mount (table 5) confirmed the certified mineral matter for Caminau, Wolfka, Spergau and Seilitz (appendix 2). Kaolinite is the dominating phase (figure 9). Non-clay mineral traces are quartz and pyrite.



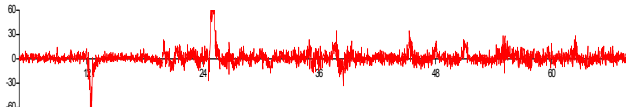
**Figure 9.** XRD patterns of German reference kaolins from randomly oriented powder mount,  $^{\circ}2\theta$  CuK $_{\alpha}$  position

*Note: Measured using Siemens D5000; The four XRD patterns from above to bottom: Caminau - bulk, Wolfka - bulk, Spergau - bulk and Seilitz - bulk, these samples were milled and sieved to  $<63 \mu\text{m}$  before measuring; the patterns show the peaks of kaolinite (Kao.), dioctahedral clay mineral (diCM): illite, montmorillonite as well as quartz and pyrite*

**Table 5. Quantitative Roentgen diffraction of German reference kaolins by “Autoquan” program (Rietveld method)**

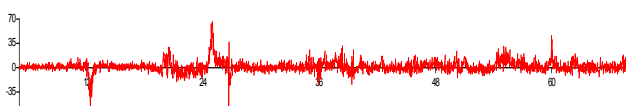
**Caminau** (ph003.raw; <63 µm, 3 s)

certified:  $Q=1.4\%$ ,  $K=84.9\%$ ,  $DSTM=14.3\%$  Rp=17.94% Rpb=24.64% R=21.40% Rwp=22.53% Rexp=10.38%

Component	Mass (%)	STDV (%)	Deviation diagram:
Kaolinitedis	<b>83</b>	3.0	
Muscovite 1M	<b>15</b>	3.0	
Quartz	<b>1</b>	0.6	

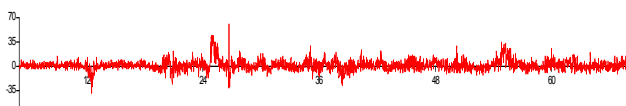
**Wolfka** (ph002.raw; <63 µm, 3 s)

certified:  $Q=15.4\%$ ,  $K=81.7\%$ ,  $DSTM=2.9\%$  Rp=17.92% Rpb=25.33% R=19.67% Rwp=23.28% Rexp=10.38%

Component	Mass (%)	STDV (%)	Deviation diagram:
Kaolinite C1, an, BISH	<b>7</b>	3.3	
Kaolinitedis	<b>79</b>	3.9	
Muscovite 1M	<b>2</b>	1.3	
Quartz	<b>12</b>	1.0	

**Spergau** (ph005.raw; <63 µm, 3 s)

certified:  $Q=15.0\%$ ,  $K=71.6\%$ ,  $DSTM=12.8\%$  Rp=17.56% Rpb=28.46% R=19.20% Rwp=22.65% Rexp=10.48%

Component	Mass (%)	STDV (%)	Deviation diagram:
Kaolinitedis	<b>72</b>	3.0	
Muscovite 1M	<b>14</b>	2.9	
Quartz	<b>13</b>	1.2	

**Seilitz** (PRO20; <32µm, 10 s)

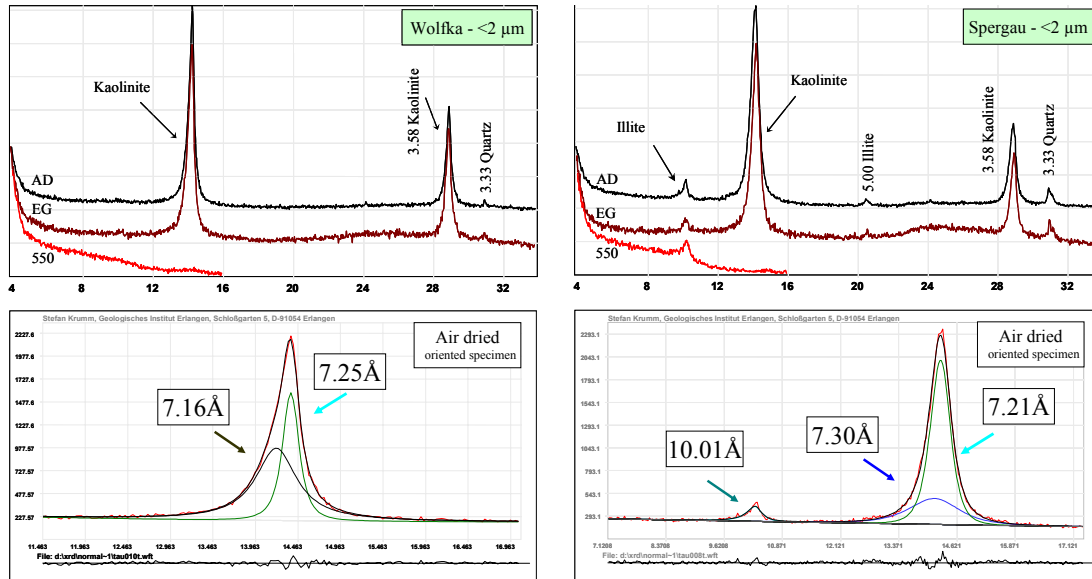
certified:  $Q=19.4\%$ ,  $K=34.1\%$ ,  $DSTM=45.0\%$

Rwp=11.17% Rexp=5.74%

Component	Mass (%)	STDV (%)
Kaolinite C1, ideal, BISH	<b>34</b>	
Muscovite 2M <sub>1</sub>	<b>45</b>	
Quartz	<b>21</b>	

Note: Analyses with powder preparation, muscovite 1M was used as model for illite dominated IS-ml phases; certified data referred to ASMW, 1988; Q: quartz, K: kaolinite, DSTM: 2:1 sheet silicate (“Dreischichtsilikat”); STDV: standard deviation





**Figure 10.** XRD patterns of Wolfka and Spergau kaolins from oriented specimens,  $^{\circ}2\theta$   $\text{CoK}_{\alpha}$  position

Note: Measured using HZG 4 / Seifert C3000; Above: completely XRD-patterns of air-dried specimen patterns (AD), ethylene-glycol saturated specimen patterns (EG) and 550 degree C heated specimen patterns (550); Bottom: fitting decomposition of air dried specimens; Left: Wolfka -  $<2 \mu\text{m}$ ; Right: Spergau -  $<2 \mu\text{m}$ ; kaolinite looks like composed by a mixture of well and poor ordered kaolinite particles (peak deconvolution by WinFit-Software (Krumm, 1994))

The German kaolin group also was analyzed with oriented specimen. Therefore, it is possible to distinguish and verify kaolinite and other clay minerals in the sample. Wolfka kaolin and Spergau kaolin contain e.g. a mixture of poor-ordered kaolinite and well-ordered kaolinite (figure 10). They are different from each other by the thickness of coherent scattering domains (CSD). In oriented profiles of Caminau and especially Seilitz, IS-ml phases were identified.

### Caminau

The kaolin formed by weathering of granodiorite in Lausitz/Saxony. Kaolinite is distributed in the sample as thick pseudo-hexagonal aggregates and also as thin, pseudo-hexagonal plates, corresponding to about 30 and 14 layers per stack ( $\sim 211$  and  $101 \text{ \AA}$  of CSD, respectively, using WinFit – Krumm, 1994). Caminau kaolin is characterized by the highest amount of kaolinite than other German reference kaolins with 84.9%. In accordance, Caminau kaolin is also characterized by a very low percentage of quartz – 1.4% by ASMW (1988). By XRD measurement, Caminau quartz peaks also presented the lowest intensity in comparison with corresponding peaks of other kaolins (figure 9). The component was confirmed by Rietveld analysis (table 5). Also an intergrowth of kaolinite and dioctahedral mica were identified by TEM (non-published information by Störr & Kasbohm, 2006).

Anatase, crandallite, goethite, hematite, ilmenite, jarosite, calcite, limonite, magnetite, monacite, pyrite, rutile, siderite, titanomagnetite, xenotime and zircon were identified in this kaolin as traces totally < 1% (ASMW, 1988).

About 44% of Caminau kaolin sample is smaller than 2  $\mu\text{m}$  (appendix 3). This kaolin has also a cation exchange capacity of 5 meq/100g (methylene blue method) and specific surface of 14  $\text{m}^2/\text{g}$  (ASMW, 1988).

### *Wolfka*

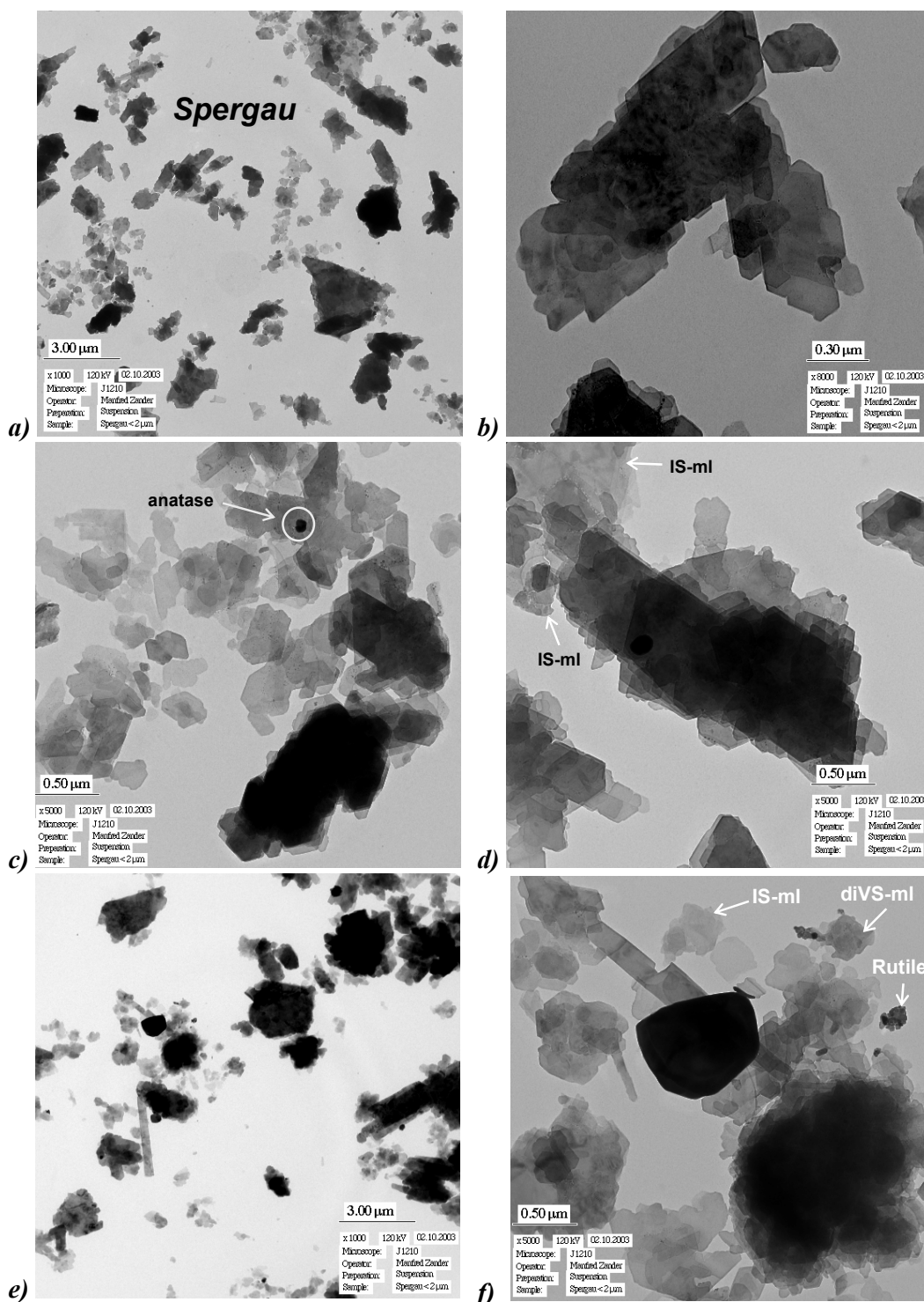
The porphyry kaolin as weathering product from Saxonia Volcanic complex in Kemmlitz contains two morphological types of kaolinite particles in the fraction <2  $\mu\text{m}$ : (i) thick, pseudohexagonal platy aggregates larger than 1  $\mu\text{m}$  and (ii) thin, pseudohexagonal plates generally smaller than 300 nm (see fig. 65 in Henning & Störr, 1986). Only rarely lath-like shape of kaolinite is also to detect in Wolfka kaolin sample. By XRD, the triplet-peak group at 20 degree  $2\theta$  in the powder diffraction showed a clear resolution of all three kaolinite peaks (figure 9). This would be interpreted as intermediate disorder of kaolinite in Wolfka sample. Considering the deconvolution (by WinFit-procedure – Krumm, 1994) of 7 Å interference, Wolfka kaolinite could be composed by kaolinite particles with a CSD of 320 Å (~ 46 layers per stack) as well ordered phase and 104 Å (~ 15 layers per stack) as higher disordered material or kaolinite with a smaller thickness per stack. Rietveld analysis of the bulk sample documents an amount of kaolinite with 86% in the sample (table 5).

In the ASMW-certification (1988) for the Wolfka reference kaolin, the low amount of 2:1 sheet silicates is characterized as IS-ml phases. However, the content of IS-ml phases is quite low (only 2.9% in mass), so that this phases were not identified clearly in the bulk XRD patterns. In traces, anatase, apatite, baryte, crandallite, goethite, hematite, jarosite, K-feldspar, calcite, monacite, pyrite, plagioclase, rutile, xenotime and zircon are listed for a total amount <1% (ASMW, 1988).

About 42% of Wolfka kaolin sample is smaller than 2  $\mu\text{m}$  (appendix 3). This kaolin has a cation exchange capacity of 5 meq/100g (methylene blue method) and specific surface of 13  $\text{m}^2/\text{g}$  (ASMW, 1988).

### *Spergau*

The kaolin deposit in Spergau, Merseburg/Saxony-Anhalt resulted from weathering of New-red Sandstone arkoses. Spergau kaolin was identified with 72% kaolinite by Rietveld quantification (table 5). The kaolinite particles appeared mainly as pseudohexagonal plates. By comparing CSD using WinFit-procedure (Krumm, 1994), Spergau kaolinite stacks are much thinner than that of Wolfka sample (figure 10). CSD values of Spergau kaolin are about 160 Å and 71 Å (about 23 layers and 10 layers per stack, respectively).

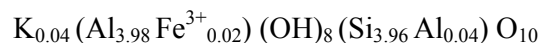


**Figure 11. TEM images of Spergau sample**

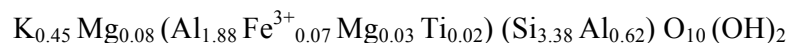
a) Overview of Spergau sample (1,000x); b) zoom of image a) (8,000x); c) & d) zoom of image a) (5,000x); e) (an other) overview of Spergau sample (1,000x) and f) zoom of image e) (5,000x)

*Note: Measured using Jeol JEM-1210; the images show the particles of kaolinite (dominating particles), Illite/smectite mixed-layer (IS-ml), quartz and anatase (rutile)*

Figure 13 shows TEM-EDX-mapping of a kaolinite particle aggregate which is imaging as A-point in the figure 12b (zoom of figure 11e). Apart from 3 main elements Al, Si, O, there are K and other minor elements. Also the Fe-enrichment through the edges of this aggregate is to note. K could be an indication for a small portion (less 5%) of former mica in this aggregate (like an intergrowth (?), noted already for Caminau kaolin). Analysis of B-point (figure 12b) gave following chemical formula of kaolinite:

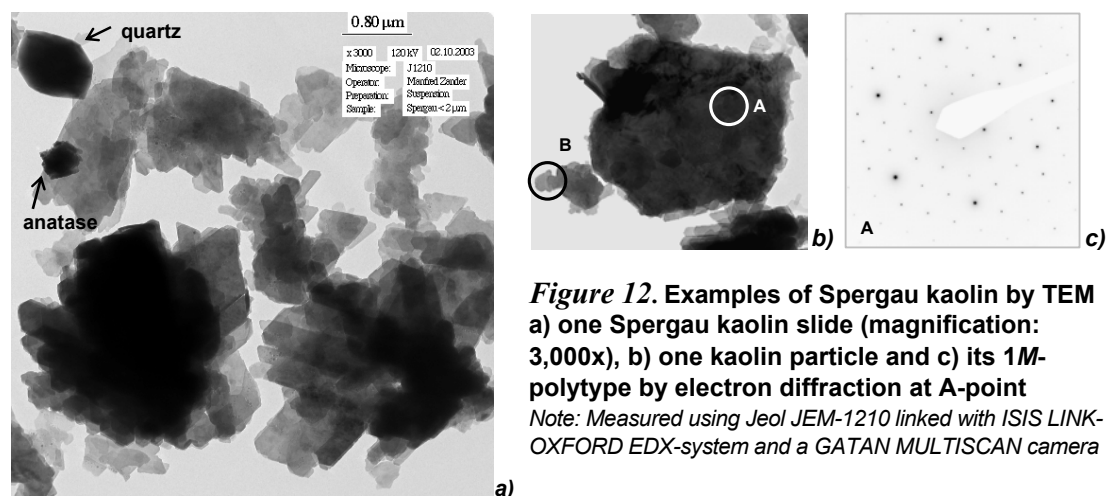
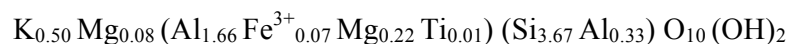


Additionally dioctahedral vermiculite, IS-ml, diVS-ml, anatase/rutile and quartz were observed (figure 11 and figure 12). Especially, illite in the sense of the international mica-classification (Rieder *et al.*, 1998), which has deficient K-amount in the interlayer, is labelled here as dioctahedral vermiculite (diVerm.) or diVerm-dominated mixed layer structures between diVerm and smectite (diVS-ml). An averaged formula of these phases is:



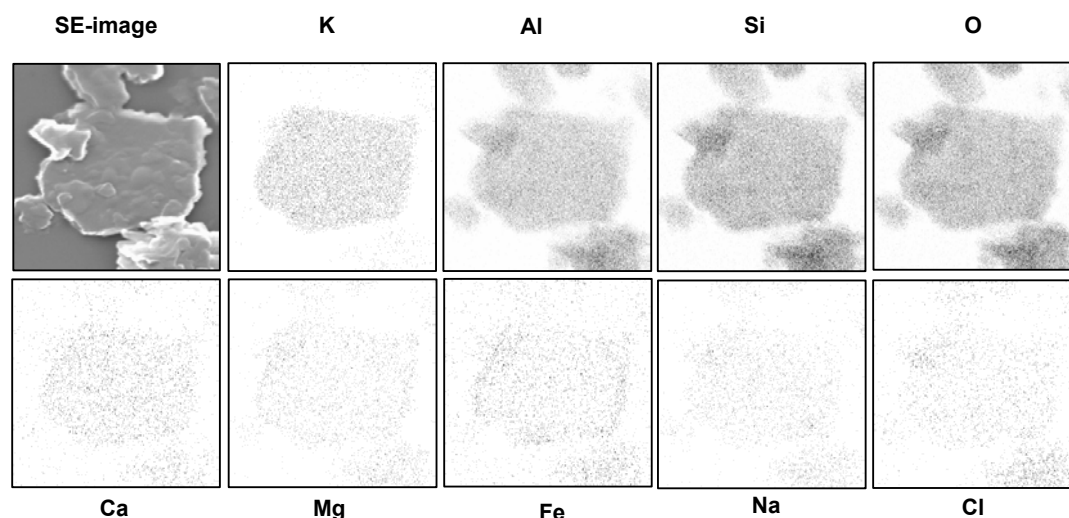
These dioctahedral vermiculite phases have a platy xenomorphous shape under TEM and could present mainly the 10 Å interference in the XRD-pattern (figure 10, right) caused by available K-amount.

The 2:1 sheet silicate component of Spergau sample, which was certified 12.8% according to ASMW (1988), is identified also as randomly interstratified IS-ml phase with 50% of smectitic layers. By TEM-EDX experiment, the chemical formula of this phase was calculated as:



**Figure 12. Examples of Spergau kaolin by TEM**  
a) one Spergau kaolin slide (magnification: 3,000x), b) one kaolin particle and c) its 1M-polytype by electron diffraction at A-point

Note: Measured using Jeol JEM-1210 linked with ISIS LINK-OXFORD EDX-system and a GATAN MULTISCAN camera



**Figure 13. Element distribution in kaolinite aggregate by TEM-EDX-mapping of Spergau kaolin**

*Note: Measured using Jeol JEM-1210 linked with ISIS LINK-OXFORD EDX-system and a GATAN MULTISCAN camera*

Anatase, crandallite, halloysite, K-feldspar, calcite, magnetite, monacite, pyrite, plagioclase, rutile and zircon are identified minerals in Spergau kaolin with total amount less than 1% (ASMW, 1988).

Remarkable higher than in Wolfka and Caminau kaolins, about 66% of Spergau kaolin sample is  $<2 \mu\text{m}$  (appendix 3). This kaolin has also higher cation exchange capacity of 7 meq/100g (methylene blue method) and specific surface of  $18 \text{ m}^2/\text{g}$  (ASMW, 1988).

### *Seilitz*

The Seilitz kaolin deposit, supplied the production of Meissen porcelain in Saxony, is the oldest active kaolin mine in the world. It is weathering product developed on pitchstones (hydrated glassy silicic volcanic rocks) of Meissen volcanic complex (Störr, 1982).

In the ASMW-certification (1988), Seilitz kaolin is characterized by 34.1% kaolinite – the lowest amount than other used German reference kaolins. By XRD experiment, in relatively comparison peak intensities, kaolinite amount of Seilitz sample is remarkable lower than the other samples (figure 9). Using Rietveld quantification, Seilitz kaolin is calculated with kaolinite amount of 34% in bulk sample (table 5). The morphology of particles in the kaolin sample is presented by sharp edges, pseudo-hexagonal plates and disorder kaolinite under TEM observation (Störr, 1982). In addition, only two kaolinite peaks at 20 degree  $2\theta$  were observed in XRD profile. By WinFit-procedure (Krumm, 1994), two obtained CSD values of 114 and 33 Å were interpreted as two corresponding types of kaolinite: thicker particle phase with about 16 layers per stack and thinner particle phase with about only 5 layers per stack.

Seilitz kaolin is also characterized by a higher amount of 2:1 sheet silicates than other kaolins. Kenj (1990) identified ~90% illitic layers in IS-ml phases as typical value by HR-TEM.

In oriented profiles of Seilitz sample, IS-ml phase was also identified. From XRD analysis of ethylene-glycolated specimen with CoK $\alpha$ , peak positions between 001/002-interference and 002/003-interference showed a difference of 9.83 ° $\Delta 2\theta$ . Applying Newmode-modelling (Moore & Reynolds, 1997 - see table 9), proportion of illitic layer in IS-ml phase is more than 90%, which is in agreement with publication mentioned above.

Accessory phases of Seilitz kaolin include anatase, ankerite, barite, crandallite, gypsum, goethite, jarosite, K-feldspar, calcite, monazite, pyrite, plagioclase, rutile and zircon with total amount <1% (ASMW, 1988).

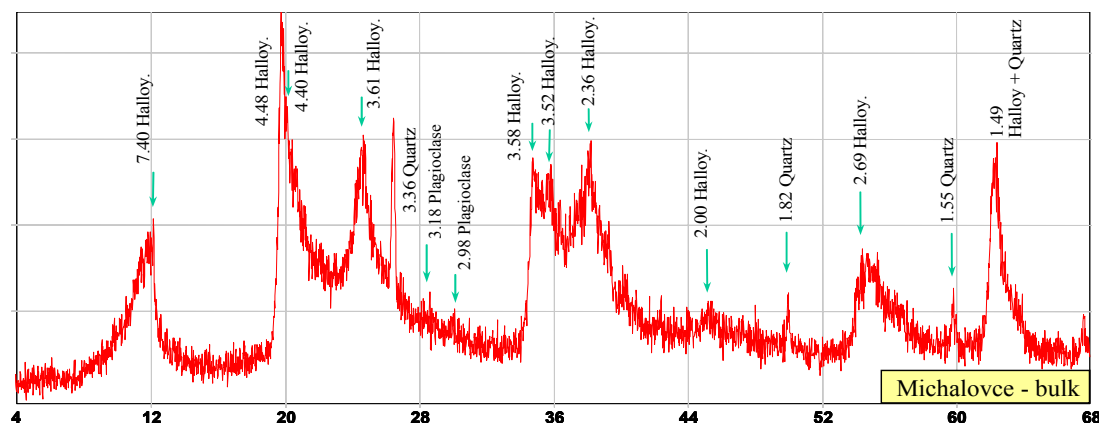
The <2  $\mu\text{m}$  fraction of Seilitz sample is approximately 68% which is the highest amount among corresponding numbers of other kaolin samples (appendix 3). Seilitz kaolin was also characterized with significant higher cation exchange capacity of about 14 meq/100g (methylen blue method) and specific surface of 17 m<sup>2</sup>/g (ASMW, 1988).

#### 4.1.2 Kaolin samples originated from Greifswald clay collection

The halloysite deposit in Michalovce/Slovakia was formed at least partially by the low-temperature hydrothermal alteration of rhyodacite (plagiorhyolite) (Kužvart, 1969).

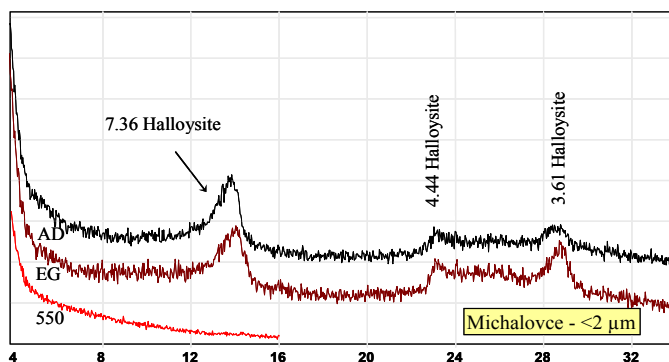
XRD patterns, which were received from the bulk samples from randomly oriented powder mount and oriented specimens of Slovakia Michalovce halloysite, were shown in figure 14 and figure 15. The obtained peaks demonstrated that the Michalovce sample contains halloysite, quartz and trace of plagioclase. 7.36 Å 001-spacing peak of halloysite indicated that Michalovce halloysite is 7 Å-halloysite type or dehydrated halloysite (as recommended by the AIPEA Nomenclature Committee) (Joussein *et al.* 2005).

Based on MacEwan (reviewed in Hillier & Ryan, 2002) about the relationship between proportion halloysite/kaolinite in the sample and changing of peak height before and after ethylene-glycol saturation, Michalovce is a pure halloysite-bearing sample or in other words, kaolinite percentage is negligible. From air-dried specimen, peak high ratio between 001-spacing peak (7.40 Å) and 002-spacing peak (3.58 Å) was (108:50=) 2.16. Corresponding ratio was identified from ethylene-glycol saturated specimen was (82:72=) 1.14. Therefore, the changing ratio was calculated as larger than 60%. With such high change of peak height intensity ratio, the sample is supposedly 100% of halloysite in comparison with kaolinite.



**Figure 14.** XRD patterns of Michalovce halloysite from powder mount,  $^{\circ}2\theta$   $\text{CuK}\alpha$  position

Note: Measured using Siemens D5000; sample was milled and sieved to  $<63\ \mu\text{m}$  before measuring; the patterns show the peaks of halloysite (Halloy.), quartz and plagioclase

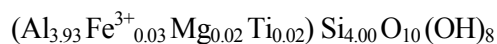


**Figure 15.** XRD patterns of Michalovce halloysite from oriented specimens,  $^{\circ}2\theta$   $\text{CoK}\alpha$  position

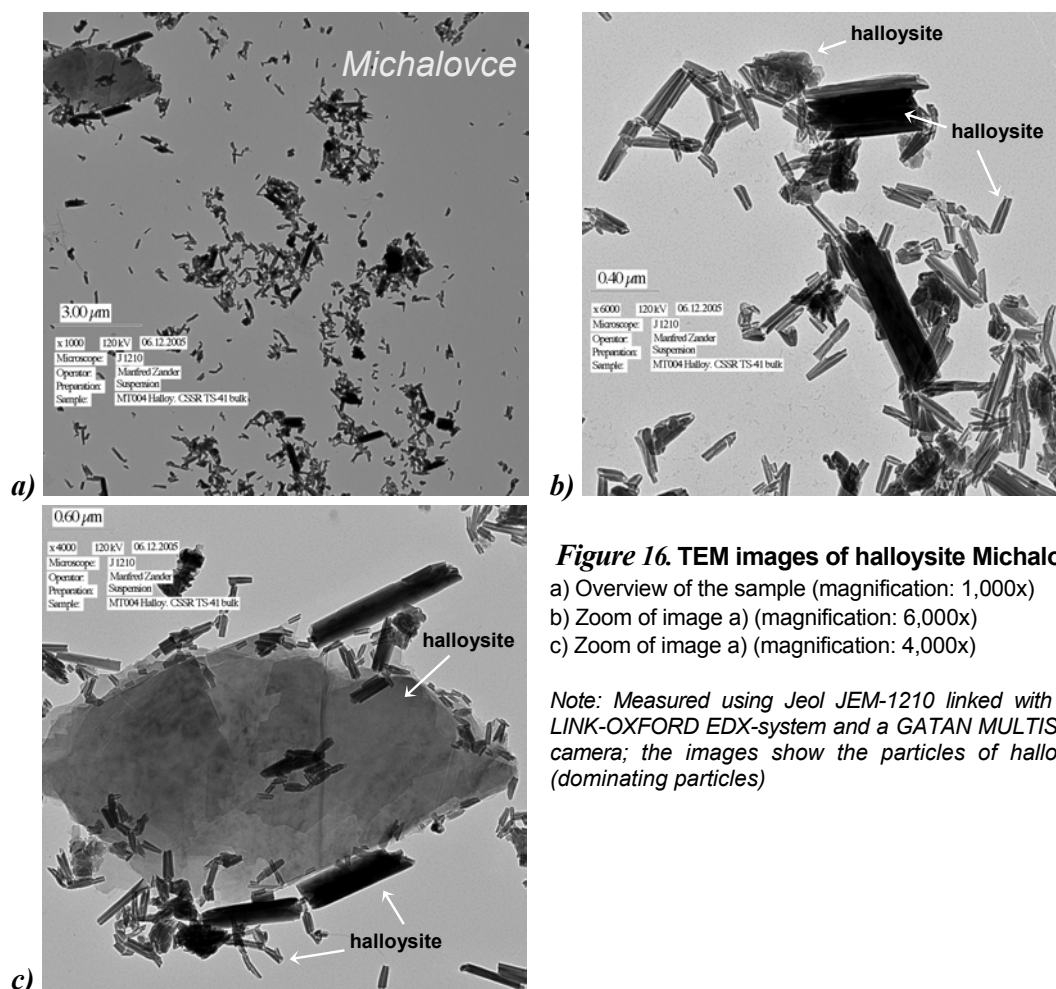
Note: Measured using HZG 4 / Seifert C3000; XRD-patterns of air-dried specimen patterns (AD), ethylene-glycol saturated specimen patterns (EG) and 550 degree C heated specimen patterns (550); the patterns show the peaks of halloysite

TEM experiment showed the tubular morphology of Michalovce halloysite (figure 16). The length of tubules particles was usually smaller than a half of micrometer and only a few exceed  $1\ \mu\text{m}$  while the diameter was  $<0.1\ \mu\text{m}$  in almost cases. The tubules shaped well with rolled ends. Occasionally, there were very big tubules, stacks of very small fragment (figure 16c) and thick plates which were broken from large tubules (figure 16b). In additions, there was presence of large and thin platy halloysite particle in the sample. Altogether, halloysite tubules are the main part of Michalovce sample from the TEM observation.

According to TEM-EDX analyses, Michalovce halloysite belongs to Al-rich halloysite, which is corresponding to the review by Joussein *et al.* (2005) that halloysite tubular form is relatively Fe-poor. Calculated empirical formula of pure dehydrated halloysite particles with average indexes from Michalovce halloysite was:



In conclusion, Michalovce sample is dominated by halloysite. The halloysite tubules make the specific and different surface area vs. kaolinite plates from other kaolin samples.



**Figure 16. TEM images of halloysite Michalovce**

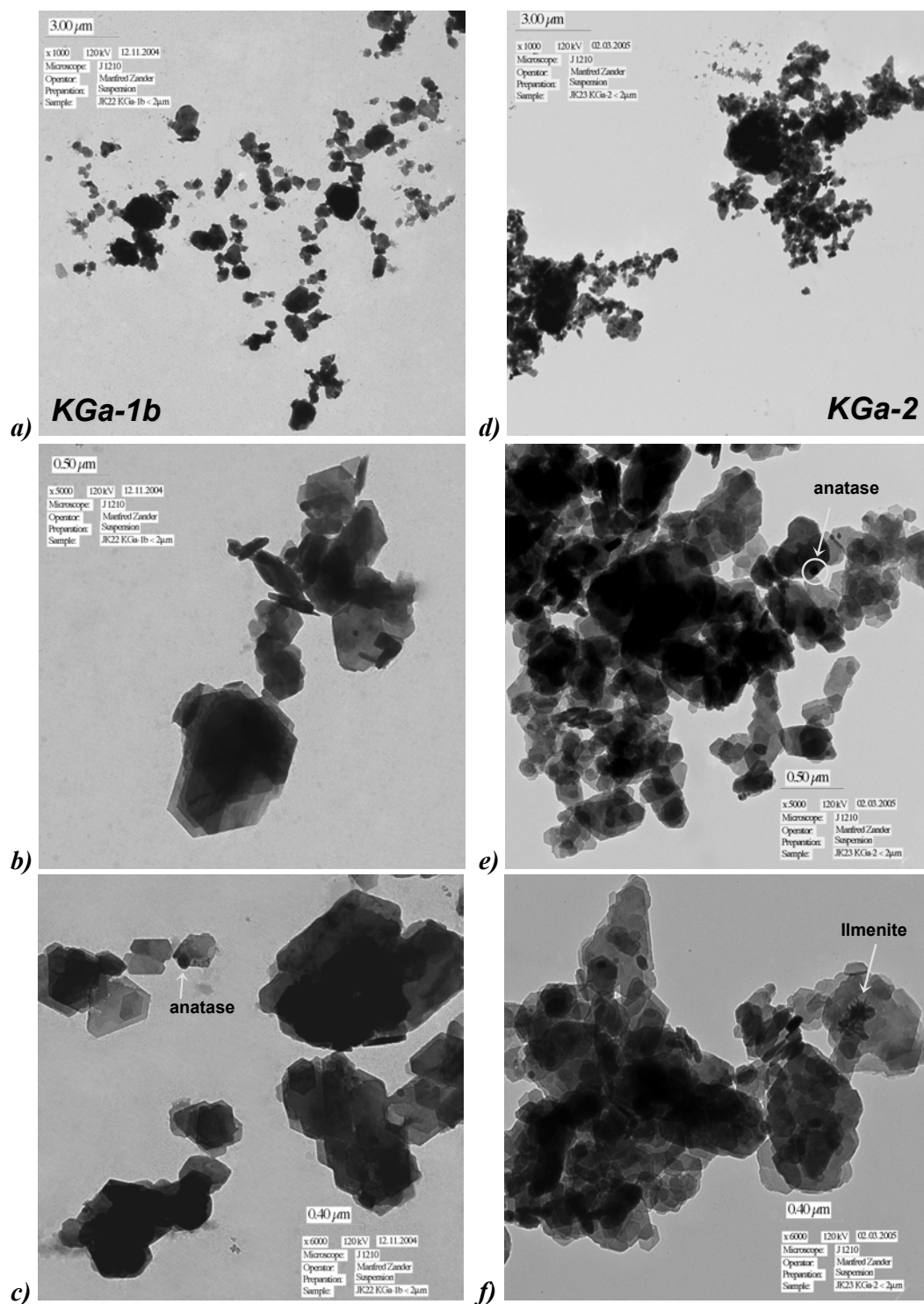
- a) Overview of the sample (magnification: 1,000x)  
b) Zoom of image a) (magnification: 6,000x)  
c) Zoom of image a) (magnification: 4,000x)

*Note: Measured using Jeol JEM-1210 linked with ISIS LINK-OXFORD EDX-system and a GATAN MULTISCAN camera; the images show the particles of halloysite (dominating particles)*

#### 4.1.3 CMS reference kaolins

The used CMS kaolins include Georgia low defect kaolin (KGa-1b or KGa-1) as weathered Tuscaloosa Formation sandstone in Wyoming/Georgia/USA and Georgia high defect kaolin (KGa-2) as lower Tertiary sedimentation in Warren/Georgia/USA. The TEM-EDX analyses showed that the two kaolins were dominated by kaolinite. By the method, it was found few indications also for kaolinite/expandable mixed-layer series, but more investigations are necessary to bring sufficient proofs for that (e.g. to avoid influence of beam damages). Only in rare detected points, observed particles were anatase (or rutile) and ilmenite. Kaolinite and kaolinite/expandable particles were pseudo-hexagonal plates. KGa-1b sample showed stacks of medium particles which have a dimension ranging from about 0.2 micrometer to over 1.0 micrometer. Almost all of these particles had good shape. KGa-2 sample presented a lot of very small particles in aggregation with medium particles.





**Figure 17. TEM images of Georgia kaolins: low defect (KGa-1b) and high defect (KGa-2)**  
a) Overview of the sample KGa-1b (magnification: 1,000x); b) & c) Zoom of image a) (magnification: 5,000x & 6,000x)  
d) Overview of the sample KGa-2 (magnification: 1,000x); e) & f) Zoom of image d) (magnification: 5,000x & 6,000x)

*Note: Measured using Jeol JEM-1210; the images show the particles of kaolinite (dominating particles), anatase (rutile), ilmenite*

The TEM observation is corresponding to the data published by van Olphen & Fripiat (1979), therein surface area of KGa-1b was 10 m<sup>2</sup>/g and that of KGa-2 was about 24 m<sup>2</sup>/g, which is much higher than that of KGa-1b. With KGa-1b (or KGa-1) sample, Ammann (2003) calculated about only 8 m<sup>2</sup>/g of surface area (methylene blue method) and accordingly about 1 meq/100g of cation exchange capacity. According to van Olphen & Fripiat (1979), the certificated cation exchange capacity values of KGa-1b and KGa-2 are 2 and 3 meq/100g, respectively. The publication also presented the general chemical compositions of the two kaolins (appendix 5).

According to Chipera & Bish (2005), KGa-1b and KGa-2 carried out by powder XRD analyses contain approximately 96% kaolinite and traces of dickite together with about 3% anatase, 1% crandallite (hydrated phosphates) and quartz (?) (KGa-1b sample) or mica and/or illite (KGa-2 sample). The proportion is obtained from both types of “processed” <2 µm size-fraction samples and “as-shipped” Source Clays.

Using QUAX software (Quantitative Phase Analysis with X-ray Powder Diffraction), Vogt *et al.* (2002) investigated that impurities in the fraction <2 µm samples of the same source Georgia kaolins are quartz (both samples), plagioclase (KGa-1b) and clinopyroxene (KGa-2) (0.5, 0.2 and 0.7% by weight, respectively). Besides, anatase was found but not quantified. The investigation also showed the grain size distribution from both samples: <2 µm fraction made up about 60% and 80% in Georgia low defect kaolin (KGa-1b) and high defect Georgia kaolin (KGa-2), respectively.

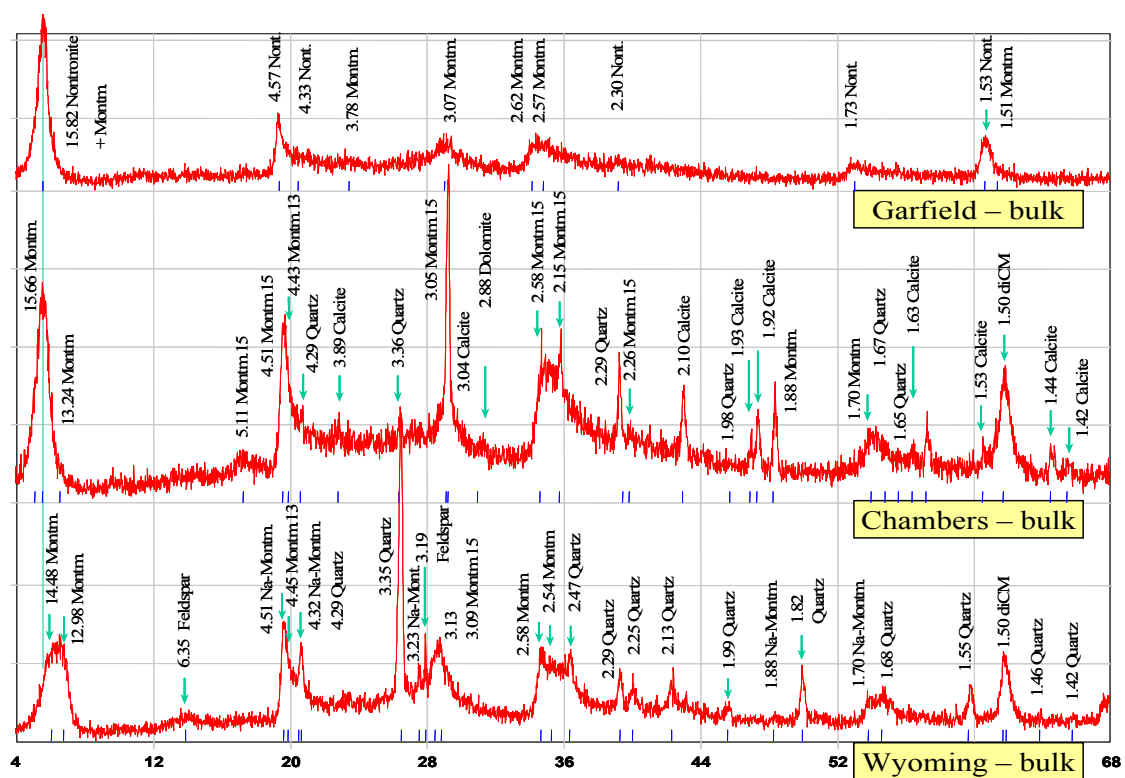
In sum, Georgia kaolins are very pure kaolinite. The impurities in both samples are not various. They are mainly quartz and anatase. The significant difference between two kaolins is particle size of kaolinite. In quantitative aspect, high defect kaolin showed the higher percentage of fine fraction and surface area. Indeed, by TEM observation in this contribution, high defect kaolin also presented much considerable density of tiny particles. Conversely, good shape kaolinite particles were preserved in low defect kaolin.

## 4.2 Bentonites

### 4.2.1 Bentonite samples originated from Greifswald clay collection

The used Greifswald collection includes Garfield, Chambers and Wyoming bentonites. These bentonite samples were certified by American Petroleum Institute Clay Mineral Standards (API). Garfield, Chambers and Wyoming bentonites were labeled by API as H-33a, H-23 and H-25, respectively.

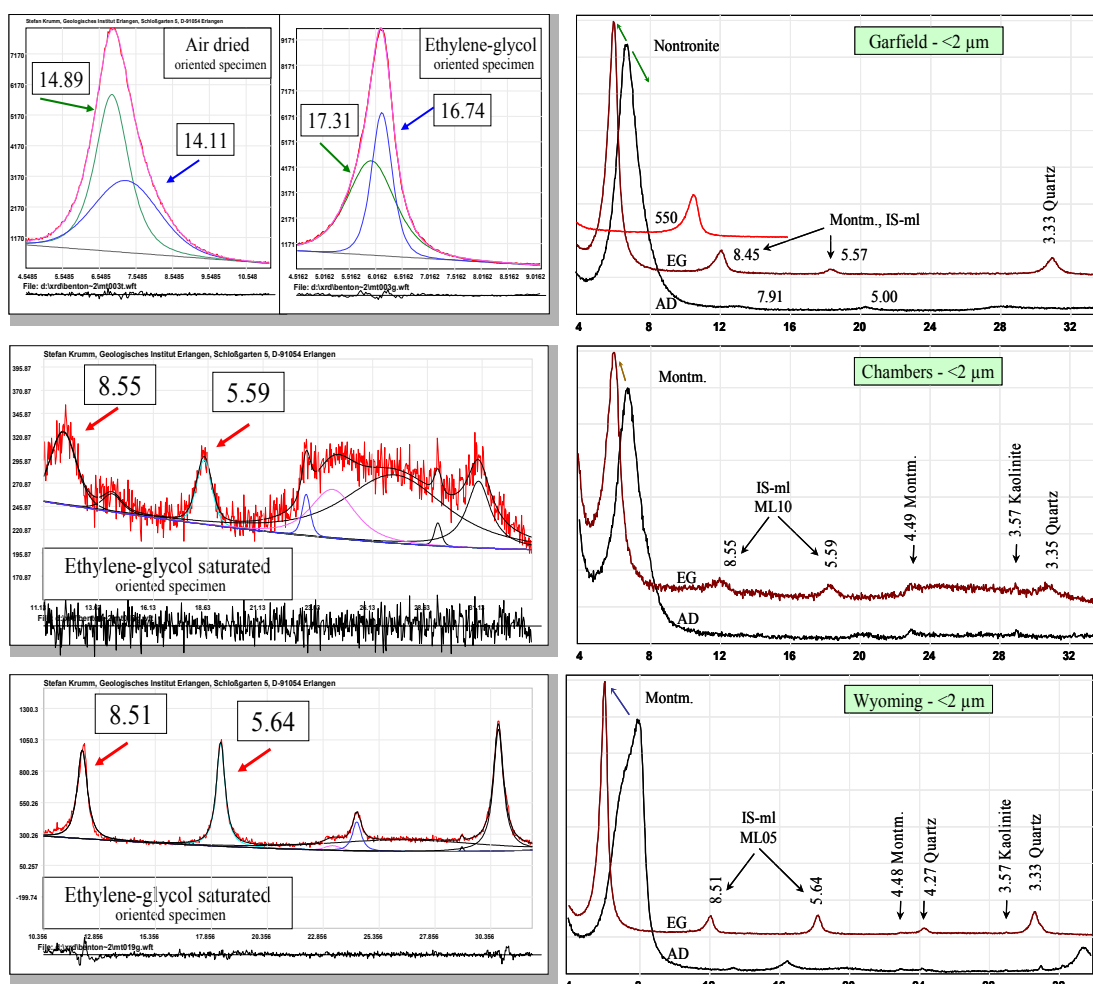
XRD patterns of these bentonites, shown in figure 18 and in figure 19, confirmed the corresponding dominated clay minerals. Garfield patterns presented nontronite and traces of montmorillonite while Chambers and Wyoming patterns showed different kinds of montmorillonite: mainly 15 Å-montmorillonite (bivalent cations in the interlayer space) was observed from Chambers sample; 13 Å-montmorillonite and 14 Å-montmorillonite (dominated by monovalent cations in the interlayer spaces) were observed from Wyoming sample. In all of three samples, the typical expandable property of smectite was obvious. Nontronite dominated bentonite is quite pure but two montmorillonite dominated bentonites contain a variety of impurities.



**Figure 18.** XRD patterns of Greifswald collection bentonites from powder mount,  $^{\circ}2\theta$   $\text{CuK}_{\alpha}$  position  
From above to bottom: patterns of nontronite Garfield, montmorillonite Chambers and Wyoming

Note: Measured using Siemens D5000; sample was milled and sieved to  $<63 \mu\text{m}$  before measuring; the patterns show the peaks of nontronite (Nont.), dioctahedral clay mineral (diCM): montmorillonite (Montm.), Na-montmorillonite (Na-Montm.) as well as quartz, calcite, domomite and feldspar

The difference among three bentonites is also presented clearly in the chemical compositions obtained from XRF analyses (table 6) because nontronite dominated Garfield bentonite is a Fe-rich smectite but the montmorillonite dominated Chambers and Wyoming bentonites are Al-rich smectites. Iron made up significant amount in the Garfield sample with iron oxide form of about 31.8% in mass. Conversely, only 2.8 and 3.3% (mass) of iron oxide were detected by XRF chemical analyses from Chambers and Wyoming samples, respectively.



**Figure 19.** XRD patterns of Greifswald collection bentonites from oriented specimens,  $^{\circ}2\theta$  CoK $\alpha$  position. From above to bottom: patterns of nontronite Garfield, montmorillonite Chambers and Wyoming.

Note: Measured using HZG 4 / Seifert C3000; right: XRD patterns including air-dried (AD), ethylene-glycol saturated (EG) and 550 degree C heated (550) specimen patterns; left: fitting decomposition of example specimens; the patterns show the peaks of nontronite, montmorillonite (Montm.), illite/smectite mixed-layer series (IS-ml), kaolinite and quartz.

**Table 6. Chemical composition (main components, oxide form) of Garfield, Chambers and Wyoming bentonites from X-Ray Fluorescence analyses, indicated in mass %**

Clay Samples	SiO <sub>2</sub> (%)	TiO <sub>2</sub> (%)	Al <sub>2</sub> O <sub>3</sub> (%)	Fe <sub>2</sub> O <sub>3</sub> (%)	MnO (%)	MgO (%)	CaO (%)	Na <sub>2</sub> O (%)	K <sub>2</sub> O (%)	P <sub>2</sub> O <sub>5</sub> (%)	LOI 1000°C (%)	H <sub>2</sub> O- (%)	Total (%)
Garfield TS-1803	40.14	0.07	5.54	<b>31.79</b>	0.01	0.69	2.07	0.23	0.17	0.05	6.50	13.86	101.10
Chambers TS-569	43.26	0.29	14.54	<b>2.81</b>	0.04	3.29	8.18	0.12	0.06	0.03	11.69	13.54	98.93
Wyoming TS-874	58.13	0.14	16.71	<b>3.30</b>	0.02	2.08	1.58	1.69	0.39	0.05	5.44	8.76	98.29

*Note: Measured using Philips PW 2404, non wetting agent or/and oxidizer, LOI at 1000°C*

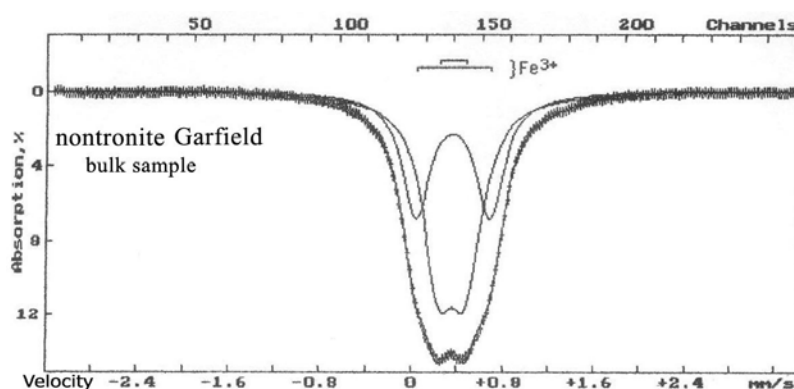
### *Garfield*

The mine, in Garfield area, near Spokane, Whitman County, Washington/USA, locating in basalt zone and the nontronite veins were formed by weathering process. Nontronite, the dominating clay mineral in this bentonite, was confirmed by clear peaks at about 15.82, 4.57, 4.33, 2.30, 1.73 and 1.53 Å in the XRD pattern of randomly oriented powder mount. Besides, montmorillonite peaks with very low intensities were obtained, too. The 001-spacing peak of nontronite overlapped with 001-spacing peak of montmorillonite (15.5 Å) to compose the asymmetric peak. This combination was verified by oriented specimen analyses (figure 19). Whilst air-dried specimen was decomposed to peaks of 14.9 Å and 14.1 Å, ethylene-glycol saturated specimen was decomposed to peaks of 17.3 Å and 16.7 Å. Therefore, it was interpreted that the first one is peak of montmorillonite and the second one is peak of nontronite. Both collapsed to approximately 10 Å peaks after heating. The spacing values at 8.45 Å and 5.57 Å obtained from ethylene-glycol saturated specimen confirmed that montmorillonite in Garfield is true montmorillonite or IS-ml with very low proportion (smaller than 5%) of illitic layer based on the interpretation about the relationship between percent illitic layer in the IS-ml series with positions of related peaks by Moore & Reynolds (1997).

The dominating 060-spacing peak at 1.53 Å (more exactly: 1.526 Å) in comparison with 1.50 Å (ratio of area of respective peaks was 38:13) verified that nontronite contributes the main part of Garfield sample. Although the pattern obtained from powder mount did not show any peak of quartz in nontronite Garfield sample, the 3.33 Å was detected from ethylene-glycol saturated specimen showing that quartz occurs in traces. This is in agreement with information from research of Huo (1997) (reviewed by Fialips *et al.*, 2002). The authors also indicated the presence of small amount of iron oxides (goethite and maghemite).

Special iron content in Garfield was studied more detail by Mössbauer spectroscopy at the St-Petersburg State University (Lessovaia, 2004 - unpublished report). The obtained spectrum of Garfield nontronite consisted of a single symmetric quadropole doublet, which presented two doublet sub-spectra (CM-7.1 and CM-7.2), is given at figure 20. These two doublets, that had the same  $\delta$  values of 0.36 mm/s and varied on  $\Delta$  of 0.24 and 0.65 mm/s, corresponded in order with *cis*- and *trans*-octahedral 2:1 layer silicates or nontronite in this sample (Goodman *et al.*, 1976; Goodman, 1978; Rozenson and Heller-Kallai, 1977; Heller-Kallai and Rozenson, 1981) (appendix 7). The difference of  $\Delta$  was affected mainly by disposition of the OH-groups which was in description of Bishop *et al.* (2002). In this case,  $\text{Fe}^{3+}$  showed slightly *cis*-vacant preference. The sample of Garfield nontronite contained structural iron about 22% by weight, which is a little higher than that of nontronite (20%) from statistical data of Stucki (2005). There was no detected sub-spectrum of tetrahedral  $\text{Fe}^{3+}$ .

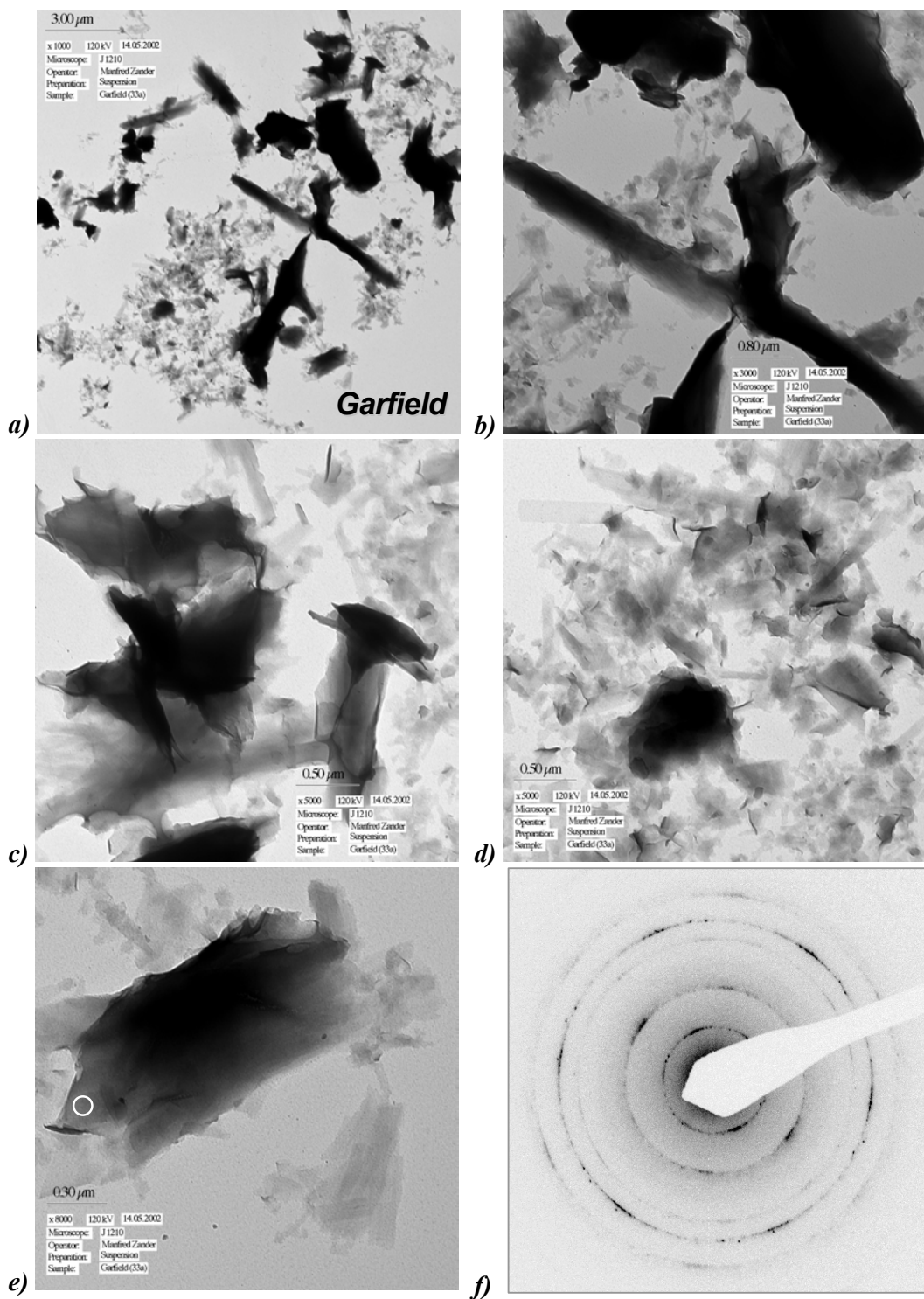
TEM-EDX analyses, in agreement with above findings from Mössbauer analysis about non-tetrahedral  $\text{Fe}^{3+}$ , gave the nontronite formula presented in table 7. Although there was the difference in the division of tetrahedral  $\text{Fe}^{3+}$  and octahedral  $\text{Fe}^{3+}$ , the charge of tetrahedral layer was calculated very close to data of Murad (1987). The tetrahedral components were also similar with published formula by Fialips *et al.* (2001) using IR technique. Morphology of nontronite particles were presented as lath-shaped xenomorphic (figure 21 b, d) and platy xenomorphic (figure 21c, e). Almost all of electron diffraction analyzed particles showed ring-like structures (figure 21f), that indicated turbostratic orientation of the layers of Garfield nontronite. The total surface area of Garfield bentonite is about 656 m<sup>2</sup>/g (Środoń & McCarty, 2006).



**Figure 20. Mössbauer spectrum of nontronite Garfield (bulk sample) at room temperature**

The spectrum showed sub-spectra of *cis*-nontronite and *trans*-nontronite (see more in appendix 7)

Note: Measured using Ms-1104Em spectrometer at St-Petersburg State University, Russia;  $^{57}\text{Co}$  isotopes resource, subspectra were fitted by Univem MS program



**Figure 21. TEM images of nontronite Garfield sample**

a) Overview of Garfield sample (1,000x); b) Zoom of image a) (3,000x); c) and d) Zoom of image a) (5,000x) e) Zoom of image a) (8,000x) and f) Electron diffractions of selected point of particle in image e)

Note: Measured using Jeol JEM-1210; the images show the particles of nontronite (dominating particles)

**Table 7. Mineral formulae [O<sub>10</sub>(OH)<sub>2</sub>] of Garfield nontronite, Chambers and Wyoming montmorillonite, based on TEM-EDX analyses**

	Interlayer					Octahedral layer					Tetra. layer		
	Ca	Mg	Na	K	Fe <sup>2+</sup>	Al	Fe <sup>3+</sup>	Fe <sup>2+</sup>	Mg	Ti	Al	Fe <sup>3+</sup>	Si
<b>Garfield: nontronite</b>													
Average	0.02	0.03	0.07	0.02	0.07	0.20	1.79	0.00	0.00	0.01	0.40	0.00	3.60
STDV	0.02	0.03	0.05	0.03	0.04	0.12	0.12	0.00	0.01	0.02	0.07	0.00	0.06
Min	0.00	0.00	0.00	0.00	0.00	0.00	1.47	0.00	0.00	0.00	0.16	0.00	3.46
Max	0.08	0.11	0.22	0.11	0.16	0.52	2.00	0.00	0.04	0.16	0.54	0.00	3.69
<i>Besson et al., 1983; by XRD, MB</i>	0.00	0.00	0.00	0.57	0.00	0.15	1.84	0.00	0.02	0.00	0.38	0.00	3.46
<i>Murad, 1987; by MB</i>	0.00	0.00	0.47	0.00	0.00	0.25	1.70	0.00	0.05	0.00	0.30	0.10	3.60
<i>Fialips et al., 2002; by IR</i>	0.00	0.00	0.40	0.00	0.00	0.32	1.82	0.01	0.02	0.00	0.39	0.00	3.61
<b>Chambers: montmorillonite</b>													
Average	0.03	0.01	0.16	0.06	0.00	1.45	0.32	0.00	0.18	0.02	0.03	0.00	3.97
<i>Cuadros, 2002; by XRF</i>	0.28	0.00	0.02	0.00	0.00	1.37	0.18	0.00	0.41	0.02	0.14	0.00	3.86
<b>Wyoming: montmorillonite</b>													
Average	0.02	0.05	0.02	0.01	0.00	1.61	0.21	0.00	0.16	0.01	0.03	0.00	3.97
STDV	0.02	0.03	0.03	0.01	0.00	0.08	0.04	0.01	0.06	0.01	0.02	0.00	0.02
Min	0.00	0.00	0.00	0.00	0.00	1.37	1.17	0.00	0.09	0.00	0.00	0.00	3.94
Max	0.07	0.09	0.09	0.03	0.00	1.68	0.33	0.02	0.27	0.03	0.06	0.00	4.00
<i>Kasbohm et al., 1998; by TEM</i>	0.07	0.00	0.22	0.04	0.00	1.54	0.17	0.00	0.26	0.00	0.05	0.00	3.95
<i>Madsen, 1998</i>	0.00	0.00	0.30	0.00	0.00	1.55	0.20	0.01	0.24	0.00	0.04	0.00	3.96
<i>Wold &amp; Eriksen, 2002; by ICP, CEC</i>	0.03	0.01	0.21	0.01	0.00	1.55	0.19	0.00	0.26	0.00	0.04	0.00	3.96

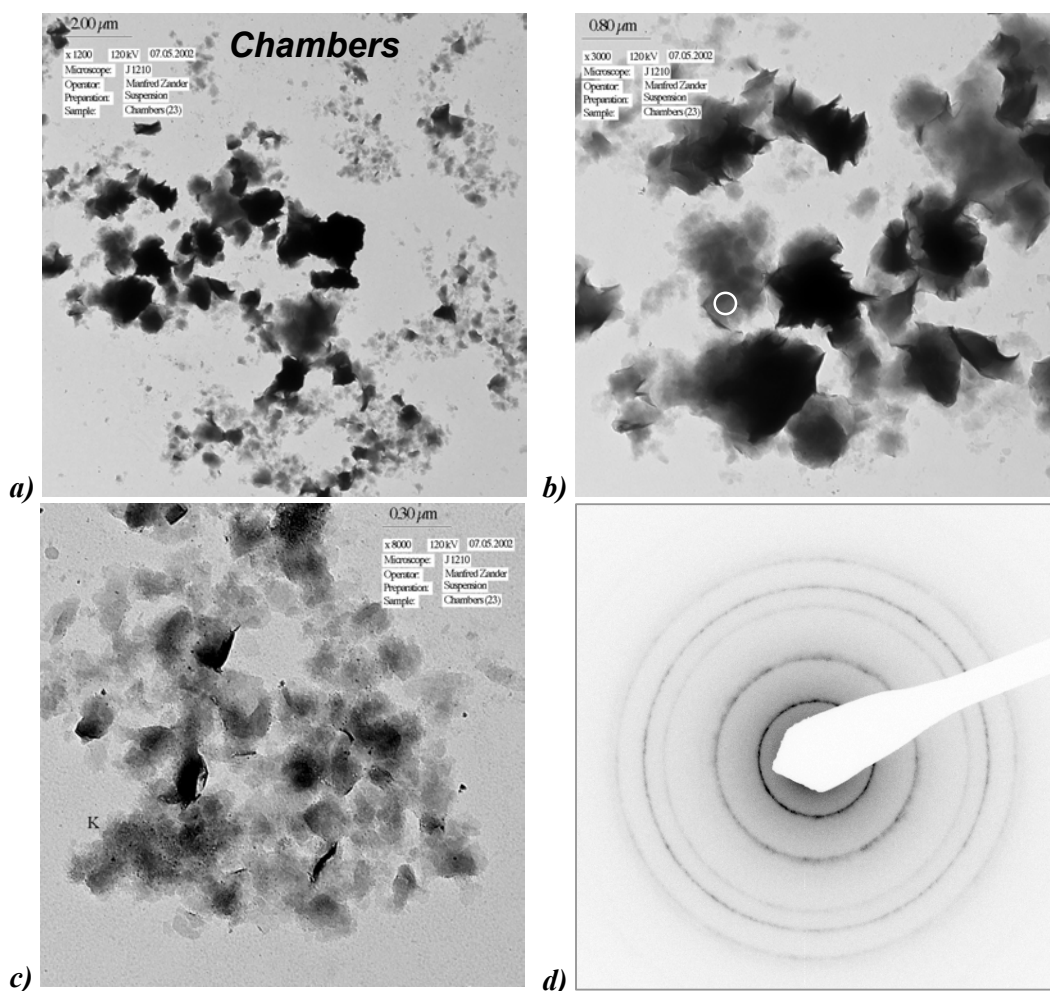
*Note: Measured using Jeol JEM-1210; Average: average index, Min: minimal index, Max: maximal index, STDV: standard deviation*

### Chambers

The altered volcanic ash bentonite originated near the Chambers siding in Apache County, Arizona/USA. By XRD experiments, for Chambers bentonite it is verified a composition of two kinds of montmorillonite: 15 Å-montmorillonite (bivalent cations in the interlayer space) and 13 Å-montmorillonite (monovalent cations in the interlayer space). They were identified not only by powder mount but also by oriented mount. The 001-spacing peaks at 15.1 and 13.0 Å (figure 19), which were decomposed from one asymmetric peak obtained from air-dried specimen, indicated to accordingly two kinds of montmorillonite. The peaks shifted to 16.8 and 18.0 Å after saturating by ethylene-glycol confirming the expandable property of smectite. However, the area ratio between the two 001-spacing



peaks from air-dried specimen pattern of about 2430:190 indicated the domination of 15 Å-montmorillonite or bication montmorillonite. This was corresponding to the much higher proportion of Ca (oxid form in mass) from XRF result. Moreover, a couple of 8.55 and 5.59 Å peaks was also identified from the ethylene-glycol saturated specimen pattern. According to Moore and Reynolds (1997) (see also table 9), the couple manifested the presence of IS-ml particles with illitic layer proportion of about 10% in the sample. The presence of IS-ml may be caused by smectite illitization towards original Chambers montmorillonite. About minor phases and impurities, Chambers pattern showed the signs of calcite, dolomite, kaolinite and quartz of which three last ones occurred as trace in the sample.



**Figure 22. TEM images of montmorillonite Chambers sample**

a) Overview of Chambers sample (1,000x); b) Zoom of image a) (3,000x); c) Zoom of image a) (8,000x) and d) Electron diffractions of selected point of particle in image b)

*Note: Measured using Jeol JEM-1210; the images show the particles of montmorillonite (dominating particles)*

The morphology of Chambers montmorillonite was observed by TEM experiment. The sample presented 2 kinds of montmorillonite particles. The larger particles, thick, curved edges and xenomorphic, had the dimension of more than 1  $\mu\text{m}$  (figure 22b). The smaller ones had only 0.10 – 0.20  $\mu\text{m}$  of dimension and occurred as single, platy xenomorphic particles (figure 22c). Both kinds showed mainly turbostratic orientation, an example is shown in figure 22d. The calculated average chemical formula of Chambers montmorillonite by TEM-EDX is shown in table 7.

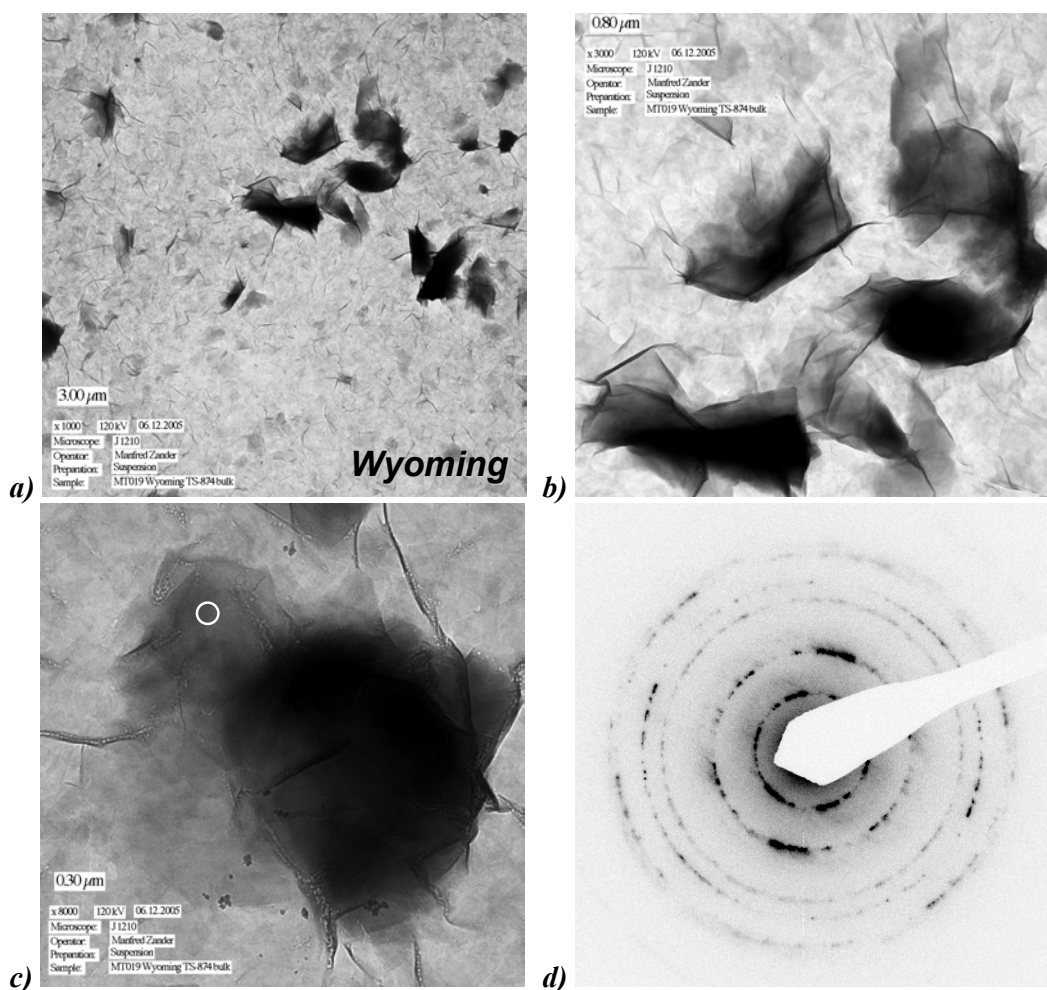
The total surface area of Chambers bentonite is about 805  $\text{m}^2/\text{g}$  (Środoń & McCarty, 2006).

### Wyoming

This type of bentonite, in Upton Area, was interbedded in Mowry shale. The deposit located in Weston/Wyoming/USA and dipped away from Black Hills uplift. The samples were characterized as bentonite dominated by 13 Å-montmorillonite and 14 Å-montmorillonite with 12.7 and 14.0 Å peaks fitted from XRD air-dried specimen profile. Relative ratio of height of these peaks was similar. By ethylene-glycol saturation, the interlayer spaces of two kinds of montmorillonite were expandable, resulting in appearance of 16.8 and 17.3 Å peaks. Similar to Chambers montmorillonite case, a couple of 8.51 and 5.64 Å peaks fitted from ethylene-glycol saturated specimen profile showed presence of IS-ml series with illitic layer proportion of 5%. Wyoming pattern presented the signs of quartz and traces of kaolinite and feldspar.

Under TEM-EDX observation, the Wyoming bentonite showed not only the large particles in approximately 1 – 2  $\mu\text{m}$  of a dimension (figure 23b, c) but also very fine particles (figure 23a). The morphology of large ones is curved edges and xenomorphic. The turbostratic orientation, demonstrated by ring-like structures of the electron spots from electron diffraction (figure 23d), is typical for structure of the Wyoming montmorillonite particles. The chemical formula of this kind of bentonite obtained from randomly selected particles is presented in table 7. The difference in the octahedral occupations and yielding interlayer in comparison with references might be caused by alteration of montmorillonite after long time in contact with water during experiment preparation. This mentioned process was discussed in some works (Kasbohm, 2003; Herbert *et al.*, 2004). In the process, Al substituted for Mg in the octahedral layer together with the dissolution of Na in the interlayer and substituted partly by Mg. Therefore, origin montmorillonite is changed to low-charge montmorillonite day after day.

Cation exchange capacity of the Upton Wyoming was calculated to about 75 meq/100g using copper complex exchange method by Ammann (2003) or about 67 meq/100g using ethylene blue method by Kahr & Madsen (1995). Total surface area of Wyoming bentonite differs from about 700  $\text{m}^2/\text{g}$  (according to Środoń & McCarty, 2006) to about 522  $\text{m}^2/\text{g}$  (according to Kahr & Madsen, 1995).



**Figure 23. TEM images of montmorillonite Wyoming sample**

a) Overview of Wyoming sample (1,000x); b) Zoom of image a) (3,000x); c) Zoom of image a) (8,000x) and d) Electron diffractions of selected point of the particle in image c)

*Note: Measured using Jeol JEM-1210; the images show the particles of montmorillonite (dominating particles)*

In general, Garfield, Chambers and Wyoming are dominated by smectites; the impurities play a minor role in the characterization of these samples. Garfield was identified as bentonite of nontronite with very high amount of iron which is in structure of nontronite mineral. In contrast, Chambers and Wyoming are aluminium-rich clays. Chambers is Ca-montmorillonite (bivalent cation), whereas Wyoming is Na-montmorillonite (monovalent cation). By TEM-EDX investigation, charges of Garfield, Chambers and Wyoming are estimated about 0.31, 0.14 and 0.16 per unit cell.

#### 4.2.2 CMS reference bentonites

In this research, hectorite SHCa-1, montmorillonite STx-1, montmorillonite SAz-1 and montmorillonite SWy-2 were included. Their properties, such as chemical composition (appendix 5) and mineral composition, were published in many documents (van Olphen & Fripiat, 1979; Chipera & Bish, 2001; Vogt *et al.*, 2002). Therefore, in this research, these samples were analyzed only by TEM-EDX with suspension of <2  $\mu\text{m}$  particles to aim to recognize the material for further experiments. The geological origin of these bentonites is reviewed and published in Moll (2001).

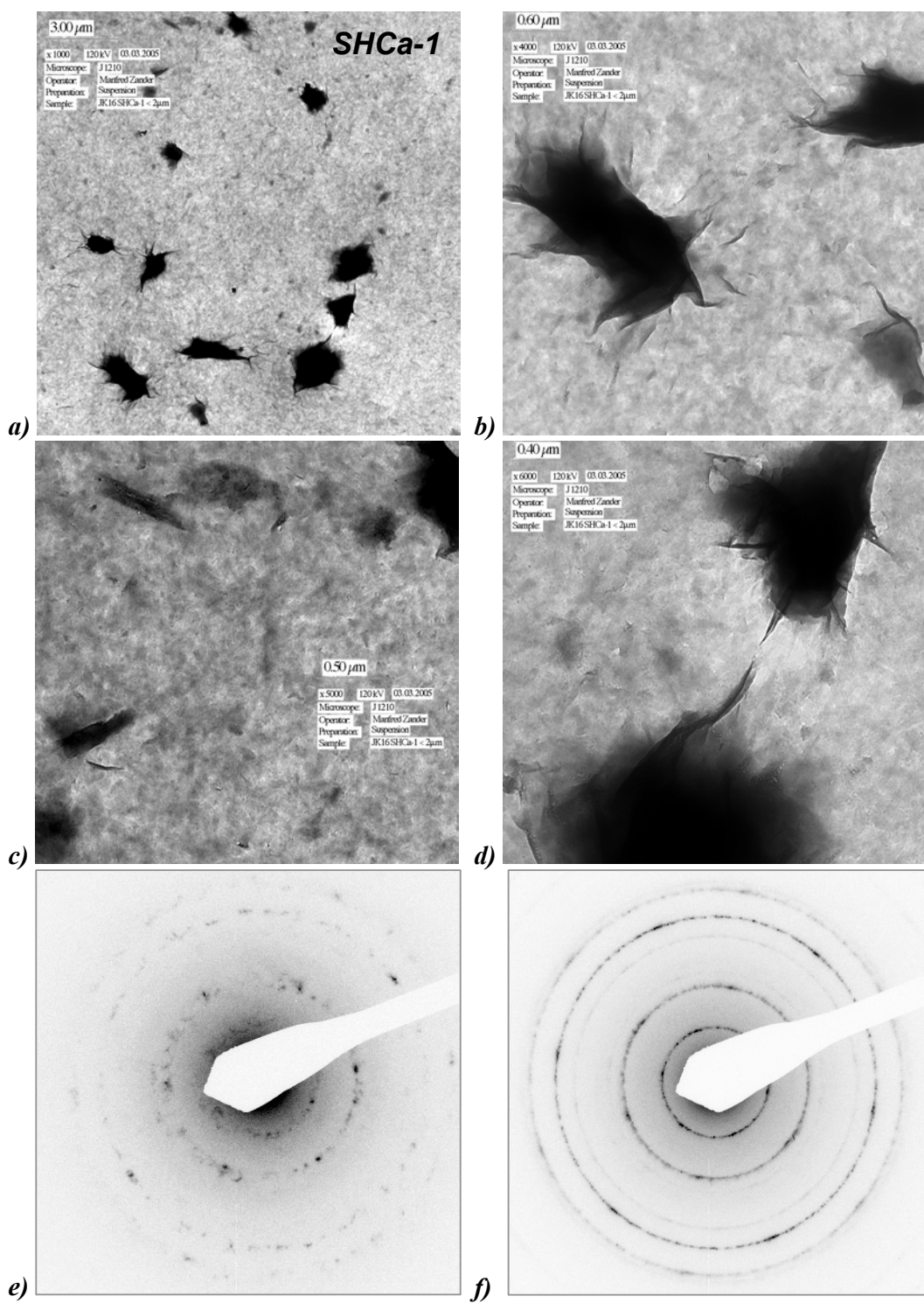
##### *SHCa-1*

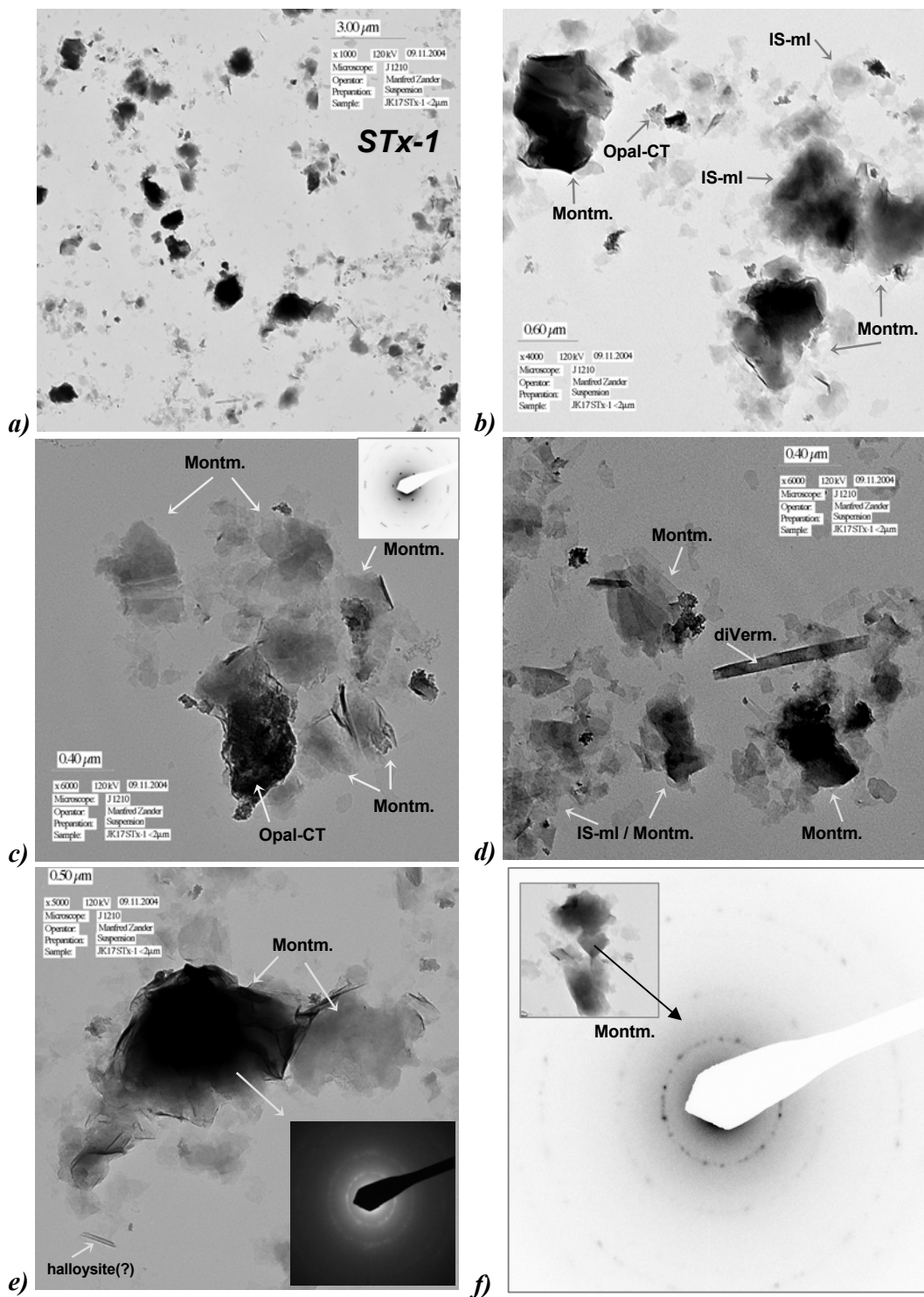
The special benonite, dominated by Li-bearing trioctahedral smectite - hectorite, is secondary product developed from Red Mountain andesite formation in county of San Bernardino, California/USA (Moll, 2001). By XRD analyses, Chipera & Bish (2001) found that bulk sample contained approximately 50% smectite together with 43% calcite, 3% dolomite, 3% quartz and 1% others (feldspar, kaolinite(?)). The hectorite presented 001-peak at 9.9 Å (d-value) in the XRD air-dried specimen profile and expanded up to 16.8 Å after ethylene-glycol saturation.

TEM observation showed that hectorite SHCa-1 sample presented very dense suspension of <2  $\mu\text{m}$  fraction. The sample includes two kinds of particle morphologies: (i) very fine, slat-shaped aggregates and (ii) about >1  $\mu\text{m}$  of dimension, nepheloid and curled particles (figure 24). Both types displayed the typical signs of expandable clay mineral. The obtained morphologies of the SHCa-1 sample are very similar with description about the hectorite located in Hector, California by Henning and Störr (1986). All of electron diffraction analyzed particles showed ring-like structures (figure 24e, f), which demonstrated the turbostratic orientation of the layer or the overlapping of the particles of hectorite in the SHCa-1 sample.

General chemical composition of the hectorite SHCa-1, according to van Olphen & Fripiat (1979), Vogt *et al.* (2002), is shown in appendix 5.

The component of <2  $\mu\text{m}$  contributed about 23% in the sample and contained approximately 97% smectite (Vogt *et al.*, 2002; Chipera & Bish, 2001). The bentonite has cation exchange capacity of about 44 meq/100g (van Olphen & Fripiat, 1979) and surface area of about 706 m<sup>2</sup>/g (Środoń & McCarty, 2006). The cation exchange capacity was also confirmed with about 47 meq/100g by Ammann *et al.* (2005).





**Figure 25. TEM images of STx-1 (Texas montmorillonite) sample**

a) Overview of STx-1 sample (1,000x); b) Zoom of image a) (4,000x); c) Zoom of image a) (6,000x) and electron diffraction of Montm. particle; d) Zoom of image a) (6,000x); e) Zoom of image a) (5,000x) and electron diffractions of Montm. particle (above)

*Note: Measured using Jeol JEM-1210; the images show the particles of montmorillonite (Montm.) (dominating particles), Illite/smectite mixed-layer (IS-mi), dioctahedral vermiculite (diVerm.), opal-CT and probably misanalyzed halloysite (halloysite(?))*

### STx-1

The white bentonite, resulted by alteration process from volcanic ash of rhyolitic composition, occurs in the Manning Formation of the upper Eocene Jackson group in county of Gonzales, Texas/USA (Moll, 2001). STx-1 includes approximately 67% smectite, 30% opal-CT, 3% impurities including quartz, feldspar, kaolinite and talc(?) (Chipera & Bish, 2001). The  $<2\ \mu\text{m}$  part still bring rich non-smectite phase as listed above. In the clay fraction composition, using XRD analyses, Chipera & Bish (2001) calculated 68% of smectite and Vogt *et al.* (2002) calculated 58% of smectite. Chemical composition of the hectorite SHCa-1 is presented in appendix 5.

By TEM observation, particle size of STx-1 bentonite (figure 25) could be classified into 2 categories. The larger one with about  $0.50\ \mu\text{m}$  of dimension occurred thick, more and curled edges particle. The smaller one appeared as thin, more and xenomorphic particle. Most of determined particles are montmorillonite or mixed-layer with high proportion (mostly 90%) of montmorillonitic layer. Chemical composition of analyzed montmorillonite was showed in table 8. This data indicated that interlayer component of STx-1 montmorillonite was various from particle to particle. K-interlayer was more stable than other interlayer elements. STx-1 montmorillonite is well-known as Ca-montmorillonite but average Ca-index is quite low from results of the study. Monovalent cations (Na and K) took a part as high as a part that bivalent cations (Ca and Mg) contributed in the interlayer.

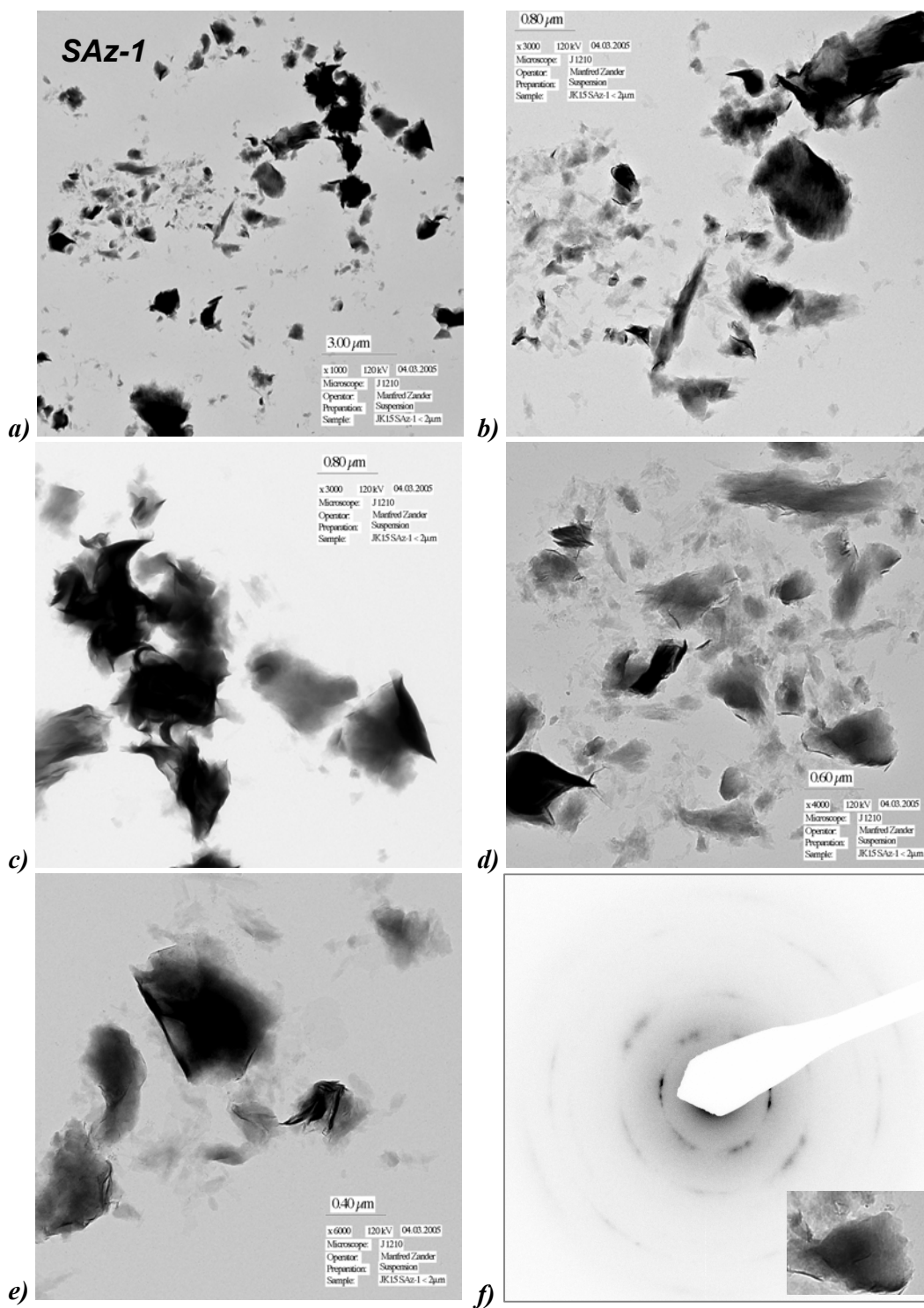
With respect to the octahedral layer component, results from TEM-EDX indicated that STx-1 montmorillonite is Fe-poor montmorillonite: octahedral layer contained dominating Al and partly Mg with low standard deviation. The published structure formula of SAZ-1 montmorillonite by van Olphen and Fripiat (1971) has a gap in octahedral layer with only 1.62 element per  $[\text{O}_{10}(\text{OH})_2]$  unit.

Layer structure of STx-1 montmorillonite studied by electronic diffraction showed a ring-like polytype (figure 25c, e, f).

The identified minor phase of STx-1 included lath-shaped dioctahedral vermiculite (figure 25), dioctahedral vermiculite/smectite mixed-layer, tubule halloysite (figure 25d), beidellite and the particles (figure 25b, c), which have chemical formula of  $\text{SiO}_2$ , were interpreted as opal-CT because its published abundant amount in  $<2\ \mu\text{m}$  composition.

STx-1 bentonite has cation exchange capacity of about 84 meq/100g (van Olphen & Fripiat, 1979; Ammann *et al.*, 2005). STx-1 surface area is of about  $741\ \text{m}^2/\text{g}$  according to Środoń & McCarty (2006).



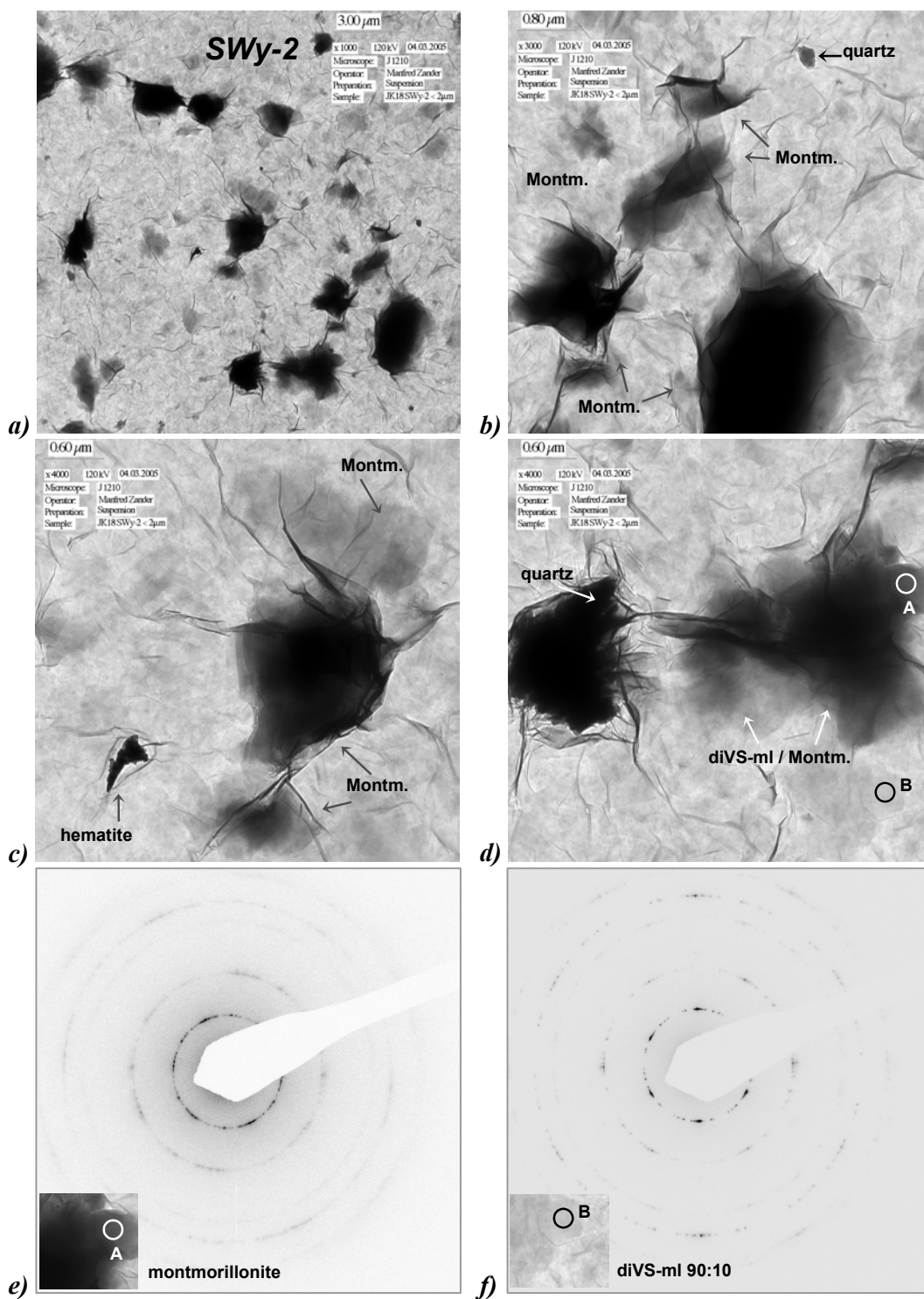


**Figure 26. TEM images of SAz-1 (Cheto, Arizona montmorillonite) sample**

a) Overview of STx-1 sample (1,000x); b) and c) Zoom of image a) (3,000x); d) Zoom of image a) (4,000x); e) Zoom of image a) (6,000x); and f) Electron diffractions of Montm. particle (bottom)

*Note: Measured using Jeol JEM-1210; the images show the particles of montmorillonite (Montm.) (dominating particles)*





**Figure 27. TEM images of SWy-2 (Wyoming montmorillonite) sample**

a) Overview of SWy-2 sample (1,000x); b) Zoom of image a) (3,000x); c) Zoom of image a) (4,000x) d) Zoom of image a) (4,000x) and A and B points for electron diffraction analyses; e) Electron diffractions of A point in image d) - montmorillonite particle and f) Electron diffractions of B point in image d) - diVS-mI 90:10 particle  
 Note: Measured using Jeol JEM-1210; the images show the particles of montmorillonite (Montm.) (dominating particles), dioctahedral vermiculite/smectite mixed-layer (IS-mI), hematite and quartz

**Table 8.** Mineral formulae [O<sub>10</sub>(OH)<sub>2</sub>] of montmorillonite and hectorite from CMS bentonites, based on TEM-EDX analyses

	Interlayer				Octahedral layer				Tetrahedral layer			
	Ca	Mg	Na	K	Fe <sup>2+</sup>	Al	Fe <sup>3+</sup>	Mg	Ti	Fe <sup>3+</sup>	Al	Si
<b>SHCa-1: Hectorite</b>												
	Ca	Mg	Na	K	Fe <sup>2+</sup>	Li <sup>+</sup>	Fe <sup>3+</sup>	Mg	Ti	Fe <sup>3+</sup>	Al	Si
CMS*	0.00	0.28	0.21	0.03	0.00	0.70	0.00	2.30	0.01	0.03	0.09	3.88
<b>STx-1: Montmorillonite</b>												
	Ca	Mg	Na	K	Fe <sup>2+</sup>	Al	Fe <sup>3+</sup>	Mg	Ti	Fe <sup>3+</sup>	Al	Si
Average	<b>0.03</b>	<b>0.08</b>	<b>0.07</b>	<b>0.04</b>	<b>0.00</b>	<b>1.63</b>	<b>0.05</b>	<b>0.31</b>	<b>0.01</b>	<b>0.00</b>	<b>0.03</b>	<b>3.97</b>
STDV	0.05	0.05	0.07	0.02	0.00	0.07	0.05	0.05	0.01	0.00	0.02	0.02
Min	0.00	0.00	0.05	0.02	0.00	1.53	0.00	0.23	0.00	0.00	0.00	3.94
Max	0.17	0.15	0.25	0.08	0.00	1.76	0.19	0.37	0.04	0.00	0.06	4.00
CMS*	0.14	0.00	0.02	0.01	0.00	<u>1.21</u>	0.05	0.36	0.02	0.00	0.00	4.00
<b>SAz-1: Montmorillonite</b>												
	Ca	Mg	Na	K	Fe <sup>2+</sup>	Al	Fe <sup>3+</sup>	Mg	Ti	Fe <sup>3+</sup>	Al	Si
Average	<b>0.05</b>	<b>0.13</b>	<b>0.00</b>	<b>0.01</b>	<b>0.00</b>	<b>1.53</b>	<b>0.07</b>	<b>0.38</b>	<b>0.01</b>	<b>0.00</b>	<b>0.00</b>	<b>4.00</b>
STDV	0.03	0.03	0.00	0.01	0.00	0.05	0.04	0.04	0.02	0.00	0.00	0.00
Min	0.00	0.06	0.00	0.00	0.00	1.39	0.00	0.29	0.00	0.00	0.00	3.95
Max	0.15	0.19	0.00	0.05	0.00	1.65	0.20	0.46	0.07	0.00	0.05	4.00
CMS*	0.20	0.00	0.18	0.01	0.00	1.36	0.06	0.56	0.02	0.00	0.00	4.00
<b>SWy-2: Montmorillonite</b>												
	Ca	Mg	Na	K	Fe <sup>2+</sup>	Al	Fe <sup>3+</sup>	Mg	Ti	Fe <sup>3+</sup>	Al	Si
Average	<b>0.07</b>	<b>0.03</b>	<b>0.01</b>	<b>0.01</b>	<b>0.00</b>	<b>1.60</b>	<b>0.17</b>	<b>0.21</b>	<b>0.01</b>	<b>0.00</b>	<b>0.03</b>	<b>3.97</b>
STDV	0.04	0.04	0.01	0.01	0.00	0.05	0.02	0.04	0.01	0.00	0.02	0.02
Min	0.02	0.00	0.00	0.00	0.00	1.56	1.13	0.15	0.00	0.00	0.00	3.94
Max	0.12	0.10	0.03	0.03	0.00	1.68	0.19	0.25	0.03	0.00	0.06	4.00
CMS*	0.06	0.00	0.16	0.03	0.00	1.51	0.21	0.27	0.01	0.00	0.01	3.99

*Note: Measured using Jeol JEM-1210; CMS\*: according to CMS resource (van Olphen & Fripiat, 1979); Average: average index, Min: minimal index, Max: maximal index, STDV: standard deviation*

*SAz-1*

Deposits of the bentonite occur in non-marine Pliocene Biodhohchi Formation, Arizona/USA. In the 1950s in district of Cheto, the production reached a maximum so that SAz-1 bentonite is also called “Cheto” bentonite. SAz-1 bentonite is very rich smectite with about 98% together with 1% quartz and 1% others (feldspar, mica, magnetite, rancieite(?), cristobalite(?), zeolite(?)) as well as amorphous phases(?) as glass or opal-A) (Chipera & Bish, 2001). However, the bentonite contains only 23% weight of <2 µm particles (Vogt *et al.*, 2002).

In own TEM-EDX research, SAz-1 smectite was also determined as very pure material. Figure 26 presented SAz-1 that montmorillonite was totally dominated. Larger montmorillonite particles, about more than 1  $\mu\text{m}$  of dimension, are xenomorphic and isometric. Edges of some of them, which are thick particles, were curled strongly (figure 26c). Smaller ones are more and slightly elongate (figure 26d).

TEM-EDX brought out a ring-like polytype of SAz-1 montmorillonite (figure 26f). Chemical formula with mean indexes of pure analyzed montmorillonite particles showing in table 8 proved that interlayer of STx-1 montmorillonite is dominated by bivalent cation. In comparison to the data published by van Olphen & Fripiat (1979), there is a difference in the octahedral components, that might caused by alteration of montmorillonite after long time in contact with water. In the process, Al substituted for Mg in the octahedral layer together with the dissolution of Na and Ca in the interlayer and substituted partly by Mg. The process was discussion by Kasbohm and his group (Kasbohm, 2003; Herbert *et al.*, 2004).

ATx-1 bentonit is certificated with quite high cation exchange capacity of 120 meq/100g (van Olphen & Fripiat, 1979) and surface area of about 764  $\text{m}^2/\text{g}$  (Środoń & McCarty, 2006). The publication of Kahr & Madsen (1995) identified its cation exchange capacity is 100 meq/100g and its surface area is 782  $\text{m}^2/\text{g}$  by methylene blue method.

### SWy-2

The benonite, one of “Wyoming bentonite” kind, is resulted as deposit of volcanic ash in to the lake of Newcastle Formation in Crook County, Wyoming/USA. Mineral composition of the bentonite is characterized as approximately 75% smectite, 8% quartz, 16% feldspar, 1% impurities involving gypsum, mica and/or illite, kaolinite(?) and/or chlorite(?) (Chipera & Bish, 2001). Research on the  $<2 \mu\text{m}$  fraction material, the authors found that it contained approximately 95% smectite and the impurities as various as in bulk sample. Vogt *et al.* (2002) suggested that the material contains about 80% amount of clay fraction. However, different from information from Chipera & Bish, the authors found augite, quartz, saponite, kaolinite and pyroxene as minor phase of SWy-2 bentonite. In this contribution, TEM-EDX results determined the presence of quartz and hematite as traces in  $<2 \mu\text{m}$  SWy-2 sample.

By TEM observation, SWy-2 presented xenomorphic and fine particles, therein finest ones look like “background” in the images (figure 27). The extremely fine particles were demonstrated as montmorillonite by EDX analyses. Montmorillonite also occurred in the dimension of about 1 - 2  $\mu\text{m}$ . The particles were curled dependently on their thickness so that folds were obvious in the “background” and the particle edge. Some

detected particles, which have the same morphology with the identified montmorillonite in this sample, were analyzed as illite/montmorillonite mixed-layer or dioctahedral vermiculite/montmorillonite mixed-layer (rarely) with about 90% of montmorillonitic layer. They had turbostratic orientation of the layers as indicated by a ring-like polytype (figure 27e, f). The presence of mixed-layer particles might be caused by slightly illitization or vermiculitization.

Chemical formula of SWy-2 montmorillonite is shown in table 8. Similarly with the case of ATx-1 montmorillonite, there is a substitution of Mg and Fe by Al in the octahedral layer in combination with the solution of Na in the interlayer, so that it caused the difference from the structure formula in literature. SWy-2 montmorillonite has richer iron in the octahedral layer than other used CMS reference bentonites. General chemical composition presented in appendix 5 also supported for that.

In publication of van Olphen & Fripiat (1979), SWy-2 cation exchange capacity is identified as 76 meq/100g. Ammann (2003) got the similar value 77 meq/100g for cation exchange capacity. According to Środoń & McCarty (2006), the surface area of ATx-1 is about 748 m<sup>2</sup>/g.

In general speaking, SHCa-1, STx-1, SAz-1 and SWy-2 were characterized as smectite-rich bentonites and high surface area. Studies by TEM-EDX showed a typical process that modifies octahedral layer components and following interlayer components. Therefore, it might cause different properties from new materials.

### 4.3 Mixed-layer dominated clay

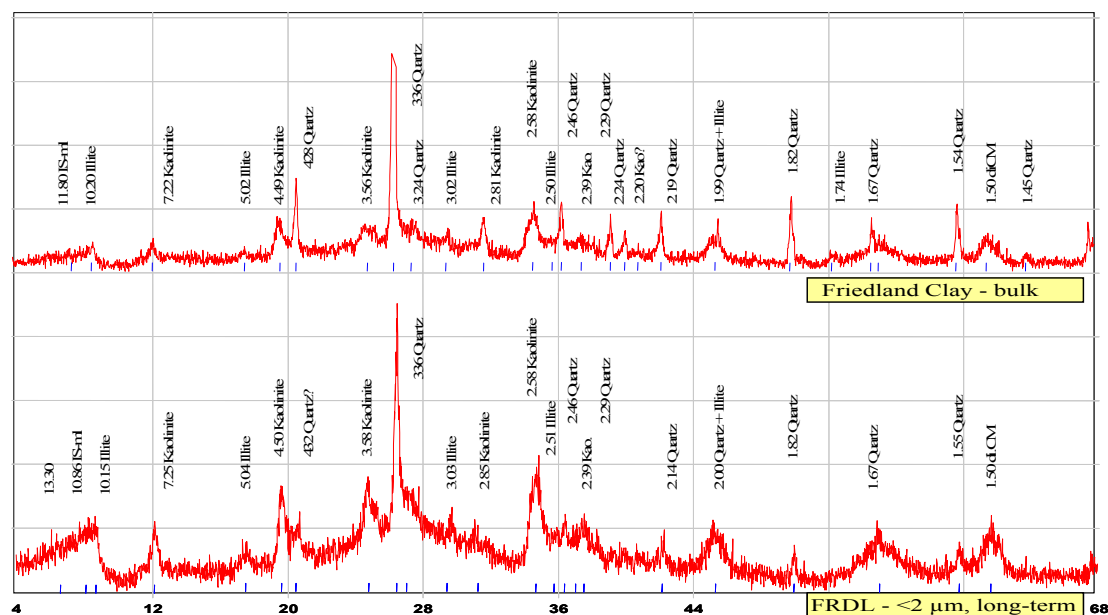
#### 4.3.1 Friedland Clay

The Eocene clay, was supplied by Pilot Vegetable Oil Technology Magdeburg e.V. (PPM e.V.), originated from Eocene marine sedimentation and located in Friedland, Mecklenburg-Western Pomerania, Germany. The geological background for the Friedland Clay is summarized in Henning & Kasbohm (1998).

This contribution used (i) bulk FRDL sample labelled as “Friedland Clay - bulk”, (ii) <2 µm FRDL sample, obtained by sedimentation after few hours in contact with water, labelled as “FRDL - <2 µm, short-term” and (iii) <2 µm FRDL sample, obtained by Atterberg sedimentation after about two months in contact with water, labelled as “FRDL - <2µm, long-term”.

Based on Henning (1971) and further measurements, Henning & Kasbohm (1998) published also the mineral matter composition of FRDL with IS-ml 50-55%, illite 20%, kaolinite + chlorite <5%, quartz 10 – 15%, feldspar <5% as well as traces of pyrite, gypsum and halite.

In own measurements, visual XRD patterns of randomly oriented samples indicated the presence of several minerals: illite, IS-ml and kaolinite as main clay mineral phases as well as quartz as main non-clay mineral phase (figure 28). In general, there was no significant variation between two spectra. However, the 13.3 Å peak of IS-ml series with bivalent cations existed only in <2 µm FRDL sample.



**Figure 28.** X-Ray Diffraction patterns of Friedland Clay samples from randomly oriented powder mount,  $2\theta$  CuK $\alpha$  position

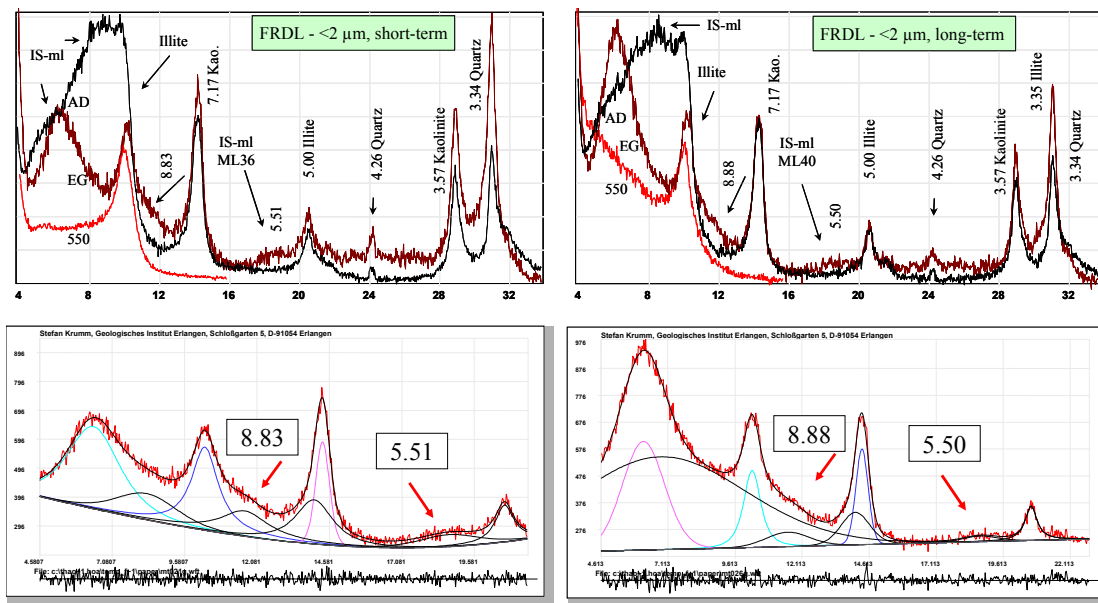
Note: Measured using Siemens D5000; Above: Friedland Clay – bulk; bottom: FRDL - <2 µm long-term in contact with water; the patterns show the peaks of kaolinite (Kao.), dioctahedral clay mineral (diCM): illite, illite/smectite mixed-layer series (IS-ml) and quartz

Experiments with oriented samples, including air-dried, ethylene-glycol saturated and 550°C heated specimens, were used to characterize the expandable layers, from both <2 µm samples (figure 29). In these FRDL samples, IS-ml presented, 11.7 and 12.0 Å peaks, which increased up to 16.0 and 16.2 Å peaks after ethylene-glycol saturation. Illite had 10.2 Å peak, which is slightly larger basal spacing than the typical 10 Å. It was possible to recognize this characterization of illite at powder diffraction, too.

**Table 9. The positions of reflections for estimating proportion of illitic layer in illite/EG-smectite**  
(according to Moore and Reynolds, 1997)

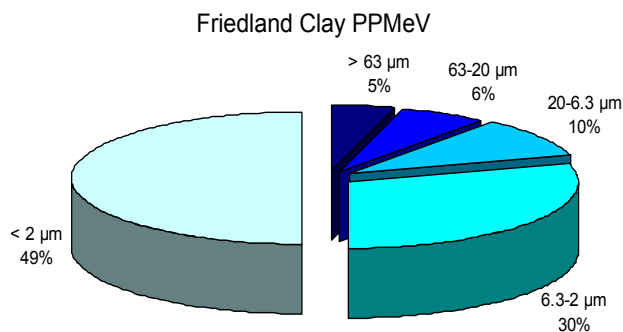
% Illite	Ordering type	001/002		002/003		
		d (Å)	°2θ	d (Å)	°2θ	°Δ2θ
10	0	8.58	10.31	5.61	15.80	5.49
20	0	8.67	10.20	5.58	15.88	5.68
30	0	8.77	10.09	5.53	16.03	5.94
40	0	8.89	9.95	5.50	16.11	6.16
50	0	9.05	9.77	5.44	16.29	6.52
60	1	9.22	9.59	5.34	16.60	7.01
70	1	9.40	9.41	5.28	16.79	7.38
80	1	9.64	9.17	5.20	17.05	7.88
90	3	9.82	9.01	5.10	17.39	8.38

Proportions of illitic layers in the illite/smectite mixed-layer were calculated according to Moore & Reynolds (1997). Based on the relationship between the d-values (Å) of 001/002 interference and 002/003 interference taken from ethylene-glycolated specimen (table 9), FRDL samples were characterized as illite/smectite mixed-layer with 35% - 40% illitic layers, respectively.



**Figure 29. XRD patterns of Friedland Clay samples from oriented specimens, °2θ CoK<sub>α</sub> position**  
Note: Measured using HZG 4 / Seifert C3000; Left: FRDL - <2 µm, short-term; right: FRDL - <2 µm, long-term; Above: completely XRD-patterns including air-dried specimen patterns (AD, solid), ethylene-glycol saturated specimen patterns (EG, dash), 550 degree C heated specimen patterns (550, solid); Bottom: fitting decomposition of example ethylene glycol saturated specimens; the patterns show the peaks of kaolinite (Kao.), dioctahedral clay mineral (diCM): illite, illite/smectite mixed-layer series (IS-ml) and quartz

The slight differences, as above description, in general mineral composition and also in the specific mixed-layer phase, were caused by different material separated by particle size. The  $<2\ \mu\text{m}$  Friedland Clay sample (FRDL -  $<2\ \mu\text{m}$ , long term) is as product of Atterberg sedimentation from untreated bulk Friedland Clay sample after 2 months contacting with water.



**Figure 30. Grain size distribution of Friedland Clay by Atterberg sedimentation**

(published in Henning & Kasbohm 1998:

$<2\ \mu\text{m} = 50\%$ ,  $2-63\ \mu\text{m} = 48\%$ ,  $>63\ \mu\text{m} = 2\%$ )

Contribution of  $<2\ \mu\text{m}$  particles

among the other larger size particles from bulk sample is drawn in figure 30. This finest part occupied about a half of whole sample. It showed appropriate result to Friedland Clay studied by Henning & Kasbohm (1998). The authors presented the material with 50% of  $<2\ \mu\text{m}$  fraction and only 2% of  $>63\ \mu\text{m}$  fraction.

With respect to chemical composition,  $<2\ \mu\text{m}$  FRDL sample obtained by Atterberg sedimentation showed much lower percentage of  $\text{SiO}_2$ ,  $\text{Al}_2\text{O}_3$ ,  $\text{Na}_2\text{O}$  than the bulk sample. It is easy to agree with this because the  $<2\ \mu\text{m}$  FRDL sample is much less of quartz particles than bulk sample and the sodium amount was washed by treatment processing.

**Table 10. Chemical composition (main components, oxide form) of bulk and  $<2\ \mu\text{m}$  Friedland Clay samples from X-Ray Fluorescence analyses in comparison with literature, indicated in mass %**

Clay Samples	$\text{SiO}_2$ (%)	$\text{TiO}_2$ (%)	$\text{Al}_2\text{O}_3$ (%)	$\text{Fe}_2\text{O}_3$ (%)	$\text{MnO}$ (%)	$\text{MgO}$ (%)	$\text{CaO}$ (%)	$\text{Na}_2\text{O}$ (%)	$\text{K}_2\text{O}$ (%)	$\text{P}_2\text{O}_5$ (%)	LOI 1000°C (%)	$\text{H}_2\text{O}$ - (%)	Total (%)
Friedland Clay - bulk	56.70	0.935	18.09	7.31	0.035	2.01	0.54	0.96	3.01	0.106	7.24	2.65	99.59
Friedland Clay $<2\ \mu\text{m}$ , long-term	51.84	0.921	23.47	6.44	0.016	2.38	0.50	0.43	3.48	0.099	8.12	1.62	99.32
IS-ml (30:70) (Kasbohm, 2003)	58.6	0.1	18.2	11.5		2.7	0.7	0.2	3.4			4.6	100.0

Clay Samples	Ba* (ppm)	Ce* (ppm)	Co* (ppm)	Cr* (ppm)	Cu* (ppm)	Ga* (ppm)	Nb* (ppm)	Ni* (ppm)	Pb* (ppm)	Rb* (ppm)	Sr* (ppm)	Th* (ppm)	U* (ppm)	V* (ppm)	Y* (ppm)	Zn* (ppm)	Zr* (ppm)
Friedland Clay - bulk	295	85	12	119	< 100	23	20	56	28	152	213	11	< 5	199	34	102	185
Friedland Clay $<2\ \mu\text{m}$ , long-term	319	86	13	156	< 100	30	20	61	46	211	227	12	< 5	267	35	169	144

Note: Measured using Philips PW 2404, non wetting agent or/and oxidizer, LOI at 1000°C

To go in detail in clay mineral distributions, TEM experiments were performed on the couple of samples: FRDL - <2  $\mu\text{m}$  with short-term in contact with water (“short-term” sample) and FRDL - <2  $\mu\text{m}$  with long term water contact (“long-term” sample). Beside a few particles of quartz, kaolinite, halloysite, anatase/rutile, feldspar and beidellite which were identified, both samples were observed as dominated by mixed-layer particles including end-members and mixed-layer series: montmorillonite, dioctahedral vermiculite, dioctahedral vermiculite/smectite mixed-layer and illite/smectite mixed-layer (figure 31 and figure 32).

The mixed-layer particles occurred mainly as xenomorphic flakes or slats, some of which formed aggregates or intergrowths with hexagonal arrangement. This overview is consistent with description about “muscovite-montmorillonite mixed-layer from Tertiary marine clay, near Friedland” by Henning and Störr (1986). There was no significant difference in morphology of illite/smectite mixed-layer series compared with dioctahedral vermiculite/smectite mixed-layer series. Mixed-layer particles were not distinguished from end-member firmly based on morphology, neither. Identified dioctahedral vermiculite minerals presented in moiré, small or very large platy crystals as well as xenomorphic particles (figure 31c). A few particles of montmorillonite were identified by TEM semiquantitatively chemical analyses but their morphology could not be distinguished from mixed-layer series (an example in figure 31c).

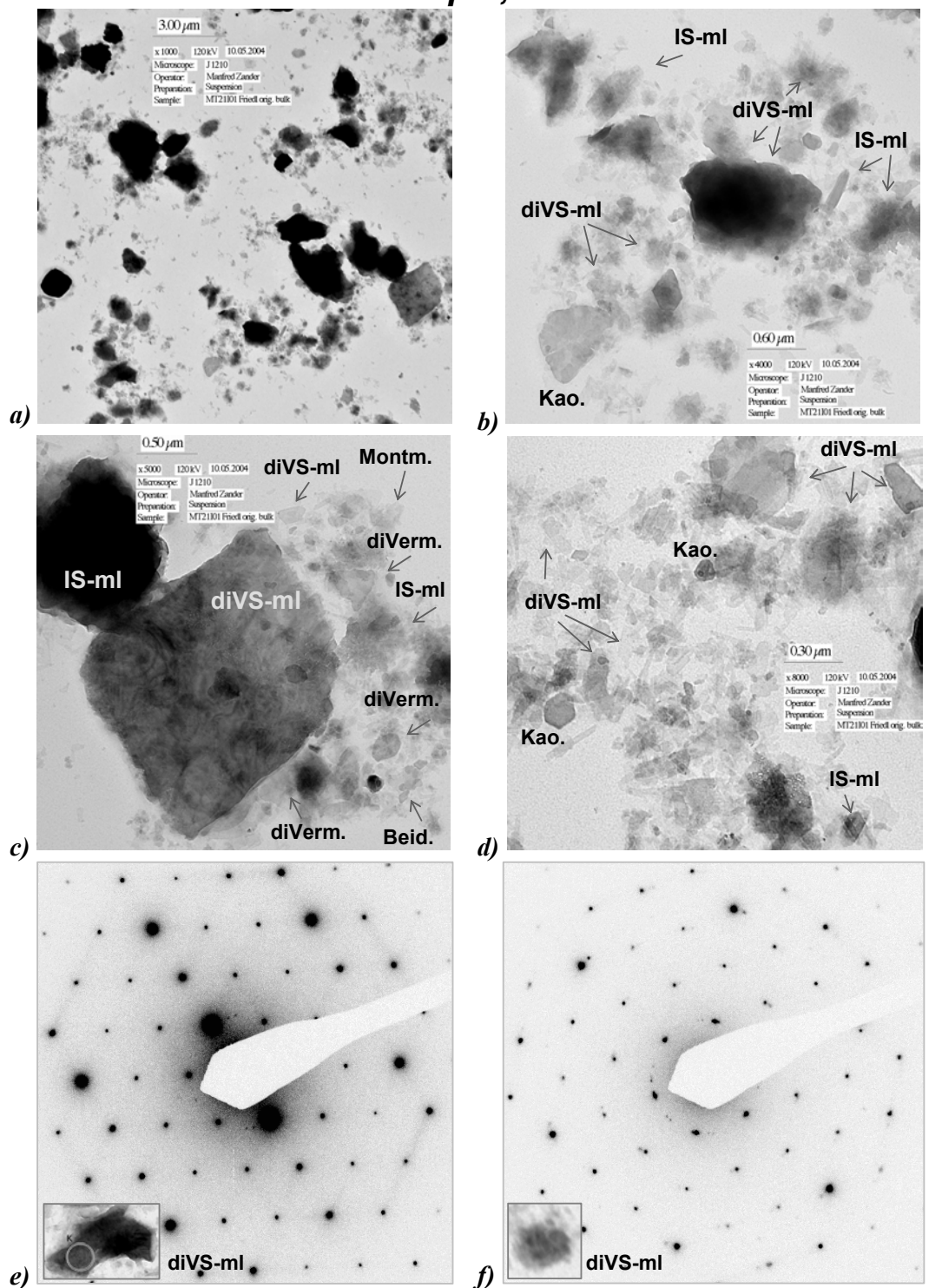
Electron diffraction patterns presented 1M-polytype for xenomorphic and flake dioctahedral vermiculite/smectite mixed-layer particles (figure 31e, f and figure 32e) as well as ring-like polytype for flake illite/smectite mixed-layer particle (figure 32f).

The frequency of mixed-layer particles was presented in figure 33. The “short-term” sample contained more mica-like particles than the “long-term” sample. In both samples, proportions of IS-ml series to diVS-ml series were calculated to relation of approximately 30:70 (30% IS-ml particles and 70% diVS-ml particles). These mixed-layer particles were also presented in ternary charge diagrams contributed from TEM-EDX results (figure 34). The attended particles of the “short-term” sample, in general, were closer to Muscovite-corner (M-corner) than the “long-term” sample. This difference is caused by tetrahedral charge and yielded octahedral charge. For research of variations in octahedral layer only, three main compositions of octahedral Al, Fe and Mg were drawn in ternary diagrams (figure 35). In octahedral ternary plot of the “short-term” sample, substitution Al by Mg showed clearly. Accordingly, octahedral Mg component in the diagram of “long-term” sample looked poorer than that of “short-term” sample.

Based on TEM analyses of individual particles, the structural formulae with average indexes of IS-ml and diVS-ml from FRDL are given in comparison with literatures in table 11.



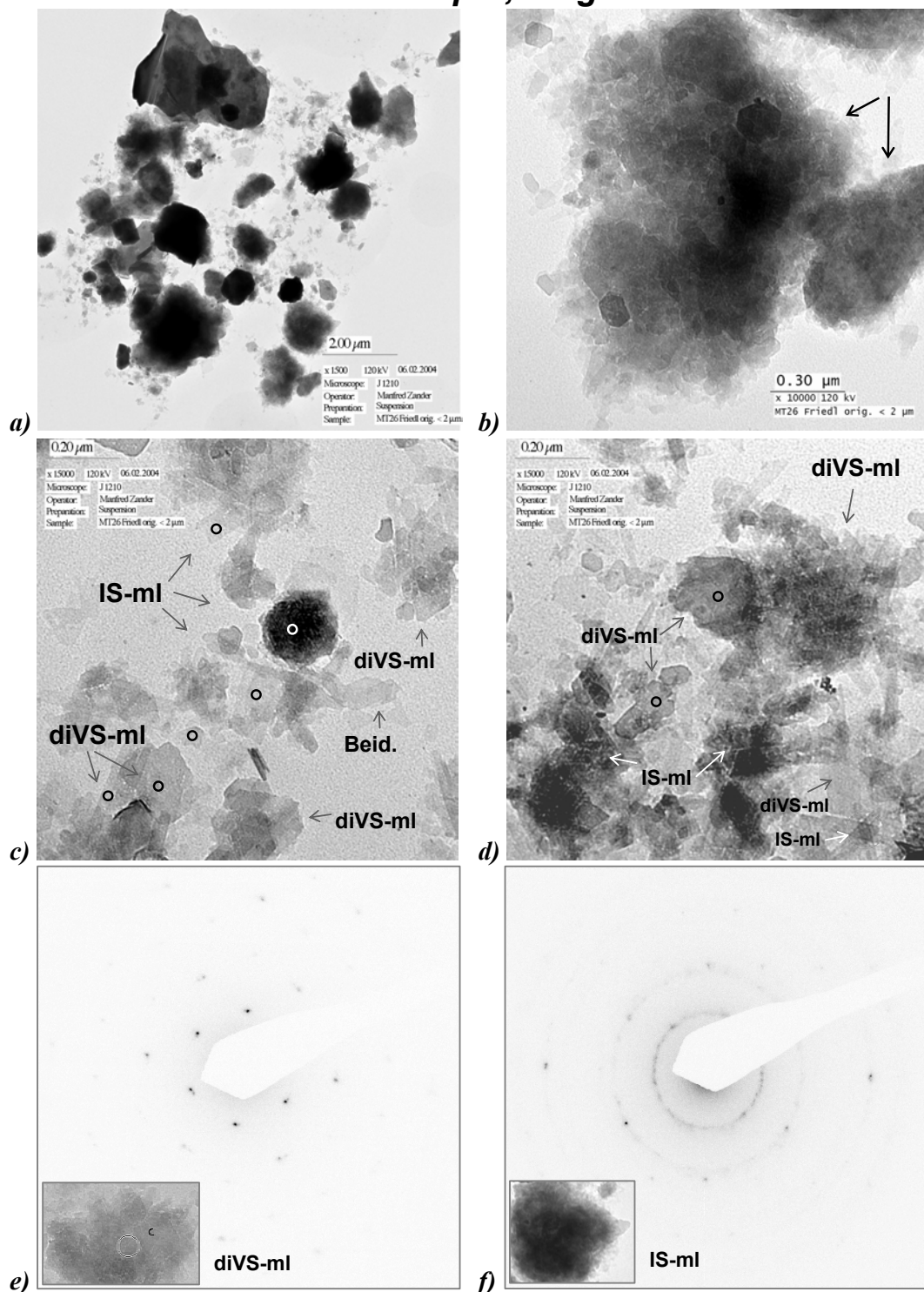
# **FRDL – <2 $\mu\text{m}$ , short-term**



**Figure 31. TEM images of FRDL - <2  $\mu\text{m}$ , short-term**  
 Note: Measured using Jeol JEM-1210; the images show the particles of dioctahedral vermiculite/smectite mixed-layer (diVS-ml), Illite/smectite mixed-layer (IS-ml), dioctahedral vermiculite (diVerm.), montmorillonite (Montm.), beidellite (Beid.) and kaolinite (Kao.)

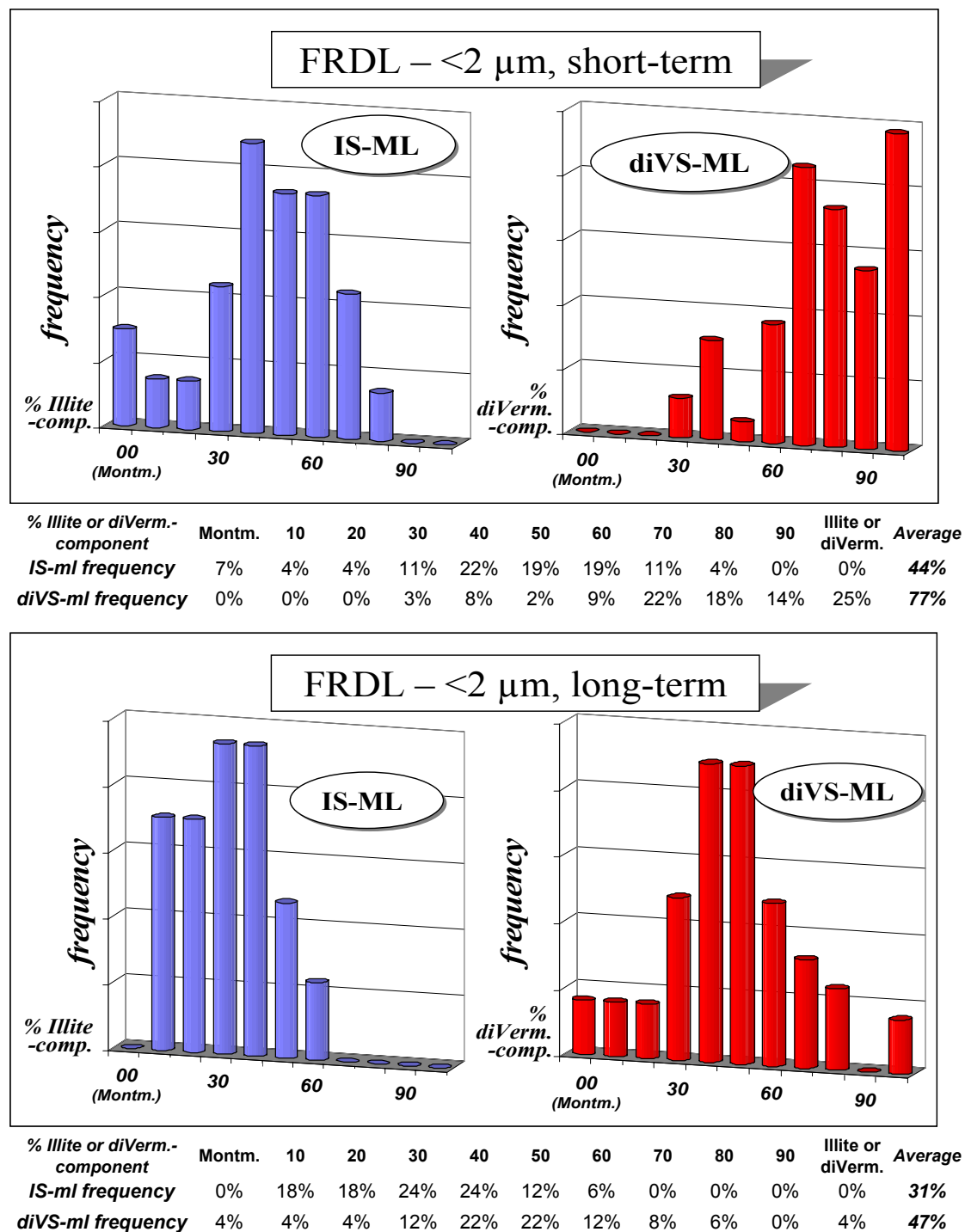
a) Overview of the sample (magnification: 1,000x)  
 b) Zoom of image a) (magnification: 4,000x)  
 c) Zoom of image a) (magnification: 5,000x)  
 d) Zoom of image a) (magnification: 8,000x)  
 e), f) Electron diffractions of diVS-ml particles presented in right bottom box

# **FRDL – <2 $\mu\text{m}$ , long-term**



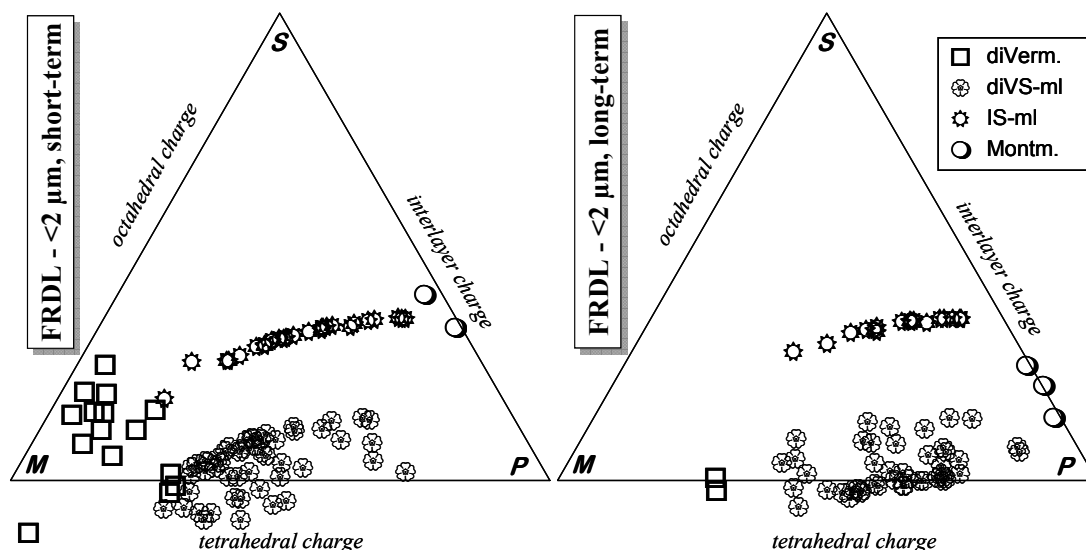
**Figure 32. TEM images of FRDL - <2  $\mu\text{m}$ , long-term**  
 Note: Measured using Jeol JEM-1210; the images show the particles of dioctahedral vermiculite/smectite mixed-layer (diVS-mI), Illite/smectite mixed-layer (IS-mI), dioctahedral vermiculite (diVerm.) and beidellite (Beid.)

a) Overview of the sample (magnification: 1,500x)  
 b) Zoom of image a) (magnification: 10,000x)  
 c) Zoom of image a) (magnification: 15,000x)  
 d) Zoom of image a) (magnification: 15,000x)  
 e), f) Electron diffractions of diVS-mI and IS-mI particles presented in right bottom box



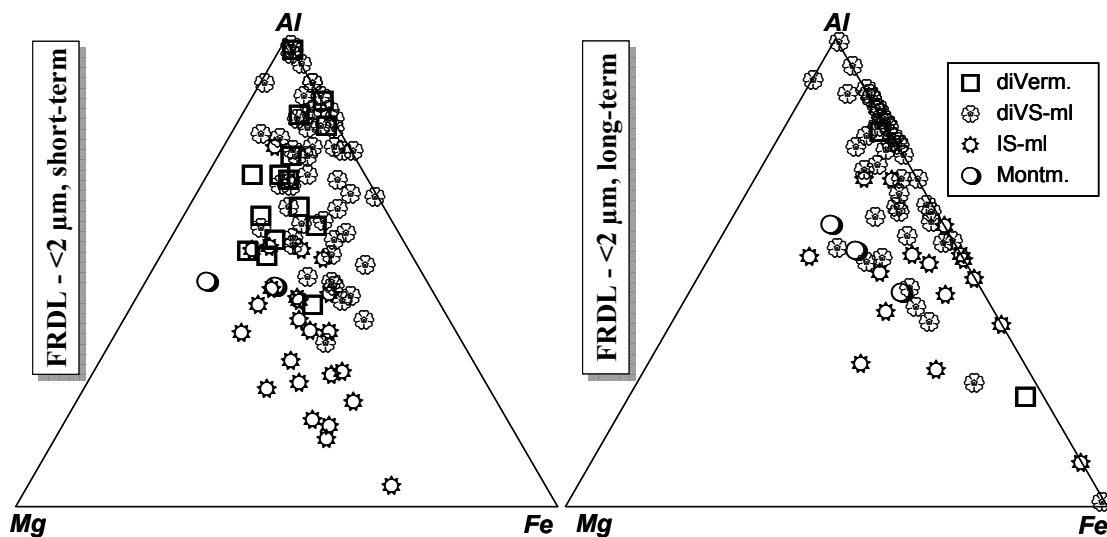
**Figure 33. Tendency of illite- and dioctahedral vermiculite-components distribution in mixed-layer series from Friedland Clay samples, based on TEM-EDX analyses**

Note: Above: histograms and table of FRDL - <2  $\mu\text{m}$ , short-term sample; Bottom: histograms and table of FRDL - <2  $\mu\text{m}$ , long-term sample; Right histograms: illite-components distribution in illite/smectite mixed-layer series (IS-ML); Left histograms: dioctahedral vermiculite-components distribution in dioctahedral vermiculite/smectite mixed-layer series (diVS-ML); % Illite- or % diVerm.-comp.: proportion of illite or dioctahedral vermiculite-component in mixed-layer series (e.g. 00% illite-comp. series: IS-ml series with 00% illite-component or montmorillonite); Montm.: montmorillonite, diVerm.: dioctahedral vermiculite; TEM-EDX measured using Jeol JEM-1210



**Figure 34. Ternary charge diagrams of end-member particles and mixed-layer particles from Friedland Clay samples, based on TEM-EDX analyses**

Note: According to Köster (1977); Ternary octahedral charge – interlayer charge – tetrahedral charge diagrams of FRDL - <2 μm, short-term (left) and FRDL - <2 μm, long-term (right); TEM-EDX Measured using Jeol JEM-1210; C corner: position of theoretical Celadonite  $KAl_2(OH)_2Si_4O_{10}$ ; P corner: position of theoretical Pyrophyllite  $Al_2(OH)_2Si_4O_{10}$ ; M corner: position of theoretical Muscovite  $KAl_2(OH)_2Si_3AlO_{10}$ ; Montm.: montmorillonite, diVerm.: dioctahedral vermiculite, diVS-mI: dioctahedral vermiculite/smectite mixed-layer, IS-mI: illite/smectite mixed layer



**Figure 35. Ternary octahedral Al-Fe-Mg diagrams of end-member and mixed-layer particles from Friedland Clay samples, based on TEM-EDX analyses**

Note: Left: from FRDL - <2 μm, short-term sample; Right: from FRDL - <2 μm, long-term sample; TEM-EDX Measured using Jeol JEM-1210; Montm.: montmorillonite, diVerm.: dioctahedral vermiculite, diVS-mI: dioctahedral vermiculite/smectite mixed-layer, IS-mI: illite/smectite mixed layer

**Table 11.** Mineral formulae [O<sub>10</sub>(OH)<sub>2</sub>] of illite/smectite and dioctahedral vermiculite mixed-layer series from original Friedland Clay samples, based on TEM-EDX analyses

<b>FRDL - &lt;2 µm, short-term</b>	<b>Interlayer</b>						<b>Octahedral layer</b>				<b>Tetra. layer</b>	
	Ca	Mg	Na	K	Fe <sup>2+</sup>	Al	Fe <sup>3+</sup>	Fe <sup>2+</sup>	Mg	Ti	Al	Si
<b>Illite/Smectite mixed-layer (Illite = 40%; Montmorillonite = 60%)</b>												
Average	0.03	0.02	0.21	0.29	0.00	1.26	0.42	0.00	0.29	0.01	0.24	3.76
STDV	0.03	0.03	0.11	0.15	0.00	0.15	0.14	0.00	0.06	0.01	0.03	0.03
Min	0.00	0.00	0.05	0.13	0.00	1.03	0.23	0.00	0.19	0.00	0.20	3.73
Max	0.08	0.09	0.35	0.54	0.00	1.43	0.66	0.00	0.36	0.03	0.27	3.80
<b>Dioctahedral Vermiculite/Smectite mixed-layer (diVerm. = 80%; Montmorillonite = 20%)</b>												
Average	0.02	0.11	0.12	0.23	0.01	1.73	0.17	0.00	0.10	0.02	0.60	3.40
STDV	0.02	0.08	0.10	0.20	0.02	0.18	0.14	0.00	0.06	0.01	0.02	0.02
Min	0.00	0.01	0.00	0.01	0.00	1.42	0.00	0.00	0.00	0.00	0.56	3.38
Max	0.06	0.29	0.31	0.57	0.07	1.97	0.45	0.00	0.18	0.04	0.62	3.44
<b>FRDL - &lt;2 µm, long-term</b>	<b>Interlayer</b>						<b>Octahedral layer</b>				<b>Tetra. layer</b>	
	Ca	Mg	Na	K	Fe <sup>2+</sup>	Al	Fe <sup>3+</sup>	Fe <sup>2+</sup>	Mg	Ti	Al	Si
<b>Illite/Smectite mixed-layer (Illite = 30%; Montmorillonite = 70%)</b>												
Average	0.01	0.12	0.00	0.26	0.00	1.50	0.28	0.00	0.14	0.00	0.19	3.81
STDV	0.01	0.03	0.00	0.04	0.00	0.18	0.13	0.00	0.07	0.00	0.01	0.01
Min	0.01	0.10	0.00	0.23	0.00	1.38	0.19	0.00	0.09	0.00	0.18	3.81
Max	0.02	0.15	0.00	0.29	0.00	1.63	0.37	0.00	0.19	0.00	0.19	3.82
<b>Dioctahedral Vermiculite/Smectite mixed-layer (diVerm. = 50%; Montmorillonite = 50%)</b>												
Average	0.04	0.07	0.00	0.14	0.03	1.74	0.21	0.00	0.04	0.01	0.38	3.62
STDV	0.02	0.04	0.01	0.10	0.05	0.15	0.11	0.00	0.07	0.01	0.02	0.02
Min	0.00	0.00	0.00	0.00	0.00	1.45	0.01	0.00	0.00	0.00	0.35	3.58
Max	0.08	0.11	0.03	0.34	0.13	1.99	0.39	0.00	0.23	0.04	0.42	3.65
<b>HGW98, &lt;2 µm (*)</b>	<b>Interlayer</b>						<b>Octahedral layer</b>				<b>Tetra. layer</b>	
	Ca	Mg	Na	K	Fe <sup>2+</sup>	Al	Fe <sup>3+</sup>	Fe <sup>2+</sup>	Mg	Ti	Al	Si
<b>Illite/Smectite mixed-layer (Illite = 30%; Montmorillonite = 70%)</b>												
Average	0.03	0.07	0.04	0.35	0.00	1.11	0.64	0.00	0.18	0.01	0.25	3.75
STDV	0.02	0.05	0.06	0.10	0.00	0.34	0.32	0.00	0.07	0.02	0.02	0.02
Min	0.01	0.03	0.00	0.29	0.00	0.54	0.43	0.00	0.09	0.00	0.23	3.72
Max	0.06	0.12	0.12	0.52	0.00	1.35	1.17	0.00	0.26	0.04	0.28	3.77
<b>Dioctahedral Vermiculite/Smectite mixed-layer (diVerm. = 60%; Montmorillonite = 40%)</b>												
Average	0.04	0.10	0.01	0.21	0.00	1.66	0.28	0.00	0.06	<0.01	0.45	3.55
STDV	0.02	0.04	0.03	0.12	0.00	0.13	0.10	0.00	0.07	0.01	0.02	0.02
Min	0.01	0.03	0.00	0.09	0.00	1.42	0.13	0.00	0.00	0.00	0.43	3.52
Max	0.06	0.18	0.10	0.43	0.00	1.87	0.44	0.00	0.19	0.01	0.48	3.57

*Note: Measured using Jeol JEM-1210; (\*): according to Henning & Kasbohm (1998); Average: average index, Min: minimal index, Max: maximal index, STDV: standard deviation*

In aim of determination of iron variations, which were observed by XRF and TEM-EDX measurements and presented above, bulk FRDL and <2  $\mu\text{m}$  FRDL (“long-term”) samples were analyzed by Mössbauer spectroscopy. MB can determine Fe-mineralogy and relative abundance of Fe-bearing minerals that cannot be obtained from XRF spectroscopy.

Mössbauer spectra of bulk and <2  $\mu\text{m}$  FRDL samples (figure 36) showed that they consisted of four quadrupole doublets, which superposed to form single asymmetric spectra. According to relative intensities and positions of these four Fe phases, it was possible to distinguish various Fe species. All of 8 phases of 2 FRDL samples had no magnetic hyperfine field, so that there was no magnetic phase, such as hematite, in these samples. According to Menil (1985) who concluded that  $\text{Fe}^{2+}$  octahedral coordination had  $\delta$  from 1.43 to 0.46 mm/s and  $\text{Fe}^{3+}$  octahedral coordination had  $\delta$  from 0.46 to 0.30 mm/s, the both FRDL samples were observed with 2 phases of  $\text{Fe}^{2+}$  and 2 phase of  $\text{Fe}^{3+}$  for each (appendix 7).

In the spectra of both samples, 2 first quadrupole doublets (CM-5.1 and CM-6.1), which had  $\delta$  about 1.24 and 1.20 mm/s together with  $\Delta$  about 1.82 and 1.74 mm/s, respectively, are commonly for a phase of  $\text{Fe}^{2+}$ -ion in silicate. In comparison with  $\Delta$  of  $\text{Fe}^{2+}$  from research of Heller-Kallai & Rozenson (1981), these phases belong to dioctahedral mica (*trans*-octahedral).

2 second quadrupole doublets of these FRDL samples were identified as other  $\text{Fe}^{2+}$  phases (CM-5.2 and CM-6.2), which are completely similar with  $\delta = 1.13$  mm/s,  $\Delta = 2.73$  mm/s and  $\Gamma = 0.36 - 0.37$  mm/s. In comparison with XRD decompositions of FRDL samples and referencing research on 2:1:1 layer minerals by Ballet *et al.* (1985), these phases were identified as octahedral  $\text{Fe}^{2+}$ -ion in chlorite.

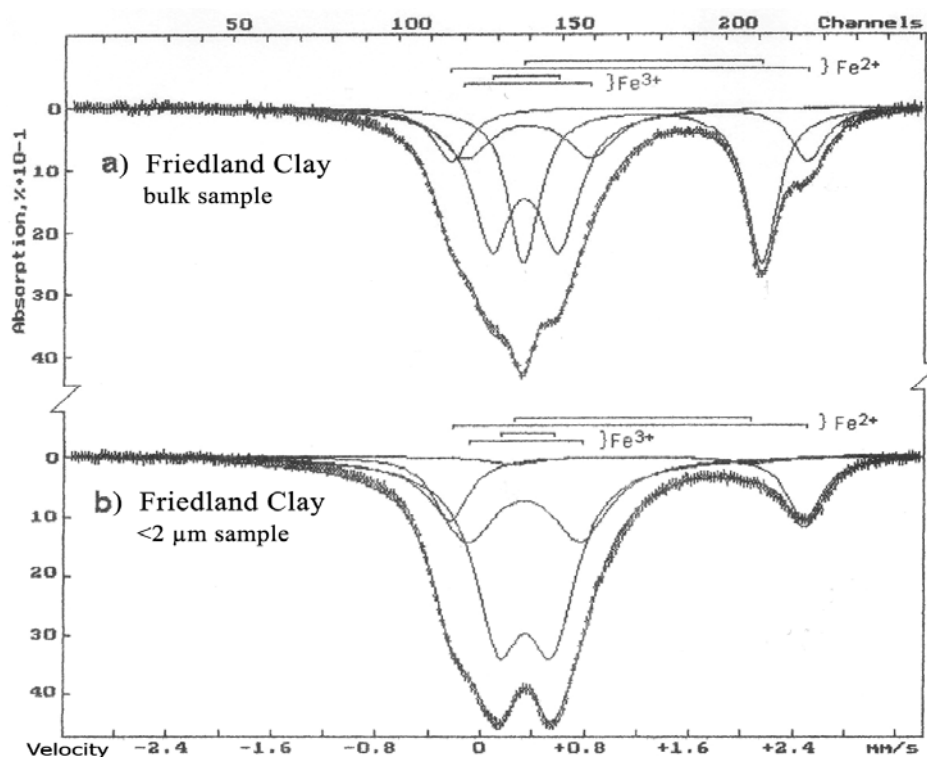
The main central doublets at about over 0.3 mm/s of  $\delta$  characterizing for  $\text{Fe}^{3+}$ -ion component in dioctahedral silicate were obtained twice in both 2 samples of FRDL and were different in  $\Delta$  values. The  $\Delta$  values of CM-5.4 and CM-6.4 (1.04 mm/s and 0.95 mm/s) were approximately twice that of CM-5.3 and CM-6.3 (0.52 mm/s and 0.42 mm/s) corresponding to the relation between  $\Delta$  of *trans*-vacant and that of *cis*-vacant. The obtained  $\delta$ ,  $\Delta$  and  $\Gamma$  are around the corresponding values of illite, montmorillonite, muscovite, glauconite from many samples studied by Heller-Kallai & Rozenson (1981) (the authors did not mention to mixed-layer mineral). Therefore, these doublets were interpreted to mixed-layer mineral which dominates in the two samples.

Summarizing XRF- and MS-measurements in combination with results from XRD and TEM analyses, it can be concluded that bulk and <2  $\mu\text{m}$  FRDL samples contained  $\text{Fe}^{2+}$ -ion in dioctahedral mica,  $\text{Fe}^{2+}$ -ion in chlorite and  $\text{Fe}^{3+}$ -ion in *cis*- and *trans*-octahedral of mixed-layer mineral. Because of significant difference in relatively height of 2 first  $\text{Fe}^{2+}$ -ion

sub-spectra (area of component), the distributions of Fe-rich dioctahedral mica of 2 samples are different. This finding is in agreement with the conclusion of more mica-like particles in “short-term” sample in comparison with “long-term” sample.

Beside the identified mixed-layer phase, illite and dioctahedral vermiculite (mica like phase), montmorillonite, kaolinite, beidellite and chlorite, FRDL also includes muscovite and glauconite as main clay minerals (Henning & Kasbohm, 1998). About the non-clay mineral phases, quartz, feldspar, calcite, dolomite, siderite, pyrite, halite, alunite, jarosite, gypsum, rozenite, roemerite and szomolnokite are identified in the clay (Henning & Kasbohm, 1998).

From the work of Ammann (2003), Friedland Clay (Friedländer) was identified with approximately 37 meq/100g of cation exchange capacity (copper complex exchange method) and approximately 280 m<sup>2</sup>/g of specific surface area. The former work by Henning & Kasbohm (1998) identified 54 meq/100g of cation exchange capacity for FRDL.



**Figure 36. Mössbauer spectra of bulk and <2 µm Friedland Clay samples at room temperature**

Each spectrum showed sub-spectra of chlorite (Fe<sup>2+</sup>), di-Mica (Fe<sup>2+</sup>) and *cis*- and *trans*- mixed-layer phases (Fe<sup>3+</sup>) (see more in appendix 7)

Note: Measured using Ms-1104Em spectrometer at St-Petersburg State University, Russia; a) Friedland Clay – bulk sample, b) Friedland Clay - <2 µm sample; <sup>57</sup>Co isotopes resource, subspectra were fitted by Univem MS program

In sum, FRDL is characterized as mixed-layer dominated clay. Whilst “FRDL - <2  $\mu\text{m}$ , short-term” sample contained mostly IS-ml series with 40% illitic layer – 60% smectitic layer and diVS-ml series with 80% dioctahedral vermiculitic layer – 20% smectitic layer, “FRDL - <2  $\mu\text{m}$ , long-term” sample contained mostly IS-ml series with 30% illitic layer – 70% smectitic layer and diVS-ml series with 50% dioctahedral vermiculitic layer – 50% smectitic layer. They are different in mica-like phase which affects also the variety of iron content. Iron amount in both samples is identified as in iron-bearing clay minerals.

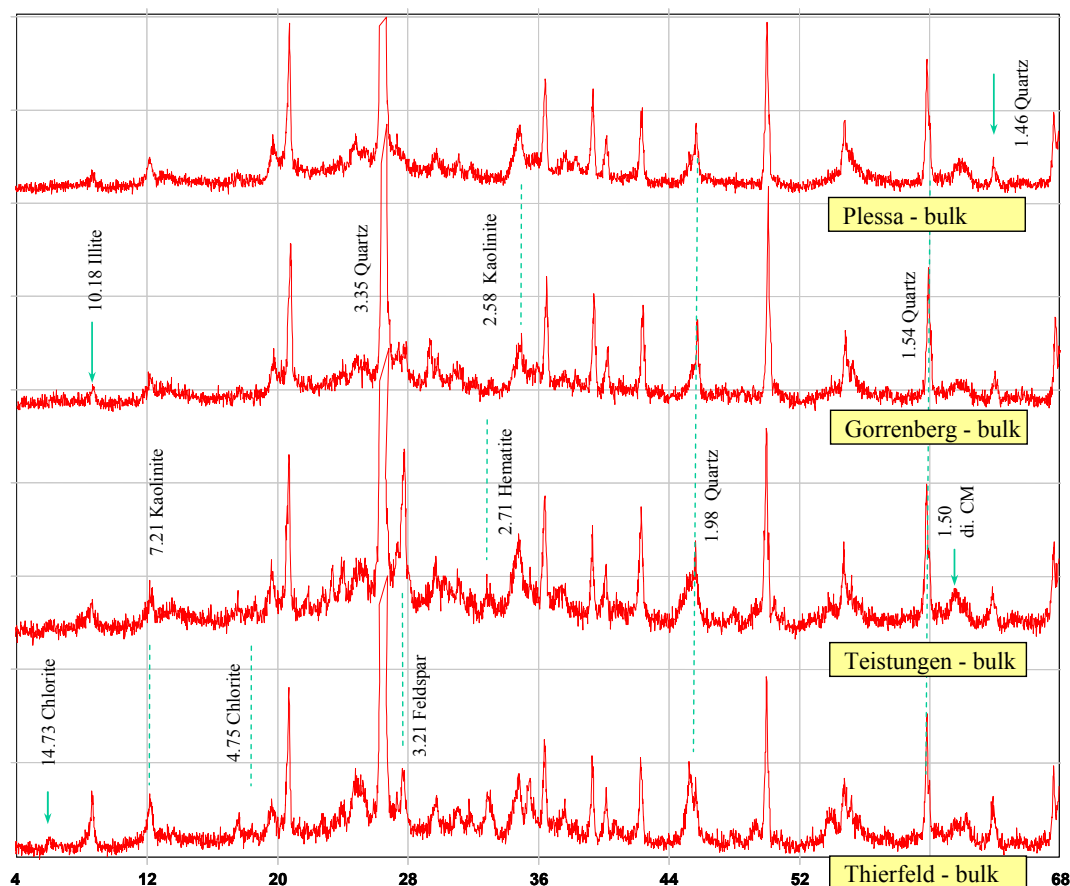
Considering the differences of TEM results between two Friedland Clay samples (figure 34, figure 35 and table 11), mineral matter of Friedland Clay was undergoing an alteration process in contact with water. Illitic particles altered to diVS-ml with increasing smectite-amount and the original IS-ml particles (40% illitic layers) showed a slight smectitization process (to 30% of illitic layers) after two months of contact with water. Linked with alteration is a rearrangement of the octahedral layer to higher Al- as well as less Mg- and Fe-amounts. The processes are combined with a reduced interlayer charge from 0.09 per unit cell for “FRDL - <2  $\mu\text{m}$ , short-term” to 0.05 per unit cell for “FRDL - <2  $\mu\text{m}$ , long-term” (the charge values are calculated from TEM-EDX analyses, table 11).



## 4.4 Mica dominated clays

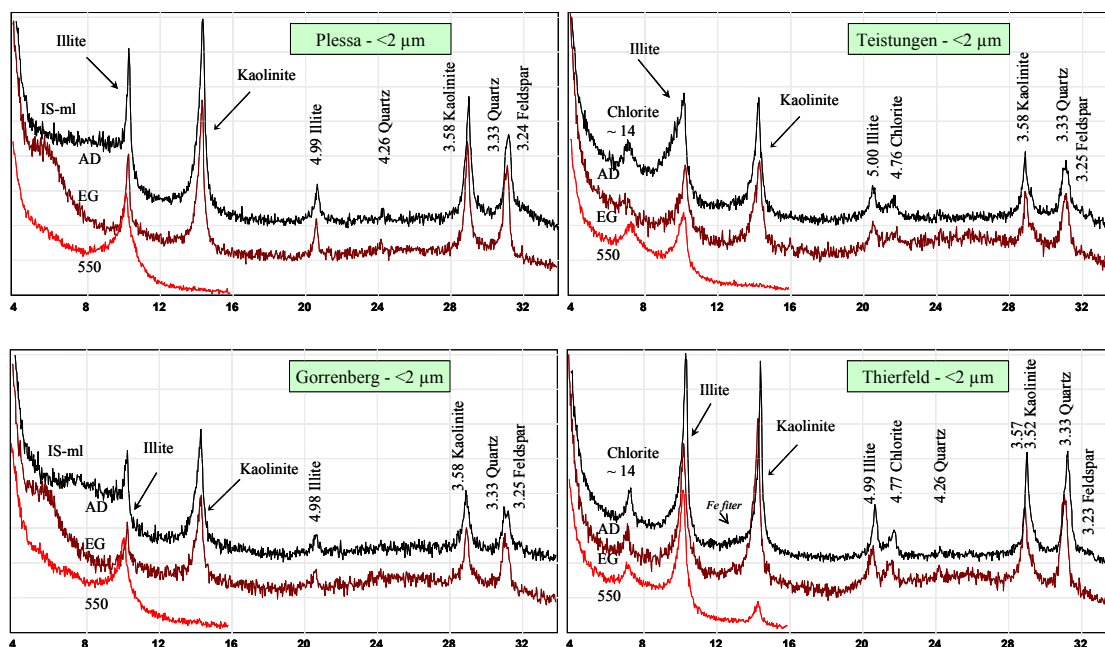
### 4.4.1 German reference clays

Representative XRD patterns, in figure 37 and figure 38, from randomly oriented powder mounts of bulk Plessa, Gorrenberg, Teistungen and Thierfeld samples and oriented specimens of their < 2  $\mu\text{m}$  fractions confirmed that the clay mineral phases of these clays include illite, kaolinite and chlorite mainly like published in Kranz *et al.* (1990). XRD patterns also demonstrated the presence of hematite, quartz and feldspar (plagioclase and orthoclase). Clay mineral phase contributed from 44% to 53% (in mass) in these clays (Kranz *et al.*, 1990; see in appendix 2). Ammann (2003) calculated that amounts of illite in total clay mineral of Plessa, Teistungen and Thierfeld were quite high as 52%, 77% and 80%, respectively. Therefore, these clays were called simplifiably as “mica dominated clays”



**Figure 37. XRD patterns of German clays from powder mount,  $^{\circ}2\theta$   $\text{CuK}\alpha$  position**

Note: Measured using Siemens D5000; From above to bottom: Plessa – bulk; Gorrenberg – bulk; Teistungen – bulk and Thierfeld – bulk; these samples were milled and sieved to <63  $\mu\text{m}$  before measuring; the patterns show the peaks of kaolinite, chlorite, dioctahedral clay mineral (di.CM): illite, illite/smectite mixed-layer series (IS-ml) as well as hematite, quartz and feldspar (plagioclase and orthoclase)



**Figure 38.** XRD patterns of German clays from oriented specimens,  $^{\circ}2\theta$  CoK $_{\alpha}$  position

Note: Measured using HZG 4 / Seifert C3000; XRD patterns including air-dried (AD), ethylene-glycol saturated (EG) and 550 degree C heated (550) specimen patterns; left above: Plessa -  $<2 \mu\text{m}$ ; left bottom: Gorrenberg -  $<2 \mu\text{m}$ ; right above: Teistungen -  $<2 \mu\text{m}$  and right bottom: Thierfeld -  $<2 \mu\text{m}$ ; the patterns show the peaks of kaolinite, chlorite, illite, illite/smectite mixed-layer series (IS-sm), quartz and feldspar

Normally, the peak at  $10 \text{ \AA}$  is composed of two major components, one wide and displaced to a position greater than  $10 \text{ \AA}$  and another narrow and centered at very close to  $10 \text{ \AA}$  (Meunier & Velde, 2004). The first one is signature of poor-ordered illite particles and the second is from the well-ordered illite particles. All of illite from German clays included such two components. From the components, any shifting under glycol saturation could not be observed.

German clays also contained kaolinite. The kaolinite had two components: well-ordered kaolinite and poor-ordered kaolinite, which were identified by oriented specimen analyses. The poor-ordered kaolinite 001-peak occurred on the position larger than  $7.2 \text{ \AA}$  and the well-ordered kaolinite peak placed at about  $7.15 \text{ \AA}$ .

### Plessa

Plessa mine is located in Bad Liebenwerda, Brandenburg/Germany. The clay contains about 53% clay mineral amount (Kranz *et al.*, 1990). Plessa had the highest percentage of kaolinite with 24% in total chemical composition among the four clays. According to the calculation by Ammann (2003), Plessa clay minerals included 52% illite, 9% smectite and 39% kaolinite whilst Teistungen and Thierfeld had no smectite phase. By XRD analysis for powder mount, Plessa also showed the lowest intensity of  $10 \text{ \AA}$  peak (figure 37).

By TEM observation, Plessa presented (i) large, thick and xenomorphic particles and (ii) small laths (figure 39a, b, c). Almost all of the particles were identified as dioctahedral vermiculite (diVerm.), which has deficient charge and K-amount in the interlayer in comparison with illite in the sense of the international mica-classification (Rieder *et al.*, 1998). Phases of diVS-ml, IS-ml, montmorillonite, beidellite as well as quartz and anatase were identified from Plessa sample. Structural formulae of analyzed clay minerals were calculated particle by particle and shown in table 12. Especially, Plessa diVerm. showed lower index of Mg but high index of Ca in opposite to the other German reference clays. This result is suitable with chemical composition by Kranz *et al.* (1990) (appendix 4).

The diVerm.-phase could present the 10 Å interference in the Plessa XRD-patterns. Using WinFit deconvolution (Krumm, 1994), Plessa diVerm. (or charge and K-deficient illite) occurred as well-ordered particles with ~40 layers per stack (CSD of 400 Å) and as poor-ordered particles with ~10 layers per stack (CSD of 100 Å). Besides, one component is overlapping with illite peak at 11.14 Å from Plessa air-dried specimen profile expanded to 16.51 Å after ethylene-glycol saturation. According to Moore & Reynolds (1997), these extensions belong to diagnostic range of illite/montmorillonite mixed-layer series, so that the presence of mixed-layer phase in Plessa is demonstrated. By electronic diffraction, diVS-ml presented a  $2M_1$  polytype (figure 39c).

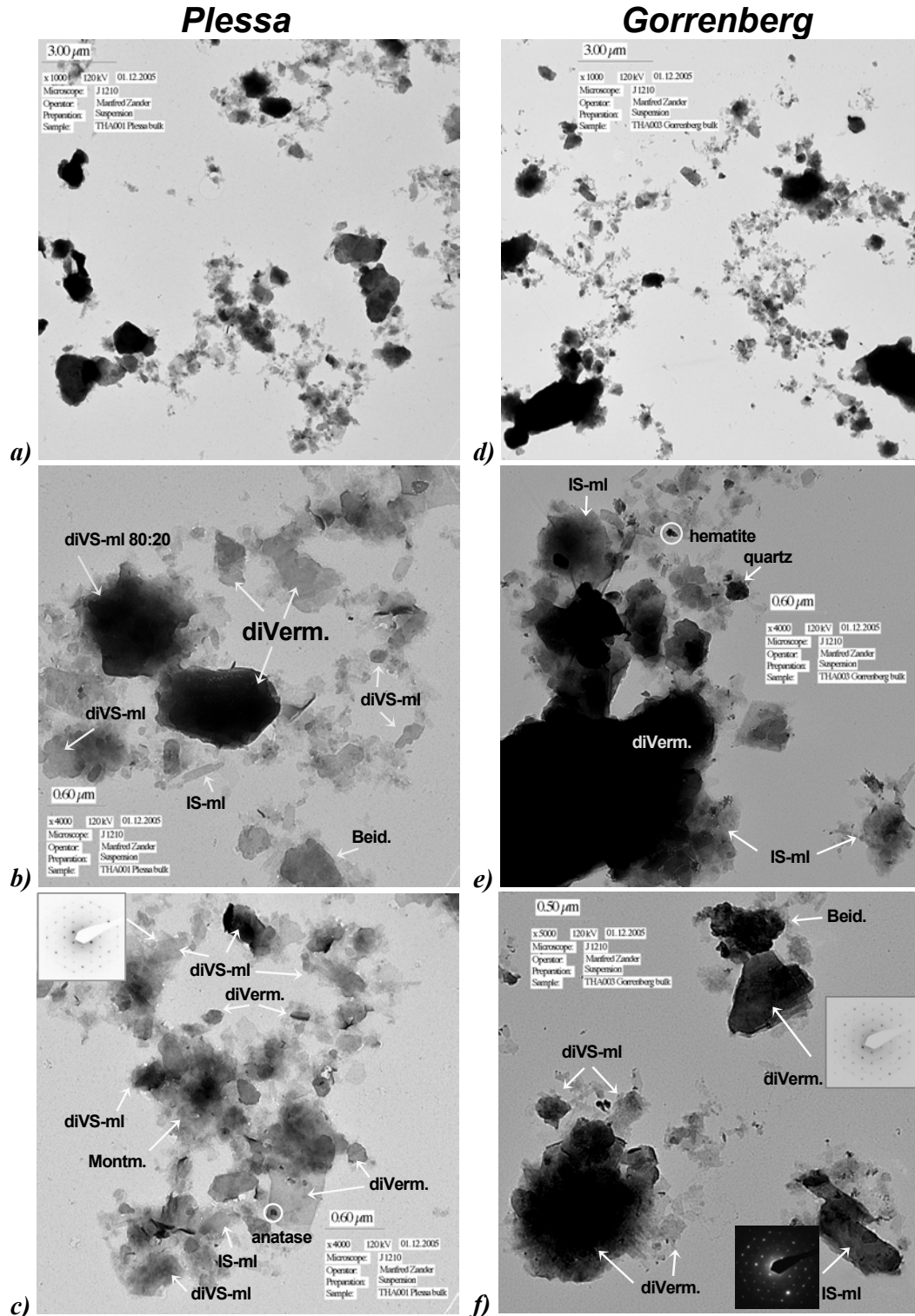
About only 27.6% of Plessa sample is smaller than 2 µm (Kranz *et al.*, 1990; see in appendix 3). According to Ammann (2003), Plessa has a cation exchange capacity of 28 meq/100g (copper complex exchange method) and the specific surface area of 200 m<sup>2</sup>/g.

### *Gorrenberg*

Gorrenberg clay is originated from Traustein, Thuringia/Germany. This clay, containing about 45% clay minerals amount (Kranz *et al.*, 1990), was characterized similarly as Plessa clay. XRD analyses confirmed the presence of 2:1 sheet silicates (illite, IS-ml), kaolinite, chlorite as well as quartz, feldspar (plagioclase and orthoclase) and hematite.

Almost all of particles identified by TEM-EDX analysis from Gorrenberg sample is dioctahedral vermiculite (charge and K-deficient illite) (figure 39d, e, f). Gorrenberg diVerm. showed  $1M$  polytype by electronic diffraction analysis (figure 39f). Two morphology types of clay particles in fraction size <2 µm were observed: thick aggregates larger than 1 µm and very fine, xenomorphic plates smaller than 0.5 µm. Accordingly, deconvolution 10 Å peak from XRD profile by WinFit obtained CDS of 320 Å (~32 layers per stack) as well ordered phase and CDS of 70 Å (~7 layers per stack) as disordered or thinner particle phase. Besides, a weak peak at 12.68 Å expanded to 16.92 Å by ethylene-glycol saturation demonstrated IS-ml and/or diVS-ml phase in Gorrenberg clay (figure 38).

The part of clay fraction size smaller 2 µm of Gorrenberg contributed about 29.6% of the bulk sample (Kranz *et al.*, 1990; see in appendix 3).



**Table 12.** Mineral formulae  $[O_{10}(OH)_2]$  of diVerm., diVS-ml, IS-ml and smectite from German clays, based on TEM-EDX analyses

	Interlayer					Octahedral layer				Tetra. layer		
	Ca	Mg	Na	K	Fe <sup>2+</sup>	Al	Fe <sup>3+</sup>	Fe <sup>2+</sup>	Mg	Ti	Al	Si
<b>Diocahedral Vermiculite</b>												
Plessa	0.17	0.04	0.13	0.14	0.04	1.81	0.13	0.00	0.06	0.02	0.81	3.20
Gorrenberg	0.04	0.13	0.04	0.29	0.02	1.61	0.22	0.00	0.06	0.08	0.81	3.19
Teistungen	0.06	0.26	0.03	0.21	0.01	1.61	0.25	0.00	0.13	0.03	0.86	3.14
Thierfeld	0.03	0.26	0.02	0.26	0.00	1.59	0.30	0.00	0.10	0.02	0.88	3.12
<b>Diocahedral Vermiculite/Smectite mixed-layer</b>												
Plessa – 70/30	0.05	0.06	0.02	0.25	0.00	1.81	0.12	0.00	0.07	0.01	0.52	3.48
Gorrenberg – 60/40	0.02	0.13	0.01	0.16	0.01	1.62	0.24	0.00	0.12	0.03	0.45	3.55
Teistungen – 70/30	0.02	0.09	0.02	0.28	0.02	1.75	0.15	0.00	0.08	0.02	0.52	3.48
Thierfeld – 70/30	0.01	0.05	0.04	0.36	0.00	1.71	0.14	0.00	0.13	0.04	0.52	3.48
<b>Illite/Smectite mixed-layer</b>												
Plessa – 50/50	0.07	0.03	0.09	0.33	0.00	1.57	0.14	0.00	0.24	0.01	0.29	3.71
Gorrenberg – 40/60	0.02	0.12	0.00	0.26	0.00	1.50	0.27	0.00	0.18	0.00	0.21	3.79
Teistungen – 50/50	0.00	0.06	0.05	0.43	0.00	1.72	0.12	0.03	0.04	0.00	0.27	3.73
Thierfeld – 50/50	0.02	0.05	0.02	0.40	0.00	1.51	0.25	0.04	0.11	0.03	0.31	3.69
<b>Beidellite</b>												
Plessa	0.12	0.03	0.03	0.04	0.00	1.88	0.16	0.00	0.05	0.00	0.62	3.38
Gorrenberg	0.03	0.04	0.02	0.05	0.05	1.78	0.25	0.01	0.00	0.04	0.54	3.46
Teistungen	0.03	0.05	0.01	0.08	0.03	1.87	0.17	0.00	0.01	0.02	0.51	3.49
Thierfeld	0.01	0.03	0.13	0.08	0.12	1.93	0.13	0.00	0.00	0.02	0.55	3.45
<b>Montmorillonite</b>												
Plessa	0.00	0.00	0.20	0.20	0.00	1.32	0.35	0.00	0.32	0.00	0.04	3.96

Note: Measured using Jeol JEM-1210; data is average index; 70/30 (and the similar ratios) means mixed-layer series with 70% of the first member (dioctahedral vermiculite or illite) and 30% of the second member (smectite); mixed-layer series did not include end-members

### Teistungen

The clay, originated from Worbis, Thuringia/Germany, includes about 44% in mass of clay mineral amount (Kranz *et al.*, 1990), therein 77% illite, 14% kaolinite and 17% chlorite (Ammann, 2003). Differently from Plessa and Gorrenberg, the chlorite peaks presented obviously in XRD patterns. Conversely, Teistungen have lowest amount of kaolinite among the German reference clays. Beside the proof about sheet silicate phase, XRD and TEM-EDX results also confirmed non-clay mineral phase including quartz, feldspar (plagioclase and orthoclase), anatase and especially hematite. The hematite phase and other iron-bearing clay phases were also determined using Mössbauer spectroscopy analyses (for details, see chapter 4.5.2).

Almost all of particles in the  $<2\ \mu\text{m}$  fraction of Teistungen was identified as diVerm. or diVS-ml with high proportion of diVerm. layer (figure 40a, b, c) because they have charge and K-deficient in the interlayer in comparison with illite in the sense of the international mica-classification by IMA (Rieder *et al.*, 1998). They are mostly fine, thin and platy except some small aggregates. The diVerm. phase, could form the  $10\ \text{\AA}$  peak, was determined as two components: a component of about 6 layers per stack and a component of about 17 layers per stack, corresponding to CSD values of  $60\ \text{\AA}$  and  $170\ \text{\AA}$ , respectively (deconvolution by WinFit). Electron diffraction determined that Teistungen diVerm. and diVS-ml particles represented  $2M_1$  polytype mostly (figure 40b). Mineral formulae of diVerm., diVS-ml as well as IS-ml and smectite (beidellite and montmorillonite) are shown in table 12.

Teistungen clay contained about 51.3% amount of  $<2\ \mu\text{m}$  fraction (Kranz *et al.*, 1990), which is much higher than those of other German reference clays. However, the clay has the specific surface area of only  $140\ \text{m}^2/\text{g}$  and a cation exchange capacity of  $17\ \text{meq}/100\text{g}$  (copper complex exchange method) (Ammann, 2003; Ammann *et al.*, 2005).

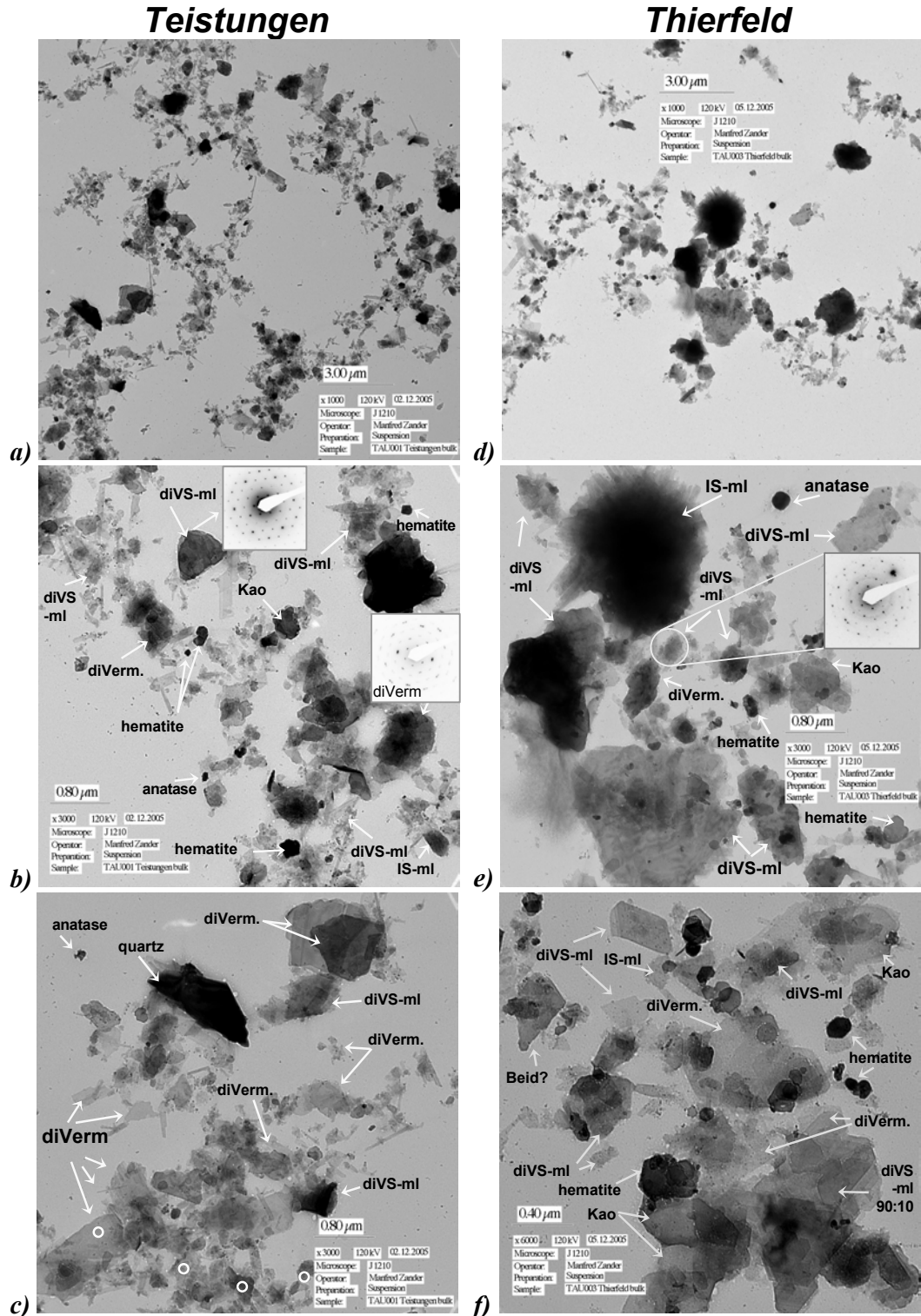
### Thierfeld

Thierfeld clay mine located in Zwickau, Saxony/Germany. The sample contained about 53% clay minerals amount (Kranz *et al.*, 1990). Ammann (2003) calculated that the clay minerals amount include 80% illite, 3% kaolinite and 17% chlorite. These clay minerals were verified by the XRD proof, too.

Thierfeld clay minerals, in the  $<2\ \mu\text{m}$  fraction, represented a variety of quite large plates, thick aggregates, slats and very fine plates (figure 40d, e, f). Deconvolution by WinFit from XRD pattern of bulk sample,  $10\ \text{\AA}$  component of Thierfeld included well-ordered phase with about 29 layers per stack (CSD =  $290\ \text{\AA}$ ) and poor-ordered phase with about 8 layers per stack (CSD =  $85\ \text{\AA}$ ). A part of the component was labelled as diVerm. or diVS-ml with high proportion of diVerm. layer in the TEM-EDX results. Figure 40e shows an example  $2M_1$  polytype of diVS-ml particle.

Especially in the Thierfeld XRD pattern of powder mount, hematite peaks were very clearly (figure 37). This hematite component, caused the very dark brown colour of Thierfeld clay, was indicated about 4.5% in the total mineral amount (Kranz *et al.*, 1990; see in appendix 2). Under TEM observation, hematite particles were commonly very small but few were about a half of micrometer in the dimension and in idiomorphic hexagonal shapes (figure 40f).

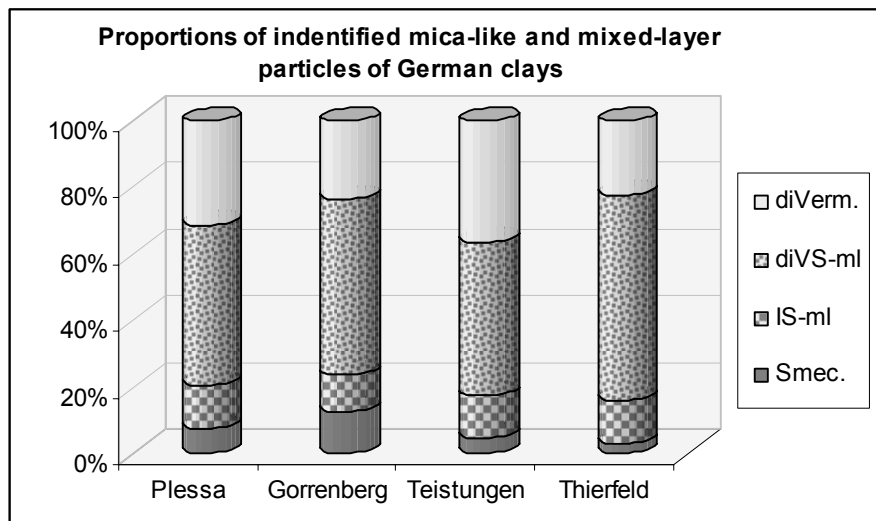
The part of  $<2\ \mu\text{m}$  contributed approximately 39.3% in the bulk Thierfeld sample (Kranz *et al.*, 1990). Its cation exchange capacity is  $14\ \text{meq}/100\text{g}$  (copper complex exchange method) and specific surface area is  $73\ \text{m}^2/\text{g}$  according to calculation by Ammann (2003).



**Figure 40. TEM images of Teistungen and Thierfeld samples**

a) Overview of Teistungen sample (1,000x); b) Zoom of image a) (3,000x) and electron diffractions of diVS-ml and diVerm. particles; c) Zoom of image a) (3,000x); d) Overview of Thierfeld sample (1,000x); e) Zoom of image d) (3,000x) and electron diffraction of diVS-ml particle; and f) zoom of image d) (6,000x)

Note: Measured using Jeol JEM-1210; the images show the particles of montmorillonite (Montm.), dioctahedral vermiculite (diVerm.), dioctahedral vermiculite/smectite mixed-layer (diVS-ml), illite/smectite mixed-layer (IS-ml), kaolinite (Kao.), beidellite(?) (Beid.?), quartz, anatase (rutile) and hematite



**Figure 41. Proportions of identified mica-like and mixed-layer particles of German clays**

*Note: Data from TEM-EDX analyses using Jeol JEM-1210; light color filling presented dioctahedral vermiculite component, confetti filling presented dioctahedral vermiculite/smectite mixed-layer component; square filling presented illite/smectite mixed-layer component and dark filling presented smectite component*

In conclusion, German clays include significant amount of dioctahedral vermiculite, which caused sharp and high  $10 \text{ \AA}$  peak in XRD patterns and were observed very often by TEM-EDX analyses. Series of diVS-ml are also the main component in German reference clays. Besides, the German clays also contain IS-ml, beidellite, chlorite and kaolinite as clay mineral phases. The frequency of the mica-like phase, smectite phase and mixed-layer phases between mica-like component and smectite component was estimated as in figure 41. Among the non-clay minerals identified in German clay samples, contents of hematite are importantly making these clays differentiated. Especially, hematite presented in remarkable content in Teistungen and Thierfeld samples. The contribution of hematite and iron-bearing minerals in total of iron amount as well as in the bulk sample was presented in the chapter “dithionite treated clays” (chapter 4.5.2).



## 4.5 Treated clays

### 4.5.1 Acid treated series

Acid treatments by HCl solution with different concentrations of acid solution and different temperatural conditions were performed to Friedland Clay. This contribution involved six treated samples including:

- FRDL, HCl 1.0 M, 100°C, 2 h (treated FRDL 5)
- FRDL, HCl 1.5 M, 60°C, 2 h (treated FRDL 6)
- FRDL, HCl 1.5 M, 100°C, 2 h (treated FRDL 10)
- FRDL, HCl 1.8 M, 100°C, 2 h (treated FRDL 13)
- FRDL, HCl 2.0 M, 80°C, 2 h (treated FRDL 14)
- FRDL, HCl 2.0 M, 100°C, 2 h (treated FRDL 16)

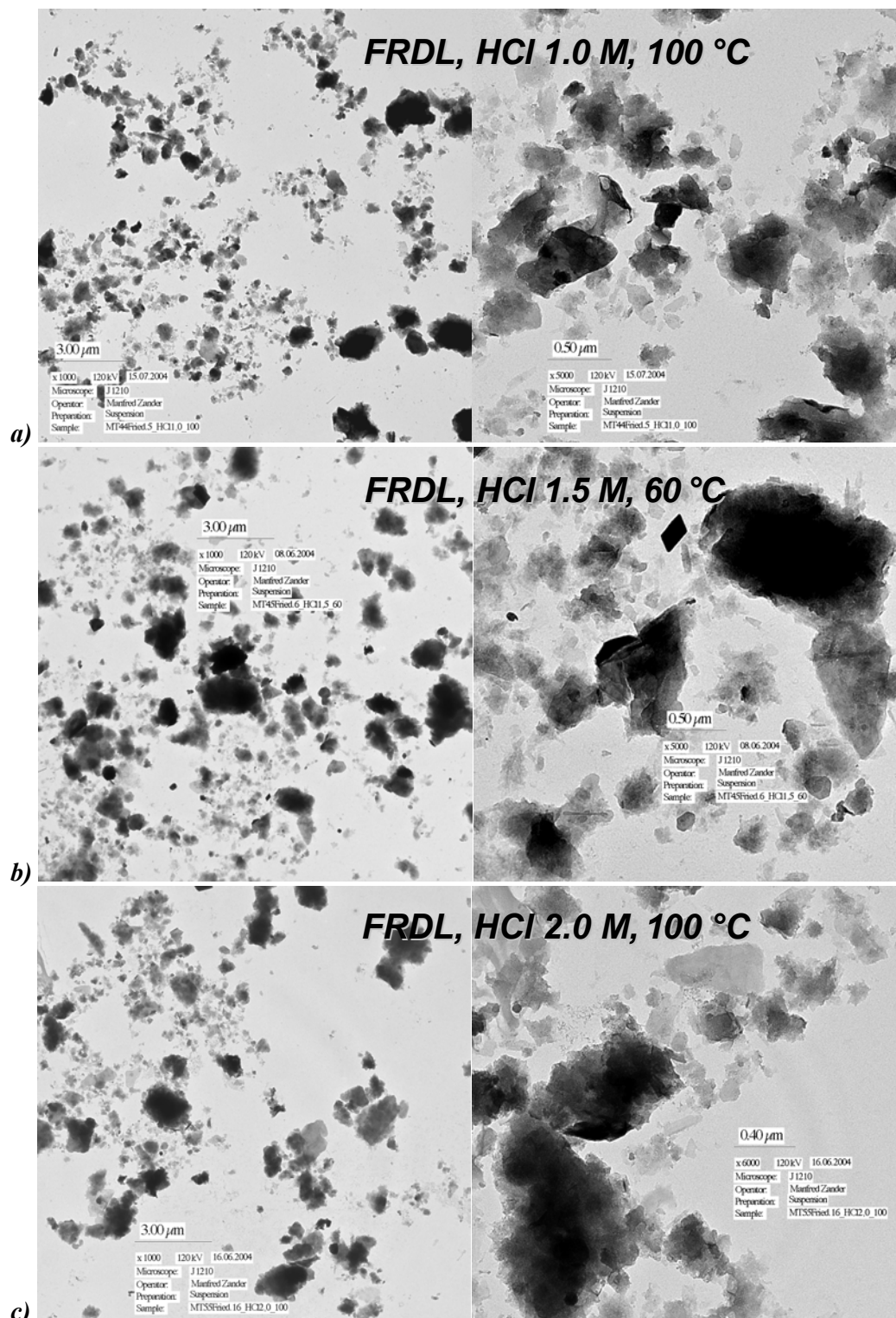
Friedland Clay was characterized as mixed-layer dominated clay including mainly IS-ml and diVS-ml series (chapter 4.3.1). Acid treatment is well-known as surface modification method towards clay minerals (Komadel & Madejová, 2006). This chapter is presenting some changes in clay matter and clay mineral phase caused by the acid treatment.

By XRF analyses, all the treated series show increase of SiO<sub>2</sub> component and decrease of some other components, especially Fe<sub>2</sub>O<sub>3</sub>, in comparison to the untreated sample (table 13). In relative comparison of the changes, the influence of thermal treatment was more effective than the rising concentration of acid.

**Table 13. Chemical composition (main components, oxide form) of HCl acid treated series of Friedland Clay in comparison with untreated sample from X-Ray Fluorescence analyses, indicated in mass %**

Clay Samples	SiO <sub>2</sub> (%)	TiO <sub>2</sub> (%)	Al <sub>2</sub> O <sub>3</sub> (%)	Fe <sub>2</sub> O <sub>3</sub> (%)	MnO (%)	MgO (%)	CaO (%)	Na <sub>2</sub> O (%)	K <sub>2</sub> O (%)	P <sub>2</sub> O <sub>5</sub> (%)	LOI 1000°C (%)	H <sub>2</sub> O- (%)	Summe (%)
1.0 M, 100°C (FRDL 5)	61.64	1.01	17.11	3.26	0.006	1.06	0.06	0.23	2.62	0.036	6.67	4.94	89.6
1.5 M, 60°C (FRDL 6)	59.66	0.98	18.49	4.27	0.008	1.37	0.06	0.24	2.97	0.042	6.51	4.71	99.3
1.5 M, 100°C (FRDL 10)	64.62	1.05	16.23	2.15	0.004	0.80	0.06	0.25	2.51	0.032	6.22	4.80	98.7
1.8 M, 100°C (FRDL 13)	64.00	1.09	16.04	2.35	0.005	0.83	0.06	0.27	2.55	0.032	6.82	4.75	98.8
2.0 M, 80°C (FRDL 14)	60.67	0.98	17.71	3.72	0.007	1.19	0.07	0.26	2.84	0.040	6.59	4.86	98.9
2.0 M, 100°C (FRDL 16)	63.18	1.06	16.89	2.43	0.005	0.92	0.06	0.24	2.69	0.032	6.35	4.90	98.8
Friedland Clay bulk, original	56.70	0.935	18.09	7.31	0.035	2.01	0.54	0.96	3.01	0.106	7.24	2.65	99.59

Note: Measured using Philips PW 2404, non wetting agent or/and oxidizer, LOI at 1000°C



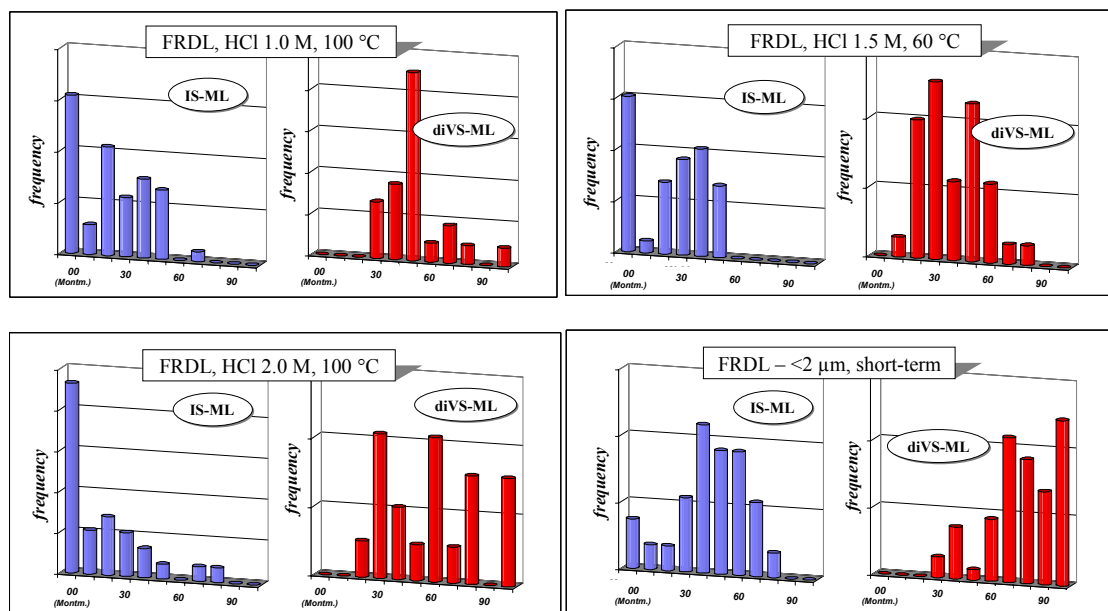
**Figure 42. TEM images of some acid treated FRDL clay samples**

a) FRDL, HCl 1.0 M, 100°C, 2 h; overview of the sample (mag.: 1,000x) (left) and a zoom image (mag.: 5,000) (right)

b) FRDL, HCl 1.5 M, 60°C, 2 h; overview of the sample (mag.: 1,000x) (left) and a zoom image (mag.: 5,000) (right)

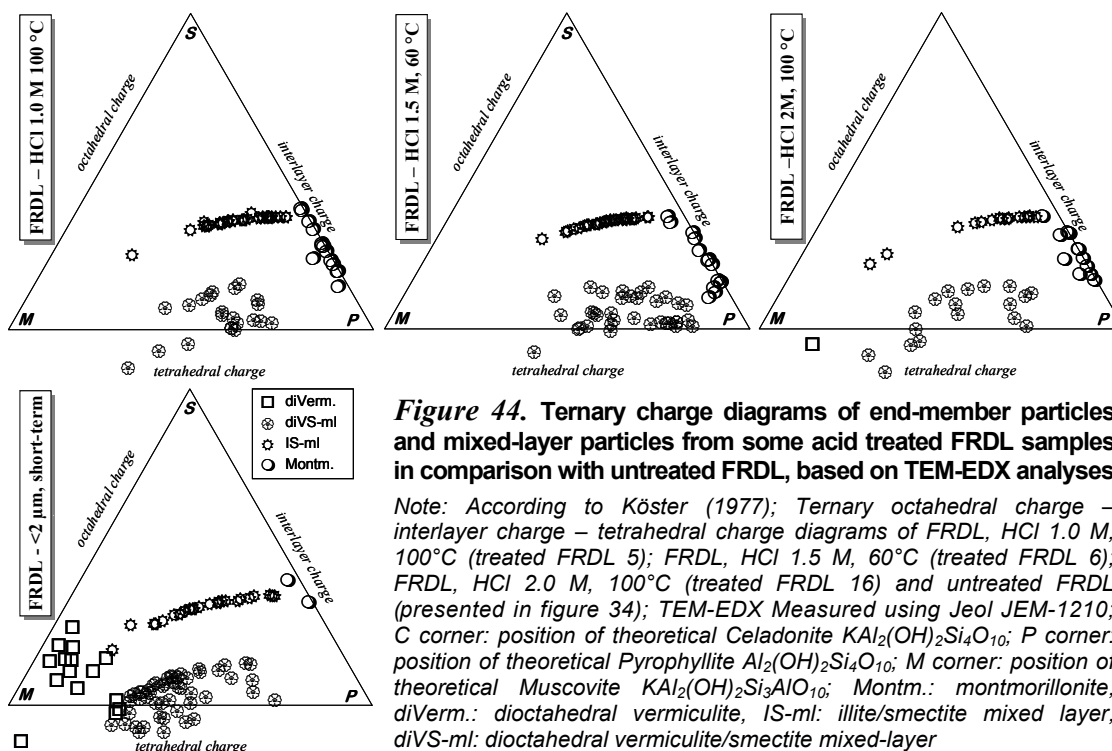
c) FRDL, HCl 2.0 M, 100°C, 2 h; overview of the sample (mag.: 1,000x) (left) and a zoom image (mag.: 6,000) (right)

*Note: Measured using Jeol JEM-1210*



**Figure 43.** Tendency of illite- and dioctahedral vermiculite-components distribution in mixed-layer series from some acid treated FRDL samples in comparison with untreated FRDL, based on TEM-EDX analyses

Note: Histograms of FRDL, HCl 1.0 M, 100°C (treated FRDL 5); FRDL, HCl 1.5 M, 60°C (treated FRDL 6); FRDL, HCl 2.0 M, 100°C (treated FRDL 16) and untreated FRDL (presented in figure 33); Right histograms: illite-components distribution in illite/smectite mixed-layer series (IS-ML); Left histograms: dioctahedral vermiculite-components distribution in dioctahedral vermiculite/smectite mixed-layer series (diVS-ML); % Illite- or % diVerm.-comp.: proportion of illite or dioctahedral vermiculite-component in mixed-layer series (e.g. 00% illite-comp. series: IS-ml series with 00% illite-component or montmorillonite); Montm.: montmorillonite, diVerm.: dioctahedral vermiculite; TEM-EDX measured using Jeol JEM-1210



**Figure 44.** Ternary charge diagrams of end-member particles and mixed-layer particles from some acid treated FRDL samples in comparison with untreated FRDL, based on TEM-EDX analyses

Note: According to Köster (1977); Ternary octahedral charge – interlayer charge – tetrahedral charge diagrams of FRDL, HCl 1.0 M, 100°C (treated FRDL 5); FRDL, HCl 1.5 M, 60°C (treated FRDL 6); FRDL, HCl 2.0 M, 100°C (treated FRDL 16) and untreated FRDL (presented in figure 34); TEM-EDX Measured using Jeol JEM-1210; C corner: position of theoretical Celadonite  $KAl_2(OH)_2Si_4O_{10}$ ; P corner: position of theoretical Pyrophyllite  $Al_2(OH)_2Si_4O_{10}$ ; M corner: position of theoretical Muscovite  $KAl_2(OH)_2Si_3AlO_{10}$ ; Montm.: montmorillonite, diVerm.: dioctahedral vermiculite, IS-ml: illite/smectite mixed layer, diVS-ml: dioctahedral vermiculite/smectite mixed-layer

**Table 14.** Mineral formulae [O<sub>10</sub>(OH)<sub>2</sub>] of illite/smectite and dioctahedral vermiculite mixed-layer series from some acid treated FRDL samples in comparison with untreated FRDL, based on TEM-EDX analyses

<b>FRDL, HCl 1.0 M, 100 °C</b>	<b>Interlayer</b>						<b>Octahedral layer</b>			<b>Tetra. layer</b>		
	Ca	Mg	Na	K	Fe <sup>2+</sup>	Al	Fe <sup>3+</sup>	Fe <sup>2+</sup>	Mg	Ti	Al	Si
<b>Illite/Smectite mixed-layer (Illite = 20%; Montmorillonite = 80%)</b>												
Average	0.03	0.07	0.07	0.18	0.00	1.52	0.26	0.00	0.12	0.01	0.12	3.88
STDV	0.04	0.04	0.06	0.10	0.00	0.08	0.07	0.00	0.05	0.01	0.02	0.02
<b>Dioctahedral Vermiculite/Smectite mixed-layer (diVerm. = 50%; Montmorillonite = 50%)</b>												
Average	0.01	0.08	0.05	0.16	0.00	1.77	0.16	0.00	0.05	0.01	0.38	3.62
STDV	0.01	0.03	0.04	0.10	0.00	0.08	0.05	0.00	0.05	0.01	0.03	0.03
<b>FRDL, HCl 1.5 M, 60 °C</b>	<b>Interlayer</b>						<b>Octahedral layer</b>			<b>Tetra. layer</b>		
	Ca	Mg	Na	K	Fe <sup>2+</sup>	Al	Fe <sup>3+</sup>	Fe <sup>2+</sup>	Mg	Ti	Al	Si
<b>Illite/Smectite mixed-layer (Illite = 20%; Montmorillonite = 80%)</b>												
Average	0.02	0.08	0.08	0.14	0.00	1.55	0.26	0.03	0.07	0.01	0.12	3.88
STDV	0.02	0.06	0.05	0.04	0.00	0.06	0.03	0.04	0.06	0.01	0.03	0.03
<b>Dioctahedral Vermiculite/Smectite mixed-layer (diVerm. = 40%; Montmorillonite = 60%)</b>												
Average	0.02	0.05	0.05	0.20	0.00	1.60	0.29	0.00	0.10	0.01	0.30	3.70
STDV	0.02	0.03	0.04	0.06	0.00	0.08	0.05	0.00	0.04	0.01	0.03	0.03
<b>FRDL, HCl 2.0 M, 100 °C</b>	<b>Interlayer</b>						<b>Octahedral layer</b>			<b>Tetra. layer</b>		
	Ca	Mg	Na	K	Fe <sup>2+</sup>	Al	Fe <sup>3+</sup>	Fe <sup>2+</sup>	Mg	Ti	Al	Si
<b>Illite/Smectite mixed-layer (Illite = 20%; Montmorillonite = 80%)</b>												
Average	0.02	0.05	0.05	0.20	0.00	1.60	0.29	0.00	0.10	0.01	0.12	3.88
STDV	0.01	0.03	0.03	0.04	0.00	0.09	0.05	0.00	0.11	0.01	0.03	0.03
<b>Dioctahedral Vermiculite/Smectite mixed-layer (diVerm. = 60%; Montmorillonite = 40%)</b>												
Average	0.02	0.06	0.05	0.31	0.00	1.74	0.14	0.00	0.11	0.02	0.43	3.57
STDV	0.02	0.04	0.05	0.03	0.00	0.06	0.03	0.00	0.04	0.02	0.04	0.04
<b>FRDL - &lt;2 µm, short-term (*)</b>	<b>Interlayer</b>						<b>Octahedral layer</b>			<b>Tetra. layer</b>		
	Ca	Mg	Na	K	Fe <sup>2+</sup>	Al	Fe <sup>3+</sup>	Fe <sup>2+</sup>	Mg	Ti	Al	Si
<b>Illite/Smectite mixed-layer (Illite = 40%; Montmorillonite = 60%)</b>												
Average	0.03	0.02	0.21	0.29	0.00	1.26	0.42	0.00	0.29	0.01	0.24	3.76
STDV	0.03	0.03	0.11	0.15	0.00	0.15	0.14	0.00	0.06	0.01	0.03	0.03
<b>Dioctahedral Vermiculite/Smectite mixed-layer (diVerm. = 80%; Montmorillonite = 20%)</b>												
Average	0.02	0.11	0.12	0.23	0.01	1.73	0.17	0.00	0.10	0.02	0.60	3.40
STDV	0.02	0.08	0.10	0.20	0.02	0.18	0.14	0.00	0.06	0.01	0.02	0.02

Note: Measured using Jeol JEM-1210; (\*): presented in table 11; Average: average index, STDV: standard deviation

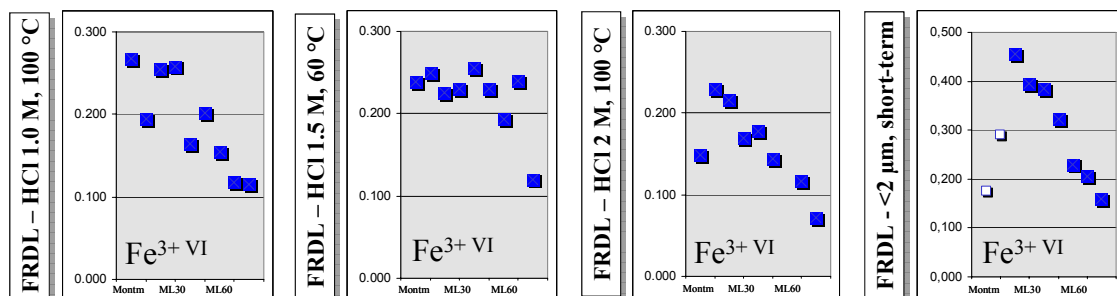
With respect to the clay mineral phases, TEM-EDX measurements were performed to characterize some selected samples. As shown in the figure 42, clay particles were modified after two hours in contact with acid solution at high temperature. Therefore, in comparison with the morphology of the untreated clay particles (figure 31), the treated clay particles show totally different morphology: non-regular plate with partly curled margin.

By XRD analyses (appendix 8), the clay minerals also became highly disordered mirrored by broader peaks. Especially, for the treated samples at 100°C (the highest temperature among all), it could not be detected any peak at position of IS-ml and diVS-ml series. That means only few layers per stack of acid treated IS-ml and diVS-ml particles.

In the treated samples, IS-ml and diVS-ml showed generally higher smectitic proportions than the untreated samples. This observation was revealed by the calculated formulae of mixed-layer particles (table 14 and figure 44). Whilst the untreated FRDL sample was determined with 40% illitic layers IS-ml particles and 80% dioctahedral vermiculitic layers diVS-ml particles (chapter 4.3.1), the acid untreated FRDL samples show IS-ml particles with only 20% illitic layers and diVS-ml particles with 40 – 60% dioctahedral vermiculitic layers (table 14 and figure 43). Between three selected treated FRDL samples, the treated sample under the condition of HCl 2.0 M and 100°C during 2 h represented less particles of the expandable clay minerals than the others (figure 44).

Based on the results obtained from TEM-EDX particles analyses of <2 µm fraction, a solution of  $\text{Fe}^{3+\text{VI}}$  component from clay minerals is determined. The untreated FRDL sample shows octahedral  $\text{Fe}^{3+}$  from 0.1 - 0.5 per unit cell while the treated FRDL samples present only 0.3 as maximal octahedral  $\text{Fe}^{3+}$  index (table 14 and figure 45).

In conclusion, acid treatment can modify and dissolve partly the expandable clay minerals of FRDL, therein much more mica-like layers were dissolved than montmorillitic layer. The treatment also reduced the expandability of mixed-layer particles and  $\text{Fe}^{3+\text{VI}}$ -amount. Among different conditions of treatment, the condition with higher temperature (100°C) and higher concentration of acid solution (HCl 2.0 M) is more effective environment.



**Figure 45.** Octahedral  $\text{Fe}^{3+}$  component of mixed-layer particles from some acid treated FRDL samples in comparison with untreated FRDL, based on TEM-EDX analyses

Note: from left to right: FRDL, HCl 1.0 M, 100°C (treated FRDL 5); FRDL, HCl 1.5 M, 60°C (treated FRDL 6); FRDL, HCl 2.0 M, 100°C (treated FRDL 16) and untreated FRDL; TEM-EDX Measured using Jeol JEM-1210

#### 4.5.2 Dithionite treated clays

The Fe-rich Teistungen and Thierfeld clays (see the part 4.4) were treated by dithionite method according to Mehra & Jackson (1960) to remove the iron oxides and hydroxides in the bulk samples. The changing after treatment was documented by XRF, XRD and Mössbauer spectroscopy (MS) analyses. Whilst XRF data showed the changing of total iron amount, XRD and MS results showed the specific phases from which iron were removed.

The decreasing in percentage of iron oxide amount from about 4.5 to 4.1% and 7.9 to 4.1% for Teistungen and Thierfeld, respectively, indicated effects of dithionite treatments. Only a low portion of iron was removed in the Teistungen sample. However, the changing in percentage of iron mass from the untreated to the treated Thierfeld showed the significant difference between the samples. Except about iron (and sodium oxide amount which is influenced by treatment material and process), the changing of other compositions were not considerable in XRF results because they were small and related to the changing of iron oxide percentage (table 15).

**Table 15. Chemical composition (main components, oxide form) of untreated and dithionite treated Teistungen and Thierfeld from X-Ray Fluorescence analyses, indicated in mass %**

Clay Samples	SiO <sub>2</sub> (%)	TiO <sub>2</sub> (%)	Al <sub>2</sub> O <sub>3</sub> (%)	Fe <sub>2</sub> O <sub>3</sub> (%)	MnO (%)	MgO (%)	CaO (%)	Na <sub>2</sub> O (%)	K <sub>2</sub> O (%)	P <sub>2</sub> O <sub>5</sub> (%)	LOI 1000°C (%)	H <sub>2</sub> O- (%)	Total (%)
Teistungen	63.12	0.816	16.25	<b>4.52</b>	0.059	2.18	0.80	1.70	3.41	0.346	4.10	1.05	98.35
Teistungen Dithionite	64.16	0.860	16.92	<b>4.06</b>	0.037	2.36	0.61	2.09	3.74	0.195	4.09	0.95	100.06
Thierfeld	59.22	1.64	17.63	<b>7.89</b>	0.091	2.16	0.61	0.85	3.35	0.337	5.01	0.77	99.56
Thierfeld Dithionite	61.49	1.70	18.64	<b>4.11</b>	0.043	2.27	0.51	1.32	3.48	0.259	5.25	0.74	99.81

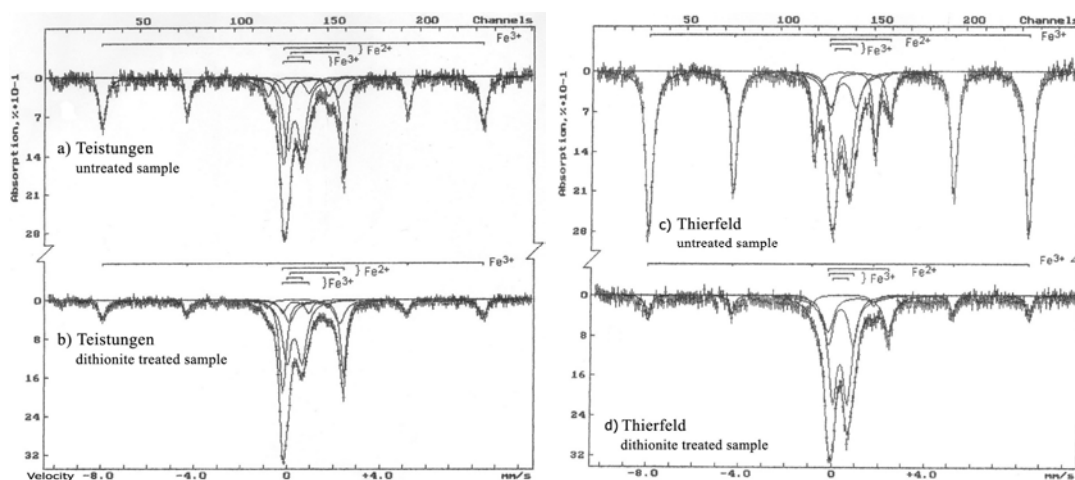
Clay Samples	Ba* (ppm)	Ce* (ppm)	Co* (ppm)	Cr* (ppm)	Cu* (ppm)	Ga* (ppm)	Nb* (ppm)	Ni* (ppm)	Pb* (ppm)	Rb* (ppm)	Sr* (ppm)	Th* (ppm)	U* (ppm)	V* (ppm)	Y* (ppm)	Zn* (ppm)	Zr* (ppm)
Teistungen	1783	86	10	58	<100	21	19	38	20	154	178	17	9	85	31	71	301
Teistungen Dithionite	1332	80	9	62	<100	23	19	35	21	189	166	13	<5	81	28	81	241
Thierfeld	825	96	22	77	<100	23	26	60	26	142	168	13	5	127	50	112	288
Thierfeld Dithionite	824	102	21	68	<100	25	25	53	22	181	173	11	5	95	32	121	273

*Note: Measured using Philips PW 2404, non wetting agent or/and oxidizer, LOI at 1000°C*

The information about the removed iron amount obtained from XRF experiments is quite similar to the results, which were obtained from MS analyses (appendix 7, figure 46), wherein iron (%) in general component decreased slightly from about 3.2 of untreated Teistungen to 2.8 of treated Teistungen and decreased drastically from 5.5 to 2.9 in the Thierfeld samples.

The Mössbauer spectra of Teistungen, Thierfeld and their dithionite treated samples consisted of a single asymmetric quadropole doublet, which represented a superposition of a sextet and four or three doublets (figure 46). The sextet sub-spectra (O-1.1, O-2.1, O-3.1 and O-4.1) with  $\delta$  of 0.37 – 0.39 mm/s,  $\Delta$  of (-0.18) - (-0.21) mm/s and magnetic hyperfine field of 50.7 - 51.1 Tesla at room temperature correspond to characterization of hematite ( $\alpha$ -Fe<sub>2</sub>O<sub>3</sub>) (Menil, 1985; Murad & Schwertmann, 1986; Murad, 1998).

Based on the  $\delta$  values, other doublets were identified as octahedral Fe<sup>2+</sup> phases (CM-1.1, CM-1.2, CM-2.1, CM-2.2, CM-3.1 and CM-4.1) and octahedral Fe<sup>3+</sup> phases (CM-1.3, CM-1.4, CM-2.3, CM-2.4, CM-3.2, CM-3.3, CM-4.2 and CM-4.3) in clay minerals (Rancourt, 1998). The obtained  $\Delta$  and  $\Gamma$  values of these doublets are in intervals of corresponding values of Al-rich dioctahedral mica or smectite, Fe-rich dioctahedral mica, trioctahedral 2:1 silicate, illite, chlorite from hundred spectra were studied by Heller-Kallai and Rozenson (1981). However, none of obtained data set was exactly fitted to reference data. This might be caused by the mixture of Fe-ion spectra from many clay minerals in one. The *cis*- and *trans*-octahedral of iron ion were carried out according to the conclusion that the  $\Delta$  values of *trans*-site is larger (approximately twice) than that of *cis*-site (Heller-Kallai & Rozenson, 1981; Ballet & Coey, 1982).



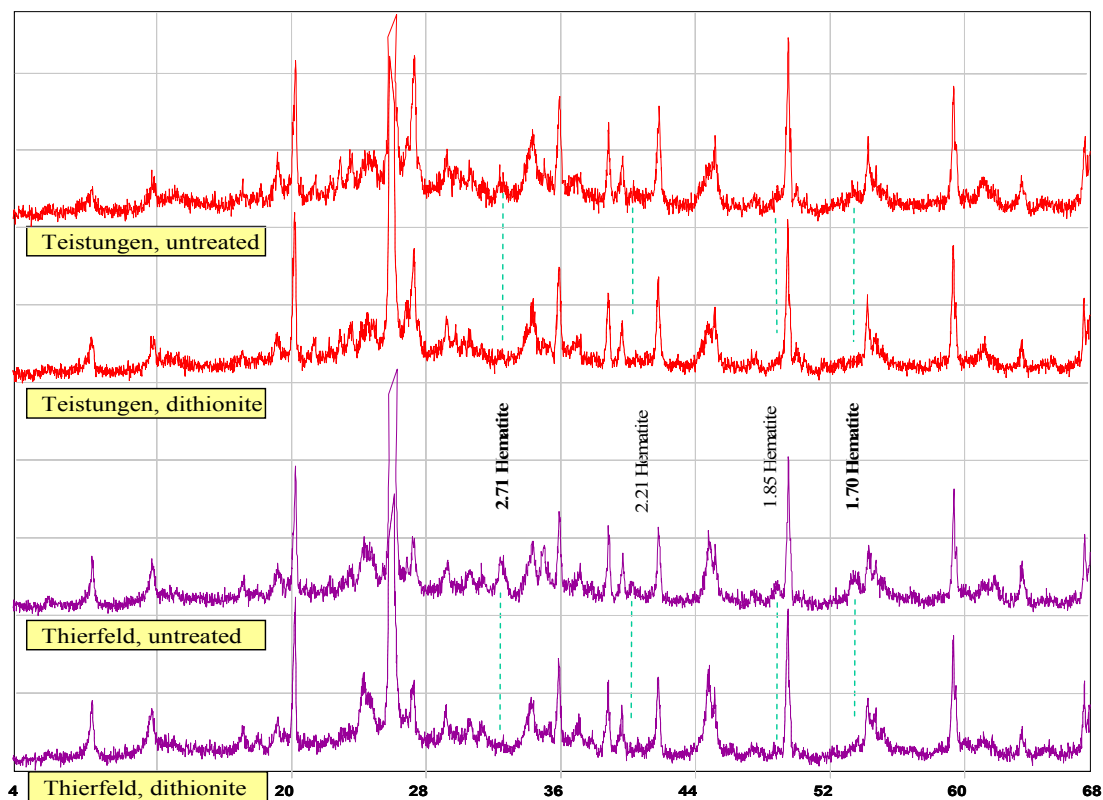
**Figure 46.** Mössbauer spectra of original and dithionite treated samples of Teistungen and Thierfeld at room temperature

Note: Measured using Ms-1104Em spectrometer at St-Petersburg State University, Russia; a) Teistungen – untreated sample (left above), b) Teistungen – dithionite treated sample (left bottom), c) Thierfeld – untreated sample (right above), and d) Thierfeld – dithionite treated sample (right bottom) ; <sup>57</sup>Co isotopes resource, subspectra were fitted by Univem MS program

As described above, Teistungen and Thierfeld samples include more than one species of dioctahedral clay minerals. Therefore, the doublets were characterized as octahedral  $\text{Fe}^{2+}$  and octahedral  $\text{Fe}^{3+}$  of the set of dioctahedral clay minerals. The sextet sub-spectra of hematite with different areas of component showed the hematite-removing amount after dithionite treatment.

The reducing of iron phase was also confirmed by XRD patterns (figure 47). The relative height of hematite peaks reduced clearly from untreated samples to corresponding dithionite treated samples.

In conclusion, performed dithionite treatment removed hematite phases in original Teistungen and Thierfeld clays. The removed iron amount in Teistungen clays is much lower than that in Thierfeld clays.



**Figure 47.** XRD patterns of original and dithionite treated samples of Teistungen and Thierfeld from powder mount,  $2\theta$   $\text{CuK}\alpha$  position

*Note: Measured using Siemens D5000; from above to bottom: untreated Teistungen, dithionite treated Teistungen, untreated Thierfeld and dithionite treated Thierfeld; these samples were milled and sieved to  $<63 \mu\text{m}$  from bulk samples before measuring; the patterns indicate changing of relatively height of hematite peaks; other peaks: see more in figure 37*



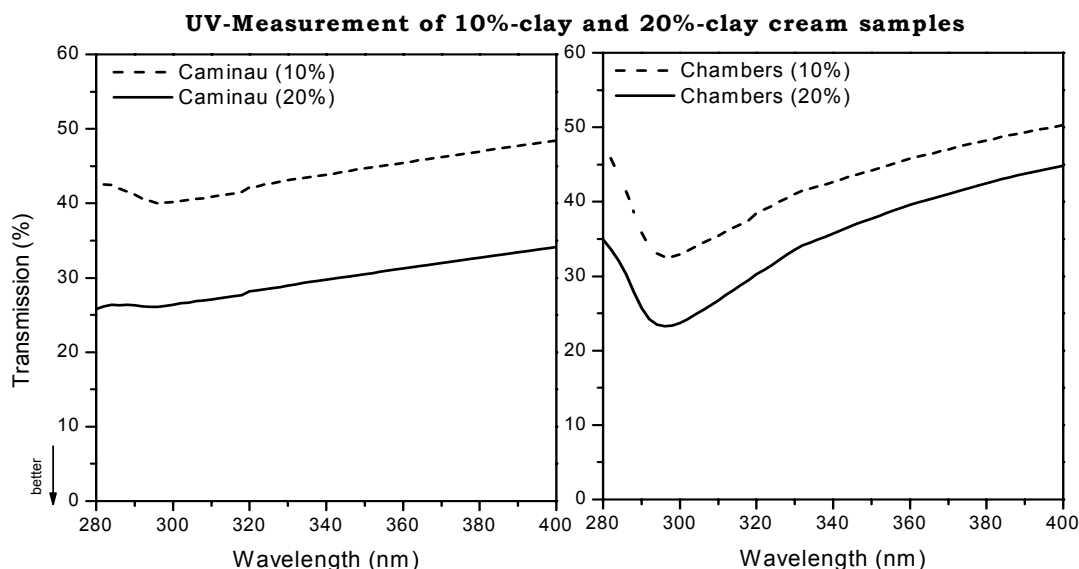
## 5 CHARACTERIZATION OF CREAM SAMPLES/UV-MEASUREMENTS

### 5.1 Pure-clay cream samples – overview

#### 5.1.1 Clay concentration

With pure-clay cream samples, two levels of clay concentration in cream sample were prepared and analyzed: 10%-clay and 20%-clay. Table 16 and table 17 showed UV-transmission results of 20%-clay cream samples and 10%-clay cream samples, respectively. Some examples in the purpose of comparing UV-absorption ability between these two clay concentration levels were shown in figure 48. Whilst average UV-transmission value of 20%-clay pure-clay cream sample of Caminau is only 28.8%, the corresponding UV-transmission value of 10%-clay sample of Caminau is as high as 43.7%. Similarly, pure-clay samples of Chamber show the average UV-transmission values for 20%-clay sample is 34.5% and for 10%-clay sample is 40.6%. It is obvious that clay amount has effect to reduce the intensity of UV-radiation. The 20%-clay cream samples absorbed much higher UV-radiation than the 10%-clay ones.

In almost cases, UV-transmission profiles obtained from the two concentration levels had the same trend. Therefore, in comparison UV-absorption abilities of the clay groups in pure-clay cream, normally only 20%-clay cream results were presented.



**Figure 48. UV-measurement in comparison clay concentration: 10%-clay and 20%-clay cream samples**

**Left: UV-transmission from Caminau kaolin; right: UV-transmission from Chambers bentonite**

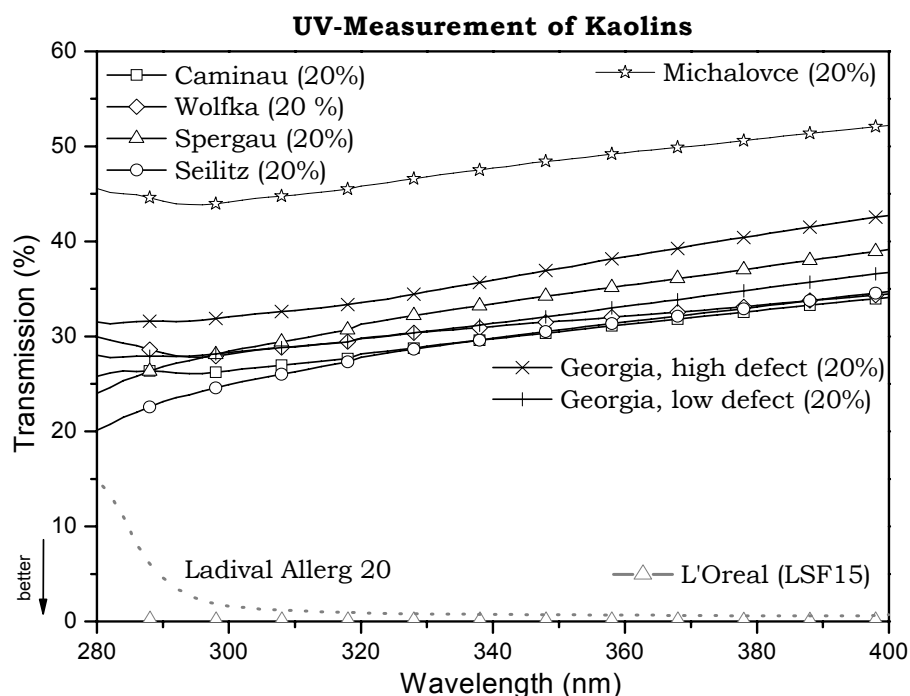
Note: Measured using AnalytikJenaAG SPECORD 50; Pure-clay cream samples of 10% and 20% of <63  $\mu\text{m}$  bulk clay with wool-wax-alcohol cream; The lower transmission proportion, the better effect by clay cream

### 5.1.2 Kaolins

Kaolin samples, Caminau, Wolfka, Spergau, Seilitz, KGa-1b (Georgia, low defect) and KGa-2 (Georgia, high defect) with kaolinite as main phase, showed absorption capacities of 20% clay-cream samples from approximately 60% to 80% of incident UV rays. In other words, obtained UV-transmission values for these kaolin samples were approximately 40% to 20% (figure 49 and table 16). Different trends of UV-transmission were not to recognize between these kaolins. Eventually, some result curves cut the others. Among these, Seilitz sample seemed to have the highest UV-absorption ability and Georgia high defect kaolin had lowest UV-absorption ability.

Especially, halloysite dominated kaolin had a notable lower UV-absorption ability than the other mentioned kaolinite bearing samples. At 300 nm of wavelength, the UV rays could transmit still nearby the half (about 47% in average) of incident light through halloysite cream screen. Whereas, the other kaolinite cream samples let pass only average 27 to 35% of incident light (table 16).

Light microscopy images of kaolins were presented in figure 50. The images show that distribution of clay in the wool-wax-alcohol cream is dispersion or dense aggregation.


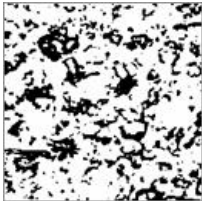
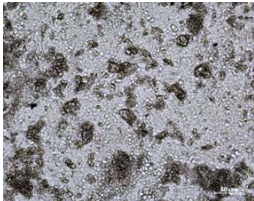
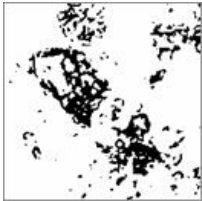
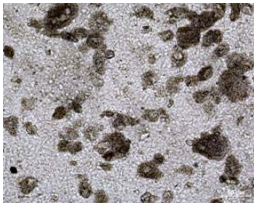
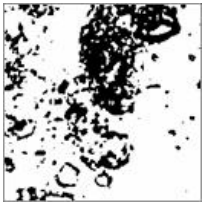
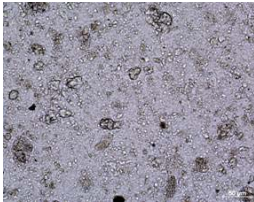
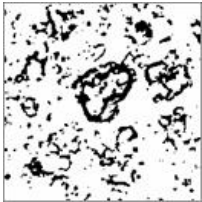
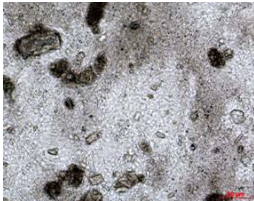
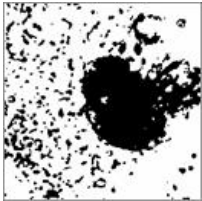

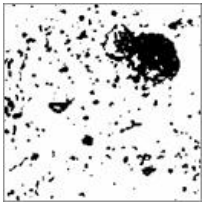
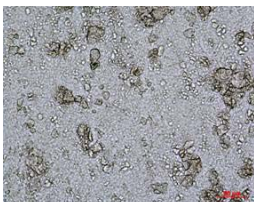



**Figure 49. UV-measurement of 20%-clay cream samples of kaolins**

**Caminau, Wolfka, Spergau and Seilitz are German reference kaolins; Georgia, low defect (KGa-1b) and Georgia, high defect (KGa-2) are CMS kaolins; halloysite Michalovce is from Greifswald collection**

Note: Measured using AnalytikJenaAG SPECORD 50; Pure-clay cream samples of <63  $\mu\text{m}$  bulk clay with wool-wax-alcohol cream; Ladival® allerg 20 and L'Oreal (LSP 15) are trade-wares (see more: [abbreviations](#)); The lower transmission proportion, the better effect by clay cream

**Figure 50.** Light microscopy images of 20%-clay cream samples of kaolins

Sample	Overview	Texture		STDV (homo- geneity)	Characterization of samples	
		50 $\mu$ m	70 $\mu$ m		Dispersion/ Aggregation	Shape of aggregates
<b>Caminau</b> (20%-clay)				112	Dispersion	-
<b>Wolfka</b> (20%-clay)				119	Aggregation	Dense
<b>Spergau</b> (20%-clay)				115	Aggregation	Dense
<b>Seilitz</b> (20%-clay)				101	Dispersion	-
<b>KGa-1b</b> (20%-clay)				87	Aggregation	Dense
<b>KGa-2</b> (20%-clay)				99	Aggregation	Dense
<b>Michalovce</b> (20%-clay) <i>halloysite</i>				107	Dispersion	-

**Table 16. UV-transmission at three selected points of 20% pure-clay cream samples**

Samples	Grain size	UV- transmission (%)			Note
		280 nm	300 nm	400 nm	
<b><i>Kaolins, pure-clay creams, 20% clay</i></b>					
Caminau	<63 µm bulk	<b>25.8</b>	<b>26.4</b>	<b>34.1</b>	German reference kaolin
Wolfka	<63 µm bulk	<b>29.9</b>	<b>28.1</b>	<b>34.5</b>	German reference kaolin
Spergau	<63 µm bulk	<b>24.0</b>	<b>28.4</b>	<b>39.1</b>	German reference kaolin
Seilitz	<63 µm bulk	<b>20.1</b>	<b>24.9</b>	<b>34.7</b>	German reference kaolin
Georgia, low defect, KGa-1b	<63 µm bulk	<b>28.0</b>	<b>28.3</b>	<b>36.7</b>	CMS reference kaolin
Georgia, high defect , KGa-2	<63 µm bulk	<b>31.5</b>	<b>32.1</b>	<b>42.7</b>	CMS reference kaolin
Michalovce (TS-41)	<63 µm bulk	<b>45.6</b>	<b>44.1</b>	<b>52.2</b>	Greifswald collection, halloysite
Wolfka <63 µm (coarse)	<63 µm	<b>30.0</b>	<b>28.2</b>	<b>34.5</b>	Sieving separation
Wolfka <2 µm (fine)	<2 µm	<b>30.1</b>	<b>29.3</b>	<b>37.1</b>	Atterberg separation
<b><i>Bentonites, pure-clay creams, 20% clay</i></b>					
Wyoming (TS-874)	<63 µm bulk	<b>19.7</b>	<b>25.3</b>	<b>40.4</b>	Greifswald collection, montmorillonite
Chambers (TS-569)	<63 µm bulk	<b>35.0</b>	<b>23.7</b>	<b>44.8</b>	Greifswald collection, montmorillonite
Garfield (TS-1803)	<63 µm bulk	<b>8.7</b>	<b>16.8</b>	<b>28.0</b>	Greifswald collection, nontronite
SHCa-1_California	<63 µm bulk	<b>30.6</b>	<b>33.3</b>	<b>43.4</b>	CMS bentonite, hectorite
STx-1_Texas	<63 µm bulk	<b>37.1</b>	<b>38.9</b>	<b>53.1</b>	CMS bentonite, montmorillonite
SAz-1_ Arizona	<63 µm bulk	<b>24.6</b>	<b>29.4</b>	<b>43.2</b>	CMS bentonite, montmorillonite
SWy-2_Wyoming	<63 µm bulk	<b>22.2</b>	<b>26.2</b>	<b>38.9</b>	CMS bentonite, montmorillonite
<b><i>Mixed-layer dominated clays, pure-clay creams, 20% clay</i></b>					
Friedland <63 µm (untreated)	<63 µm bulk	<b>18.8</b>	<b>22.4</b>	<b>32.9</b>	Friedland Clay PPM e.V.
Friedland <2 µm (Atterberg)	<2 µm	<b>16.2</b>	<b>22.3</b>	<b>40.3</b>	FRDL - <2 µm, long-term
FRDL, HCl 1.0 M, 100°C, 2 h	<63 µm bulk	<b>14.6</b>	<b>19.7</b>	<b>32.5</b>	Treated Friedland Clay 5
FRDL, HCl 1.5 M, 60°C, 2 h	<63 µm bulk	<b>14.6</b>	<b>19.0</b>	<b>32.3</b>	Treated Friedland Clay 6
FRDL, HCl 1.5 M, 100°C, 2 h	<63 µm bulk	<b>12.6</b>	<b>19.3</b>	<b>31.7</b>	Treated Friedland Clay 10
FRDL, HCl 1.8 M, 100°C, 2 h	<63 µm bulk	<b>13.3</b>	<b>19.7</b>	<b>32.8</b>	Treated Friedland Clay 13
FRDL, HCl 2.0 M, 80°C, 2 h	<63 µm bulk	<b>10.5</b>	<b>16.2</b>	<b>29.8</b>	Treated Friedland Clay 14
FRDL, HCl 2.0 M, 100°C, 2 h	<63 µm bulk	<b>19.0</b>	<b>25.1</b>	<b>37.0</b>	Treated Friedland Clay 16
<b><i>Mica dominated clays, pure-clay creams, 20% clay</i></b>					
Plessa	<63 µm bulk	<b>23.3</b>	<b>13.5</b>	<b>31.5</b>	German reference clay
Gorrenberg	<63 µm bulk	<b>19.1</b>	<b>11.0</b>	<b>25.5</b>	German reference clay
Teistungen (untreated)	<63 µm bulk	<b>14.8</b>	<b>9.5</b>	<b>22.1</b>	German reference clay (untreated)
Thierfeld (untreated)	<63 µm bulk	<b>8.3</b>	<b>4.6</b>	<b>15.1</b>	German reference clay (untreated)
Teistungen, dithionite	<63 µm bulk	<b>14.7</b>	<b>10.2</b>	<b>24.7</b>	Treated Teistungen
Thierfeld, dithionite	<63 µm bulk	<b>13.3</b>	<b>13.3</b>	<b>25.2</b>	Treated Thierfeld
<b><i>Reference materials</i></b>					
Ferrum Oxydatum Rubrum		<b>0.6</b>	<b>0.2</b>	<b>0.2</b>	Pharmacy material, Fe <sub>2</sub> O <sub>3</sub>
Ferrum Oxydatum Flavum		<b>0.3</b>	<b>&lt;0.1</b>	<b>&lt;0.1</b>	Pharmacy material, Fe(OH) <sub>3</sub>
TiO <sub>2</sub> 1%		<b>32.4</b>	<b>27.3</b>	<b>23.7</b>	Anatase
TiO <sub>2</sub> 8%		<b>1.5</b>	<b>1.1</b>	<b>1.0</b>	Anatase
L'Oreal (LSP 15)		<b>0.2</b>	<b>&lt;0.1</b>	<b>&lt;0.1</b>	Trade-ware cream, SPF 15
Ladival® allerg 20		<b>15.0</b>	<b>1.6</b>	<b>0.7</b>	Trade-ware cream, SPF 20

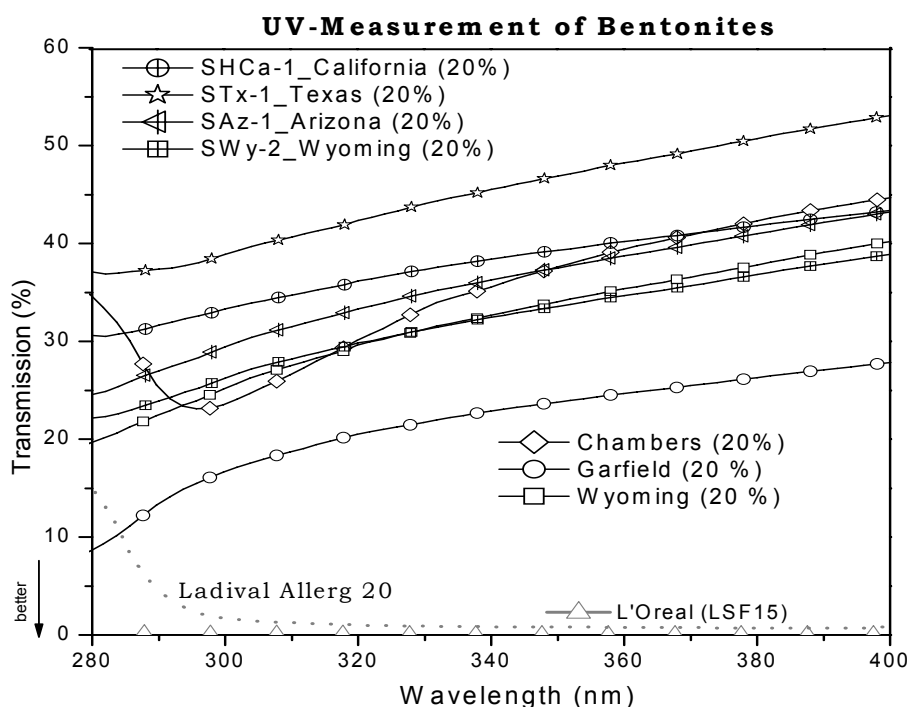
*Note: Measured using AnalytikJenaAG SPECORD 50*

### 5.1.3 Bentonites

Bentonite cream samples had complete different UV-absorption behaviors from those of kaolin bearing creams (figure 51). Garfield let pass only approximately 9% to 28% of incident rays (from 280 nm to 400 nm, respectively) (table 16). This group had result series, from highest absorption ability of nontronite Garfield to the lowest absorption ability of montmorillonite Texas.

Absorption in the whole UV area was very much larger from Garfield than from the other bentonites. In the series, montmorillonite Chambers had result line that diverges from others, especially in the UV-B range. Na-montmorillonite or Wyoming bentonite, which is common used in cosmetics and pharmacy, had medium UV-absorption capacity among this group. This material absorbs UV rays better than other bentonite samples but the result is still far from the result of Garfield nontronite. Approximate 10% of transmission unit was the difference between UV-transmission of Wyoming and UV-transmission of Garfield.

Observation from light microscopy shows that matrix of bentonite and wool-wax-alcohol cream is dispersion or aggregation with honey-comb and/or porous shape (figure 52).



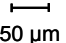
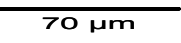
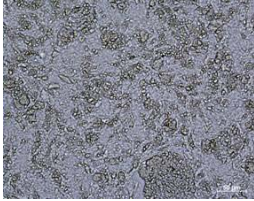
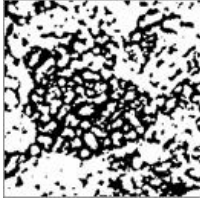
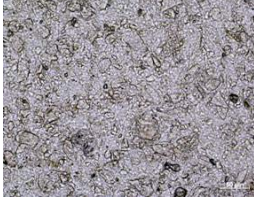
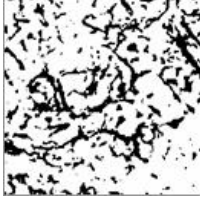
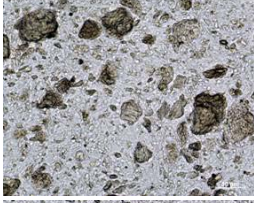
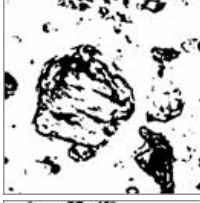
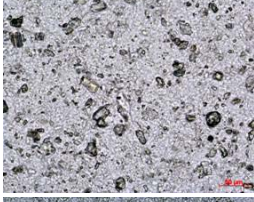
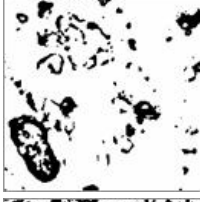


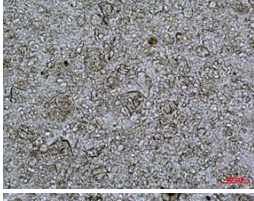
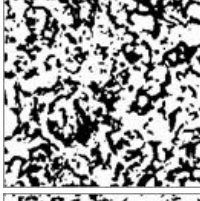
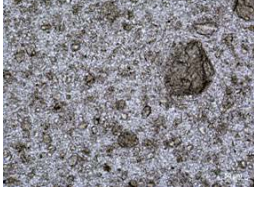
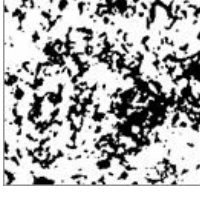
**Figure 51. UV-measurement of 20%-clay cream samples of bentonites**

**SHCa-1, STx-1, SAz-1 and SWy-2 are CMS bentonites; Chambers, Garfield and Wyoming are Greifswald collection bentonites**

Note: Measured using AnalytikJenaAG SPECORD 50; Pure-clay cream samples of <63  $\mu\text{m}$  bulk clay with wool-wax-alcohol cream; Ladival® allerg 20 and L'Oreal (LSP 15) are trade-wares (see more: [abbreviations](#)); The lower transmission proportion, the better effect by clay cream



**Figure 52. Light microscopy images of 20%-clay samples of bentonites**

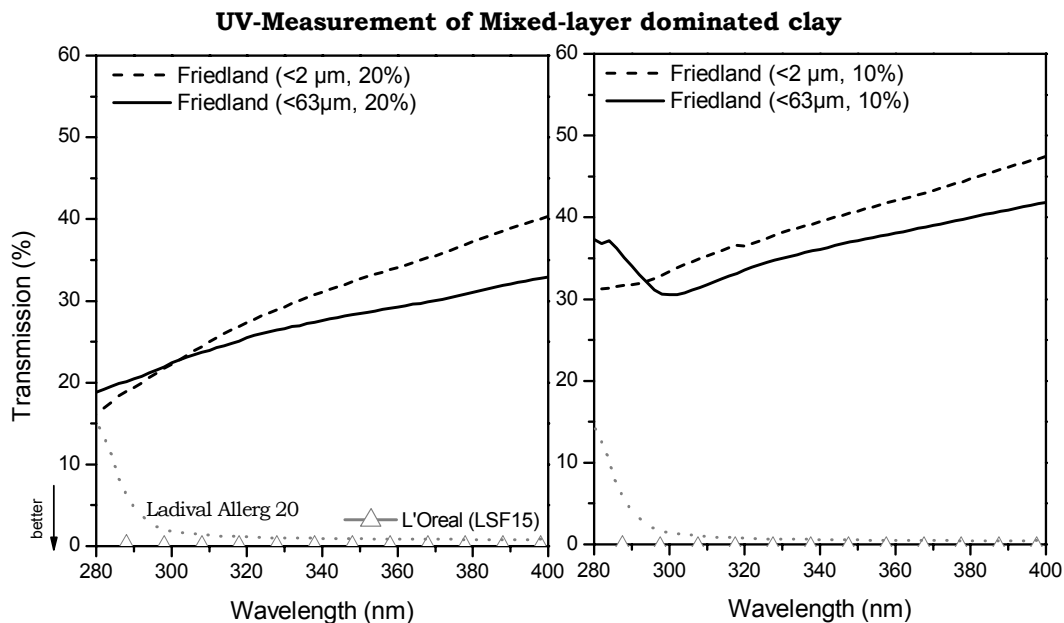
Sample	Overview	Texture	STDV (homo- geneity)	Characterization of samples	
				Dispersion/ Aggregation	Shape of aggregates
		 			
<b>Wyoming</b> (20%-clay)			126	Aggregation	Porous (honey-comb)
<b>Chambers</b> (20%-clay)			107	Aggregation	Unclosed honey-comb
<b>Garfield</b> (20%-clay)			110	Aggregation	porous
<b>SHCa-1</b> (20%-clay)			93	Dispersion	-
<b>STx-1</b> (20%-clay)			123	Dispersion	-
<b>SAz-1</b> (20%-clay)			124	Dispersion	-
<b>SWy-2</b> (20%-clay)			124	Aggregation	porous

### 5.1.4 Mixed-layer dominated clay

The figure 53 shows result spectra from Friedland Clay (from PPMeV) which were characterized as mixed-layer dominated clay (chapter 4.3). Clay cream samples, made from 20% of untreated bulk FRDL (milled to  $<63\ \mu\text{m}$ ) and  $<2\ \mu\text{m}$  FRDL (long-term)<sup>11</sup>, showed the UV-transmission approximately 19% to 33% and 16% to 40% (table 16). With 10%-clay pure-clay cream sample, at three selected points (280, 300 and 400 nm), UV-transmission results of bulk FRDL are 37.3, 30.5 and 41.8%, whilst UV-transmission results of  $<2\ \mu\text{m}$  FRDL (long-term) are 31.3, 33.4 and 47.4%, respectively.

From 280 nm to 300 nm, strong UV-B range,  $<2\ \mu\text{m}$  FRDL (long-term) absorbed UV rays better than  $<63\ \mu\text{m}$  bulk FRDL. Conversely, from 300 nm to 400 nm - UV-A range and one part of UV-B range,  $<63\ \mu\text{m}$  bulk FRDL exposed the better ability of UV-absorption.

Under light microscopy, 20%-clay cream sample of bulk FRDL represented the porous aggregation distribution like cream samples of bentonites (figure 59).



**Figure 53. UV-measurement of 10%- and 20%-clay cream sample of mixed-layer dominated clay**

**UV-transmission from 20%-clay cream samples (left) and 10%-clay cream samples (right) of  $<2\ \mu\text{m}$  Friedland Clay and  $<63\ \mu\text{m}$  bulk Friedland Clay**

Note: Measured using AnalytikJenaAG SPECORD 50; Pure-clay cream samples with wool-wax-alcohol cream; Ladival® allerg 20 and L'Oreal (LSP 15) are trade-wares (see more: [abbreviations](#)); The lower transmission proportion, the better effect by clay cream

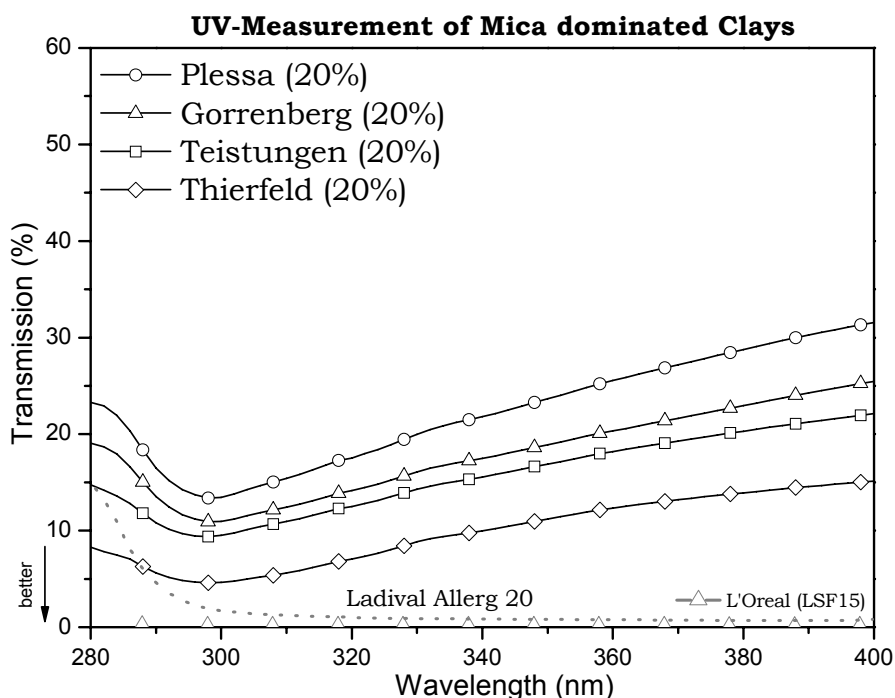
<sup>11</sup> The  $<2\ \mu\text{m}$  FRDL material, which was obtained by Atterberg sedimentation from bulk sample under long-term contact with water for two months, is labeled as "FRDL -  $<2\ \mu\text{m}$ , long-term" (see chapter 4.3)

### 5.1.5 Mica dominated clays

All clay cream samples, which were made from Plessa, Gorrenberg, Teistungen and Thierfeld with 20% of clay, were analyzed. They showed the high UV-absorption capacity. The best result curve was from Thierfeld clay. It was observed that UV-absorption abilities decreased in order of Thierfeld, Teistungen, Gorrenberg and Plessa (figure 54). In the figure, results of all of clay cream samples had the same trend. They got the highest absorption or lowest transmission at about 298 nm of wavelength.

UV-transmission of Thierfeld was approximately 8% at the minimal point and 15% at the maximal point (table 16). In beginning of UV-B range, the short and high energy area, this group absorbed from about 77% (Plessa) and 92% (Thierfeld) at 280 nm and increased to 87% and 95% at 298 nm. Moreover, in this area, Thierfeld reached a lower value of transmission than the trade-ware Ladival® allerg 20. From 298 nm to 400 nm, UV-absorption decreased gradually to 68% and 85%.

Matrix of 20%-clay pure-clay samples of clays were also observed by light microscopy (figure 55). All of the clays mix with wool-wax-alcohol cream to form dense aggregation matrix.




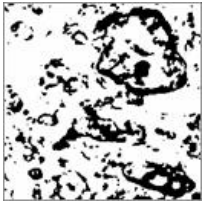
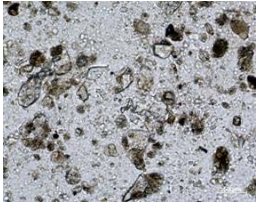
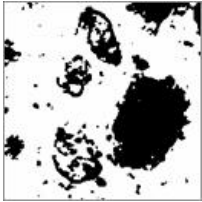
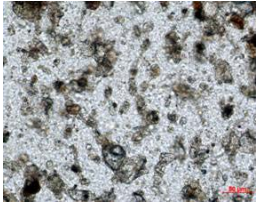
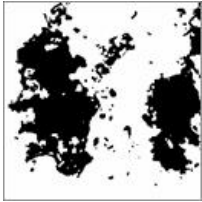
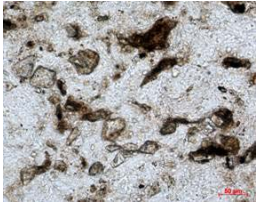
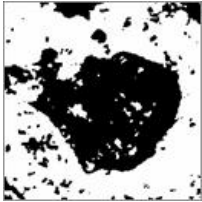
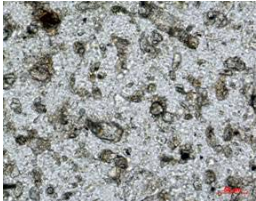

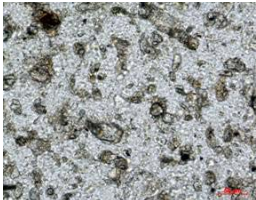
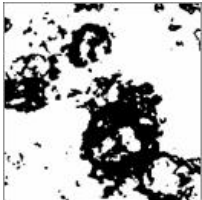
**Figure 54. UV-measurement 20%-clay cream samples of mica dominated clays**

**Plessa, Gorrenberg, Teistungen and Thierfeld are German reference clays**

Note: Measured using AnalytikJenaAG SPECORD 50; Pure-clay cream samples of <63 µm bulk clay with wool-wax-alcohol cream; Ladival® allerg 20 and L'Oreal (LSP 15) are trade-wares (see more: [abbreviations](#)); The lower transmission proportion, the better effect by clay cream



**Figure 55.** Light microscopy images of 20%-clay cream samples of clays

Sample	Overview	Texture		STDV (homo- geneity)	Characterization of samples	
		50 µm	70 µm		Dispersion/ Aggregation	Shape of aggregates
<b>Plessa</b> (20%-clay)				111	Aggregation	sub-dense
<b>Gorrenberg</b> (20%-clay)				115	Aggregation	Dense
<b>Teistungen</b> (20%-clay)				121	Aggregation	Dense
<b>Thierfeld</b> (20%-clay)				105	Aggregation	Dense
<b>Teistungen, dithionite</b> (20%-clay)				118	Aggregation	Dense
<b>Thierfeld, dithionite</b> (20%-clay)				115	Aggregation	Dense

In general, as the contribution observed, different clay samples have different UV-transmission values or different UV-absorption ability. In the kaolin series, all kaolinite dominated kaolins have quite close UV-transmission values meanwhile halloysite dominated sample has significant lower UV-absorption ability. Conversely, from the bentonite series, all of them are dominated by smectites but have complete different behaviour of UV-transmission. Therefore, the parameters which affected abilities of UV-transmission were expected to bring out. Besides, in the mica dominated clay series, Thierfeld showed the much lower UV-transmission. Therefore, some characteristics of the clay could play an important role. The levels of influences of mentioned parameters or characteristics were also expected to be determined.

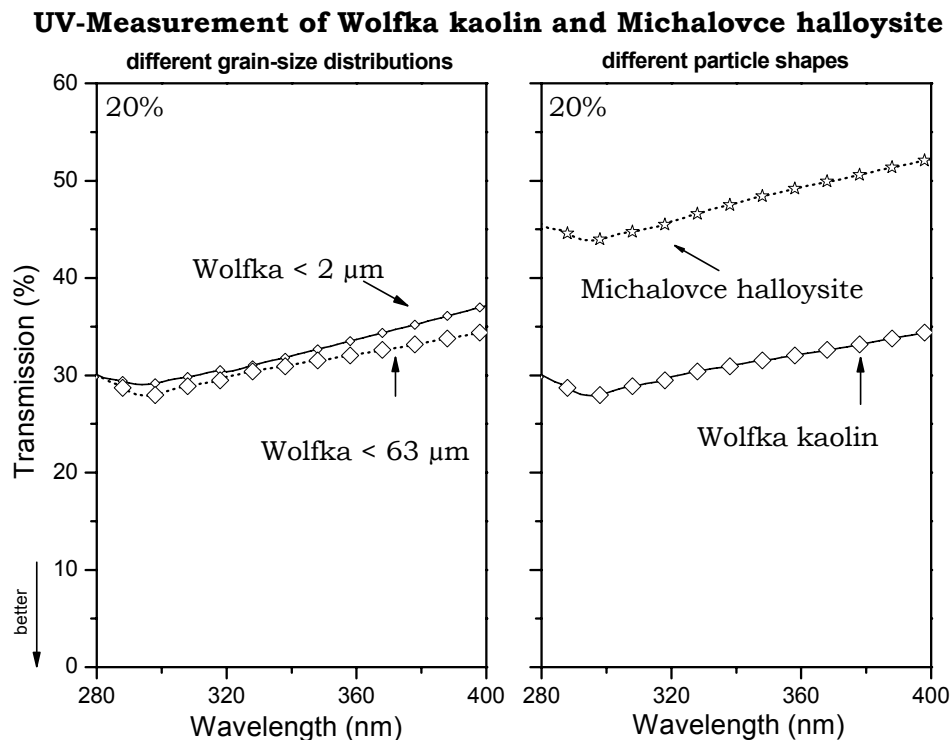
Concerning distribution of clay and ointment cream, whilst bentonites and mixed-layer dominated clay mostly presented the structure of dispersion or aggregation with porous or honey-comb shape, kaolins and mica dominated clays showed the structure of dense aggregation or dispersion. The influence level of distribution between clays and ointment cream to the UV-transmission levels was also considered.

## 5.2 Clay samples with different particle parameters

### 5.2.1 Particle sizes

The left side of figure 56 visualizes to results of  $<63 \mu\text{m}$  bulk and  $<2 \mu\text{m}$  Wolfka cream samples. The  $<63 \mu\text{m}$  bulk sample, was separated by sieving from bulk sample, containing about 86% kaolinite and 12% quartz (part 4.1.1). And the  $<2 \mu\text{m}$  sample, which was obtained by Atterberg sedimentation from original bulk sample, was composed by about 80% kaolinite and 17% IS-ml phases (Störr, 1982). Therefore, these two kaolin samples are not only different in particle size but also different in mineral matter. However, these UV-transmission result curves are quite similar. The difference in UV-transmission, which could be caused by particle size difference as well as mineralogical component difference, was not observed clearly. The problem was also met with  $<63 \mu\text{m}$  bulk and  $<2 \mu\text{m}$  Friedland Clay samples (the above chapter 5.1.4).

Chapter 5.5 also will present the UV-transmission of clay-fungi cream with different parameters.



**Figure 56. UV-measurement of 20%-clay cream samples of Wolfka and Michalovce**

UV-transmission from 20%-clay cream samples of  $<2 \mu\text{m}$  and  $<63 \mu\text{m}$  bulk Wolfka (left) and from 20%-clay cream samples of  $<63 \mu\text{m}$  bulk Michalovce halloysite kaolin and Wolfka kaolin (right)

Note: Measured using AnalytikJenaAG SPECORD 50; Pure-clay cream samples of clay with wool-wax-alcohol cream; The lower transmission proportion, the better effect by clay cream

### **5.2.2 Particle shapes**

On the right side of figure 56, the difference between Wolfka kaolin and Michalovce halloysite was significant. It is about 15-18% of transmission unit. Michalovce halloysite contains mostly tabular halloysite, whereas, Wolfka is platy kaolinite dominated kaolin. As described above, Wolfka and other kaolinite dominated kaolins had quite similar UV-transmission values. And as can be seen in the figure 49, Michalovce halloysite cream sample had much lower UV-absorption ability than other kaolin cream samples.

Because of these observations, roles of particle size and particle shape which could affect the UV-transmission degrees are considered and will be discussed in the following chapter 7.6. Especially, it was expected that the sample with finer grain size distribution generated the higher surface area can protect more effectively UV-radiation, but the experiment with different grain size distributions of Wolfka and Friedland Clay showed the opposite trend. Therefore, the relationship between the factor, which played a role in these results, and the grain size separation should be determined.

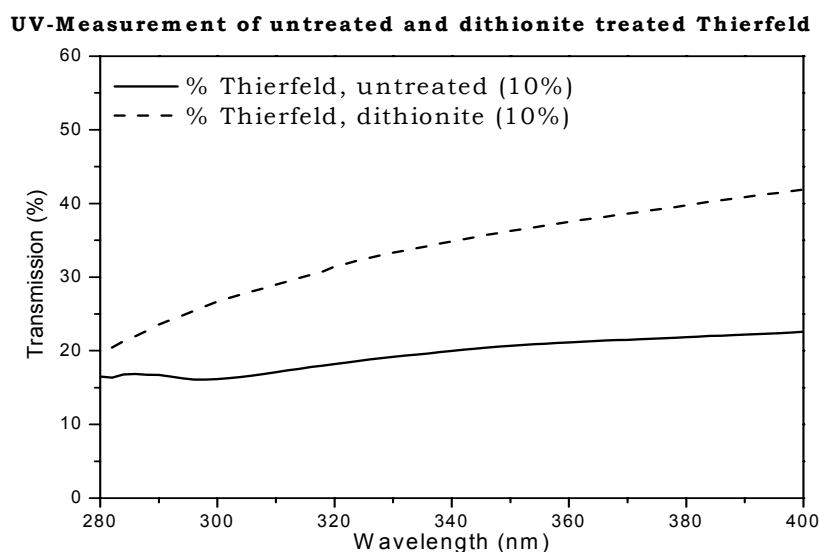
### 5.3 Iron-reduced samples

Whilst 20%-clay cream samples of untreated Thierfeld clay let pass only about 8 – 15% of UV-radiation, 13 – 25% UV-radiation could transmit through the 20%-clay cream samples of dithionite treated Thierfeld clay (table 16 and figure 54). That changing should be considered. A similar changing was also observed for Teistungen clay. UV-transmission of the cream samples (20% clay) of dithionite treated Teistungen was measured about 15 - 25% of incident UV ray, which is a little bit higher than UV-transmission of corresponding cream samples of untreated Teistungen (15 - 22%) (table 16 and figure 54). The main difference in the mineralogy of Thierfeld and Teistungen between original and dithionite treated samples is the reduced hematite contribution by dithionite treatment (XRD traces: figure 47; XRF analyses: table 15 and Mössbauer spectroscopy analyses: figure 46 and appendix 7).

With 10%-clay cream samples, UV-transmission of untreated Thierfeld was obtained about 17 – 23% and UV-transmission of dithionite treated Thierfeld was obtained about 20 – 42% (figure 57 and table 17).

Similarly to the untreated clays, the cream samples of dithionite treated Teistungen and Thierfeld have dense aggregation distribution (figure 55).

Difference of UV-transmission between untreated and dithionite treated samples also obtained from analyses of clay in combination with nanosuspension of a fungi kind (will be presented in chapter 5.5).



**Figure 57. UV-measurement of 10%-clay cream samples of untreated Thierfeld and its dithionite treated sample**

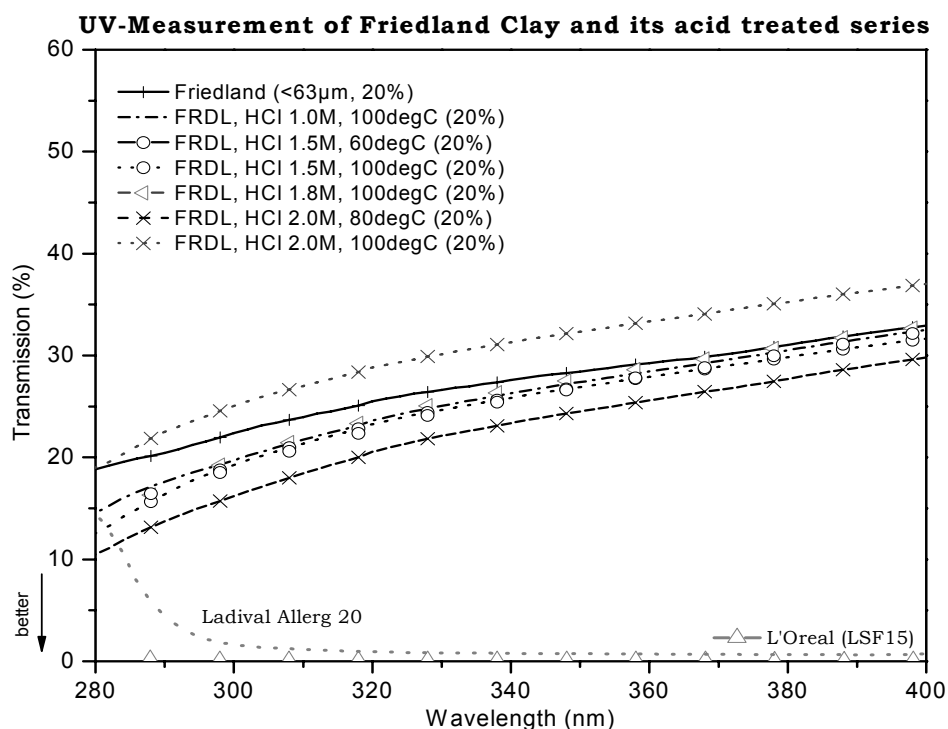
Measured using AnalytikJenaAG SPECORD 50; Pure-clay cream samples of <63 µm bulk clay with wool-wax-alcohol cream; The lower transmission proportion, the better effect by clay cream

## 5.4 Acid treated samples

With respect to the UV-absorption behaviour of some treatments on clay, not only the original bulk Friedland Clay but also its HCl treated series were analysed by UV-measurement (figure 58 and table 16). The obtained results showed that almost of all 20%-clay cream samples of treated clay samples represented the higher UV-absorption abilities than the original clay sample. It is looking like a formation of an optimum of UV-absorption for the sample treated under the condition of HCl 2.0 M, 80°C, 2 hours. More intensive acid treatment, such as the treatment with HCl 2.0 M with 100°C for 2 hours, is causing a reducing of UV-absorption behavior again. With 20%-clay, the treated clay cream sample transmitted 10 – 30% incident UV ray whilst the untreated clay cream sample transmitted 19 – 33% incident UV ray.

The distribution between clay particles of acid treated FRDL sample with wool-wax-alcohol cream looks more aggregative in comparison with untreated sample (figure 59).


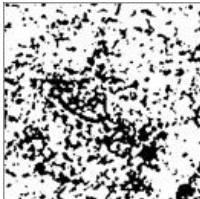
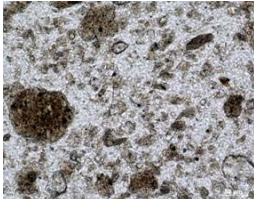
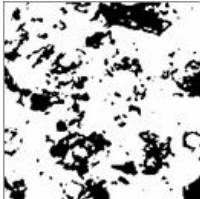
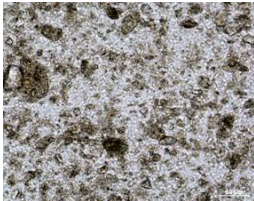
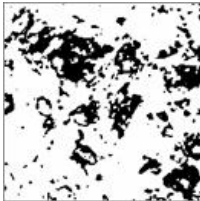
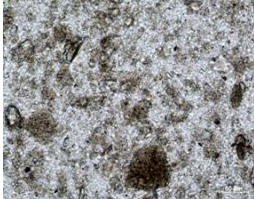
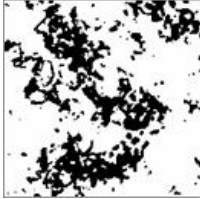
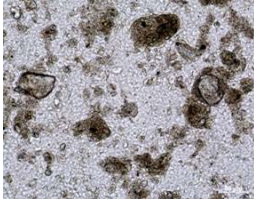
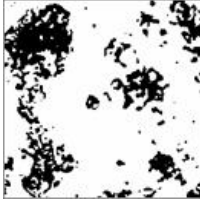

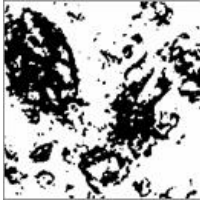
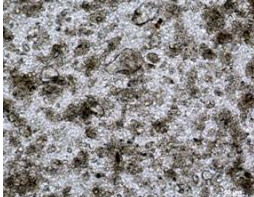
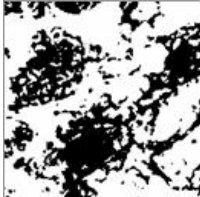
Chapter 5.5 also will present UV-measurement of one special sample of acid treated Friedland Clay and the untreated one in the system of clay-fungi creams.



**Figure 58. UV-measurement of 20%-clay cream samples of untreated Friedland Clay and its acid treated series**

Measured using AnalytikJenaAG SPECORD 50; Pure-clay cream samples of <63 µm bulk clay with wool-wax-alcohol cream; Friedland: untreated Friedland Clay PPM e.V. and FRDL, HCl -M, -degC: acid treated series of Friedland Clay with treated condition such as acid concentration (M) and temperature (degC), the treatment time is 2 hours; Ladival® allerg 20 and L'Oreal (LSP 15) are trade-wares (the lower transmission proportion, the better effect by clay cream)

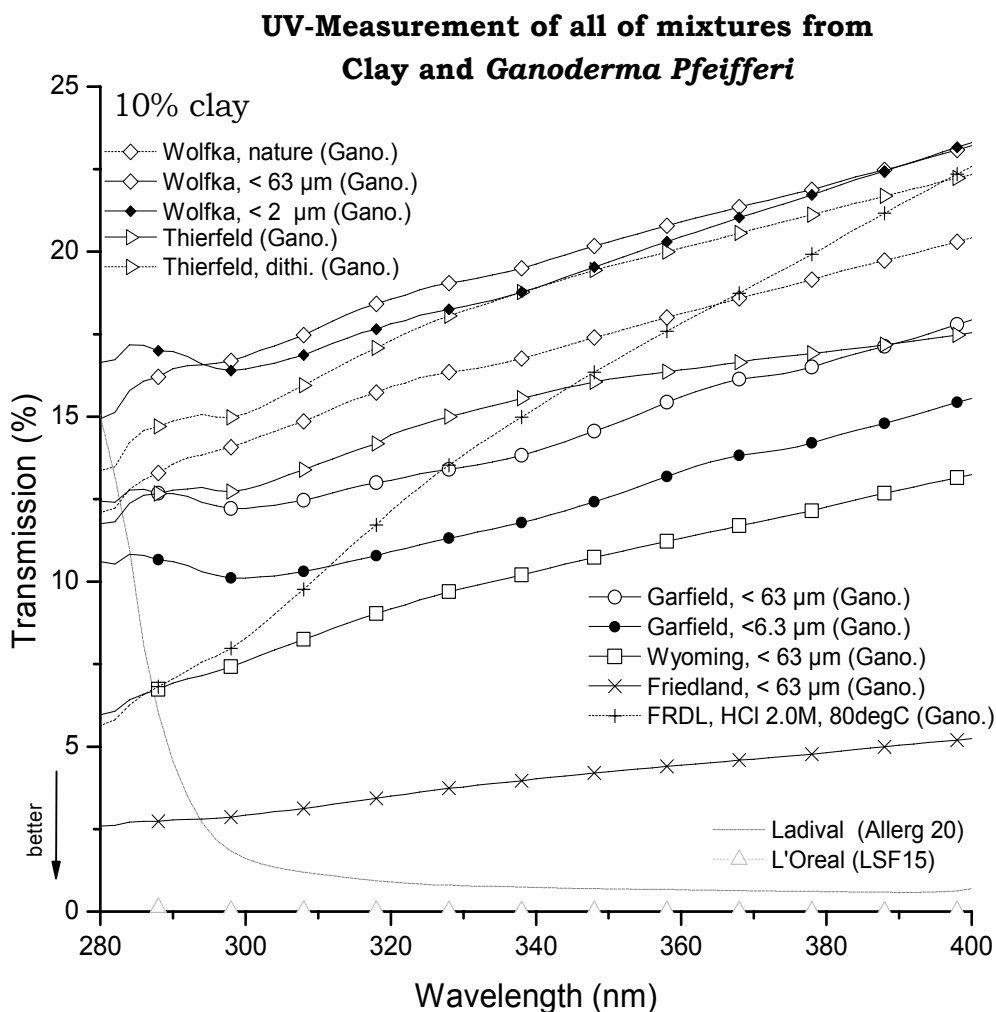
**Figure 59.** Light microscopy images of 20%-clay cream samples of Friedland Clay series

Sample	Overview	Texture		STDV (homo- geneity)	Characterization of samples	
		50 $\mu$ m	70 $\mu$ m		Dispersion/ Aggregation	Shape of aggregates
FRDL - untreated (20%-clay)				109	Aggregation	porous
FRDL – HCl 1.0 M, 100 °C (20%-clay)				119	Aggregation	sub-dense
FRDL – HCl 1.5 M, 60 °C (20%-clay)				120	Aggregation	sub-dense
FRDL – HCl 1.5 M, 100 °C (20%-clay)				118	Aggregation	sub-dense
FRDL – HCl 1.8 M, 100 °C (20%-clay)				111	Aggregation	sub-dense
FRDL – HCl 2.0 M, 80 °C (20%-clay)				116	Aggregation	sub-dense
FRDL – HCl 2.0 M, 100 °C (20%-clay)				124	Aggregation	sub-dense



## 5.5 Clay-fungi cream samples - combination with *Ganoderma pfeifferi*

The clay-fungi cream samples are the combination of clay sample and nanosuspension of fungi kind *Ganoderma pfeifferi* (see more in chapter 3.2.1). The concentration of clay amount in the sample is about 10% by weight in comparison with amount of wool-wax-alcohol cream. Various selected clay samples were performed in combination with the fungi suspension.




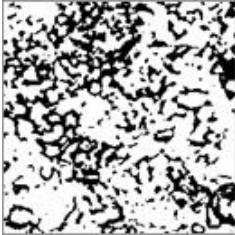

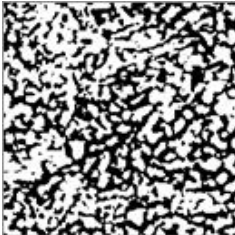
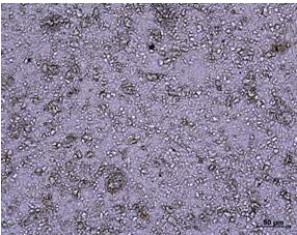
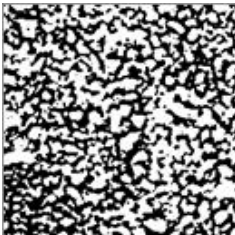
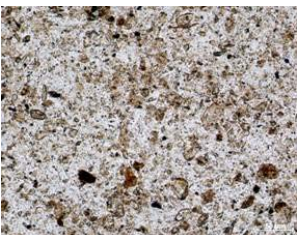
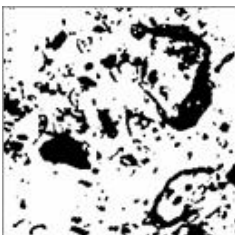

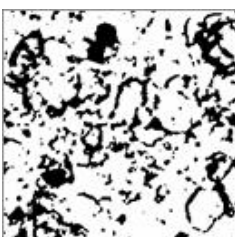
**Figure 60. UV-measurement of clay-fungi cream samples**

**UV-transmission from clay-fungi cream samples: mixtures of 10%-clay and fungi nanosuspension**


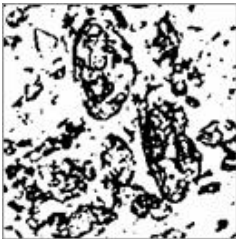
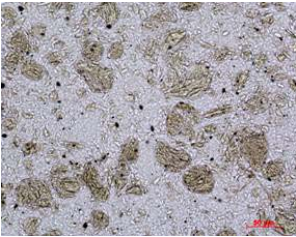
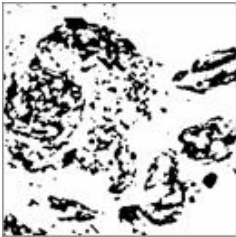
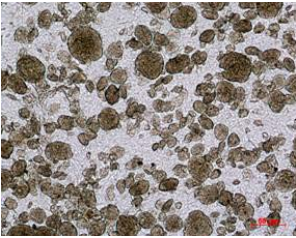
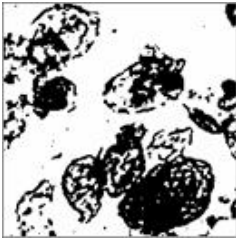

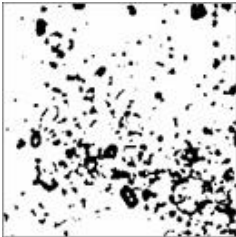

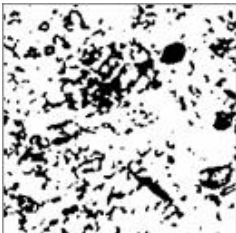
Measured using AnalytikJenaAG SPECORD 50; Clay-fungi cream samples of clay with fungi nanosuspension and wool-wax-alcohol cream (0.1 gram: 1ml: 1gram); Wolfka, nature = natural Wolfka; Wolfka, <63 $\mu\text{m}$  = <63 $\mu\text{m}$  Wolfka by milling and sieving; Wolfka, <2  $\mu\text{m}$  = <2  $\mu\text{m}$  Wolfka; Thierfeld = <63  $\mu\text{m}$ , untreated Thierfeld; Thierfeld, dithi. = <63  $\mu\text{m}$ , dithionite treated Thierfeld; Garfield, <63  $\mu\text{m}$  = <63  $\mu\text{m}$  Garfield by milling and sieving; Garfield, <6.3  $\mu\text{m}$  = <6.3  $\mu\text{m}$  Garfield by Atterberg sedimentation; Wyoming, <63 $\mu\text{m}$  = <63  $\mu\text{m}$  Wyoming; Friedland, <63  $\mu\text{m}$  = <63  $\mu\text{m}$  untreated Friedland Clay; FRDL, HCl 2.0 M, 80 deg C = acid treated Friedland; Ladival® allerg 20 and L'Oreal (LSP 15) are trade-wares (see more: [abbreviations](#)); (the lower transmission proportion, the better effect by clay cream)



**Figure 61.** Light microscopy images of clay-fungi cream samples  
(10%-clay and fungi nanosuspension)

Sample	Overview	Texture	STDV (homo- geneity)	Characterization of samples	
				Dispersion/ Aggregation	Shape of aggregates
		<div>50 <math>\mu</math>m</div> <div>70 <math>\mu</math>m</div>			
Wolfka, nature + fungi <i>Gano. pfeifferi</i> nano- suspension			120	Dispersion	-
Wolfka, <63 $\mu$ m + fungi <i>Gano. pfeifferi</i> nano- suspension			127	Dispersion	-
Wolfka, <2 $\mu$ m + fungi <i>Gano. pfeifferi</i> nano- suspension			127	Dispersion	-
Thierfeld, + fungi <i>Gano. pfeifferi</i> nano- suspension			111	Aggregation	Sub- Dense
Thierfeld, dithionite + fungi <i>Gano. pfeifferi</i> nano- suspension			121	Aggregation	Sub- Dense

**Figure 61.** Light microscopy images of clay-fungi cream samples (*cont.*)

Sample	Overview	Texture	STDV (homo- geneity)	Characterization of samples	
				Dispersion/ Aggregation	Shape of aggregates
Wyoming, <63 $\mu\text{m}$ + fungi <i>Gano. pfeifferi</i> nano- suspension		 50 $\mu\text{m}$ 70 $\mu\text{m}$	119	Aggregation	Porous
Garfield, <63 $\mu\text{m}$ + fungi <i>Gano. pfeifferi</i> nano- suspension			94	Aggregation	Porous
Garfield, <6.3 $\mu\text{m}$ + fungi <i>Gano. pfeifferi</i> nano- suspension			119	Aggregation	Porous
FRDL, untreated + fungi <i>Gano.</i> <i>pfeifferi</i> nano- suspension			87	Dispersion	-
FRDL, HCl 2.0 M, 80 °C + fungi <i>Gano.</i> <i>pfeifferi</i> nano- suspension			105	Dispersion	-

**Table 17. UV-transmission at three selected points of 10% pure-clay cream samples and 10% clay-fungi (*Ganoderma pfeifferi*) cream samples**

		UV- transmission (%) of 10% pure-clay cream			UV- transmission (%) of 10% clay-fungi cream		
Clay samples	Wavelength	280 nm	300 nm	400 nm	280 nm	300 nm	400 nm
Wolfka, nature	bulk	-	-	-	12.1	14.2	20.4
Wolfka, <63 µm	<63 µm bulk	35.6	33.4	40.5	14.9	16.8	23.2
Wolfka, <2 µm	<2 µm	40.0	34.2	43.6	16.6	16.4	23.3
Wyoming (TS-874)	<63 µm bulk	33.2	34.5	47.7	6.0	7.6	13.3
Garfield, <63 µm (TS-1803)	<63 µm bulk	13.3	15.8	29.8	12.4	12.2	17.9
Garfield, <6.3 µm (TS-1803)	<6.3 µm	-	-	-	10.6	10.1	15.6
FRDL, untreated	<63 µm bulk	37.3	30.5	41.8	2.6	2.9	5.2
FRDL, HCl 2.0 M, 80°C, 2 h	<63 µm bulk	16.2	19.8	32.7	5.6	8.3	22.6
Thierfeld, untreated	<63 µm bulk	16.5	16.2	22.6	11.8	12.8	17.5
Thierfeld, dithionite	<63 µm bulk	19.9	26.7	41.9	13.4	15.1	22.3

*Note: Measured using AnalytikJenaAG SPECORD 50*

In general, the series of UV-absorption abilities or UV-transmission results were observed, and UV-absorption increased clearly with clay-fungi cream samples in comparison with corresponding pure-clay cream samples (figure 60 and table 17).

In Wolfka cream sample series, sample of bulk Wolfka with natural particle size distribution and without any treatment showed the best results. The UV-transmission difference between the samples of <63 µm Wolfka and the samples of <2 µm Wolfka was not to define. Clay-fungi cream samples of three of them presented approximately 12 -23% UV-transmission.

Untreated Thierfeld and dithionite treated Thierfeld represented UV-transmission of their clay-fungi cream samples from 12 – 22% of incident UV-radiation. The samples of untreated Thierfeld absorb UV ray better than the samples of treated Thierfeld but the difference is not so large: it is only 1 - 4 percent unit whilst the UV-transmission difference between 10%-clay pure-clay cream samples of them is about 3 – 19 percent unit.

Two result profiles of Garfield show the UV-transmission from 10 – 18%. The observed UV-absorption abilities are higher than those of Wolfka group and Thierfeld group. The fungi-cream of finer Garfield, <6.3 µm of particle size, showed the better UV-absorption ability than the bulk Garfield milled and sieved to <63 µm. The difference is about 1 - 2 percent unit.

Concerning the untreated and the treated Friedland Clay samples, conversely the cases of pure-clay cream that presented the higher UV-absorption ability of the acid treated Friedland Clay (condition: HCl 2.0 M, 80°C, 2 hours) than the untreated one, clay-fungi cream samples of the acid treated Friedland Clay showed the lower absorption potential. The UV-transmission potential of acid treated one was changed significantly depending on the UV wavelength.

Interestingly, some clay-fungi cream samples showed significant improvement of UV-absorption in comparison with corresponding pure-clay cream samples, such as Wyoming bentonite and original Friedland Clay.

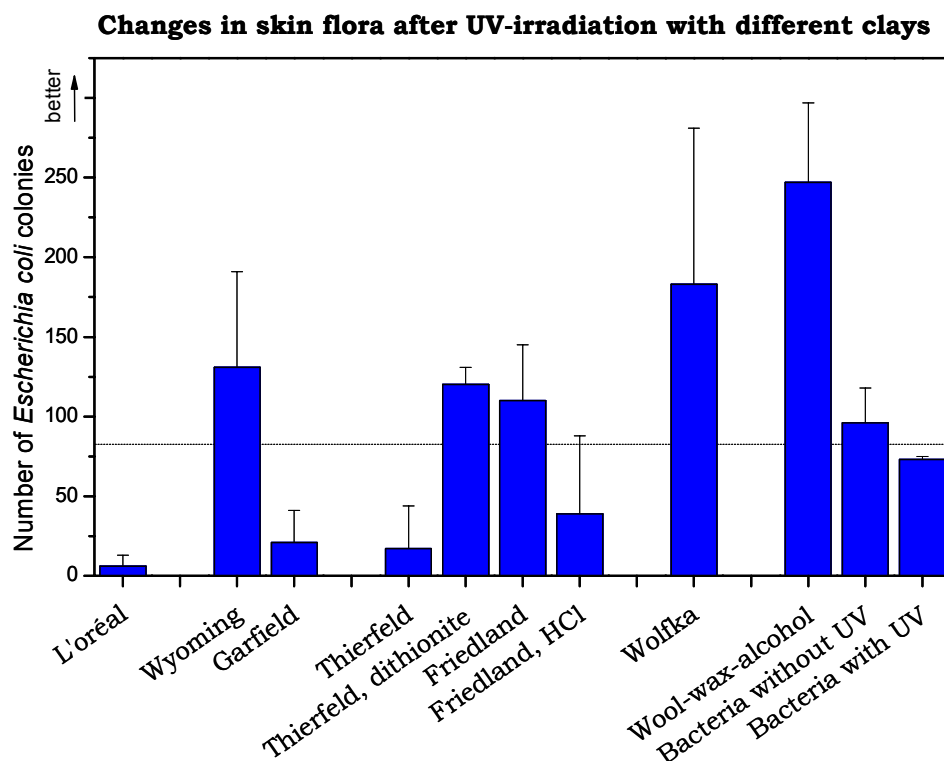
The matrix of clay-fungi cream was observed by light microscopy (figure 61). The distribution between clay and nanosuspension looks differently from sample to sample.

In summary, besides the general increasing of UV protection ability of clay in combination with *Ganoderma pfeifferi*, the other trends of UV-transmission changing might be influenced by some characteristics of clay samples. The mentioned characteristics will be discussed. Notably, it is considerable the interaction between clay and nanosuspension of the fungi, that differs from the system of pure-clay cream samples.

## 6 RESULTS OF BIO-EXPERIMENTS IN CREAM SAMPLES

### 6.1 Changes in skin flora after UV-irradiation with different clays

The ability of attacking some kinds of common bacteria such as *Escherichia coli* is a proof for photocatalytic effect of  $\text{TiO}_2$ . This property was demonstrated by the former research (chapter 2.3). That's why it was the target for this contribution to examine the influence of clay matter bearing creams in comparison with  $\text{TiO}_2$ -bearing suncreams on such the skin flora *E. coli*. The experiments were performed by skin model test with mouse-ear *in vivo*. As the above description in chapter methodology 3.2.3, the number of *E. coli* germ colony, which was available after experiments with UV-irradiation during 30 seconds, represented the safety of the used media or the coated cream samples. The higher number of the colony shows the more safety of the clay towards the skin flora.



**Figure 62. Changes in skin flora *E. coli* after UV-irradiation with different clays (20%-clay pure-clay cream samples)**

Performed by Biometec GmbH, Greifswald; Wyoming, Garfield, Thierfeld, Friedland (Friedland Clay) and Wolfka: from untreated, bulk <63  $\mu\text{m}$  clay samples; Thierfeld, dithionite = dithionite treated Thierfeld; Friedland, HCl = acid treated Friedland Clay under condition of HCl 2.0 M, 80 °C, 2 hours; Wool-wax-alcohol: sample without any clay; L'Oréal: trade-ware with LSP 15; bacteria without UV and bacteria with UV are control samples; dash line means to divide samples with skin flora attacking behaviour and samples with skin flora protecting behaviour; The higher number of colony, the more safety clay cream towards the skin flora

The figure 62 shows the results of some selected pure-clay cream samples in comparison with the trade-ware L'Oreal. The TiO<sub>2</sub>-bearing L'Oreal has a high UV protection ability (SPF 15), but this cream attacks also clearly the skin flora expressing through the very few available *E. coli* colonies after experiment.

Behaviour of the involved clay bearing samples can be subdivided generally into two main groups: (i) samples with skin flora attacking behaviour like L'Oreal: Garfield, untreated Thierfeld and acid treated Friedland Clay (by HCl 2.0 M, 80°C, 2 hours) and (ii) samples with skin flora protecting behaviour: Wyoming, dithionite treated Thierfeld, untreated Friedland Clay and Wolfka.

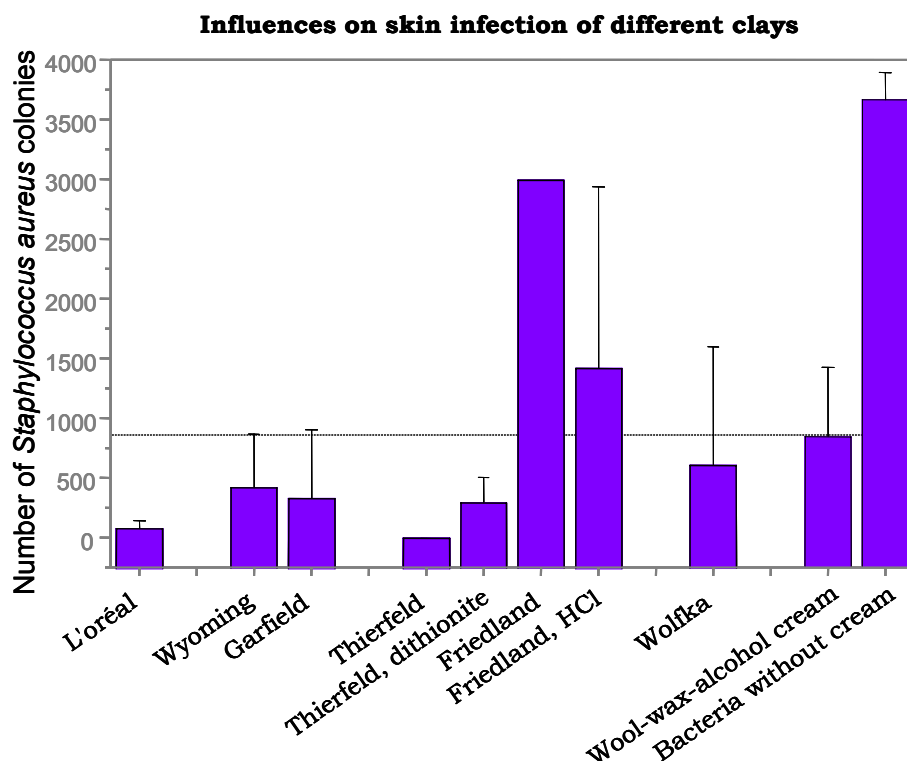
In agreement with L'Oreal cream, the three samples with the skin flora attacking behaviour (group i) have a quite high UV-absorption ability (average UV-transmission values of untreated Thierfeld, Garfield and acid treated Friedland Clay were 9.3, 17.8 and 18.8%, respectively). This UV-absorption degree is also higher than that of the investigated samples with the skin flora protecting behaviour (group ii) with 17.3, 28.5, 24.7 and 30.8% as average UV-transmission values for dithionite treated Thierfeld, Wyoming, untreated Friedland Clay and Wolfka, respectively. This situation is promoting to find a further parameter, which influences the clay matter behaviour concerning the skin flora. Normally, a higher UV protection degree should let expecting also a lower effect to the skin flora. This additional parameter is not linked alone with the influence of UV-radiation (the *E. coli* tests showed only a small difference between two control samples with and without UV-irradiation in figure 62).



## 6.2 Influences on skin infection of different clays

Behaviour of clays towards skin infections was determined by skin model test on mouse-ear *in vivo* using infectious bacteria *Staphylococcus aureus* (figure 63). Based on the experiment results, the involved clay bearing samples were subdivided generally into two main groups. One group (i) including Wyoming, Garfield, untreated Thierfeld, dithionite treated Thierfeld and Wolfka. This group has behaviour of destroying skin infection like L'Oreal cream, which presented very low number of *S. aureus* colonies in comparison with control sample (wool-wax-alcohol cream). Conversely, the other group (ii), including untreated Friedland Clay and acid treated Friedland Clay (by HCl 2.0 M, 80°C, 2 hours), has behaviour of protecting skin infection. They seem to provide suitable media for infectious *S. aureus*.

In general, different clays can affect skin infection at different levels. Some of clays can limit the bacterial growth, so that they can reduce the infection.



**Figure 63. Influences on skin infection *S. aureus* of different clays (20%-clay pure-clay cream samples)**

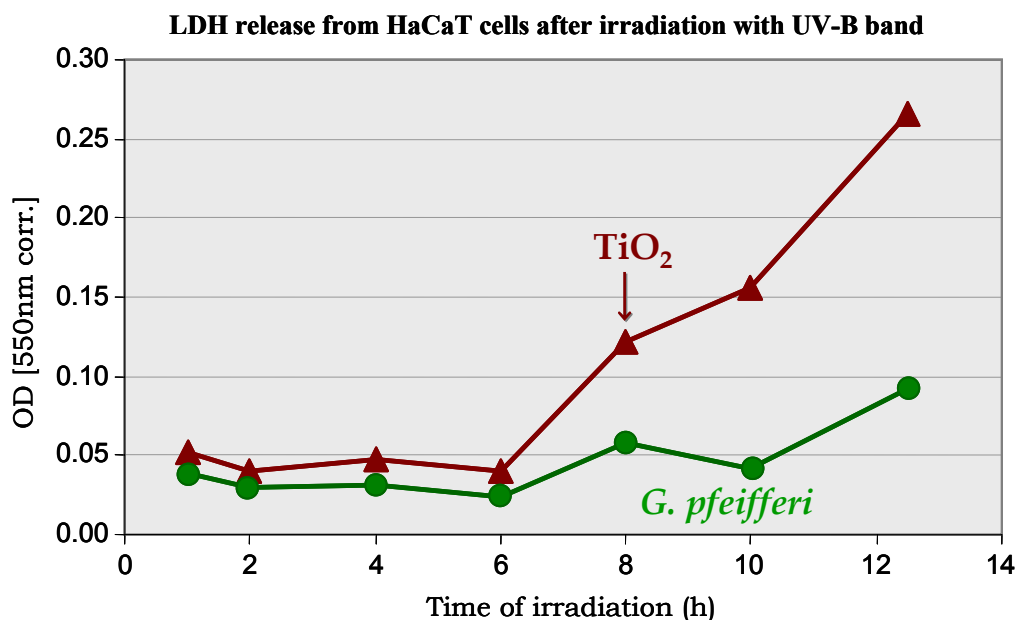
Performed by Biometec GmbH, Greifswald; Wyoming, Garfield, Thierfeld, Friedland (Friedland Clay) and Wolfka: from untreated, bulk <63 µm clay samples; Thierfeld, dithionite = dithionite treated Thierfeld; Friedland, HCl = acid treated Friedland Clay under condition of HCl 2.0 M, 80°C, 2 hours; Wool-wax-alcohol: sample without any clay; L'Oreal: trade-ware with LSP 15; bacteria without cream is control sample; dash line means to divide samples with bacteria attacking behavior and samples with bacteria protecting behaviour

### 6.3 Improving the protection ability of skin cream

To improve the protection ability of skin cream, the combination of *Ganoderma pfeifferi* suspension with different clays were tested because the *G. pfeifferi* extracts were demonstrated having suitable properties for controlling infection and skin problem inhibition.

In these *in vitro* Lactate DeHydrogenase (LDH) tests, in comparison with obtained results from suspension of 0.5%  $\text{TiO}_2$ , extract from *G. pfeifferi* impressed with very low concentration of LDH release, especially after more than 6 hours of UV-irradiation. Therefore, *G. pfeifferi* expressed the positive property towards the skin cells versus suspension of  $\text{TiO}_2$  even with very low concentration.

The experiments gave a proof for the using fungi kind *Ganoderma pfeifferi* in skin cream. Beside the known anti-aging effect, the species of fungi can improve the protection abilities of cream samples as presented in UV-measurement (as showed in chapter 5.5) as well as in the *in vitro* test.



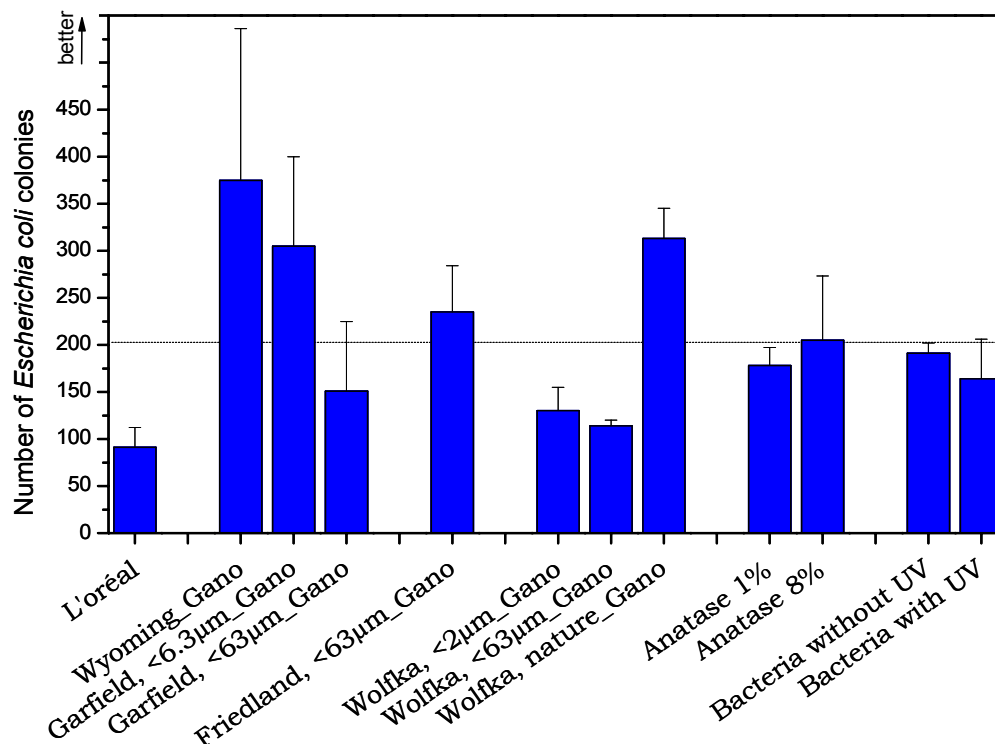
**Figure 64.** LDH release from HaCaT cells after irradiation with UV-B band under the influences of suspension of  $\text{TiO}_2$  (0.5%) and *Ganoderma pfeifferi*

Performed by Biometec GmbH, Greifswald; analysed samples were prepared as suspension; using medical UV-B (broad band, maximum 311 nm); the LDH releases were determined corresponding to optical density (OD) at 550 nm; the higher OD value (or the higher concentration of LDH release), the more toxicity of material



## 6.4 Changes in skin flora after UV-irradiation with different mixtures of clay and fungi

**Changes in skin flora after UV-irradiation with different mixtures of clay and fungi**



**Figure 65. Changes in skin flora *E. coli* after UV-irradiation with different mixtures of clay and nanosuspension of *G. pfeifferi* (10%-clay clay-fungi cream samples)**

Performed by Biometec GmbH, Greifswald; Wyoming\_Gano, Garfield, <63µm\_Gano, Friedland, <63µm\_Gano, Wolfka, <63µm\_Gano: mixtures of untreated, bulk <63 µm clay samples with *G. pfeifferi*; Garfield, <6.3µm\_Gano: mixture of fine part, <6.3 µm, of Garfield with *G. pfeifferi*; Wolfka, <2µm\_Gano: mixture of fine part, <2 µm, of Wolfka with *G. pfeifferi*; Wolfka, nature\_Gano: mixture of Wolfka as natural size with *G. pfeifferi*; Anatase 1% and Anatase 8%: mixtures of anatase and wool-wax-alcohol without *G. pfeifferi*; bacteria without UV and bacteria with UV are control samples; dash line means to divide samples with skin flora attacking behavior and samples with skin flora protecting behaviour; The higher number of colony, the more safety clay cream towards the skin flora

The tests with skin flora *E. coli* for mixtures of clay and nanosuspension of *G. pfeifferi* were also carried out. The figure 65 presents the changes of colonies with different selected clay-fungi cream samples after 30 seconds under UV irradiation.

In this visualization, it is also possible to subdivide the samples into two groups according to results of counted *E. coli* colonies. One group (i) has skin flora attacking behaviour like TiO<sub>2</sub>-bearing L'Oreal, anatase 1% and anatase 8% - these materials presented generally lower numbers of colonies than other samples after experiments.

This group includes mixtures of *Ganoderma pfeifferi* with <63 µm Garfield, <63 µm Wolfka and <2µm Wolfka samples. These clay-fungi cream samples have also average UV-transmission values of 14.2, 18.3 and 18.8%, respectively. The other group (ii) has skin flora protecting and partially stimulating behaviour expressing the stronger growth of bacteria. This group involves mixtures of the fungi with <63 Friedland Clay (untreated), Wyoming, <6.3 µm Garfield and natural Wolfka samples. These samples have generally higher UV-absorption abilities in comparison with other clay-fungi samples. Their corresponding average UV-transmission values are 3.6, 9.0, 12.1 and 15.6%.

In general, it is notable here that the samples with high UV-absorption potential or low degree of passing UV-radiation also protect the skin flora. Therefore, UV protection property of clay-fungi may be connected with skin flora protection behaviour. However, because of the regardless difference between the numbers of colonies obtained from the control samples (plates of bacteria with and without UV-irradiation), some additional parameters which influences the behaviour of clay-fungi mixtures is also expected to be determined.

## 7 DISCUSSION

### 7.1 General UV protection behaviour of clays and clay minerals

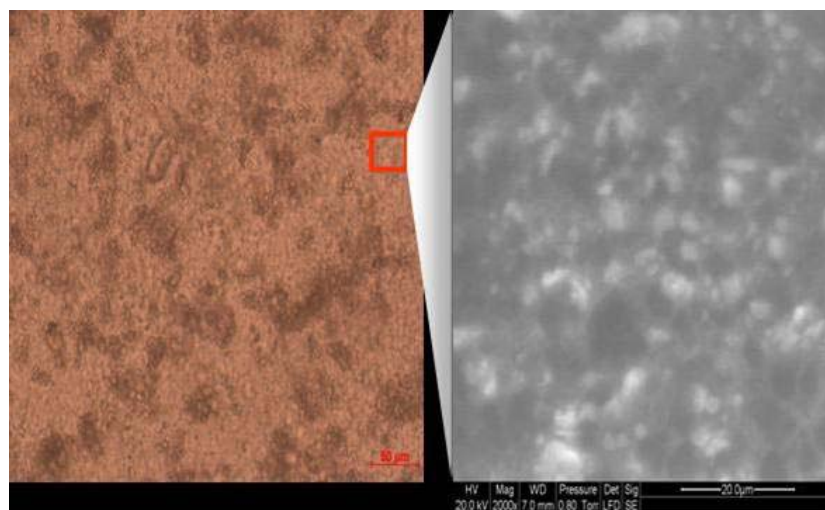
#### 7.1.1 UV protection potential of clays and clay minerals in pure-clay creams

Clays show a potential in UV protection to absorb or to reflect UV-radiation. The analyzed pure-clay cream samples did not show only a level of UV-transmission result, but they are obtained with different results and different levels of UV-transmission behaviour.

From analyses of four clay groups carried out, it was observed that kaolins have a lower UV protection level than bentonites and mixed-layer dominated clays; and mica dominated clays have a higher UV protection level than the other clays. The quite low UV-transmission results from nontronite Garfield and hematite-rich Thierfeld suggest an iron influence. This study was also considering effects of particle parameters. However, the samples in different grain size distributions showed an unexpected difference: the sample with finer grain size distribution showed a slight lower UV protection ability. An additional treatment, acid treatment, was mentioned in the Friedland Clay series to examine any changing in UV-transmission level. The obtained results showed that the activation of clays can improve UV protection, especially with sample treated in the condition of HCl 2.0 M and 80°C during 2 hours.

In the pure-clay creams, clay particles (pretreated by mixing with glycerol) are distributed in ointment wool-wax-alcohol cream with dispersion as well as aggregation. Samples of bentonites and mixed-layer dominated clay showed the aggregations with different levels of porosity (e.g. honey-comb in Wyoming, Garfield and open structure in Chambers, SWy-2 and Friedland Clay) and also the dispersions (other samples). Samples of kaolins and clays showed mostly blocky, dense aggregations except for the dispersion of Caminau and Seilitz samples. But, from an ESEM image (figure 66), clay particles, which were also found under the wool-wax-alcohol cream, can be seen. That means clay matter could cover the whole area of cream slide. The distributions of clay particles in ointments did not show a clear agreement or trend with UV-transmission levels.

Therefore, influences of iron, acid treatment and particle parameters are taken for discussion in detail in corresponding three next chapters 7.3, 7.4 and 7.6 to bring out specific UV protection behaviour of clays and clay minerals. The structure of the system of pure-clay creams is also discussed in chapter 7.2.



**Figure 66.** Light microscopy image (left) and ESEM image (right) from <63 µm bulk Wolfka kaolin cream (20% of clay)

Note: ESEM image is analyzed using microscopy FEI Quanta 600 (EDAX microanalysis) at Institute of Soil science, University of Hamburg

### 7.1.2 UV protection potential of clays and clay minerals in clay-fungi creams

Clays presented also completely different behaviours when mixing with nanosuspension of fungi *Ganoderma pfeifferi*. The UV protection behaviours of all fungi-clay cream samples increase in comparison with the corresponding pure-clay cream samples.

In general, the clay-fungi cream samples of kaolins showed the higher UV-transmission value than other groups. Grain size distribution influence is also considered in the mixing with the nanosuspension. The sample of Wolfka in natural size distribution presented the best results in comparison with finer grain size distributions using grinding and Atterberg sedimentation. The iron trend, which was observed with pure-clay cream series, does not appear in the clay-fungi cream series. In additions, the acid treated Friedland Clay, which presented much lower UV-transmission value than the untreated clay in pure-clay cream system, showed drastic reducing in UV protection ability, especially in the UV-A area.

In the clay-fungi creams, distribution of clay particles in nanosuspension is considered. The suspension of fungi extracted by plantacare (aqueous solution of decyl glucoside) can interact with clays. The interaction might present different levels depending on the charges of the clays. In the system, clay could absorb the long-chain molecular (decyl glucoside). The dispersive or aggregative distributions between clay particles and nanosuspension and ointment observed under light microscopy may be related to the charge.

Therefore, detailed discussion about some specific properties of clay, which influences the interaction between clay and nanosuspension causing changes of UV protection behaviour from pure-clay system to clay-fungi system, is considered in later chapters, especially chapter 7.2 and chapter 7.5.

### **7.1.3 Effects of clays media towards skin flora and skin infection**

Concerning changes of skin flora after UV-radiation with clays and mixtures of clay and fungi as well as skin infection with clays, different clays showed a completely various behaviour in interaction with bacteria. With pure-clay cream samples, towards both kinds of skin flora and skin infection, bacteria are limited to grow by clay characterized with mostly higher UV protection ability and they are “supported” by clay characterized with mostly lower UV protection ability. Conversely, in mixing with nanosuspension of fungi, the UV protection abilities and positive intensities of interaction with skin flora of clays are in an agreement. Hence, the interaction between pure-clay and clay-fungi cream samples with skin flora and skin infection is discussed in detail in the chapter 7.7.

## 7.2 Structure of clay particles in cream

### 7.2.1 Structure of clay particles and wool-wax-alcohol ointment in pure-clay creams

In the process of preparing pure-clay cream samples, clay was premixed with glycerol and subsequently mixed with ointment wool-wax-alcohol cream. Because of the preparation manner, interlayer spaces of clay minerals in the clay samples can be dominated mostly by glycerol.

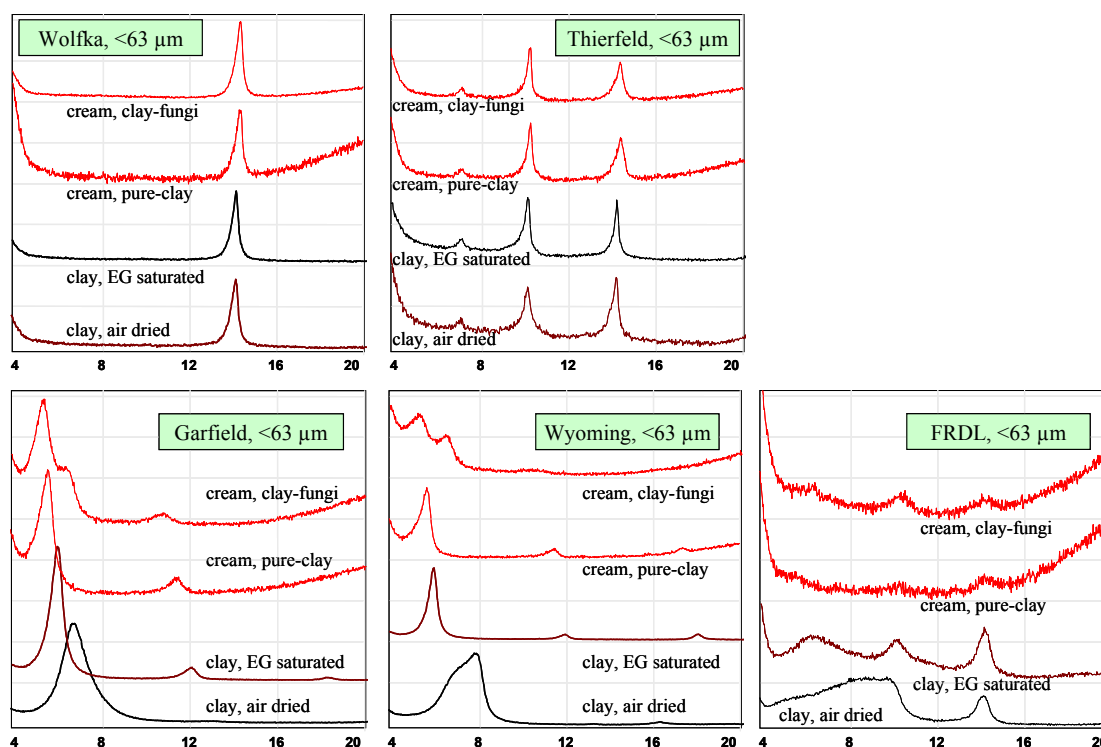
Wool-wax-alcohol cream contains wool-wax-alcohol, sorbitanum trioleinicum GOT and vaseline with a ratio 2.5 : 3 : 100. The dominating vaseline itself includes 50 - 80% liquid phase of isoparaffin and olefincarbohydrate. The solid phase of vaseline is composed by 10 - 20% of crystalline component (n-paraffin) and 90 - 80% of microcrystalline component (isoparaffin with low amount of alicycle) (Voigt & Bornschein, 1975).

The XRD analyses of pure-clay cream samples of Wolfka and Thierfeld, dominated by non-expandable clay minerals, did not show any change of peak positions in comparison with clay matter (figure 67 and table 18). Therefore, glycerol and wool-wax-alcohol are not interlamellary in these samples.

Concerning clay minerals with layer-charge, the examples of Garfield, Wyoming and Friedland Clay show shifting of 001-spacing from 14.9 Å, 14.0 Å and 11.7 Å (air-dry specimens) to 19 & 18 Å, (pure-clay cream samples) after milling with glycerol and wool-wax-alcohol cream (figure 67 and table 18). The first shifting level (i) of about 18 Å corresponds to expansion of interlayer space by glycerol. The second yielded shifting (ii), about 19 Å, could be caused by absorption liquid vaseline component from wool-wax-alcohol cream in interlayer. The second mentioned interaction is also proved by XRD-results from clay-fungi cream samples.

The clay samples dominated by expandable clay minerals (such as bentonites and illite/smectite mixed-layer dominated clays) can absorb glycerol and liquid vaseline component of wool-wax-alcohol cream in interlayer. Otherwise, clay samples characterized mostly by non-expandable clay minerals distribute wool-wax-alcohol cream only in the voids between particles.

Light microscopy observation supports for imagination about structure of clay particles in the pure-clay cream samples. Kaolins and mica dominated clays showed that mostly distribution of coarse aggregate or dispersion structure is dominating (figure 50 and figure 55). However, because glycerol and liquid vaseline can expand the interlayer of expandable particles, bentonites and mixed-layer clays showed commonly disaggregation of stacks representing finer distribution under light microscopy (figure 52 and figure 59).



**Figure 67.** XRD patterns of selected clay samples and their cream samples,  $^{\circ}2\theta$  CoK $_{\alpha}$  position

Note: Measured using HZG 4 / Seifert C3000; measured from 2 to 20  $^{\circ}2\theta$ ; XRD patterns including 10%-clay clay-fungi cream sample (cream, clay-fungi), 20%-clay pure-clay cream sample (cream, pure-clay), ethylene-glycol saturated specimen of clay sample (clay, EG saturated) and air-dried specimen of clay sample (clay, air dried), left to right and above to bottom: Wolfka, Thierfeld, Garfield, Wyoming and Friedland Clay

**Table 18.** 001-spacing d-values of clay minerals from XRD patterns of clay samples, pure-clay cream samples and clay-fungi cream samples

		d-values of 001-spacing (Å)			
		Clay, Air dried	Clay, EG saturated	Cream, Pure-clay (*)	Cream, Clay-fungi (**)
Wolfka, <63 $\mu\text{m}$	<63 $\mu\text{m}$ bulk	7.2	7.2	7.2	7.2
Thierfeld, untreated	<63 $\mu\text{m}$ bulk	9.9	10.0	10.0	10.0
Garfield, <63 $\mu\text{m}$ (TS-1803)	<63 $\mu\text{m}$ bulk	14.9	17.3	17.9 area (i) 18.7 area (ii)	15.7 area (i') 18.9 area (ii)
Wyoming (TS-874)	<63 $\mu\text{m}$ bulk	14.0	17.3	18.0 area (i) 19.1 area (ii)	15.6 area (i') 19.1 area (ii)
FRDL, untreated	<63 $\mu\text{m}$ bulk	11.7	16.0	19.0 area (ii)	16.0 area (i')

Note: (\*): mixture of clay, glycerol and liquid vaseline bearing wool-wax-alcohol cream; (\*\*): mixture of clay, plantacare bearing nanosuspension of fungi and liquid vaseline bearing wool-wax-alcohol cream; (i): expansion by glycerol; (ii): expansion by liquid vaseline and (i'): expansion by plantacare

Measured using HZG 4 / Seifert C3000; deconvolution using WinFit-procedure (Krumm, 1994)

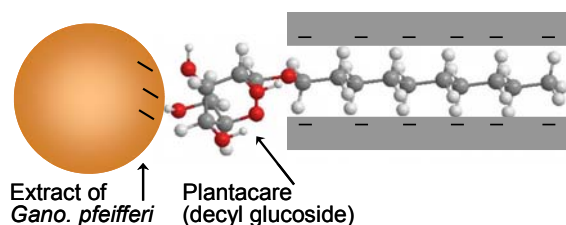
### 7.2.2 Structure of clay particles and fungi capsules in clay-fungi creams

In the process of preparing clay-fungi cream samples, primarily nanosuspension of fungi extracted by plantacare was milled with wool-wax-alcohol cream. Consequently, this matter was milled to homogeneous with the clay samples.

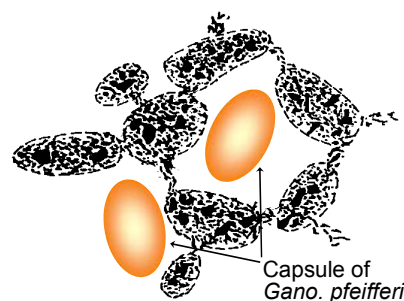
The used plantacare is aqueous solution of decyl glucoside, which is characterized as active long-chain. The glucose head of plantacare has a positive charge under low pH-value. Therefore, the positive charged heads of plantacare demobilize negative charged lipid-like *Ganoderma pfeifferi*'s extract (figure 68). The plantacare chain can enter interlayer of clay minerals as showing in figure 68. The XRD experimental information also supports for that. The patterns of clay-fungi cream samples show also two different observations: no peak shifting with clay sample dominated by non-expandable clay minerals such as samples of Wolfka and Thierfeld; and peak shifting (001-spacing and 002-spacing) with clay sample dominated by expandable clay minerals such as samples of Garfield, Wyoming and Friedland Clay (figure 67 and table 18).

#### *Clays dominated by non-expandable clay minerals*

With non-expandable clay samples, for example Wolfka and Thierfeld, fungi capsules can only distribute in the voids between clay particles (figure 69). Using XRD analyses, there is no indicator for the entering in interlamellar (figure 67 and table 18). The larger variable charge yields the larger voids between the clay particles, so that the fungi capsules are more aggregated in the matrix. In figure 61, the images of clay-fungi creams also show that the Thierfeld sample has more aggregative structure than the Wolfka sample in according to the higher variable charge of mica dominated clay Thierfeld than kaolinite dominated Wolfka kaolin.



**Figure 68. Plantacare-bearing fungi capsules in interlayer of clay particles**  
Structure of clay particles in clay-fungi creams



**Figure 69. Plantacare-bearing fungi capsules in voids of clay particles**  
Structure of clay particles in clay-fungi creams - emulsion homogenization

(adopted to Pusch & Yong, 2006)



### ***Clays dominated by expandable clay minerals***

The two yielded expansions, (i') the first is about 16 Å and (ii) the second is about 19 Å, are discussed now. The second one is equal to the above mentioned second expansion yielded from pure-clay cream samples. Therefore, it refers to the expansion caused by liquid vaseline or wool-wax-alcohol cream, which is used in both types of cream samples. The first expansion at 16 Å indicates a monolayer order of the plantacare chain in the interlayer space, the glucose head is outside the clay stack because of its large size (C-O and C-C bonds are about 100 Å) (figure 68).

Whilst the cream sample of Garfield shows that expansion by liquid vaseline is about 3.2 times higher than expansion by plantacare (19 Å : 16 Å peak areas = 710: 220), the cream sample of Wyoming shows corresponding number only about 1.5 times (220: 150). The sample of Friedland Clay presents only the plantacare-expansion (figure 67). Because the plantacare chain is neutral, so that it can occupy the interlayer space only under the low charge condition.

Comparing the layer charge, Friedland Clay is characterized as mixed-layer dominated clay including a part of IS-ml and a part of diVS-ml (4.3.1). Its charge is estimated about 0.09 per unit cell. Montmorillonite dominated in Wyoming bentonite is also characterized as low-charge smectite with about 0.16 per unit cell. Garfield, dominated by nontronite, has high-charge, which is about 0.31 per unit cell. The charge values are estimated from obtained clay mineral formulae by EDX-TEM measurements (chapter 4.2.1). Therefore, the order of decreasing layer charge is Garfield > Wyoming > Friedland Clay.

The observed images under light microscopy also showed the matrix of clay particles with fungi capsules and wool-wax-alcohol cream (figure 70). The different levels of porous of aggregated structures seem to belong to the structure of clay samples. The more dispersive structure was observed from clay-fungi cream sample of Friedland Clay in comparison with structures of clay-fungi cream samples of Wyoming and Garfield.



**Figure 70. Clay-fungi cream matrix of selected clays dominated by expandable clay minerals**

*Images taken by light microscopy, see also figure 61*

In sum, the structure of clay particle in the cream sample, including pure-clay cream samples and clay-fungi cream samples, depends on the layer charge of clay minerals. With clay samples dominated by non-expandable clay minerals, wool-wax-alcohol cream and/or fungi capsule arrange in the voids between particles. The larger void makes the more aggregative structure. With clay samples dominated by expandable clay minerals, liquid vaseline of wool-wax-alcohol cream can enter partly in the interlayer and/or plantacare linked with fungi extract also can enter in the interlayer. A low charge of expandable clay mineral supports a higher absorption of plantacare. The lower charge of the expandable clay minerals supports for more homogeneous structure of clay-fungi cream sample.

### 7.3 Iron effect on UV-absorption ability of clays and clay minerals

#### 7.3.1 Presence of iron effect of clays and clay minerals in ointment

In chapter 5, few indications were summarized that iron amount of the samples could have a certain effect to improve the UV-absorption ability of clay minerals. In the system wool-wax-alcohol cream and 20 % clay minerals admixtures, nontronite Garfield as well as German reference clays Teistungen and Thierfeld show a high ability for UV-absorption (figure 51 and figure 54). These three samples are characterized by the high amount of  $\text{Fe}_2\text{O}_3$  in the chemical analyses in comparison to other involved samples.

Therefore,  $\text{Fe}_2\text{O}_3$  could influence the UV protection property of the clays. Data from samples of pharmacy products,  $\text{Fe}_2\text{O}_3$  (ferrum oxydatum rubrum) with about 0.3% and  $\text{Fe}(\text{OH})_3$  (ferrum oxydatum flavum) with about 0.1% of UV-transmission, demonstrated that the amount of iron has significant effect on the UV protection behaviour. That's why, the possible influence of iron, presenting generally as total  $\text{Fe}_2\text{O}_3$ -amount in chemical composition of clay or especially as non-clay phases (for example: hematite) and/or clay phases (for example:  $\text{Fe}^{3+}$  in octahedral layer of sheet silicates), is discussed in detail now.

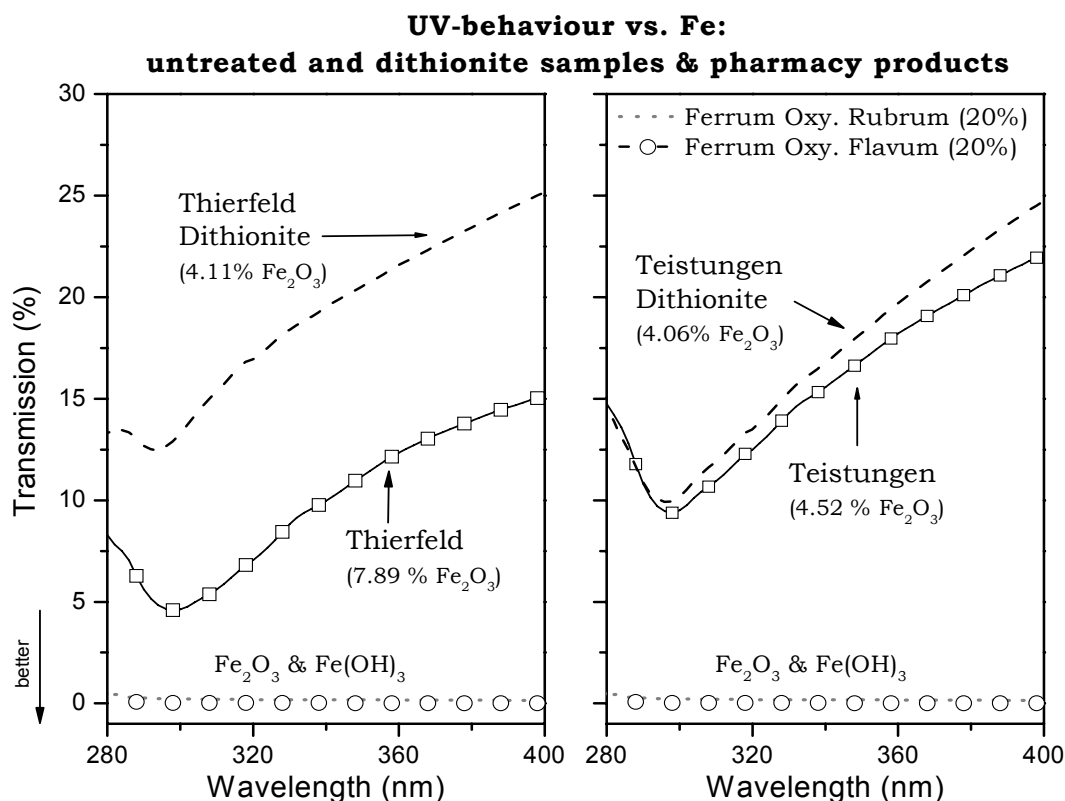
To understand the mentioned effect of  $\text{Fe}_2\text{O}_3$ , not only the untreated sample of Thierfeld and Teistungen but also their treated ones were analyzed by UV-measurement. As presented in the chapter 5.3, the obvious changes of UV-transmission values from untreated samples to the corresponding dithionite treated samples of 20%-clay samples as well as 10%-clay samples were observed.

Figure 71 shows the patterns of 20%-clay pure-clay cream samples of original and dithionite treated Thierfeld and Teistungen as well as pharmacy products in comparison with corresponding amount of total  $\text{Fe}_2\text{O}_3$ . The distances between patterns of original and treated samples seem to be connected with differences between reducing  $\text{Fe}_2\text{O}_3$ -amounts by dithionite treatment: about 7.9% of UV-transmission difference of couple of Thierfeld samples is corresponding to about 3.8% weight of  $\text{Fe}_2\text{O}_3$  reducing, meanwhile 1.1% of UV-transmission difference of couple of Teistungen samples is corresponding to about 0.5% weight of  $\text{Fe}_2\text{O}_3$  reducing.

#### *Mineralogy and Fe-bearing phases for Teistungen & Thierfeld samples*

The positions of Fe-atoms in the mineral matter of untreated and treated Teistungen and Thierfeld samples are differentiated by Mössbauer spectroscopy analyses (figure 46 and appendix 7).

Teistungen, untreated:	1.1 % of total Fe in dioctahedral clay minerals as $\text{Fe}^{2+}$
	1.1 % of total Fe in dioctahedral clay minerals as $\text{Fe}^{3+}$
	1.0 % of total Fe in hematite as $\text{Fe}^{3+}$ (~ 1.4 % hematite)
Teistungen, dithionite:	1.3 % of total Fe in dioctahedral clay minerals as $\text{Fe}^{2+}$
	1.1 % of total Fe in dioctahedral clay minerals as $\text{Fe}^{3+}$
	0.4 % of total Fe in hematite as $\text{Fe}^{3+}$ (~ 0.6 % hematite)
Thierfeld, untreated:	0.5 % of total Fe in dioctahedral clay minerals as $\text{Fe}^{2+}$
	1.7 % of total Fe in dioctahedral clay minerals as $\text{Fe}^{3+}$
	3.3 % of total Fe in hematite as $\text{Fe}^{3+}$ (~ 4.7 % hematite)
Thierfeld, dithionite:	0.5 % of total Fe in dioctahedral clay minerals as $\text{Fe}^{2+}$
	2.0 % of total Fe in dioctahedral clay minerals as $\text{Fe}^{3+}$
	0.4 % of total Fe in hematite as $\text{Fe}^{3+}$ (~ 0.5 % hematite)



**Figure 71. UV-behaviour vs. iron amount: untreated Thierfeld, Teistungen, their dithionite treated samples and pharmacy products**

Measured using AnalytikJenaAG SPECORD 50; UV-measurement of 20%-clay pure-clay cream samples of <63  $\mu\text{m}$  bulk clay with wool-wax-alcohol cream; The lower transmission proportion, the better effect by clay cream

Teistungen and Thierfeld, were characterized by TEM-EDX analyses with  $<2\ \mu\text{m}$  component, composed mostly of diVerm. and diVerm.-rich diVS-ml, therein  $\text{Fe}^{3+}$  in octahedral layers is lower than 3% of  $\text{Fe}_2\text{O}_3$ -amount per particle. That means there is a low degree of Fe-incorporation in the pattern of clay minerals. After dithionite treatments,  $\text{Fe}^{3+}$  components in octahedral layers were more or less unchanged. Hence, the intensity of reduced UV protection ability is comparable with the amount of dissolved hematite by dithionite processing.

Another possible factor, which may influence the UV protection theoretically, is the distribution and orientation of particles. However, the observation (figure 55) shows that creams of untreated and treated Teistungen and Thierfeld have the similar dense aggregation structures. Therefore, there is no additional influence of particles' arrangements in the creams to expect.

Summarizing the discussion of the two samples Teistungen and Thierfeld and their treated materials, only the different iron-amount (corresponding to different amount of hematite) seems to be responsible for the different intensity of UV absorption in those samples.

### ***UV-transmission and total $\text{Fe}_2\text{O}_3$ -amount of all samples***

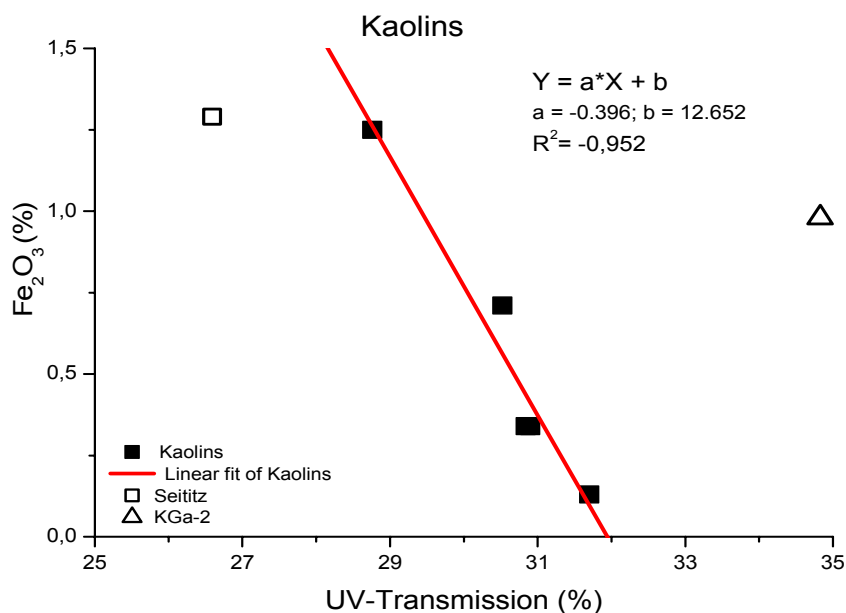
The average UV-transmission values (as average value of the three selected points at 280 nm, 300 nm and 400 nm of wavelength) together with  $\text{Fe}_2\text{O}_3$ -amount in total chemical composition of bulk sample were selected for correlation diagrams in figure 72, figure 73 and figure 74.

### ***Kaolins***

Data of kaolin series contributed the figure 72, therein data from four kaolin samples Caminau, Wolfka, Spergau and low defect Georgia kaolin KGa-1b, are in a linear relationship. It is imaging that higher  $\text{Fe}_2\text{O}_3$ -amount will absorb more UV-radiation. The exception points are from Seilitz and high defect Georgia kaolin KGa-2.

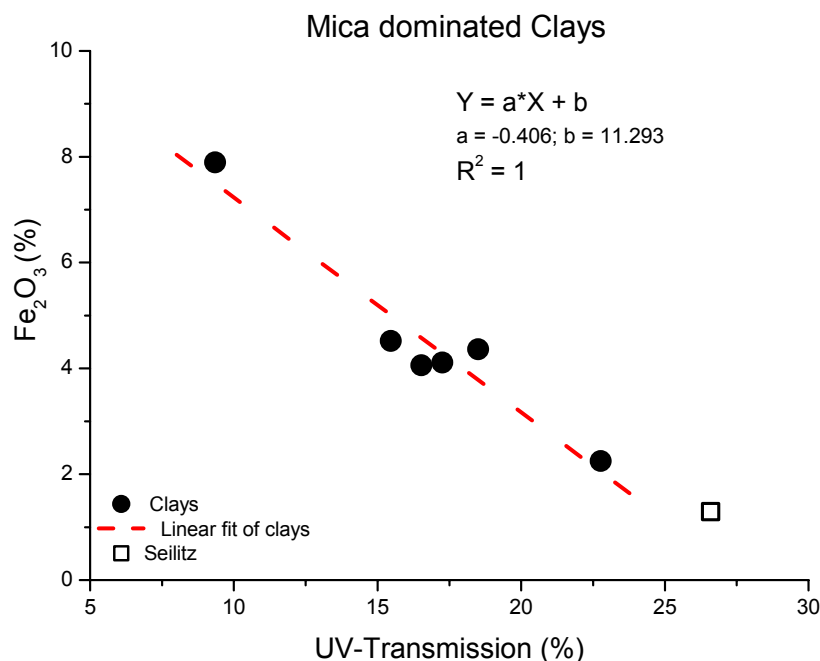
The Fe-contribution in clay minerals of these four samples is less than  $\frac{1}{3}$  of total Fe. The further  $\frac{2}{3}$  of total Fe are covered by a large number of Fe-bearing trace minerals:

Caminau ( $\text{Fe}_2\text{O}_3$ : 1.25%):	goethite, hematite, ilmenite, jarosite, limonite, magnetite, pyrite, siderite, titanomagnetite
Wolfka ( $\text{Fe}_2\text{O}_3$ : 0.34%):	goethite, hematite, jarosite, pyrite
Spergau ( $\text{Fe}_2\text{O}_3$ : 0.71%):	magnetite, pyrite
KGa-1b ( $\text{Fe}_2\text{O}_3$ : 0.17%):	Fe could be covered by Fe-contribution in kaolinite structure



**Figure 72. Relationship between Fe<sub>2</sub>O<sub>3</sub>-amount and UV-transmission of kaolins**

Note: UV-transmission values from 20%-clay pure-clay cream samples; solid squares present the kaolin samples including Caminau, Wolfka, Spergau and KGa-1 samples; the line is a linear fit of these four kaolins; empty square presents Seilitz sample and empty triangle presents KGa-2 sample



**Figure 73. Relationship between Fe<sub>2</sub>O<sub>3</sub>-amount and UV-transmission of clays**

Note: UV-transmission values from 20%-clay pure-clay cream samples; solid rounds present the clay samples including Plessa, Gorrenberg, untreated Teistungen, treated Teistungen, untreated Thierfeld and treated Thierfeld samples; dash line is linear fit of the clays and empty square presents Seilitz sample

Because of the large variability of Fe-bearing phases in the four kaolin samples, the Fe-amount is to be considered as one of the main factors in this sample group to absorb UV-radiation.

Comparing the mineral composition of Seilitz and high defect Georgia kaolin KGa-2 with the other mentioned kaolins, it is to note that these two samples have a different general clay mineral matter than the other four samples. Seilitz was characterized with lowest amount of kaolinite (34%) and highest amount of 2:1 sheet silicates (45%, mostly as IS-ml with 90% of illitic layers) in comparison with other German kaolins (chapter 4.1.1). In Seilitz kaolin,  $\text{Fe}^{3+}$  was determined as  $\text{Fe}^{3+}$  in octahedral layer of IS-ml series. KGa-2 was determined as high defect kaolin with much higher total surface area than the other kaolins (chapter 4.1.3). The results by TEM-EDX indicate the existence of a remarkable amount of KE-ml phases with 40% of expandable layers in KGa-2.

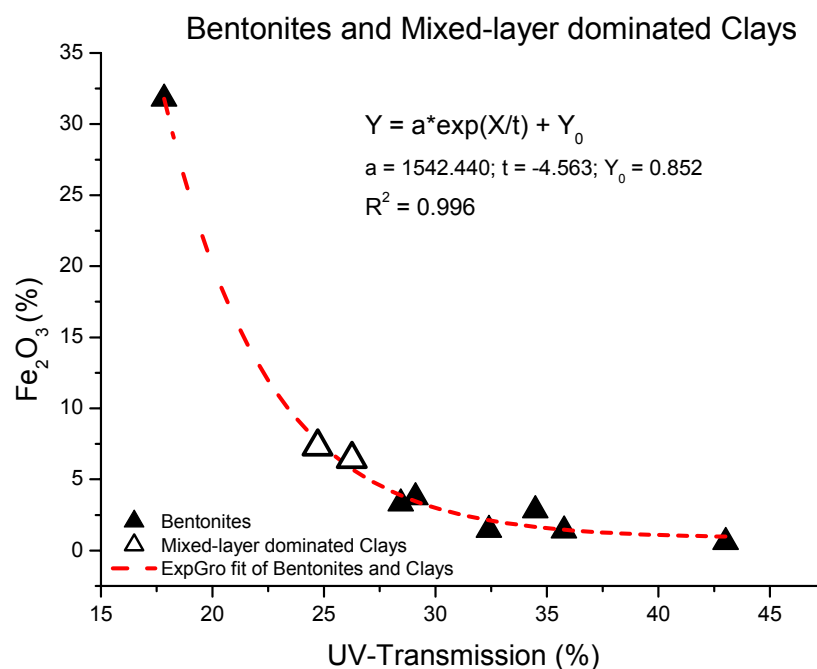
#### *Mica dominated clays*

Similarly, figure 73 shows a linear relationship between  $\text{Fe}_2\text{O}_3$ -amount and average UV-transmission values obtained from mica dominated clay series (Plessa, Gorrenberg, untreated Teistungen, treated Teistungen, untreated Thierfeld and treated Thierfeld). The figure also includes the presence of Seilitz kaolin. The sample is very close to the linear fit line of clays. It is notable again that Seilitz includes nearby a half of 2:1 sheet silicate, which is characterized as IS-ml phase with 90% illitic layer. Therefore, the Seilitz is also close to the mica dominated clay series.

Similar to Teistungen and Thierfeld, Plessa and Gorrenberg were characterized as materials composed mostly by diVerm. and diVerm.-rich diVS-ml in  $<2\ \mu\text{m}$  component (using TEM-EDX analyses). The Fe-amounts of these two clays, Plessa and Gorrenberg with 2.25% and 4.36% weight of  $\text{Fe}_2\text{O}_3$  respectively, are distributed mostly as  $\text{Fe}^{3+}$  in octahedral layers of mica-like components.

#### *Bentonites and mixed-layer dominated clays*

In opposite to the cases of kaolins and mica dominated clays, from the data of bentonite series (Garfield, Chambers, Wyoming, SHCa-1, STx-1, SAz-1 and SWy-2) and mixed-layer dominated clays (untreated bulk sample and  $<2\ \mu\text{m}$  sample of Friedland Clay), the fitting is not a linear relationship, but exponential relationship (figure 74). Therefore, it is quite clear that the relationship between  $\text{Fe}_2\text{O}_3$ -amount and UV-transmission of bentonite as well as mixed-layer dominated clay is different from those of clays and kaolins.



**Figure 74. Relationship between Fe<sub>2</sub>O<sub>3</sub>-amount and UV-transmission of bentonites and mixed-layer dominated clay**

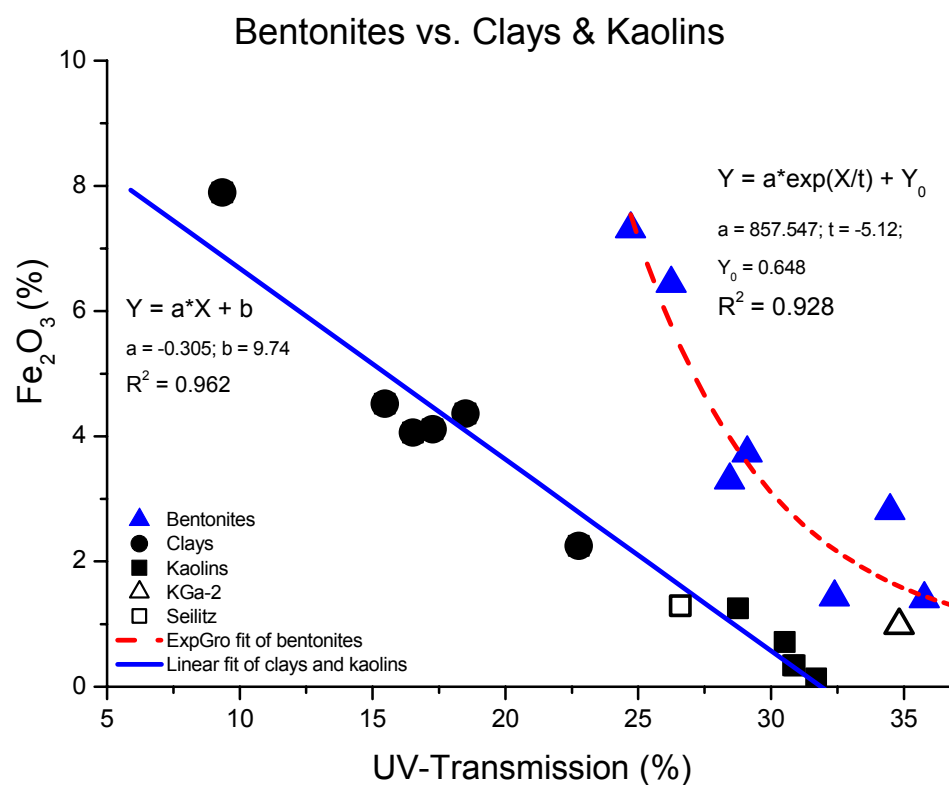
Note: UV-transmission values from 20%-clay pure-clay cream samples; solid triangles present the bentonites including Garfield, Chambers, Wyoming, SHCa-1, STx-1, SAz-1 and SWy-2 samples; empty triangles present bulk and <2 μm untreated Friedland Clay samples; dash curve is exponential fit of the bentonite and mixed-layer dominated clay series

The bentonites have no phase of iron non-clay minerals, except for SAz-1 which contains magnetite and Garfield which contains goethite and maghemite in traces. The bulk and <2 μm Friedland Clay samples contain about 15% of Fe<sub>2</sub>O<sub>3</sub>-amount in chlorite phase (by Mössbauer spectroscopy analyses). The main distributions of Fe-amount in the bentonites and clays are Fe-ion in smectites or mixed-layer series.

These Fe-amounts in structure of clay minerals are mainly responsible for the UV-absorption capacity of bentonites and mixed-layer dominated clays (shorten as bentonites). In comparison to the relationship between amounts of Fe<sub>2</sub>O<sub>3</sub> and UV-transmission values analyzed from kaolins and mica dominated clays, the bentonites have lower UV-absorption ability than the kaolins and the clays for the same amount of Fe<sub>2</sub>O<sub>3</sub> (figure 75). The higher degree of dispersion of the particles in the ointment and the commonly porous aggregates (partially, honey comb-like), observed from pure-clay cream samples of bentonites, is overlapping the Fe-influence and is reducing generally the UV-absorption in comparison to clays and kaolins.



With the observation about the case of Seilitz as well as both determined relationships all are linear ones. It is thus possible to connect kaolin series and mica dominated clay series. Figure 75 presents this linkage. Almost all presences of kaolin and mica dominated clay samples are combined in one. The figure also presents the series of bentonites and mixed-layer dominated clays. Although it is expressed in the same scale and excluding the special point of Garfield, which is very rich  $\text{Fe}_2\text{O}_3$ -amount in chemical composition, the series of bentonite and mixed-layer clay do not tie to the other series. They are in different exponential relationship. However, presence of KGa-2 is close to the series of bentonite and mixed-layer dominated clay. That is possibly because of some characteristics of KGa-2 kaolin, which was determined with remarkable amount of kaolinite/expandable phase (with 40% of expandable layers), are similar to characteristics of smectite or mixed-layer phase.



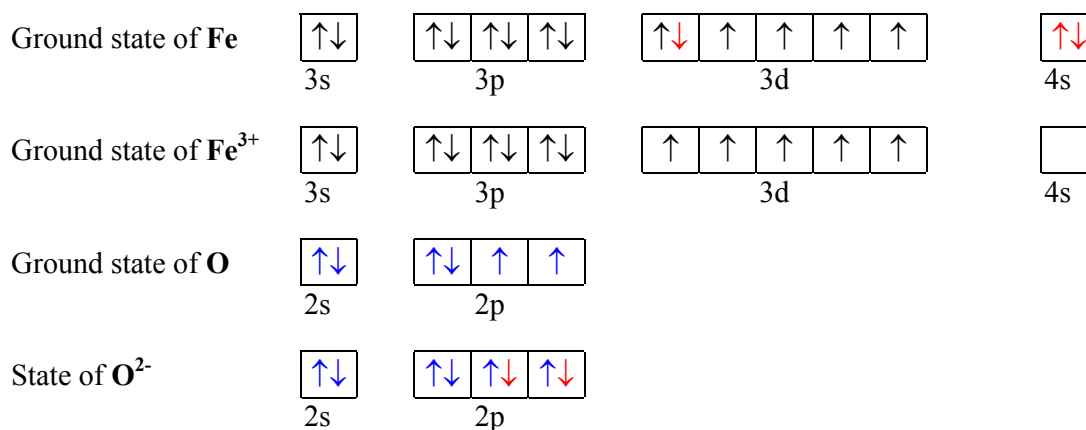
**Figure 75. Bentonites versus clays and kaolins in the aspect of relationship between  $\text{Fe}_2\text{O}_3$ -amount and UV-transmission**

Note: UV-transmission values from 20%-clay pure-clay cream samples; solid triangles present the bentonites including Chambers, Wyoming, SHCa-1, STx-1, SAz-1 and SWy-2 and bulk and  $<2 \mu\text{m}$  untreated Friedland Clay samples; dash curve is exponential fit of the bentonite and mixed-layer dominated clay series; empty triangle presents KGa-2 sample; dark squares present kaolins including Caminau, Wolfka, Spergau and KGa-1 samples; empty square presents Seilitz sample; dark rounds present clays including Plessa, Gorrenberg, untreated Teistungen, treated Teistungen, untreated Thierfeld and treated Thierfeld samples and solid line is line fit of the kaolins and clays

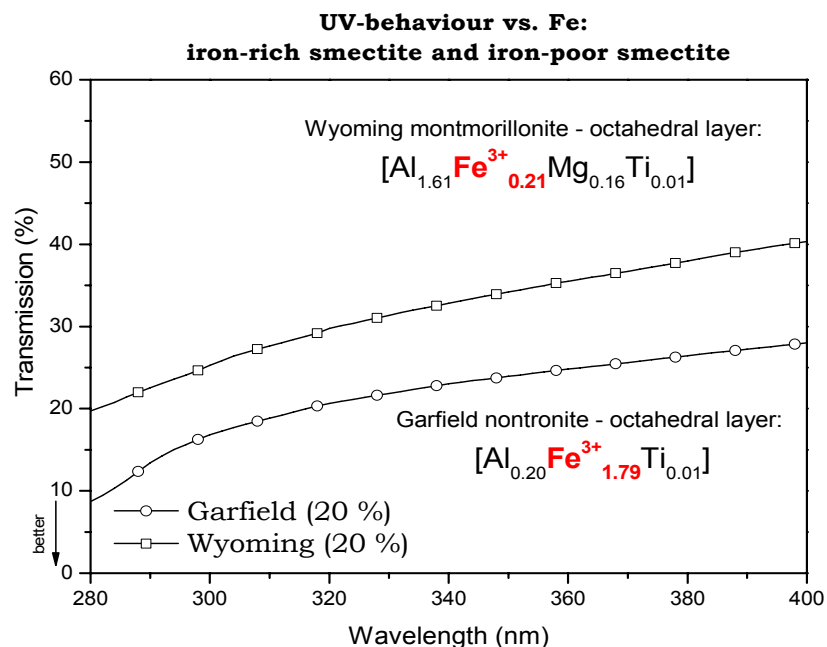
Based on the above discussion, it can be concluded that total  $\text{Fe}_2\text{O}_3$ -amount in clay relates to UV-transmission level. The octahedral Fe-amount and Fe-bearing trace minerals are responsible for that. For kaolin and mica dominated clay the relationship is a linear trend. For bentonite and mixed-layer dominated clay the relationship is exponential trend. The absorption abilities of bentonite and mixed layer structures are lower for the same Fe-amount than absorption abilities of kaolin and clay.

### ***Role of Fe - electron configuration***

In previous proofs and discussion, hematite is contributed to UV-transmission behaviour. Hematite with formula  $\text{Fe}_2\text{O}_3$  is bonded from  $\text{Fe}^{3+}$  and  $\text{O}^{2-}$ , whose electron configurations are presented in figure 76. Theoretically, similar to the case of  $\text{TiO}_2$  (chapter 2.3), there is empty orbital in the electron configuration of  $\text{Fe}^{3+}$ , so that some electrons can absorb energy to change to the higher energy level. The absorption is demonstrated by experiments and electronic spectra of  $\text{Fe}^{3+}$  oxides (including hematite) in the near UV in a publication of Sherman & Waite (1985). Moreover, Kormann *et al.* (1989) demonstrated that hematite ( $\alpha\text{-Fe}_2\text{O}_3$ ) expresses negligible photocatalytic effect in comparison to photocatalytic effect of  $\text{TiO}_2$  and  $\text{ZnO}$ . Combining the theoretical and experimental properties of hematite with UV-measurement proofs, it can be concluded that hematite plays a role of absorption to UV-radiation in clay matter.



**Figure 76. Electron configuration of outermost orbital shell of Fe and O and their ionic states**  
 $\text{Fe}^{3+}$  ( $Z_{\text{Fe}} = 26$ ) and  $\text{O}^{2-}$  ( $Z_{\text{O}} = 8$ ) are associated by ionic bond to form  $\text{Fe}_2\text{O}_3$ . At promoted state, 4s orbital of  $\text{Fe}^{3+}$  is empty.



**Figure 77. UV-behaviour vs. iron amount: iron-rich Garfield and iron-poor Wyoming**

Measured using AnalytikJenaAG SPECORD 50; UV-measurement of 20%-clay pure-clay cream samples of <63  $\mu m$  bulk clay with wool-wax-alcohol cream; The lower transmission proportion, the better effect by clay cream

With the respect to iron in clay mineral phase, octahedral  $Fe^{3+}$  in the structure of clay mineral has also an electron configuration with empty orbital (see figure 77), so that it can also absorb photons, theoretically. The experiments demonstrated octahedral layer  $Fe^{3+}$  can express this ability through the case of nontronite Garfield sample with low value of UV-transmission. Garfield bentonite was characterized as quite pure bentonite dominated by nontronite. Its iron was demonstrated using TEM-EDX and Mössbauer spectroscopy analyses as obvious  $Fe^{3+}$  represents in nontronite mineral.

A comparison between octahedral iron-rich smectite and octahedral iron-poor smectite is presented in figure 79. Wyoming bentonite, characterized as dominating aluminum-rich smectite with only 0.21  $Fe^{3+}$  per  $[O_{10}(OH)_2]$  unit, shows obviously higher UV-transmission level than Garfield bentonite which has 1.79  $Fe^{3+}$  per  $[O_{10}(OH)_2]$  unit. Both samples do not include any other iron-rich phase.

In summary, it can be concluded that UV-absorption ability of iron-rich clay is better than iron-pure clay. However, the phases of iron in the clay as well as mineral properties of the clay play some role in the UV-absorption ability. This contribution exhibits that kaolins and mica dominated clays show a linear relationship between  $Fe_2O_3$ -amount (in total chemical composition) and UV-transmission (of 20%-clay pure-clay cream sample), meanwhile bentonites and mixed-layer dominated clays show an exponential relationship.

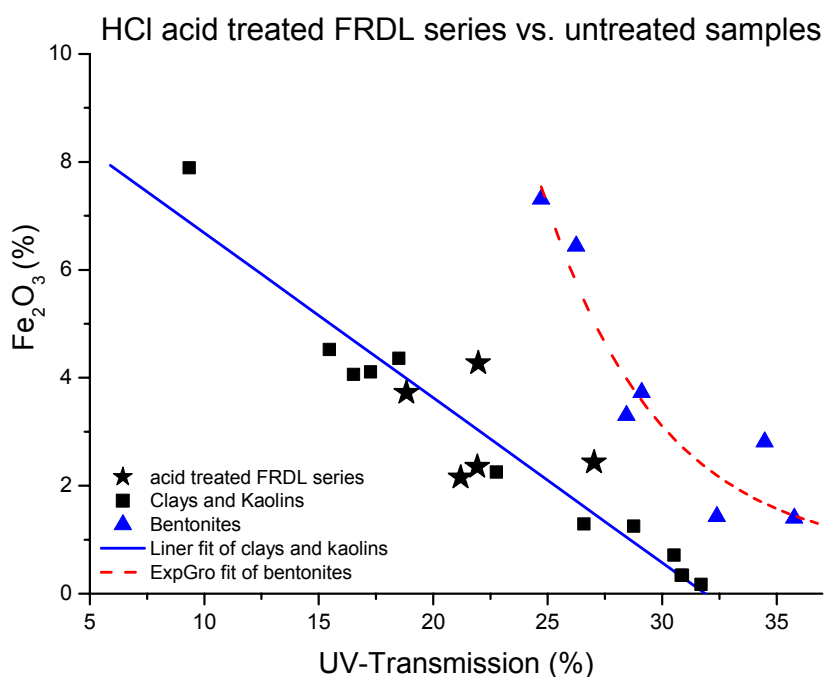
### 7.3.2 Role of iron in mixture with nanosuspension of fungi *G. pfeifferi*

The obtained UV-transmission results of clay-fungi cream samples (figure 60 and table 17) and  $\text{Fe}_2\text{O}_3$ -amount of the clays are now discussed. Although, Thierfeld showed the better UV-absorption ability than iron-reduced Thierfeld, both of the clays presented lower UV-absorption ability than natural Wolfka ( $\text{Fe}_2\text{O}_3$ -amount of iron-reduced Thierfeld is still higher than that of natural Wolfka). Moreover, UV-absorption level of iron-poor Wyoming is clearly higher than that of iron-rich Garfield. Therefore, the influence of Fe, which was found in the clay - wool-wax-alcohol system, seems to be changed vice versa. It is possible that Fe effect is overlapped by another parameter such as interaction between clay particles and nanosuspension of fungi. The next chapter 7.5.2 discusses about the mentioned parameter.

## 7.4 Acid treatment and changing of UV protection ability

In chapter 5.4, it was observed that UV-absorption abilities of acid treated FRDL series increase in comparison with the untreated one. However, iron was dissolved partly by acid treatment (chapter 4.5.1), so that the relationship between  $\text{Fe}_2\text{O}_3$ -amounts and UV-transmission values of acid treated FRDL series is not linked with the trend represented for bentonites in the chapter 7.3.1 (figure 74).

Using  $\text{Fe}_2\text{O}_3$ -amount obtained by XRF analyses and the average UV-transmission values of 20%-clay pure-clay cream samples, the correlation diagram of these two parameters is drawn in figure 78 for series of acid treated samples in comparison with the bentonites vs. mica dominated clays and kaolins. The figure shows that the points indicated for samples of HCl acid treated FRDL series are closer to the trend line of mica dominated clays and kaolins than the trend curve of bentonites and mixed-layer dominated clays. This behaviour might be influenced by expandability that is difference between these two groups: group of mica dominated clays and kaolins vs. group of bentonites and mixed-layer dominated clays.



**Figure 78. HCl acid treated Friedland Clay series versus untreated samples in the aspect of relationship between  $\text{Fe}_2\text{O}_3$ -amount and UV-transmission**

Note: UV-transmission values from 20%-clay pure-clay cream samples; solid stars present the involved acid treated Friedland Clay series (chapter 5.4), see also legend in figure 75

Under the treatment with solution of acid HCl and high temperature during 2 hours, mixed-layer particles were modified to finer particles and fewer layers per stack (chapter 4.5.1). The acid treated clay sample made decrease of the expandability because of low pH environment.

By light microscopy observation, images of cream samples of acid treated FRDL series also showed the more aggregative structures than those of the untreated one (STDV parameters of treated samples images are mostly higher than that of untreated sample image) (figure 59). It is a proof for the less expandability of acid treated series in comparison to the untreated sample.

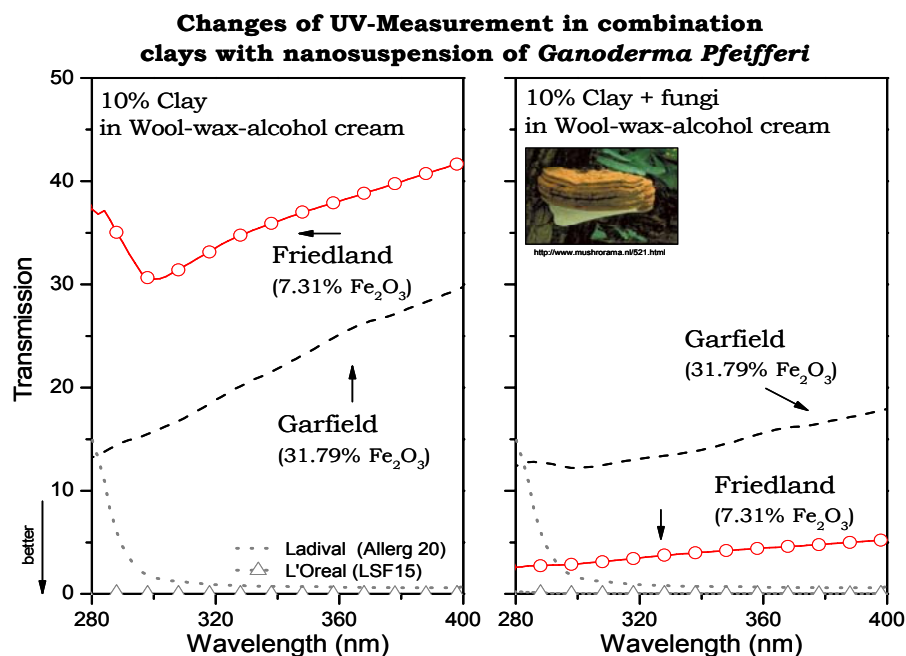
In summary, the acid treatment decreases expandability of mixed-layer particles that causes the UV-absorption ability of treated sample becoming like non-expandable clay minerals (kaolinite and mica). Hence, the UV-transmission level relates to the  $\text{Fe}_2\text{O}_3$ -amount as the lineal relationship (discussed in chapter 7.3.1).

## 7.5 Increasing of UV-absorption potential in clay-fungi combination and meaning of clay charge

### 7.5.1 Increasing of UV-absorption potential in combination of clays and nanosuspension fungi *G. pfeifferi*

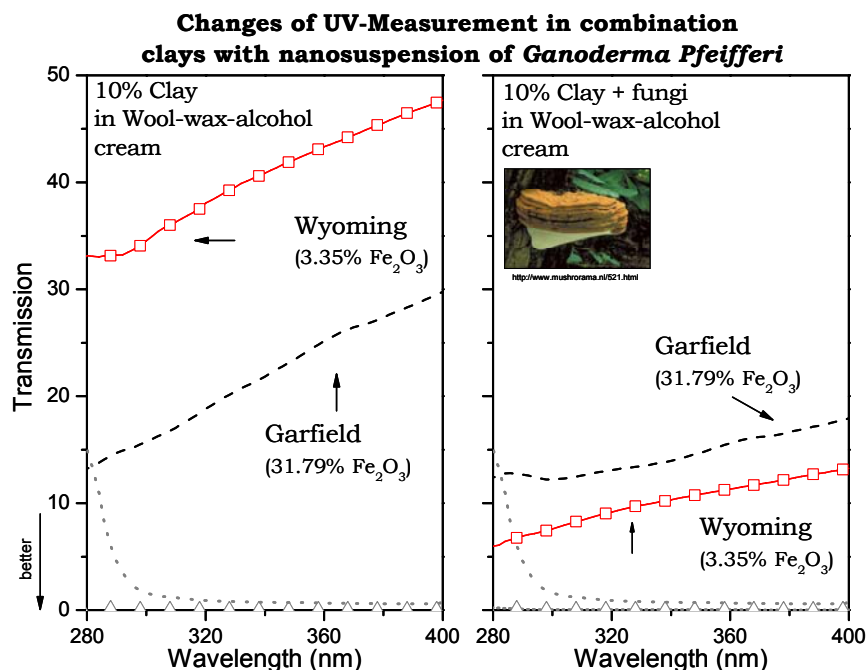
Chapter 5.5 presented UV-measurements of some clay-fungi cream samples from selected clay samples. It was observed, when combining the clays with nanosuspension of fungi *Ganoderma pfeifferi*, that the obtained UV-transmission is improved remarkably in comparison with UV-transmission levels of corresponding pure-clay cream samples with the same amount of clays (10% per woo-wax-alcohol cream by weight) (table 17).

This reducing effect varies with different selected clays. The clay-fungi cream samples of Garfield samples showed a little improvement of UV protection potential. Clear increases in UV protection potential were obtained from groups of Thierfeld samples (Thierfeld – untreated and Thierfeld - dithionite), Wolfka samples (Wolfka - <63  $\mu\text{m}$  and Wolfka - <2  $\mu\text{m}$  and Wolfka – nature) and acid treated Friedland Clay sample (HCl 2.0 M, 80°C, 2 h). Strong improvements were yielded from samples of Wyoming and Friedland Clay. The comparisons are shown in figure 79 and figure 80.



**Figure 79. Changes of UV-measurements in combination clays with nanosuspension of *Ganoderma pfeifferi*: Garfield and Friedland Clay**

Measured using AnalytikJenaAG SPECORD 50; UV-measurement of 10%-clay pure-clay and 10%-clay clay-fungi cream samples of <63  $\mu\text{m}$  bulk clay; The lower transmission proportion, the better effect by clay cream



**Figure 80. Changes of UV-measurements in combination clays with nanosuspension of *Ganoderma pfeifferi*: Garfield and Wyoming**

Measured using AnalytikJenaAG SPECORD 50; UV-measurement of 10%-clay pure-clay and 10%-clay clay-fungi cream samples of <63  $\mu\text{m}$  bulk clay; The lower transmission proportion, the better effect by clay cream

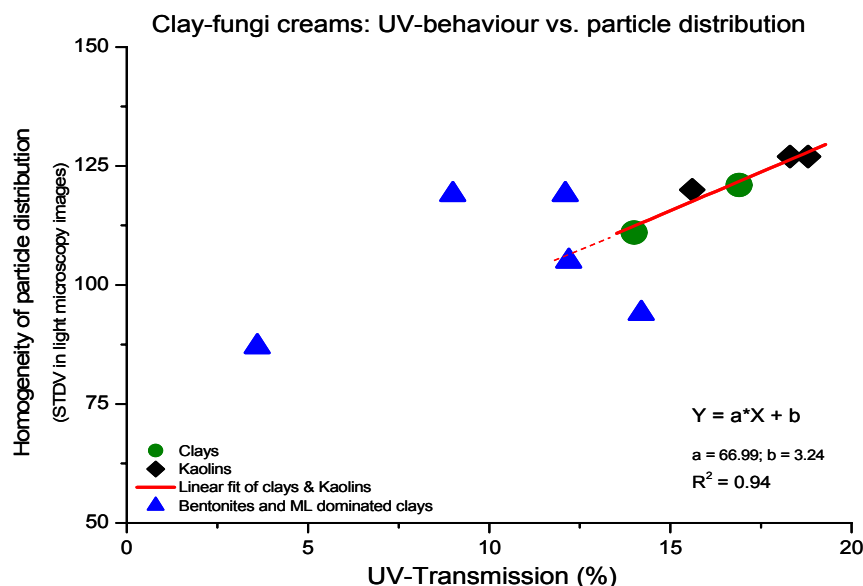
These two figures also present Fe<sub>2</sub>O<sub>3</sub>-amount of the clay samples. It is obvious to recognize that UV protection behaviour of clay-fungi cream samples does not follow the influence of Fe<sub>2</sub>O<sub>3</sub> in the clay sample. Other factor which could influence effectively the UV-absorption abilities of the clay-fungi cream samples is the degree of distribution between clay particles and nanosuspension, may be linked with the charge of clays.

### 7.5.2 Influence of charge of clay: non-expandable clay and expandable clay

From the light microscopy images, parameter STDV was calculated to estimate degree of homogeneity of mineral particles in the clay-fungi system. Therefore, the parameter STDV can represent levels of aggregation or dispersion of clay particles in the cream matrix. The results and images were presented in figure 61.

Correlating STDV numbers to the UV-transmission values of clay-fungi cream sample, it is drawn in figure 81. The figure shows that kaolins and mica dominated clays represent different behaviours concerning particle distribution versus UV protection ability from bentonites and mixed-layer dominated clays. It may be caused by the different behaviours of non-expandable clay versus expandable clay.





**Figure 81. UV-behaviour vs. particle distribution in the clay-fungi creams' system**

Note: UV-transmission values from 10%-clay clay-fungi cream samples; solid triangles present the bentonites and mixed-layer dominated clays including Wyoming, Garfield - <63 µm, Garfield - <6.3 µm, FRDL - HCl 2.0 M, 80°C, 2 h (treated FRDL) and FRDL - untreated; dark squares present kaolins including Wolfka - nature, Wolfka - <63 µm and Wolfka - <2 µm; dark rounds present clays including Thierfeld - untreated and Thierfeld - dithionite treated; and solid line is linear fit of the kaolins and clays, the triangle closed to the solid line by dash line presents treated FRDL which is reduced the expandability by acid treatment

For clays with non-expandable clay minerals, a lower degree of homogeneity of particle distribution (higher STDV) indicates a lower density of clay particles in the aggregate for a volume of cream. This situation allows a higher transmission of UV-radiation through the cream. For clays with more expandable sheet silicates, another mechanism shown in figure 81 is to consider. Higher degree of homogeneity (lower value for STDV in light microscopy image) corresponds directly to reduce of a passing of UV-radiation. Interaction between clay particles and the fungi capsule, a system which includes wool-wax-alcohol cream, plantacare (aqueous solution of long-chain decyl glucoside) and extract of fungi *Ganoderma pfeifferi*, is concentrated to discuss now.

#### ***Clays dominated by non-expandable clay minerals***

The Wolfka series are dominated by kaolinite, so that they have only a variable charge at the edge of particles. The untreated and dithionite reduced Thierfeld samples were characterized as materials including mostly diVerm. and diVerm.-rich diVS-ml in clay mineral phases, so that they have edge charge and also low layer charge. Therefore, the fungi capsule is distributed mostly in the voids of clay particles as was concluded in chapter discussion 7.2.2.

The Wolfka sample as natural material without any grinding and treatment shows a decrease of UV-transmission. This “native” Wolfka presents a more non-smoothed distribution of grain size diameter than other Wolfka samples, so that the voids among particles are smaller than those of the others. These small voids are limiting the mobility or separation of fungi capsules including long-chain decyl glucoside. In other words, clay particles of Wolfka kaolin and fungi capsules distribute homogeneously and the distribution of natural Wolfka is more homogeneous than the distributions of the other Wolfka samples. By experiments using light microscopy, this discussion is also supported by dispersion arrangement observed from matrixes of Wolfka clay-fungi cream samples (image of clay-fungi cream of natural Wolfka has lowest STDV in comparison with those of  $<63\ \mu\text{m}$  and  $<2\ \mu\text{m}$  Wolfka) (figure 61).

Similarly, the cases of untreated and treated Thierfeld samples might be caused by edge charge or voids among clay particles. The treated Thierfeld, with the higher UV-transmission than the untreated Thierfeld sample, was slightly enriched with  $\text{Na}^+$  (demonstrated by XRF results, table 15). The larger voids among clay particles could be formed in comparison with the voids formed by untreated Thierfeld. The light microscopy images also showed the more aggregative distribution (higher STDV) of treated Thierfeld particles than untreated Thierfeld particles (figure 61). The higher dispersion's degree of particles and the higher value of variable charge for the dithionite treated Thierfeld sample could be responsible for a better stabile homogenisation of fungi capsule and clay particles.

With the determined structures, the UV protection behaviour of the clay-fungi cream samples of Wolfka series and Thierfeld couple could be resulted partly by UV-absorption ability of the clay samples themselves and partly by UV-absorption ability of fungi capsules. The UV-absorption abilities of clay samples are under the iron effect as the mention in chapter 7.3.1. With the same amount of fungi suspension, it seems, that the own UV-absorption ability of Ganoderma compounds and its stabile homogenous distribution in the cream affect the UV-behaviour much stronger than the specific UV-absorption capacity of the clay minerals.

### *Clays dominated by expandable clay minerals*

In previous discussion, the negative charged capsules are fixed at the positive charged plantacare-heads. The plantacare molecules are embedded in the interlayer space. This consolidated structure is stabilizing a durable homogenous distribution of Ganoderma-capsules in the cream.

In the previous chapter 7.2.2, it is determined that layer charge decreases in the order Garfield > Wyoming > Friedland Clay. Moreover, Garfield and Wyoming smectites have similar surface area (656 m<sup>2</sup>/g for Garfield or 522 – 700 m<sup>2</sup>/g for Wyoming), so that the adsorption domain (= specific surface / charge) of Garfield is much lower than that of Wyoming because of much higher layer charge of Garfield smectite. Caused by grain size separation, the surface area of sample Garfield - <6.3 µm increases significantly from sample Garfield - <63 µm, so that the adsorption domain of Garfield - <6.3 µm is higher than that of Garfield - <63 µm. Wyoming has also lower adsorption domain than Friedland Clay because of two times higher layer charge of Wyoming in comparison with Friedland Clay. In summary, the adsorption domain increases with the less layer charge in the following order: Garfield - 63µm < Garfield - 6.3 µm << Wyoming < Friedland Clay. With acid treated Friedland Clay, because of the high disorder of clay particles caused by acid treatment, the adsorption domain of treated sample is lower than the untreated sample.

Belonging to the above order of adsorption domain, the plantacare-molecules fixing the fungi capsules are more distributed interlayer spaces with a higher adsorption domain size. Therefore, the distribution of fungi capsule is more dispersive stabilised in the matrix of those clay particles. In the other words, the fungi capsule is less concentrative or aggregative in the layer surface. The observed light microscope images support partly for this discussion (figure 61 and figure 70).

In agreement to the discussion on the role of plantacare in low charged clay minerals, the UV-transmission values of clay-fungi cream samples decrease in the same above mentioned order: Garfield - 63µm < Garfield - 6.3 µm << Wyoming < Friedland Clay and acid treated Friedland Clay < Friedland Clay (untreated sample). Therefore, in this case, the UV-absorption potential of clay-fungi cream samples could belong to the permanent charge of expandable layers.

Conclusively, combination with nanosuspension of *Ganoderma pfeifferi* makes the UV-absorption ability of cream samples of clay increasing. Especially, a sample with a low charge for expandable layers, like Friedland Clay (untreated, bulk sample), reaches a quite low UV-transmission level, see Friedland Clay with only 3.6% in average. This value is equal to SPF 27 with UV-A broad band absorption (the estimation is presented in chapter 2.4). In comparison with Ladival® (SPF 20) (figure 79), sample of Friedland Clay showed a higher UV-transmission value in UV-A area. But in UV-B area, from 280 to 295 nm, UV-transmission value of Friedland Clay is noteworthy lower, which means better. In chapter 2.4, it is noted that “the biological effectiveness of UV-radiation increases by a factor of over 1000 as the wavelength changes from UV-A to UV-B”. Therefore, UV-absorption potential of clay-fungi cream of Friedland Clay is considerable.

The property which supports for Friedland Clay having such high UV-absorption potential is a “low-charge” smectite. In this situation plantacare in the interlayer space of clay minerals is immobilizing fungi capsules in cream. Non-expandable clay particles with effective charges only at the edges adsorb fungi capsules in the voids between particles, so that the UV-absorption ability affected partly by additional characterization of clay sample (such as iron amount) and partly by the size of the voids. The high dispersion of fungi capsules with expandable clay particles is the higher UV-absorption potential.

## 7.6 Influences of particle parameters on UV protection ability of clay minerals

### 7.6.1 Influence of particle size observed from different grain size distributions

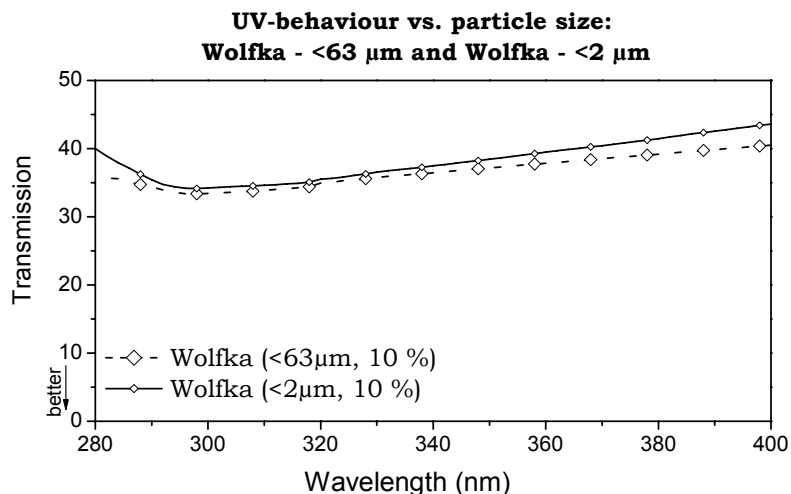
To investigate influence of particle size, the UV protection potential was determined from different grain size distributions of the same original sample. A finer grain size distribution will increase a homogenization of pore size between the grain and it will be arisen a higher specific surface area.

#### *Pure-clay creams*

Comparing pure-clay cream samples of Friedland Clay (FRDL), the difference in UV-transmission value is small (table 16 and figure 53). The UV protection level of cream sample of FRDL -  $<2\ \mu\text{m}$  is better at UV-B area but is lower at UV-A area than that of FRDL -  $<63\ \mu\text{m}$  bulk. In the whole UV area, average UV transmission result of 20%-clay of pure-clay cream samples of FRDL -  $<2\ \mu\text{m}$  and FRDL -  $<63\ \mu\text{m}$  bulk are about 26.3% and 24.7%, respectively. FRDL -  $<2\ \mu\text{m}$  is better, because protection in UV-B (stronger effective) is more necessary than protection in UV-A as well as this cream sample is smoother than the cream of FRDL -  $<63\ \mu\text{m}$ . Correspondingly, FRDL -  $<2\ \mu\text{m}$  and FRDL -  $<63\ \mu\text{m}$  contains about 6.4% and 7.3% of  $\text{Fe}_2\text{O}_3$ -amount (by XRF measurements).

The lower  $\text{Fe}_2\text{O}_3$ -amount of  $<2\ \mu\text{m}$  fraction could explain for the higher UV-transmission for cream sample of FRDL -  $<2\ \mu\text{m}$  in the overall interval of UV. The behaviour of  $<2\ \mu\text{m}$  fraction in UV-B area indicates influence of an additional grain size effect. Normally, it would expect a higher  $\text{Fe}_2\text{O}_3$ -amount in FRDL -  $<2\ \mu\text{m}$  because of enrichment of Fe-bearing mixed-layer series in  $<2\ \mu\text{m}$  fraction. But during the Atterberg sedimentation to win the full  $<2\ \mu\text{m}$  fraction, clay particles had been in contact with water for two months. Therefore, the contact led to clay particles undergoing alteration processes, a therein illitic particles altered to diVS-ml and smectitization process is happened with IS-ml particles. Furthermore, octahedral  $\text{Fe}^{3+}$ -amount was reduced during these alteration process. These alterations also reduced the interlayer charge of expandable mixed-layer series (see chapter 4.3.1).

The expected additional grain size effect for UV-B area could be explained by intercalation. Liquid vaseline compound filled the interlayer space and expanding from about  $12\ \text{\AA}$  to  $19\ \text{\AA}$  supporting more homogenous particle distribution or reducing the clay particle-free area in the cream on this way.



**Figure 82. UV-behaviour vs. particle size: Wolfka – <63  $\mu\text{m}$  and Wolfka - <2  $\mu\text{m}$**

Measured using AnalytikJenaAG SPECORD 50; UV-measurement of 10%-clay pure-clay cream samples of clay with wool-wax-alcohol cream; The lower transmission proportion, the better effect by clay cream

The pure-clay cream samples of Wolfka, which contains about 42% of <2  $\mu\text{m}$  fraction, were prepared with <63  $\mu\text{m}$  bulk and <2  $\mu\text{m}$  clay matters. Correspondingly, the surface area of <63  $\mu\text{m}$  sample is smaller than that of <2  $\mu\text{m}$ . However, the UV-transmission values of cream sample of <63  $\mu\text{m}$  is slightly higher than those of <2  $\mu\text{m}$  as shown in figure 82 (see also in chapter 5.2.1). Therefore, the difference (average about 2% of transmission unit) may be linked with the reducing of goethite, hematite, jarosite, pyrite phases in Wolfka sample. The reduce Fe-amount could also explain the not better UV protection of this finer (<2  $\mu\text{m}$ ) material. The another effect by grain size distribution is not to expect for non-expandable clay minerals.

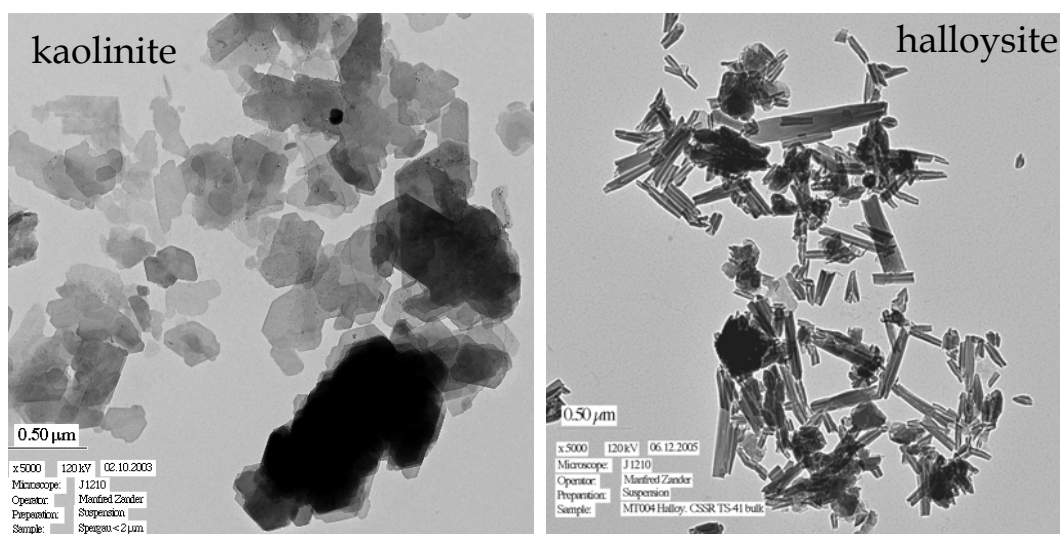
### ***Clay-fungi creams***

Comparing UV-transmission of the three included samples: fungi-clay creams natural Wolfka, <63  $\mu\text{m}$  Wolfka and <2  $\mu\text{m}$  Wolfka, the natural Wolfka is the best one (chapter 5.5, figure 60 and table 17). Concerning the distribution between clay particles and fungi capsules, natural Wolfka is also more homogenous than the others (figure 61 and figure 81). In chapter 7.5.2, it was discussed about the link between UV protection potentials of the clay-fungi cream series and their cream distributions; therein the more homogeneity of particle distribution is the better UV-absorption ability (figure 81). To explain for the more dispersive structure of natural Wolfka, the grinding to get certain fraction may produce the additional edge charge on clay particles, so that the voids among clay particles are enlarged affecting on higher concentration of fungi capsule in the voids.

With the case of expandable Garfield samples,  $<6.3\ \mu\text{m}$  Garfield showed the better UV-absorption possibility than the  $<63\ \mu\text{m}$  Garfield. Concerning the influence on UV-absorption by distribution of cream matrix, chapter 7.5.2 concluded that the higher dispersion of plantacare-molecules fixing the fungi capsules in the interlayer space of expandable clay minerals causes the higher UV protection potential. Because of thinner particles,  $<6.3\ \mu\text{m}$  Garfield has a higher degree of occupied interlayer by plantacare in comparison with larger fraction size, so that it causes the higher possibility in absorption UV-radiation.

### 7.6.2 Influence of different particle shapes concerning ability of covering

In this study, the sample of halloysite dominated Michalovce kaolin was also investigated. In comparison with all of the other clays, Michalovce showed significantly the lowest UV protection potential (figure 49). Chapter 5.2.2 presented the comparison of UV-transmission values between pure-clay cream samples of Wolfka and Michalovce (figure 56). The 20%-clay cream sample of Michalovce presented 15 - 18% UV-transmission lower than that of Wolfka. However, Wolfka has only 0.3% weight of  $\text{Fe}_2\text{O}_3$  and Michalovce contains approximately 0.5% weight of  $\text{Fe}_2\text{O}_3$  (calculated from TEM-EDX analyses).



**Figure 83. TEM images of kaolinite and halloysite**

Left: Wolfka sample, magnification: 5,000x; Right: Michalovce sample, magnification: 5,000x

*Note: Observed using Jeol JEM-1210*

This problem may connect with the shapes of clay minerals. Different from other clay samples, Michalovce dominated by tubules of halloysite while Wolfka and other used samples were dominated by plates or slats of kaolinite, smectites, mica-like and mixed-layer particles (figure 83). For certain amount of sample on cream slide, the surface area of Michalovce is too small to cover totally the cream matrix, so that UV-radiation can transmit easily. However, by comparison of all surface area data of used clay samples (chapter 4) with corresponding UV-transmission values (chapter 5), none correlation behaviour was defined. Therefore, it may also mean that the surface area is not an effective factor for UV protection ability but it is a key to warrant the covering cream area.

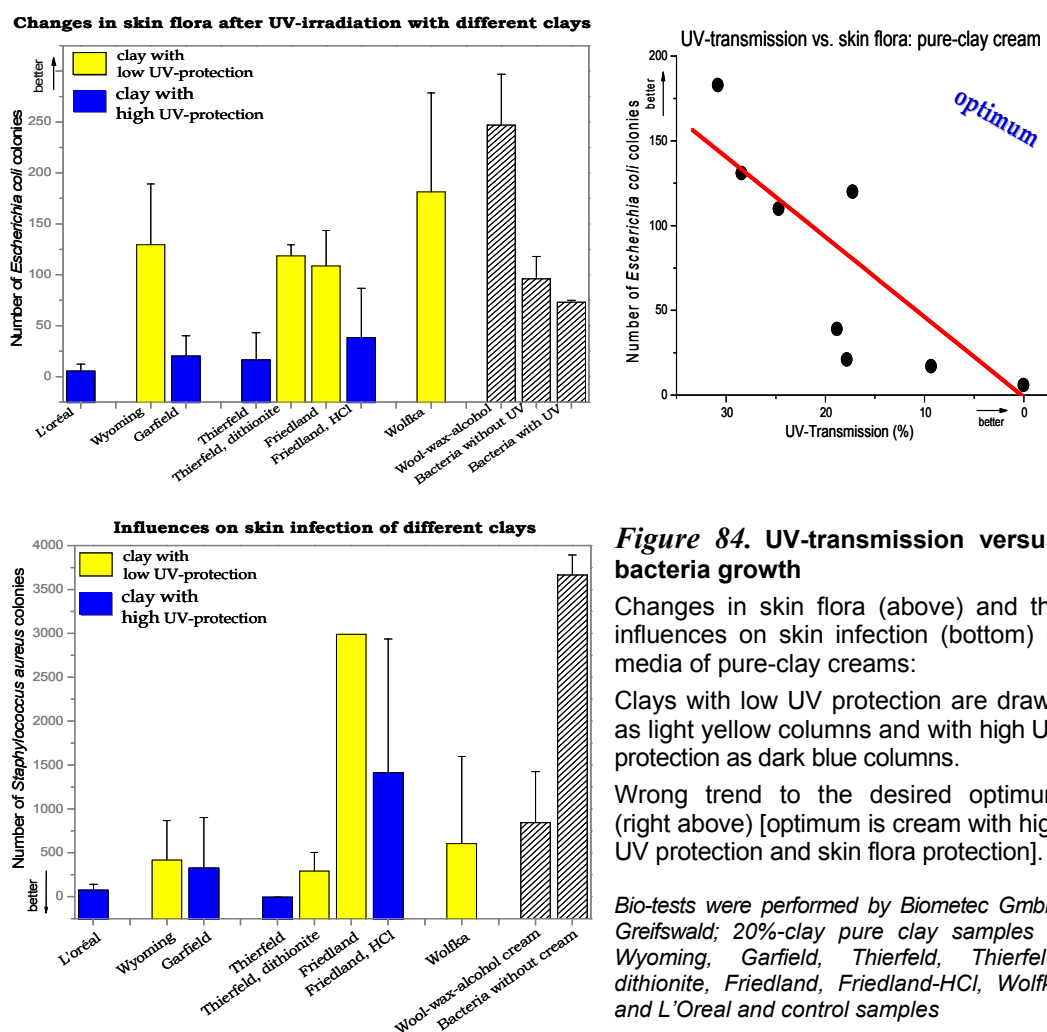
Conclusively, slat and platy shapes of clay mineral are necessary to create enough surface area for covering the cream slide to protect UV-radiation. For expandable clays, particle size distribution influences the cream homogeneity to affect UV-absorption ability. Especially, finer grain size distribution causes more disperse structure of clay particles and plantacare linked with fungi extraction generating better UV-absorption possibility. For non-expandable clays, grain size distribution has no directly effect to UV protection ability of cream. However, the small fraction preparation by grinding can increase the edge charge to decrease the UV-absorption ability of clay-fungi cream; and/or small fraction separation by Atterberg sedimentation can decrease the iron amount, so that it decrease the UV-absorption ability of pure-clay cream.



## 7.7 Interaction between clay creams with skin flora and skin infection

### 7.7.1 Charges of clay minerals affect growth of skin flora and infectious bacteria

The bio-test with pure-clay cream samples showed significantly different changes of skin flora and infectious bacteria (chapter 6.1 & 6.2 and following figure 84). These differences promote to find the parameter which affects on changes of the colonies. Especially, the experiment with skin flora after UV-irradiation (figure 84 left above) shows that the mentioned parameter is not linked clearly with the influence of UV-radiation because the reducing of bacteria growth from the control sample with UV-radiation is not significantly lower than that from the control sample without UV-radiation. That is reason why the discussion has to consider more clay mineral properties in order to explain this behaviour seen in figure 84. Additionally the discussion has to consider a different behaviour of bacteria in wool-wax-alcohol ointment: *E. coli* show a promoted growth in the ointment (figure 84 left above) but *S. aureus* is underpressed in the ointment (figure 84 left bottom).



### ***Pure-clay creams with skin flora *E. coli****

The creams of Garfield, Thierfeld and acid treated Friedland Clay, which have high absorption abilities, were expected to have the skin flora protecting behaviour but they show only fewer survived colonies in comparison with other creams (figure 84 left above).

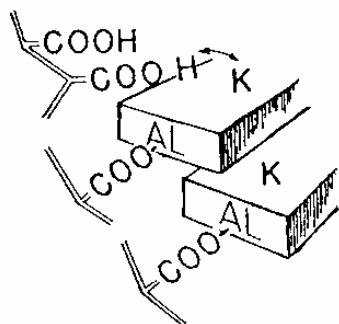
Garfield is characterized as nontronite dominated high charge bentonite with 0.31 per unit cell (chapter 4.2.1). The Thierfeld clay has high variable charge and additionally very high charge in tetrahedral layer of the involved chlorite component (17%) and mica-like component (80%). In the same group of attacking skin flora with Garfield and Thierfeld, acid treated Friedland Clay (by HCl 2.0 M, 80°C, 2 hours) possibly have also high charge. The untreated Friedland Clay charge is estimated about 0.09 per unit cell (chapter 4.3.1). However, because of alteration by acid treatment, the treated Friedland Clay sample have an increase of edge charge in comparison with the untreated Friedland Clay one (using light microscopy, acid treated Friedland Clay sample also showed the much more aggregative in structure in comparison with untreated one (figure 59)).

Conversely, the creams of Friedland Clay, Wyoming, dithionite treated Thierfeld and Wolfka obtained with low absorption abilities have the skin flora protecting behaviour.

Similarly to Friedland Clay, Wyoming was determined as low charge smectite with about 0.16 per unit cell (chapter 4.2.1). In comparison to the original Thierfeld clay, the sample of iron-reduced Thierfeld might be partly decreased with the charge because of slight Na<sup>+</sup>-enrichment (detected by XRF analyses). Especially, Wolfka has only edge charge, so that the sample could has much lower charge than the other samples.

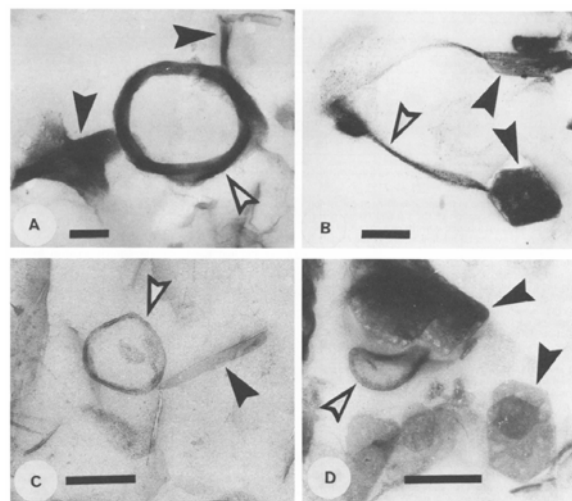
As discussed above, the higher charged media have attacking behaviour towards skin flora while the lower charged media support for skin flora to grow. Therefore, the behaviour of clay cream may depend on the charge: the growth of bacteria is limited by the charge of clay matter.

The influence of the charge towards bacteria can be explained by the fact that bacteria are bonded to clay minerals using their positive charge organic molecules and the negative charge clay particle as simulated in figure 85 (Pusch & Yong, 2006). Therefore, the bacteria are immobilized stronger in the higher charged media. For example, the bacteria are bonded at surface of smectite particles and/or at edge of kaolinite particles as showed in pictures by Walker *et al.* (1989) (figure 86). In addition, the voids among clay particles can also immobilize bacteria, so that they are limited from growing. The trend of the yielded skin flora growth connects with the decreasing trend of total charge from corresponding clays media.



**Figure 85.** Bonding mechanism of organic molecules and clay minerals.

(Pusch & Yong, 2006)



**Figure 86.** Bacteria are affected by charge of clay mineral *B. subtilis* and *E. coli* walls and envelopes (empty arrow) absorbed to smectite and kaolinite (solid arrow)

(Walker et al., 1989)

#### **Pure-clay creams with infectious bacteria *S. aureus***

In figure 84 (left bottom), it is to recognize that wool-wax-alcohol cream bearing system does not support an additional growth of *S. aureus* - only one exception: Friedland Clay. The acid treatment has slightly reduced the additional input for *S. aureus* growth by Friedland Clay. Wyoming and Garfield show comparable behaviours, so that, beside the influence of charge, there is additional factor affecting bacteria growth.

Studying on cell biology of *S. aureus*, Skarr et al. (2004) proved that heme iron is imported by this kind of bacteria. Friedland Clay is also characterized with 7.3% of  $\text{Fe}_2\text{O}_3$ -amount that is higher than the  $\text{Fe}_2\text{O}_3$ -amount of treated Friedland Clay with 3.7%. The samples of Garfield and Thierfeld are also iron-rich but they have also high charge, so that the infectious bacteria are limited from growing.

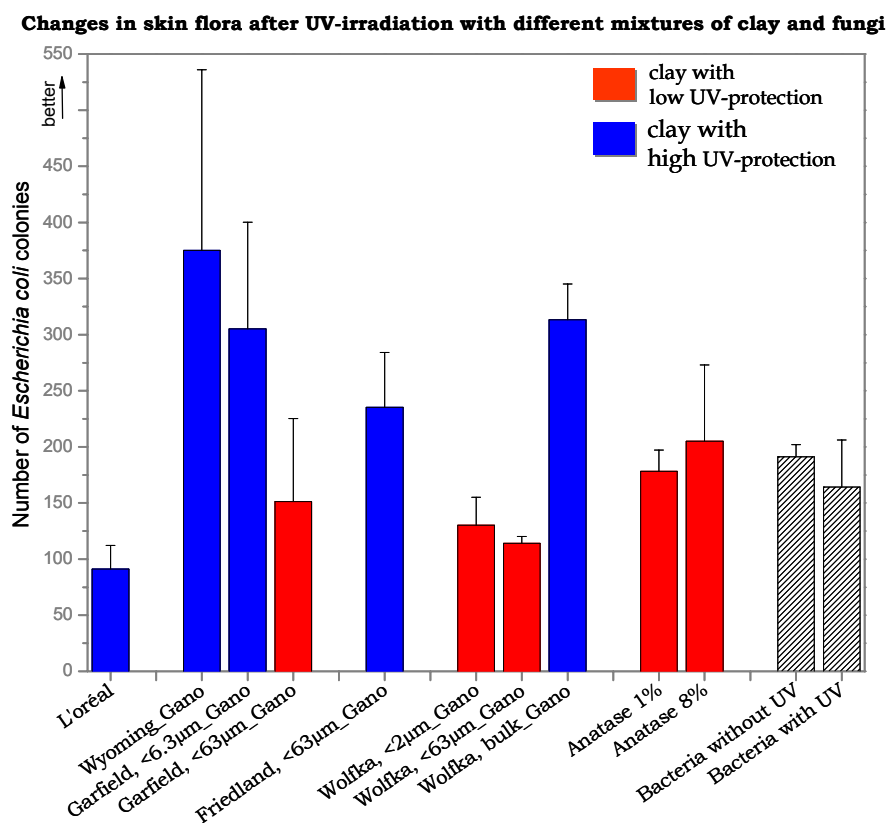
Combining the goal of protection UV-radiation (that is effective by high  $\text{Fe}_2\text{O}_3$ -amount) and the safety towards human skin through experiment with skin flora, the optimal clay may be the clay that has low total charge and high amount of  $\text{Fe}_2\text{O}_3$  (for example, Friedland Clay). Within the selected samples, the pure-clay cream samples are far from the optimum concerning both UV protection and safety to skin (figure 84). Besides, low-charge and iron-rich clay is suitable environment for the growth of infectious bacteria. However, the high charge clay may be not safe for the human skin but suitable for anti skin infection.

### 7.7.2 Clay-fungi combination as an opportunity concerning safety to human skin

The combination with fungi *Ganoderma pfeifferi* improved the protection ability of skin cream (chapter 6.3 & 6.4). Besides the advantage of the fungi, clay-fungi cream also showed the optimal setting that material with high UV protection ability has also high safety concerning skin thorough skin flora test (figure 87).

The previous chapter concluded that the lower charge clay is more protectively to the skin, meanwhile the chapter 7.5 demonstrated that combination of fungi *Ganoderma pfeifferi* and clays, especially the low charge expandable clays, improve the UV protection potential. Therefore, the clay-fungi cream samples of Wyoming, <6.3  $\mu\text{m}$  Garfield, natural Wolfka and Friedland Clay, which presented the high UV-absorption potential, showed the behaviour of protecting skin flora.

Therefore, combining clay with fungi offers the opportunity to get the optimal cream material which can be safe for applying onto human skin because of the UV protecting behaviour as well as the bio-protecting behaviour. Combining with the point concerning UV protection potential, the trend to look for low charge expandable clay may give rise to the optimal material.



**Figure 87. UV-transmission versus bacteria growth**  
**Changes in skin flora with clay groups of low and high UV protection**  
 Performed by Biometec GmbH, Greifswald; 10%-clay clay-fungi cream samples of Wyoming, Garfield-<6.3 $\mu\text{m}$ , Garfield-<63 $\mu\text{m}$ , Friedland-<63 $\mu\text{m}$ , Wolfka-<2 $\mu\text{m}$ , G Wolfka-<63 $\mu\text{m}$ , Wolfka,-nature, Anatase 1% and Anatase 8% and control samples; The higher number of colony, the more safety clay cream towards the skin flora

## SUMMARY

The non-natural substances in commonly used UV protection creams such as  $\text{TiO}_2$ , are known to have a photocatalytic side effect, which is very harmful to human skin. On the other hand, clays and clay minerals have been known to be good for human health and have been used widely in traditional applications as well as pharmacy and cosmetic industries. However, there is very little information on their UV-absorption properties. This study presents here some properties of clays and clay minerals concerning UV protection potential, which can be very helpful for the development of new UV protection cream generation.

In order to obtain the goals of this study, different clay samples including kaolins: Caminau, Wolfka, Seilitz, Spergau, KGa-1b, KGa-2, Michalovce (halloysite); bentonite: Garfield (nontronite), Chamber, Wyoming, SHCa-1 (hectorite), SAz-1, STx.-1, SWy-1; IS- and diVS-mixed-layer dominated clay: Friedland Clay; and mica dominated clays: Plessa, Gorrenberg, Teistungen, Thierfeld were investigated. They were characterized by XRD, TEM-EDX, XRF, Mössbauer spectroscopy, Atterberg sedimentation and dithionite treatment analyses. The clay-containing cream samples were analyzed by UV-transmission measurement, light microscopy observation and skin model test.

All the results, taken together allowed us to draw some following conclusions:

**1.** Clays and clay minerals have potential to absorb UV-radiation. Different types of cream samples: pure-clay cream (20%-clay or 10%-clay in wool-wax-alcohol cream ointment by weight) and clay-fungi cream (10%-clay in mixture of wool-wax-alcohol cream and nanosuspension of fungi *Ganoderma pfeifferi* by weight), have different UV-transmission results.

1.1. Each pure-clay cream had a different UV-transmission value indicating that clays can absorb UV themselves.

1.2. Different UV-transmission results obtained for different clay-fungi creams showed that clays have an effect on UV absorption of the system.

1.3. Because clays may have effects on skin flora and skin infectious bacteria, their safeness on human skin should be taken care of when using clays in skin cream.

**2.** The structures of clay particles in cream were shown to be dependent on the layer charge of clay minerals. The expandable clays have completely different properties from the non-expandable ones.

2.1. In pure-clay cream system, expandable clay minerals absorb glycerol and liquid vaseline compound of wool-wax-alcohol cream while in clay matter containing only non-expandable phases, wool-wax-alcohol cream distributes in the voids between particles.

2.2. In fungi-clay cream system, whilst wool-wax-alcohol cream and/or fungi capsule arrange only in the voids between particles of non-expandable phases, plantacare linked with fungi extract can enter into the interlayers of expandable phases. The lower layer charge of the expandable clays supports more homogeneous structure of clay-fungi cream sample.

**3.** The total amount of  $\text{Fe}_2\text{O}_3$  in chemical composition of clay plays a key role in determining the UV-absorption ability of the clay matter. Moreover, the UV-absorption ability also depends on the expandable or non-expandable property of the clay.

3.1. The average UV-transmission level obtained from cream samples with 20%-clay in wool-wax-alcohol cream related to the total  $\text{Fe}_2\text{O}_3$  amount of non-expandable phase in a linear relationship but in an exponential relationship for that of expandable phase. With the same high  $\text{Fe}_2\text{O}_3$ -amount, kaolins and mica dominated clays absorb UV-radiation better than bentonites and mixed-layer dominated clays. For example, the samples of mica dominated Thierfeld and nontronite Garfield with the  $\text{Fe}_2\text{O}_3$ -amount of about 8% and 32% absorbed about 91% and 82% in average, respectively.

3.2. The trend of iron amount in mixture clay and nanosuspension of fungi is overprinted by layer charge property, which is affecting structure of clay particles in cream.

**4.** Acid treatment decreased the expandability of mixed-layer dominated Friedland Clay so that UV-absorption abilities of acid treated clay matters were similar with non-expandable clays (kaolins and mica dominated clays). Although the treatment dissolved a part of iron in the clay matter, it could increase the UV-absorption ability of treated one. Harsh treatment such as 2.0 M HCl at 100°C, can change seriously characteristics of Friedland Clay generating reducing its UV-absorption ability.

**5.** Clays can be extremely useful for human skin when combining with nanosuspension of fungi *Ganoderma pfeifferi*. The studies were performed on the mixtures of wool-wax-alcohol cream and nanosuspension obtained by the extraction of fungi mass by using plantacare (aqueous solution of long-chain decyl glucoside) together with clay. Clay characterized with lipophilic property plays a role for emulsion homogenization in distribution with the nanosuspension and the ointment.

5.1. The combination of clays and nanosuspension increased its UV-absorption ability. Moreover, the increase is considerable compared to Friedland Clay and Wyoming.

5.2. The interaction of clay minerals with nanosuspension or homogenization of cream is critical for UV-absorption ability of cream. Therefore, the UV-absorption potential of cream depends on the charge of clay minerals. The characterization of low charge of expandable clay mineral is an advantage for such combination.

**6.** Particle parameters such as particle size (grain size distribution) and particle shape of clay minerals also play also influences in UV protection potential of clay, especially in the clay-fungi cream system.

6.1. In expandable clays, the clay matter with finer grain size supports the more homogeneous particle distribution in order to increase the UV-absorption ability. For non-expandable clays, the higher charge (e.g. caused by grinding) decreases the homogenous distribution between clay particles and fungi capsule thus decreasing UV-absorption ability of cream. Furthermore, during the Atterberg sedimentation to get finer grain size, a  $\text{Fe}^{3+\text{VI}}$ -amount can be reduced in the alteration processes; hence changing its UV-absorption ability.

6.2. In addition, the ability of covering a large area or typical flat and platy shape of clay mineral is a real advantage for UV protection potential of clay. In other words, clay matter characterized by too small surface area is not able to protect UV-radiation strongly (e.g. halloysite dominated kaolin).

**7.** The skin model test was performed *in vivo* in mouse ears with skin flora *Escherichia coli* (irradiated under UV-radiation during 30 seconds) and infectious bacteria *Staphylococcus aureus* in order to determine the effects of cream samples on skin under UV irradiation and skin infection.

7.1. Clay minerals prevented bacteria from growing by attracting them to the surface charge or edge charge of clay minerals. The clay matter with higher charge is the less favourable environment for skin flora as well as for infectious bacteria. Because the trend reaching high UV-absorption links with high  $\text{Fe}_2\text{O}_3$ -amount, so that the optimal pure-clay cream for human skin in terms of UV protection should be a low charge clay with high  $\text{Fe}_2\text{O}_3$  content, such as Friedland Clay. Besides, the iron-rich clay may support for growing of the infectious bacteria.

7.2. Combination with nanosuspension of *Ganoderma pfeifferi* protects for skin flora growth. The low charge expandable clay not only has high UV-absorption ability but also has high safety towards skin flora. Therefore, it is a great candidate in the search of materials for UV protection cream.

**8.** From the results of characterization of clays and clay minerals properties in UV protection cream, this study brings some following outlooks:

8.1. The clays dominated by low-charge expandable clay minerals can be the optimal solution in mixture with UV-protection active organic materials like *Ganoderma pfeifferi*. The interaction between expandable clay mineral and the emulsifier plantacare is the reason for this preferred direction.

8.2. The short-term alteration upon on contacting with water can reduce the layer charge of expandable clay minerals. This process should be taken care of when obtaining low-charge expandable clay minerals.



## REFERENCES

- ALLEN, J., 2001: *Ultraviolet Radiation: How It Affects Life on Earth – on NASA's Earth Observatory website*. URL: <http://earthobservatory.nasa.gov/Library/UVB/printall.php> (accessed January 20, 2006).
- AMMANN, L., 2003: *Cation exchange and adsorption on clays and clay minerals*. Dissertation - Christian-Albrechts-Universität Kiel.
- AMMANN, L.; BERGAYA, F.; LAGALY, G., 2005: *Determination of the cation exchange capacity of clays with copper complexes revisited*. Clay Minerals 40(4): 441-453.
- ARPANSA, 2003: *Ultraviolet Radiation reference - Resource Guide for UV Protective Products 2003 - Information Section*. Australian Radiation Protection and Nuclear Safety Agency. URL: [http://www.arpansa.gov.au/uvrg/pubs/uv\\_ref.pdf](http://www.arpansa.gov.au/uvrg/pubs/uv_ref.pdf) (accessed April 20, 2006).
- AS/NZS, 1993: *Standards Australia/Standards New Zealand™, Sunscreen products-evaluation and classification, Report No. AS 2604*. Sydney/Wellington, 1993.
- AS/NZS, 1997: *Standards Australia/Standards New Zealand™, Sunscreen products-evaluation and classification, AS/NZS 2604:1997*. Sydney/Wellington, 1997.
- AS/NZS, 1998: *Standards Australia/Standards New Zealand™, Sunscreen products-evaluation and classification, AS/NZS 2604:1998*. Sydney/Wellington, 1998.
- ASMW, 1988: *Katalog der vom ASMW geeichten Normalproben.- Amt für Standardisierung, Meßwesen und Warenprüfung (ASMW), Ausgabe 1988/89, Berlin 1988*.
- BAADSGAARD, O., 1991: *In vivo ultraviolet irradiation of human skin results in profound perturbation of the immune system : relevance to ultraviolet-induced skin cancer*. Arch. Dermatol. 127: 99-109.
- BAILEY, S. W.; CHAIRMAN, 1980: *Summary of recommendations of AIPEA nomenclature committee on clay minerals*. Am. Mineral. 65: 1-7.
- BALLET, O.; COEY, J.M.D.; BURKE, K.J., 1985: *Magnetic properties of sheet silicates; 2:1:1 layer minerals*. Phys. Chem. Miner. 12: 370-378.
- BESSON, G.; BOOKIN, A. S.; DAINYAK, L. G.; RAUTUREAU, M.; TSIPURSKY, S. I.; TCHOUBAR, C.; DRITS, V. A., 1983: *Use of diffraction and Mössbauer methods for the structural and crystallochemical characterization of nontronites.- J. Appl. Cryst., 16: 374-383*.
- BISHOP, J.; MURAD, E.; DYAR, M.D., 2002: *Influence of octahedral and tetrahedral cation substitution on the structure of smectites and serpentines as observed through infrared spectroscopy*. Clay Minerals, 37: 617-628.
- BISSETT, D.L.; HANNON, D.P.; ORR, T.V., 1989: *Wavelength dependence of histological, physical, and visible changes in chronically UV-irradiated hairless mouse skin*. Photochem Photobiol. 50 (6): 763-769.
- BURGETH, G.; KISCH, H., 2002: *Photocatalytic and photoelectrochemical properties of titania-chloroplatinate (IV)*. Coordination Chemistry Reviews 230: 41-47.
- CAI, R.; KUBOTA, Y.; SHUIN, T.; SAKAI, H.; HASHIMOTO, K.; FUJISHIMA, A., 1992b: *Induction of cytotoxicity by photoexcited TiO<sub>2</sub> particles*. Cancer Res. 52 (8): 2346-2348.

- CAI, R.; HASHIMOTO, K.; FUJISHIMA, A.; KUBOTA, Y., 1992a. *Conversion of photogenerated superoxide anion into hydrogen peroxide in TiO<sub>2</sub> suspension system*. Journal of Electroanalytical Chemistry, 326 (1-2): 345-350.
- CARRETERO, I., 2002: *Clay minerals and their beneficial effects upon human health. A review*. Appl. Clay Sci. 21 (3-4): 155-163.
- CHEL, V.G.; OOMS, M.E.; POPP-SNIJDERS, C.; PAVEL, S.; SCHOTHORST, A.A.; MEULEMANS, C.C.; LIPS, P., 1998: *Ultraviolet irradiation corrects vitamin D deficiency and suppresses secondary hyperparathyroidism in the elderly*. J Bone Miner Res. 13 (8): 1238-1242.
- CHIPERA, S.J. and BISH, D.L., 2001: *Baseline studies of the clay minerals society source clays: powder X-ray diffraction analyses*. Clays and Clay Minerals 49 (5): 398 - 409.
- CLECHET, P.; MARTELET, C.; MARTIN, J.R.; OLIER, R., 1979: *Photoelectrochemical behaviour of TiO<sub>2</sub> and formation of hydrogen peroxide*. Electrochimica Acta 24 (4), 457-461.
- COBLENTZ, W.W., 1932: *The Copenhagen meeting of the Second International Congress on Light*. Science 76: 412-415.
- COLE, C., 2001: *Sunscreen protection in the ultraviolet A region: how to measure the effectiveness*. Photodermatol. Photoimmunol. and Photomed. 17 (1): 2-10.
- Colipa, 2004: *Activity Report 2004*. European Cosmetic, Toiletry and Perfumery Association (www.colipa.com).
- COUTURE, REX A. and DYMEK, ROBERT F., 1996: *A reexamination of absorption and enhancement effects in X-ray fluorescence trace element analysis*. Am. Mineral. 81: 639-650.
- CTFA, 2004: *Australia/New Zealand Sunscreen Standard: AS/NZS 2604:1998 - SPF Test Method: Comparative summary (May 2004)*. The Cosmetic, Toiletry and Fragrance Association of Australia, Inc.
- CUARDROS, J., 2002: *Structural insights from the study of Cs-exchanged smectites submitted to wetting-and-drying cycles*. Clay Minerals 37: 473-486.
- de FABO, E.C; NOONAN, F.P.; FREDERICK, J.E., 1990: *Biologically effective doses of sunlight for immune suppression at various latitudes and their relationship to changes in stratospheric ozone*. Photochem. Photobiol. 52: 811-817.
- de GRUIJL, F.R. and van der LEUN, J.C., 1994: *Estimate of the wavelength dependency of ultraviolet carcinogenesis in humans and its relevance to the risk assessment of stratospheric ozone depletion*. Health Physics 67: 319-325.
- de GRUIJL, F.R.; STERENBORG, H.J.; FORBES, P.D.; DAVIES, R.E.; COLE, C.; KELFKENS, G.; van WEELDEN, H.; SLAPER, H. and van der LEUN, J.C., 1993: *Wavelength dependence of skin cancer induction by ultraviolet irradiation of albino hairless mice*. Cancer Res. 53: 53-60.
- Del HOYO, C.; VICENTE, M.A.; RIVES, V., 1998: *Application of phenyl salicylate-sepiolite systems as ultraviolet radiation filters*. Clay Mineral 33: 467-474.
- Del HOYO, C; VICENTE, M.A; RIVES, V., 2001: *Preparation of drug-montmorillonite UV-radiation protection compounds by gas-solid adsorption*. Clay and Clay Minerals 36: 541-546.
- DESROSIERS, K.; INGRAHAM, W.; van MATRE, A., 2005: *TiO<sub>2</sub> Photocatalysis for Organics*. Course ENVE 325 - Environmental Air Quality, California Polytechnic State University, URL: <http://ceenve.calpoly.edu/cota/enve436/projects/TiO2b/TiO2-Organics.html> (accessed January 10, 2005).

- DIFFEY, B.L., 1991: *Solar ultraviolet radiation effects on biological systems*. Review in Physics in Medicine and Biology 36 (3): 299-328.
- DIFFEY, B.L., 2002: *Sources and measurement of ultraviolet radiation*. Methods 28: 4-13.
- DIFFEY, B., 2004: *Climate change, ozone depletion and the impact on ultraviolet exposure of human skin*. Phys. Med. Biol. 49: R1-R11.
- DRITS, V.A.; SAKHAROV, B.A.; DAINYAK, L.G.; SALYN, A.L.; and LINDGREEN, H., 2002: *Structural and chemical heterogeneity of illite-smectites from Upper Jurassic mudstones of East Greenland related to volcanic and weathered parent rocks*. Am. Mineral. 87 (11-12): 1590–1607.
- DUNFORD, R.; SALINARO, A.; CAI, L.Z.; SERPONE, N.; HORIKOSHI, S.; HIDAKA, H.; KNOWLAND, J., 1997: *Chemical oxidation and DNA-damage catalyzed by inorganic sunscreen ingredients*. FEBS Letters 418 (1-2): 87-90.
- FDA, 1999: *Sunscreen Drug Products for Over-the-Counter Human Use; Final Monograph, Federal Register 64-27666*. U.S. Food and Drug Administration, Rockville, MD, URL: <http://www.fda.gov/cder/fdama/fedreg/sunscreen.pdf> (Posted 5/21/99, accessed 1/2/2006)
- FIALIPS, CLAIRE-ISABELLE; HUO, D.; YAN, L.; WU, J. and STUCKI, J.S. (2002): *Effect of Fe oxidation state on the IR spectra of Garfield nontronite*. Am. Mineral. 87: 630–641
- GIES, P.H.; ROY, C.R.; TOOMEY, S.; MCLENNAN, A., 1998: *Protection against solar ultraviolet radiation*. Mutat Res. 422 (1): 15-22.
- GOODMAN, B.A., 1978: *The Mössbauer spectra of nontronites: consideration of an alternative assignment*. Clays and Clay Minerals 26: 176–177.
- GOODMAN, B.A.; RUSSELL, J.D.; FRASE, A.R.; WOODHAMS, F.D., 1976: *A Mössbauer and I.R. spectroscopic study of the structure of nontronite*. Clays and Clay Minerals 24: 53–59.
- GOSWAMI, D.Y., 1999: *Recent developments in photocatalytic detoxification and disinfection of water and air* – in Grossman, G. (Ed.) Proceedings of the ISES 1999 Solar World Congress.
- GOSWAMI, Y., 2003: *Targeting Bioterrorism - Detoxification*. URL: <http://rgp.ufl.edu/research/bioterrorism.html> (updated 2003).
- HELLER-KALLAI, L. and ROZENSON, I., 1981: *The Use of Mössbauer Spectroscopy of Iron in Clay Mineralogy*. Phys. Chem. Minerals 7: 223-238.
- HENNING, K.-H. & STÖRR, M., 1986: *Electron micrographs (TEM, SEM) of clays and clay minerals*. Akademie-Verlag Berlin [Schriftenreihe für geologische Wissenschaften, Bd. 25]: 352 pp.
- HENNING, K.-H. & KASBOHM, J., 1998: *Mineralbestand und Genese feinkörniger quartärer und präquartärer Sedimente in Nordostdeutschland unter besonderer Berücksichtigung des „Friedländer Tones“*, 3-5.9.1998. [Berichte der Deutschen Ton- und Tonmineralgruppe e.V., Band 6]: 147 – 162.
- HENNING, K.-H., 1971: *Mineralogische Untersuchung des eozänen Tones der Lagerstätte Friedland (Bezirk Neubrandenburg)*. Ber. Dt. Ges. Geol. Wiss., 16 (5): 5-39.
- HERBERT, H.-J.; KASBOHM, J.; HENNING, K.-H., 2004: *Long-term behaviour of the Wyoming bentonite MX-80 in high saline solutions*. Applied Clay Sciences 26: 275-291.
- HIDAKA, H.; HORIKOSHI, S.; SERPONE, N. and KNOWLAND, J., 1997: *In vitro photochemical damage to DNA, RNA and their bases by an inorganic sunscreen agent on exposure to UVA and UVB radiation*. Photochemistry and Photobiology A: Chemistry 111 (1-3): 205-213.

- HILLIER, S. and RYAN, P. C., 2002: *Identification of halloysite (7 Å) by ethylene glycol solvation: the 'MacEwan effect'*. Clay Minerals 37: 487–496.
- JAEGER, C.D. and BARD, A.J., 1979: *Spin trapping and electron spin resonance detection of radical intermediates in the photodecomposition of water at TiO<sub>2</sub> particulate systems*. J Phys Chem 83: 3146-3152.
- JCPDS International Center for Diffraction Data, 1978: *ASTM - set 28 & 29 of the power diffraction file*, USA.
- JCPDS International Center for Diffraction Data, 1979: *Power diffraction file: alphabetical index inorganic materials*, USA.
- JOUSSEIN, E.; PETIT, S.; CHURCHMAN, J.; THENG, B.; RIGHI, D. AND DELVAUX, B., 2005: *Halloysite clay minerals - a review*. Clay Minerals 40 (4): 383-426.
- JUDIN, V. P.S., 1993: *The lighter side of TiO<sub>2</sub>*. Chemistry in Britain 29: 503-505.
- JULICH *et al.*, 2004: *Biologically active compounds of Ganoderma pfeifferi DSM 13239*. U.S. Pat. No. 6,726,911.
- KAHR G. & MADSEN F.T., 1995: *Determination of the cation exchange capacity and the surface area of bentonite, illite, and kaolinite by methylene blue adsorption*. Applied Clay Science 9: 327-336.
- KASBOHM, J., 2003: *Zur Langzeitstabilität von Na-Montmorillonit in hochsalinaren Lösungen*. Habilitationsschrift - Universität Greifswald.
- KASBOHM, J.; HENNING, K.-H.; HERBERT, H.-J., 1998: *Transmissionselektronenmikroskopische Untersuchungen am Bentonit MX80 – in: Henning, K.-H.; Kasbohm, J. (Hrsg.): Beiträge zur Jahrestagung Greifswald, 3.-5.9.1998*. Berichte der Deutschen Ton- und Tonmineralgruppe e.V., Band 6: 228-236.
- KASBOHM, J.; TARRAH, J.; HENNING, K.-H., 2002: *Transmissionselektronen-mikroskopische Untersuchungen an Feinfraktionen der Ringversuchsprobe „Ton Stoob“ – in: Ottner, F.; Gier, S. (Hrsg.): Beiträge zur Jahrestagung Wien, 18.-20.9. 2002*. Berichte der Deutschen Ton- und Tonmineralgruppe e.V., Band 9: 71 – 84.
- KENJ, H., 1990: *Angewandte geologisch-mineralogisch und technologische Untersuchungen am Seilitzer Kaolin*. Dissertationsarbeit - Universität Greifswald.
- KERR, P.F. (Ed.), 1951: *Preliminary reports reference clay minerals American Petroleum Institute - Research Project 49*. Columbia University, New York.
- KLOPROGGE, J.T., JANSEN, J.B.H., and GEUS, J.W., 1990. *Characterization of synthetic Na-beidellite*. Clays and Clay Minerals 38 (4): 409-414.
- KNOWLAND, J.; MCKENZIE, E.A.; MCHUGH, P.J.; CRIDLAND, N.A., 1993: *Sunlight-induced mutagenicity of a common sunscreen ingredient*. FEBS Lett. 324: 309–313.
- KOMADEL, P. and MADEJOVÁ, J., 2006: *Acid activation of clay minerals. Chapter 7.1 – in: Bergaya, F., Theng, B.K.G., and Lagaly, G. (Eds.) Handbook of Clay Science*. Elsevier, Amsterdam.
- KORMANN, C.; BAHNEMANN, D.W. & HOFFMANN, M.R., 1989. *Environmental photochemistry: Is iron oxide (hematite) an active photocatalyst? A comparative study: α-Fe<sub>2</sub>O<sub>3</sub>, ZnO, TiO<sub>2</sub>*. J. Photochem. Photobiol., A: Chem. 48: 161-169.

- KÖSTER H. M., 1977: *Die Berechnung kristallchemischer Strukturformeln von 2:1-Schichtsilikaten unter Berücksichtigung der gemessenen Zwischenschichtladungen und Kationenaustauschkapazitäten, sowie die Darstellung der Ladungsverteilung in der Struktur mittels Dreieckskoordinaten*. Clay Miner. 12: 45-54.
- KRANZ, G.; RUCHHOLZ, M.; MARX, E., 1990: *Neue Referenzmaterialien - Kaoline und Tone*. Silikatechnik 41 (10): 330 – 333.
- KRUMM, S., 1994: *WINFIT 1.0 - A Computer Program for X-ray Diffraction Line Profile Analysis*. Acta Universitatis Carolinae Geologica, 38, XIIIth Conference on Clay Mineralogy and Petrology, Praha, 253-261.
- KUŽVART, M., 1969: *Kaolin Deposits of Czechoslovakia* – in: Malkovský, M. and Vachtl, J. (Eds.): *Proceedings of Symposium I - Kaolin Deposits of the World: A - Europe*. Report of the Twenty-Third Session, Szechoslovakia 1968/ International Geological Congress, Prague Vol. 15, 47–73.
- LIM, H.W.; GILCHREST, B.A.; COOPER, K.D.; BISCHOFF-FERRARI, H.A.; RIGEL, D.S., CYR, W.H.; MILLER, S.; de LEO, V.A.; LEE, T.K.; DEMKO, C.A.; WEINSTOCK, M.A.; YOUNG, A.; EDWARDS, L.S.; JOHNSON, T.M.; STONE, S.P., 2005: *Sunlight, tanning booths, and vitamin D*. J Am Acad. Dermatol. 52: 868-876.
- LINDEQUIST, U; NIEDERMEYER, T.H. J. AND JÜLICH, W.-D., 2005: *The pharmacological potential of mushrooms*. Evid Based Complement Alternat Med. 2 (3): 285-99.
- LONGSTRETH, J.D.; de GRUIJL, F.R.; KRIPKE, M.L.; TAKIZAWA, Y. & van der LEUN, J.C., 1994: *Effects of Increased Solar Ultraviolet Radiation on Human Health*. – in: van der Leun J.C. (Ed.), *Environmental Effects of Ozone Depletion: 1994 Assessment*. United Nations Environment Programme (UNEP): 23-48.
- MacKIE, R.M., 2000: *Effects of Ultraviolet Radiation on Human Health*. Radiation Protection Dosimetry 91: 15-18.
- MacLAUGHLIN, J.A.; ANDERSON, R.R.; HOLICK, M.F., 1982: *Spectral character of sunlight modulates the photosynthesis of previtamin D3 and its photoisomers in human skin*. Science.: 1001-1003.
- MADSEN, F. T., 1998: *Clay mineralogical investigations related to nuclear waste disposal*. Clay Minerals 33: 109–129.
- MALLA, P.B., and DOUGLAS, L.A., 1987: *Problems in identification of montmorillonite and beidellite*. Clays and Clay Minerals 35 (3): 232-236.
- McKINLAY, A.F. and DIFFEY, B.L., 1987: *A reference action spectrum for ultra-violet induced erythema in human skin*. In *Human Exposure to Ultraviolet Radiation: Risks and Regulations*. W.F. Passchier and B.F.M. Bosnjakovich (Eds.): International Congress Series. 83-87.
- MEHRA, O.P., and JACKSON, M.L., 1960: *Iron oxide removal from soils and clays by a dithionite-citrate system buffered with sodium bicarbonate*. Clays Clay Miner. 7: 317-327.
- MENIL, F., 1985: *Systematic Trends of the <sup>57</sup>Fe Mossbauer isomer shifts in (FeO<sub>n</sub>) and (FeF<sub>n</sub>) polyhedra*. J. Phys. Chem. Solids. 46 (7): 763-789.
- MEUNIER, A.; LANSON, B. and VELDE, B., 2004: *Composition variation of illite-vermiculitesmectite mixed-layer minerals in a bentonite bed from Charente (France)*. Clay Minerals (39): 317–332.
- MEUNIER, A. and VELDE, B., 2004: *Illite*. Springer, 286 pp. (Reviews in Clays and Clay Minerals, 52 (6) 792-795, 2004.)

- MEUNIER, A.; LANSON, B. and BEAUFORT, D., 2000: *Vermiculitization of smectite interfaces and illite layer growth as a possible dual model for illitesmectite illitization in diagenetic environments: a synthesis*. Clay Minerals (35): 573–586.
- MEUNIER, A. and VELDE, B., 1989: *Solid solutions in I/S mixed-layer minerals and illite*. Am. Mineral. 74 (9-10): 1106–1112.
- MOAN, J. and PEAK, M.J., 1989: *Effects of UV radiation on cells*. J. Photochem. Photobiol. B. Biol. 4: 21–34.
- MOLL, W.F., Jr., 2001: *Baseline studies of the Clay Minerals Society source clays: geological origin*. Clays and Clay Minerals 49 (5): 374–380.
- MOORE, DUANE E., & REYNOLDS, ROBERT C., JR., 1997: *X-Ray Diffraction and the Identification and Analysis of Clay Minerals*. 2nd Edition, Oxford University Press, 378 pp. (Reviews in Am. Mineral. 84: 689–690.)
- MURAD, E., 1987: *Mössbauer spectra of nontronites: structural implications and characterization of associated iron oxides*. - Zeitschr. Pflanzenernährung Bodenk. 150: 279–285.
- MURAD, E.; SCHWERTMANN, U., 1986: *Influence of Al Substitutions and Crystal Size on the Room-Temperature Mossbauer Spectrum of Hematite*. Clays and Clay Minerals 34: 1–6.
- MURAD, E., 1998: *Clays and clay minerals: What can Mössbauer spectroscopy do to help understand them?* Hyperfine Interactions 117: 39–70.
- MURRAY, H.H., 1997: *Clays for our future*. Proceeding of the 11<sup>th</sup> International Clay Conference, Ottawa, Canada: 3–11.
- MURRAY, H.H., 2005: *Current Industrial Applications of Clays*. Unpublished paper and Presentation in the 13<sup>th</sup> International Clay Conference, Tokyo, Japan.
- NEWMAN, A.C.D., 1987: *Chemistry of Clays and Clay Minerals*. Longman Scientific and Technical, Harlow, Essex, UK. 480 pp.
- NRPB, 2002: *Report of the Advisory Group on Non-ionising Radiation (AGNIR): Effects of Ultraviolet Radiation on Human Health*. Documents of the NRPB, 13 (1): 282 pp. (URL: [http://www.hpa.org.uk/radiation/publications/documents\\_of\\_nrpb/](http://www.hpa.org.uk/radiation/publications/documents_of_nrpb/))
- Parmentier GmbH & Co KG, 2004: *Lanowax EP distilled grade - Wollwachsalkohol Ph. Eur. 4.03*. URL: <http://www.lanolin.de/auswahl.htm?lanowax.htm> (updated 2004, accessed June 28, 2005).
- PEAK, J.G. and PEAK, M.J., 1991: *Comparison of initial yields of DNA-to-protein crosslinks and single-strand breaks induced in cultured human cells by far- and near-ultraviolet light, blue light and X-rays*. Mutat. Res./Fundamental and Molecular Mechanisms of Mutagenesis, 246: 187–191.
- PRYOR, W.A., 1986: *Oxy-Radicals and Related Species: Their Formation, Lifetimes, and Reactions*. Annu Rev Physiol. 48: 657–667.
- RANCOURT, D.G., 1998: *Mössbauer spectroscopy in clay science (REVIEW)*. Hyperfine Interactions 117: 3–38.
- RIEDER, M. et al., 1998: *Nomenclature of the micas*. Am. Mineral. 83, 1366 (1–7p).
- ROSENBERG, PHILIP E., 2002: *The nature, formation, and stability of end-member illite: A hypothesis*. Am. Mineral. (87): 103–107.
- ROZENSON, I.; HELLER-KALLAI, L., 1977: *Mössbauer spectra of dioctahedral smectites*. Clays and Clay Minerals 25: 94–101.



- RPA, 2004: *Comparative Study on Cosmetics Legislation in the EU and Other Principal Markets with Special Attention to so-called Borderline Products* (Final Report – August 2004 prepared for European Commission, DG Enterprise). Risk & Policy Analysts Limited, UK (www.rpaltd.co.uk).
- SEDAC: *Action Spectra*. Stratospheric Ozone and Human Health Project – on Socioeconomic Data and Applications Center's (SEDAC) website. URL: <http://sedac.ciesin.org/ozone/docs/AS.html> (accessed January 18, 2006).
- SERPONE, N.; SALINARO, A.; EMELINE, A., 2001: *Deleterious effects of sunscreen titanium dioxide nanoparticles on DNA: efforts to limit DNA damage by particle surface modification* – in Catherine J. Murphy (Ed.) Proc. SPIE Vol. 4258, Nanoparticles and Nanostructured Surfaces: Novel Reporters with Biological Applications 2: 86-98.
- SERPONE, N.; SALINARO, A.; EMELINE, A.V.; HORIKOSHI, S.; HIDAKA, H. and ZHAO, J., 2002: *An in vitro systematic spectroscopic examination of the photostabilities of a random set of commercial sunscreen lotions and their chemical UVB/UVA active agents*. Photochem. Photobiol. Sci., 2002, 1, 970–981.
- SETLOW, R.B., 1974: *The wavelengths in sunlight effective in producing cancer: a theoretical analysis*. Proceedings of the National Academy of Sciences U.S.A. 71: 3363-3366.
- SHERMAN D.M. AND WAITE T.D., 1985: *Electronic spectra of Fe<sup>3+</sup> oxides and oxide hydroxides in the near-IR to near-UV*. Amer. Mineral. 70: 1262-1269.
- SKAAR, E.P.; HUMAYUN, M.; BAE, T.; deBORD, K.L; and SCHNEEWIND, O., 2004: *Iron-Source Preference of Staphylococcus aureus Infections*. Science. 305: 1626 - 1628.
- ŚRODOŃ, J.; ELSASS, F.; MCHARDY, W. J.; MORGAN, D. J., 1992: *Chemistry of illite-smectite inferred from TEM measurements of fundamental particles*. Clay Minerals 27 (2): 137-158.
- ŚRODOŃ, J. and McCARTY, D.K., 2006: *Total surface area, surface charge density, cation exchange capacity and water retention in smectites*. – in: Bridging Clays - Joint meeting Groupe Francais des Argiles & The Clay Minerals Society, 3 - 7 June 2006, France.
- STARKEY, H.C.; BLACKMON, P.D.; and HAUFF, P.L., 1984: *The routine mineralogical analysis of clay-bearing samples*. Washington, DC, US Geological Survey, 32 pp (US Geological Survey Bulletin 1563).
- STÖRR M., 1982. *Die Kaolinlagerstätten der Deutschen Demokratischen Republik*. Akademie-Verlag Berlin: 226 pp.
- STUCKI, J. W. 2006: *Properties and behaviour of iron in clay minerals. Chapter 8* – in: Bergaya, F., Theng, B.K.G., and Lagaly, G. (Eds.) *Handbook of Clay Science*. Elsevier, Amsterdam.
- TAN, M.H.; COMMENS, C.A.; BURNETT, L.; SNITCH, P.J., 1996: *A pilot study on the percutaneous absorption of microfine titanium dioxide from sunscreens*. Australas J Dermatol 37: 185-187.
- Unions NSW, 2005: *Sun Safety at work - Labor Council of New South Wales (NSW) Policy on protection from ultraviolet radiation for outdoor workers*. The Local Government Association of NSW and the Shires Association of NSW. URL: [http://www.lgsa.org.au/resources/documents/Sun\\_Safety\\_policy\\_301105.pdf](http://www.lgsa.org.au/resources/documents/Sun_Safety_policy_301105.pdf) (accessed April 20, 2006).

- VICENTE, M. A.; ELSASS, F.; MOLINA, E.; ROBERT, M., 1997: *Palaeoweathering in slates from the Iberian Hercynian Massif (Spain): investigation by TEM of clay mineral signatures*. Clay Minerals 32 (3): 435-451.
- VICENTE, M.A.; SANCHEZ-CAMAZANO, M.; SÁNCHEZ-MARTÍN, M.J.; Del ARCO, M.; MARTÍN, C.; RIVES, V.; VICENTE-HERNÁNDEZ, J., 1989: *Adsorption and desorption of N-Methyl 8-Hydroxy Quinoline Methyl Sulfate on Smectite and the potential use of the clay-organic product as an ultraviolet radiation collector*. Clay and Clay Minerals 37 (2): 157-163.
- VOGT, C.; LAUTERJUNG, J. and FISCHER, R. X., 2002: *Investigation of the clay fraction (<2 µm) of the Clay Minerals Society reference clays*. Clays and Clay Minerals 50 (3): 388 - 400.
- VOIGT, R. and BORNSCHEIN, M., 1975: *Lehrbuch der pharmazeutischen Technologie*. Veb Verlag Volk und Gesundheit. 272 – 275.
- WALKER, S.G.; FLEMMING, C.A.; FERRIS, F.G.; BEVERIDGE, T.J. AND BAILEY, G.W., 1989: *Physicochemical interaction of Escherichia coli cell envelopes and Bacillus subtilis cell walls with two clays and ability of the composite to immobilize heavy metals from solution*. Appl Environ Microbiol., 55 (11): 2976–2984.
- WARREN, E. A. and CURTIS, C. D., 1989: *The chemical composition of authigenic illite within two sandstone reservoirs as analysed by ATEM*. Clay Minerals (24): 137-156.
- WELLMER, F.-W.; KOSINOWSKI, M., 2005: *A hierarchy of natural resources with respect to sustainable development*. Zeitschrift der Deutschen Gesellschaft für Geowissenschaften 156 (2): 247-260.
- WOLD, S.; ERIKSEN, T. E., 2002: *Diffusion of lignosulfonate colloids in compacted bentonite*. Workshop on 'Clay Microstructure and its Importance to Soil Behaviour', Lund, Oct. 15-17, 2002: 74-86.
- WONG, J.C.F and PARISI, A.V., 1998: *Assessment of ultraviolet radiation exposures in photobiological experiments*. Proc. Protection Against the Hazards of UVR, Internet Photochemistry and Photobiology. URL: <http://www.photobiology.com/UVR98/wongrev/index.htm> (accessed February 01, 2006).
- YOUNG, A.R.; CHADWICK, C.A.; HARRISON, G.I.; NIKAIIDO, O.; RAMSDEN, J.; POTTEN, C.S., 1998: *The similarity of action spectra for thymine dimmers in human epidermis and erythema suggests that DNA is the chromophore for erythema*. J. Invest. Dermatol. 111: 982-988.
- ZÖLLER, M. H., 1993: *Charakterisierung von Illitkristallen durch konvergente Elektronenbeugung* - in: Graf v. Reichenbach, H. (Hrsg.): *Hydratation und Dehydratation von Tonmineralen – Beiträge zur Jahrestagung Hannover, DTTG 1992: Berichte der Deutschen Ton- und Tonmineralgruppe e.V., Band 2: 211-220*.



## APPENDIX

### *Appendix 1. Determined clay minerals with d-values by Å and related intensities based on the JCPDS International Center for Diffraction Data*

14-0164				29-1487		02-0462		12-204		29-1498		13-0135		3173 (*)		07-0166		05-0490	
Kaolinite-1\ITA\RG				Halloysite-7Å		Illite, 1M		Na-Montm.		Montm.-13 Å		Montm.-15 Å		Nontronite		Chlorite		Quartz, low	
Al <sub>2</sub> Si <sub>2</sub> O <sub>5</sub> (OH) <sub>4</sub>				Al <sub>2</sub> Si <sub>2</sub> O <sub>5</sub> (OH) <sub>4</sub> (metahalloysite)		KAl <sub>2</sub> (Si <sub>3</sub> AlO <sub>10</sub> ) (OH) <sub>2</sub>		Na <sub>x</sub> (AlMg) <sub>2</sub> Si <sub>4</sub> O <sub>10</sub> (OH) <sub>2</sub>		Na <sub>0.3</sub> (Al,Mg) <sub>2</sub> Si <sub>4</sub> O <sub>10</sub> (OH) <sub>2</sub> .4H <sub>2</sub> O		Ca <sub>0.2</sub> (Al,Mg) <sub>2</sub> Si <sub>4</sub> O <sub>10</sub> (OH) <sub>2</sub> .H <sub>2</sub> O		Na <sub>0.33</sub> Fe <sub>2</sub> (Si,Al) <sub>4</sub> O <sub>10</sub> (OH) <sub>2</sub>		(Fe,Al,Mg) <sub>6</sub> (Si,Al) <sub>4</sub> O <sub>10</sub> (OH) <sub>8</sub>		SiO <sub>2</sub>	
7.170	100	2.064	20	7.300	65	10.000	80	12.900	100	13.600	100	15.000	100	9.986	100	14.000	60	4.260	35
4.478	35	1.997	35	4.420	100	5.030	80	6.550	10	5.160	12	5.010	60	4.555	44	7.080	100	3.343	100
4.366	60	1.987	35	3.620	60	4.520	60	4.510	70	4.460	65	4.500	80	4.354	36	4.681	30	2.458	12
4.186	45	1.974	20	2.560	25	3.630	80	4.320	10	2.560	18	3.770	20	3.625	17	3.523	50	2.282	12
4.139	35	1.952	20	2.370	1	3.350	100	4.120	10	1.690	8	3.500	10	3.329	26	2.821	10	2.237	6
3.847	40	1.939	35	1.681	16	3.100	80	3.250	20	1.495	12	3.300	10	3.116	21	2.682	4	2.128	9
3.745	25	1.921	20	1.483	30	2.900	80	2.580	20			3.020	60	2.688	11	2.619	30	1.980	6
3.579	80	1.906	5			2.600	100	2.245	5			2.580	40	2.589	17	2.574	20	1.817	17
3.420	5	1.897	25			2.470	60	1.876	5			2.500	40	2.585	6	2.469	10	1.801	1
3.376	35	1.870	20			2.390	80	1.700	20			2.260	10	2.408	22	2.405	20	1.672	7
3.155	20	1.845	25			2.270	40	1.503	40			2.150	10	2.403	15	2.279	10	1.659	3
3.107	20	1.838	35			2.180	40					1.880	10	2.239	5	2.014	20	1.608	1
2.754	20	1.810	20			2.140	80					1.700	30	2.239	4	1.893	5	1.541	15
2.566	35	1.789	25			1.990	100					1.500	50	2.152	7	1.828	5	1.453	3
2.553	25	1.710	25			1.720	20					1.493	50	1.975	4	1.765	5	1.418	1
2.535	35	1.689	25			1.650	80					1.285	20	1.660	8	1.722	5	1.382	7
2.519	10	1.681	25			1.510	80							1.658	5	1.666	5	1.375	11
2.495	45	1.669	40			1.420	20							1.525	5	1.560	20	1.372	9
2.385	25	1.660	40			1.380	20							1.516	7	1.523	10	1.288	3
2.347	40	1.656	10			1.350	60							1.352	6	1.483	5		
2.338	40	1.649	40			1.340	60									1.427	5		
2.305	5	1.633	30			1.300	60									1.411	5		
2.293	35	1.620	70													1.393	5		
2.253	20	1.607	30													1.339	5		
2.237	5	1.594	10																
2.218	10	1.586	60																
2.197	20	1.572	10																
2.186	20	1.553	30																
2.173	5	1.545	40																
2.151	10	1.537	40																
2.133	20	1.514	5																
2.116	10	1.505	5																
2.093	10	1.489	90																
2.080	5																		

09-0466				3714 (*)		3348 (*)		06-0710		13-0534	
Albite, ordered				Plagioclase		Orthoclase		Pyrite, syn		Hematite, syn	
NaAlSi <sub>3</sub> O <sub>8</sub>				(Na,Ca)(Si,Al) <sub>4</sub> O <sub>8</sub>		KAlSi <sub>3</sub> O <sub>8</sub>		FeS <sub>2</sub>		Fe <sub>2</sub> O <sub>3</sub>	
6.390	20	1.851	2	4.045	81	4.218	57	3.128	35	3.660	25
5.940	2	1.844	3	3.896	17	3.937	18	2.709	85	2.690	100
5.590	2	1.829	4	3.761	27	3.774	74	2.423	65	2.510	50
4.030	16	1.824	18	3.755	39	3.616	16	2.212	50	2.285	2
3.857	8	1.804	6	3.645	34	3.465	51	1.916	40	2.201	30
3.780	25	1.785	8	3.370	24	3.308	100	1.633	100	2.070	2
3.684	20			3.232	52	3.285	58	1.564	14	1.838	40
3.663	16			3.212	62	3.249	29	1.503	20	1.690	60
3.509	10			3.207	94	3.229	76	1.445	25	1.634	4
3.484	2			3.183	100	2.989	58			1.596	16
3.375	8			3.139	43	2.902	25			1.484	35
3.196	100			3.022	23	2.767	22			1.452	35
3.151	10			2.951	28	2.601	20			1.349	4
2.964	10			2.933	18	2.574	38			1.310	20
2.933	16			2.840	25	2.166	26				
2.866	8			2.523	31	2.006	15				
2.843	2			2.508	20	1.798	25				
2.787	2			2.125	15	1.496	26				
2.639	6			1.833	16	1.287	14				
2.563	8			1.775	26	1.277	14				
2.538	2										
2.511	2										
2.496	6										
2.460	6										
2.443	4										
2.431	2										
2.405	2										
2.388	4										
2.320	4										
2.278	2										
2.189	4										
2.125	8										
2.119	6										
2.076	2										
2.035	2										
2.000	2										
1.980	4										
1.927	2										
1.889	8										

*Note: (\*) source: CHICHAGOV, A.V. et al (created: 1997): Crystallographic and Crystallochemical Database for Mineral and their Structural Analogues. Institute of Experimental Mineralogy, Russia. URL: <http://database.iem.ac.ru/mincryst/> (new full revision: 2000, accessed: 2005)*

**Appendix 2. Mineralogical composition of German reference kaolins and German reference clays, indicated in mass %**

(according to (a) ASMW, 1988; (b) Kranz et al., 1990)

(a) Reference Kaolins	Caminau	Wolfka	Spergau	Seilitz
Quartz	1.4	15.4	15.0	19.4
Kaolinite	84.9	81.7	71.6	34.1
2:1 Mineral (*)	14.3	2.9	12.8	45.0
Others	<1	<1	<1	<1
(*)	Illite Muscovite	IS-ml	IS-ml	Illite IS-ml

(b) Reference Clays	Plessa	Gorrenberg	Teistungen	Thierfeld
Quartz	40.8	38.3	34.4	32.6
Kaolinite	24.4	16.8	11.2	19.0
2:1 Mineral (*)	28.5	27.0	25.0	28.5
Feldspar (**)	5.0	10.0	19.1	7.7
Chlorite	not detected	1.7	7.9	6.4
Hematite	not detected	1.4	1.8	4.5
Rutile/Anatase	1.0	1.0	<1.0	1.5
Calcite	not detected	3.0	not detected	not detected
Dolomite	not detected	not detected	<1.0	not detected
(*)	Smectite Mixed-layer Illite	Smectite Mixed-layer Illite	Mixed-layer	Illite
(**)	Orthoclase	Plagioclase Orthoclase	Plagioclase Orthoclase	Plagioclase Orthoclase

**Appendix 3. Grain size distribution of German reference kaolins and German reference clays, indicated in %**

(adapted to (a) ASMW, 1988; (b) Kranz et al., 1990)

	(a) Reference Kaolins				(b) Reference Clays			
	Caminau	Wolfka	Spergau	Seilitz	Plessa	Gorrenberg	Teistungen	Thierfeld
> 20 µm	1.5	1.4	5.2	2.8	38.4	31.4	16.4	18.1
20-6.3 µm	18.3	15.2	13.5	15.6	19.5	20.2	14.7	25.5
6.3-2 µm	35.8	41.6	15.2	14	14.5	18.8	17.6	17.1
<2 µm	44	41.8	66.1	67.6	27.6	29.6	51.3	39.3

**Appendix 4. Chemical composition (main components, oxide form) of German reference kaolins and German reference clays, indicated in mass %**  
(according to (a) ASMW, 1988; (b) Kranz et al., 1990)

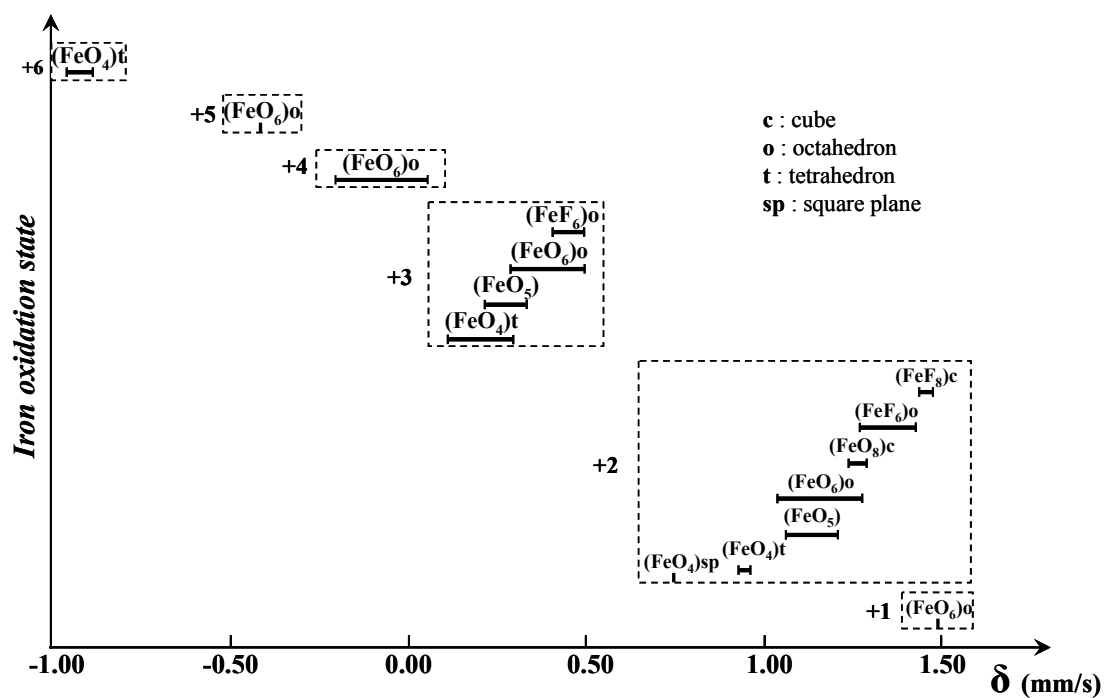
Samples	SiO <sub>2</sub> (%)	TiO <sub>2</sub> (%)	Al <sub>2</sub> O <sub>3</sub> (%)	Fe <sub>2</sub> O <sub>3</sub> (%)	MgO (%)	CaO (%)	Na <sub>2</sub> O (%)	K <sub>2</sub> O (%)	LOI (%)
<b>(a) Reference Kaolins</b>									
Caminau	46.16	0.61	37.05	1.25	0.20	0.14	0.03	1.53	12.86
Wolfka	53.75	0.16	32.84	0.34	0.11	0.13	0.016	0.10	12.12
Spergau	53.81	0.73	31.23	0.71	0.36	0.18	0.069	1.09	11.16
Seilitz	61.50	0.29	23.87	1.29	1.07	0.27	0.035	4.09	7.18
<b>(b) Reference Clays</b>									
Plessa	68.92	1.13	16.96	2.25	0.73	0.27	0.95	2.46	5.49
Gorrenberg	65.77	1.09	14.40	4.36	1.26	2.86	0.87	2.45	6.28
Teistungen	65.58	0.79	16.22	4.39	2.23	0.76	1.62	3.5	4.31
Thierfeld	60.22	1.67	17.92	7.89	2.10	0.47	0.66	3.29	5.09

**Appendix 5. Chemical composition (main components, oxide form) of The Clay Minerals Society reference clays (kaolins and bentonites), indicated in mass %**  
(according to a) van Olphen & Fripiat (1979) and b) Vogt et al. (2002))

Clay Samples	Ref.	SiO <sub>2</sub> (%)	TiO <sub>2</sub> (%)	Al <sub>2</sub> O <sub>3</sub> (%)	Fe <sub>2</sub> O <sub>3</sub> (%)	FeO (%)	MnO (%)	MgO (%)	CaO (%)	Na <sub>2</sub> O (%)	K <sub>2</sub> O (%)	P <sub>2</sub> O <sub>5</sub> (%)	LOI (%)
<b>KGa-1b</b> Georgia low defect kaolin	a)	44.2	1.39	39.7	<b>0.13</b>	0.08	<0.01	0.03	n.d.	0.013	0.05	0.03	13.78
<b>KGa-2</b> Georgia high defect kaolin	a)	43.9	2.08	38.5	<b>0.98</b>	0.15	n.d.	0.03	n.d.	<0.01	0.07	0.05	13.77
<b>SHCa-1</b> California hectorite	a)	34.7	0.04	0.7	<b>0.02</b>	0.25	0.01	15.3	23.4	1.26	0.13	0.01	21.80
	b)	52.1	0.20	15.2	<b>1.40</b>		0.07	7.54	0.12	n.d.	0.05	0.01	24.17
<b>STx-1</b> Texas montmorillonite	a)	70.1	0.22	16.0	<b>0.65</b>	0.15	0.01	3.69	1.59	0.27	0.08	0.03	6.54
	b)	62.2	0.22	14.5	<b>0.58</b>		0.01	4.57	0.12	n.d.	0.04	0.02	18.33
<b>SAz-1</b> Arizona montmorillonite	a)	60.4	0.24	17.6	<b>1.42</b>	0.08	0.10	6.46	2.82	0.06	0.19	0.02	9.91
	b)	52.5	0.20	15.2	<b>1.43</b>		0.07	7.44	0.18	n.d.	0.05	0.01	23.61
<b>SWy-2</b> Wyoming montmorillonite	a)	62.9	0.09	19.6	<b>3.35</b>	0.32	<0.01	3.05	1.68	1.53	0.53	0.05	6.06
	b)	57.3	0.11	17.9	<b>3.73</b>		0.01	3.91	0.05	n.d.	0.12	0.02	17.38

Note: n.d.: not detected

*Appendix 6. Isomer shifts at room temperature for various  $(\text{Fe}^{m+}\text{F}_n)$  and  $(\text{Fe}^{m+}\text{O}_n)$  polyhedra  
(according to Menil, 1985)*



**Appendix 7. Mössbauer spectroscopy analyses with selected iron-bearing clay samples**

Clay Samples	Component of spectrum	Isomer shift $\delta$ (mm/s)	Quadrupole splitting $\Delta$ (mm/s)	Line-width FWHM $\Gamma$ (mm/s)	Magnetic hyperfine field $H_i$ (T)	ion in general component $Fe^*$ (%)	area of component $I$ (%)	ion mass in phase $Fe^{**}$ (%)	Coeff. of ionoxidation $Fe_0$	Fe-ion phases
Teistungen	O-1.1 ( $Fe^{3+}$ )	0.37	-0.20	0.35	50.9		32.01	1.01		Hematite
	CM-1.1 ( $Fe^{2+}$ )	1.14	2.61	0.32	0		27.19	0.86		diCM, <i>cis</i>
	CM-1.2 ( $Fe^{2+}$ )	1.15	2.06	0.40	0	3.16	6.97	0.22	0.66	diCM, <i>trans</i>
	CM-1.3 ( $Fe^{3+}$ )	0.33	0.65	0.49	0		27.70	0.88		diCM, <i>cis</i>
	CM-1.4 ( $Fe^{3+}$ )	0.36	1.14	0.58	0		6.13	0.19		diCM, <i>trans</i>
Teistungen Dithionite	O-2.1 ( $Fe^{3+}$ )	0.37	-0.18	0.35	50.7		15.42	0.44		Hematite
	CM-2.1 ( $Fe^{2+}$ )	1.13	2.63	0.32	0		31.69	0.90		diCM, <i>cis</i>
	CM-2.2 ( $Fe^{2+}$ )	1.19	2.16	0.58	0	2.84	14.99	0.43	0.53	diCM, <i>trans</i>
	CM-2.3 ( $Fe^{3+}$ )	0.33	0.67	0.47	0		32.21	0.91		diCM, <i>cis</i>
	CM-2.4 ( $Fe^{3+}$ )	0.39	1.13	0.36	0		5.69	0.16		diCM, <i>trans</i>
Thierfeld	O-3.1 ( $Fe^{3+}$ )	0.38	-0.21	0.36	50.9		60.00	3.31		Hematite
	CM-3.1 ( $Fe^{2+}$ )	1.12	2.59	0.40	0		8.69	0.48		diCM, <i>cis</i>
	CM-3.2 ( $Fe^{3+}$ )	0.35	0.65	0.47	0	5.52	21.90	1.21	0.91	diCM, <i>cis</i>
	CM-3.3 ( $Fe^{3+}$ )	0.39	1.13	0.52	0		9.41	0.52		diCM, <i>trans</i>
Thierfeld Dithionite	O-4.1 ( $Fe^{3+}$ )	0.39	-0.20	0.35	51.1		12.23	0.35		Hematite
	CM-4.1 ( $Fe^{2+}$ )	1.12	2.59	0.47	0		16.72	0.48		diCM, <i>cis</i>
	CM-4.2 ( $Fe^{3+}$ )	0.35	0.67	0.47	0	2.87	46.23	1.33	0.83	diCM, <i>cis</i>
	CM-4.3 ( $Fe^{3+}$ )	0.38	1.08	0.58	0		24.82	0.71		diCM, <i>trans</i>

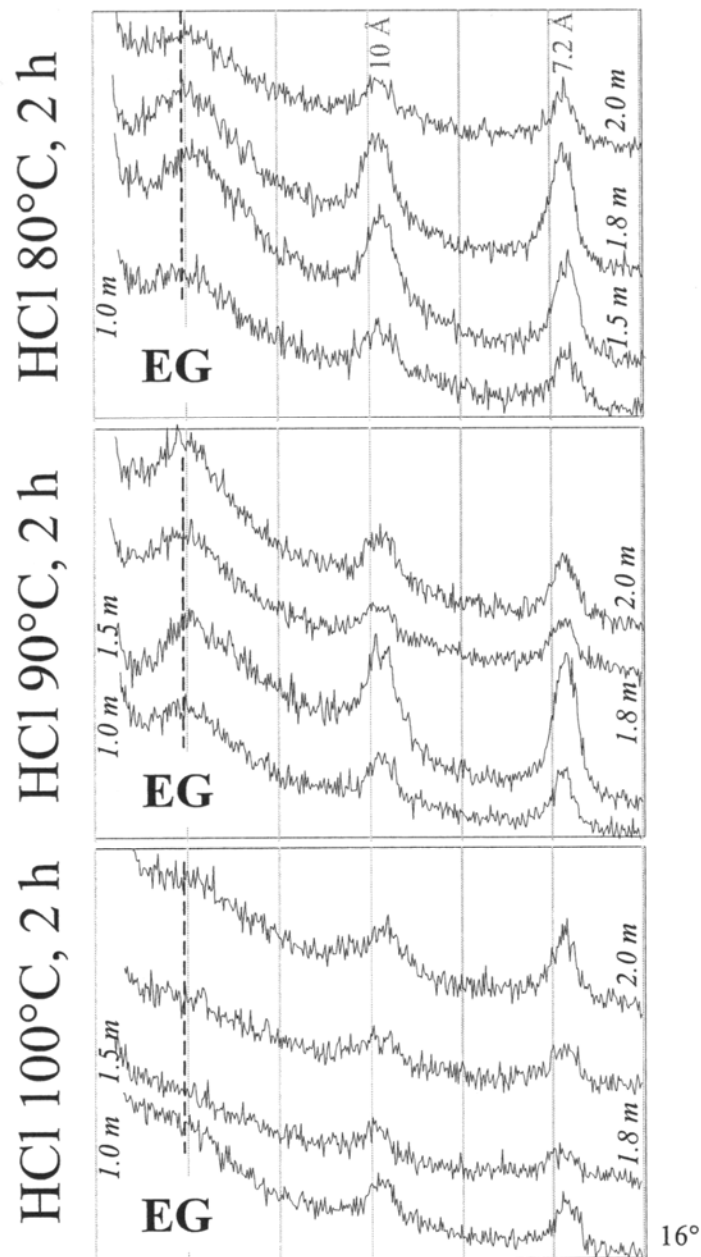
Note: Measured using Ms-1104Em at room temperature (about 300 K), Doppler-velocity and  $^{57}Co$  isotopes resource

**Appendix 7. Mössbauer spectroscopy analyses with selected iron-bearing clay samples (cont.)**

Clay Samples	Component of spectrum	Isomer shift $\delta$ (mm/s)	Quadrupole splitting $\Delta$ (mm/s)	Width of line FWHM $\Gamma$ (mm/s)	Magnetic hyperfine field $H_i$ (T)	ion in general component $Fe^*$ (%)	area of component $I$ (%)	ion mass in phase $Fe^{**}$ (%)	Coeff. of ionoxidation $Fe_0$	Fe-ion phases
Friedland Clay bulk	CM-5.1 ( $Fe^{2+}$ )	1.24	1.82	0.28	0	5.11	31.16	1.59	0.55	di-Mica, <i>trans</i>
	CM-5.2 ( $Fe^{2+}$ )	1.13	2.73	0.36	0		14.04	0.72		Chlorite
	CM-5.3 ( $Fe^{3+}$ )	0.34	0.52	0.41	0		43.97	2.25		ML mineral, <i>cis</i>
	CM-5.4 ( $Fe^{3+}$ )	0.37	1.04	0.38	0		10.84	0.55		ML mineral, <i>trans</i>
Friedland Clay <2 $\mu m$	CM-6.1 ( $Fe^{2+}$ )	1.20	1.74	0.37	0	4.50	2.95	0.13	0.80	di-Mica, <i>trans</i>
	CM-6.2 ( $Fe^{2+}$ )	1.13	2.73	0.37	0		16.34	0.74		Chlorite
	CM-6.3 ( $Fe^{3+}$ )	0.35	0.42	0.40	0		57.44	2.58		ML mineral, <i>cis</i>
	CM-6.4 ( $Fe^{3+}$ )	0.34	0.95	0.45	0		23.26	1.05		ML mineral, <i>trans</i>
Nontonite Garfield	CM-7.1 ( $Fe^{3+}$ )	0.36	0.24	0.34	0	22.22	59.48	13.22	1.00	Nontronite, <i>cis</i>
	CM-7.2 ( $Fe^{3+}$ )	0.36	0.65	0.31	0		40.52	9.00		Nontronite, <i>trans</i>

Measured using Ms-1104Em at room temperature (about 300 K), Doppler-velocity and  $^{57}Co$  isotopes resource

ML mineral: mixed-layer mineral, *cis* or *trans* means Fe-ion phase in *cis*-octahedral or *trans*-octahedral in accordingly mineral



**Appendix 8. XRD patterns of HCl acid treated series with different concentrations of acid solution and different temperatural conditions,  $^{\circ}2\theta$  CoK $_{\alpha}$  position**

(according to KASBOHM & HOANG, 2004 (working paper))

*Note: Measured using HZG 4 / Seifert C3000; XRD patterns including ethylene-glycol saturated (EG) specimen patterns; from above to the bottom: three groups of treated samples in according to three temperature levels: 80°C, 90°C and 100°C; within each group is including samples in according to different except treated sample concentrations of acid solution: 1M, 1.5M, 1.8M and 2M; the patterns show the peaks of mixed-lay series (except treated samples under temperature of 100°C), mica-like mineral and kaolinite*



## Appendix 9. Ingredient of Ladival® trade-ware cream series

(according to STADA GmbH, Bad Vilbel, Germany, URL: <http://www.ladival.de/>)

<b>Ingredient</b>	<b>Function for product</b>	<b>Function for skin</b>
4-Methylbenzylidene Camphor	-	UV-B filter
Acrylates/C10-30 Alkyl Acrylate Crosspolymer Sodium	consistency, gel-matrix	-
Alcloxa	-	skin regeneration
Alcohol Denat.	to cure	skin regeneration
Aloe Barbadensis Gel	-	moisture, refrigerant, regeneration
Aqua	solution	-
Arachis Hypogaea	oil phase	greasing, pleasantness
Ascorbic Acid	anti-oxidation	-
Ascorbyl Palmitate	anti-oxidation	-
Bisabolol	-	depressant
Butyl Methoxydibenzoylmethane	-	UV-A filter
Buxus Chinensis	oil phase	greasing, pleasantness
C12-15 Alkyl Benzoate	-	pleasantness
C20-40 Alkyl Stearate	consistency	pleasantness
Candelilla Cera	consistency	pleasantness
Caprylic/Capric Triglyceride	oil phase	greasing, pleasantness
Cera Alba	consistency	pleasantness
Cetyl Alcohol	consistency	-
Cetyl Palmitate	consistency	-
Cocoglycerides	oil phase	greasing, pleasantness
Disodium EDTA	complexing agent	-
Glycerin	wetting agent	wetting disperser
Glyceryl Oleate	emulsifier, PEG-free	-
Glycine	buffer constant	-
Hydrogenated Cocoglycerides	consistency	pleasantness
Hydrogenated Palm Oil	consistency	pleasantness
Hydroxyethyl Ethylcellulose	gel creator	-
Isoamyl p-Methoxycinnamate	-	UV-B filter
Isopropyl Myristate	oil phase	greasing, pleasantness
Isopropyl Palmitate	oil phase	greasing, pleasantness
Lactic Acid	buffer constant	moisture
Magnesium Aluminium Silicate	gel creator	-
Magnesium Stearate	consistency	-
Magnesium Sulfate	consistency	-
Octyl Methoxycinnamate	-	UV-B filter
Octyl Triazone	-	UV-B filter
Octyldodecanol	oil phase	greasing, pleasantness
Panthenol	provitamin B5	moisture, depressant
Pentylene Glycol	-	moisture, pleasantness
Phenoxyethanol	conservation	-
Phenyl Trimethicone	-	pleasantness
Planktonextract (and) Lecithin	-	regeneration
Polyglyceryl-2 Dipolyhydroxystearate	emulsifier, PEG-free	-
Polyglyceryl-3 Methylglucose Distearate	emulsifier, PEG-free	-
Propylene Glycol	wetting agent	moisture
Propylene Glycol Dicaprylate/Dicaprate	oil phase	greasing, pleasantness
PVP/VA Copolymer	film creator	-
Ricinus Communis	oil phase	greasing, pleasantness
Sodium Carbomer	consistency	-
Sodium Lactate	buffer constant	moisture
Titanium Dioxide	-	UV-A, UV-B filter
Titanium Dioxide, Alumina, Simethicone	-	UV-A, UV-B filter
Tocopherol	anti-oxidation	vitamin E, pleasantness, radical captor
Tocopheryl Acetate	anti-oxidation	vitamin E, pleasantness, radical captor
Vanillin	flavour	flavour, odor
Xanthan Gum	consistency	-
Zea Mays	gel creator	-
Zinc Oxide	-	UV-A, UV-B filter
Zinc Sulfate	stabilization agent	-

## CURRICULUM VITAE

**HOANG-MINH Thao** (*Hoàng Thị Minh Thảo*) Vietnamese

### Personal information:

Date of birth	01.6.1979
Place of birth	Quang Ninh, Vietnam
Parents	HOANG Minh Tru & DINH Thi Thuy
Marital status	Single
Nationality	Vietnamese
Religion	None

### Education and work experience:

1985-1994	Primary and secondary school in Cam Pha, Quang Ninh, Vietnam
1994-1997	Baccalaureate - High school in Cam Pha, Quang Ninh, Vietnam
1997-2001	B.Sc. in Geology - Honors Program, Hanoi National University, Vietnam
2001-2003	Researcher and Teaching Assistance - Faculty of Geology, Hanoi University of Science, Hanoi National University, Vietnam
2002-2003	Diploma of Equivalent in Geosciences and Environment - “Joint Educational Training Center Hanoi-Greifswald” program
2003-2006	Ph.D. student in Applied Geology - Institute of Geography and Geology, Ernst-Moritz-Arndt University of Greifswald, Germany

### Others

Language	Vietnamese (mother tongue), English (fluent), German (elementary)
----------	---

### List of publications

1. NGUYỄN Văn Nhân, **HOÀNG Thị Minh Thảo**, 2002. *Geochemical-mineralogical characteristics of lead-zinc ores in the Tú Lệ area*. Journal of Geology, Series A, Hanoi, 271, 7-8/2002, p.24 - 30 (in Vietnamese: *Đặc điểm địa hoá - khoáng vật quặng chì-kẽm vùng mỏ Tú Lệ*).
2. NGUYỄN Văn Nhân, **HOÀNG Thị Minh Thảo**, 2002. *Geochemical - mineralogical characteristics of precious rare elements of Cu - Ni sulphide ore type in Northwestern Vietnam*. Journal of Sciences - Natural sciences and technology, Vietnam national University, Hanoi, T.XVIII, 3, p.18 - 24 (in Vietnamese: *Đặc điểm địa hoá - khoáng vật các nguyên tố quý hiếm trong quặng sulphide đồng-niken Tây Bắc Việt Nam*).
3. NGUYỄN Văn Nhân, **HOÀNG Thị Minh Thảo**, 2002. *Mineralogical characteristics of tin - silver ores in some polymetal deposits at Ngân Sơn*. Journal of Geology, Series A, Hanoi, 274, 1-2/2003 (in Vietnamese: *Đặc điểm khoáng vật quặng vùng mỏ đa kim thiếc - bạc Ngân Sơn*).
4. BÙI Học, PHẠM Khánh Huy, **HOÀNG Thị Minh Thảo**, 2005. Groundwater management in Việt Nam. Journal of Geology, Series B, Hanoi, 25, p.26-30.

### List of working papers

1. Jörn KASBOHM, **HOANG Thị Minh Thao**, 2004: *Phasenanalytische Charakterisierung mineralogischer Veränderungen an säurebehandelten Proben des ‚Friedländer Tons‘*. Abschlussbericht, 51 pp.
2. ĐỖ Văn Chương, NGÔ-ĐỨC Thành, **HOÀNG Thị Minh Thảo**, NGUYỄN Thị Hồng Liễu, VŨ Thị Anh Tiềm, NGUYỄN Thị Hồng Anh, DƯƠNG Ngọc Cường, 2005: *The Sumatra earthquakes and the Indian Ocean Tsunami, 26/12/2004*. Vietnamese Geosciences Group. E-book (in Vietnamese: *Động đất Sumatra và sóng thần Ấn Độ Dương 26/12/2004*).

## List of proceedings and abstracts

1. **HOÀNG Thị Minh Thảo**, 2000. *The Material Composition and forming conditions of Gold in Phuoc Son area, Vietnam*. Vietnam National University. University Contest of Student's Scientific Researches, 2000, Hanoi, Vietnam; Proceedings, Vol.5, p.142 (in Vietnamese).
2. ĐÀM Quang Minh, **HOÀNG Thị Minh Thảo**, TRẦN Thị Thanh Thúy, 2001. *Computer software for mineralogical controlling*. Vietnam National University. University Contest of Student's Scientific Researches, 2001, Hanoi, Vietnam; Proceedings, Vol.6 p.121-122 (in Vietnamese).
3. **HOÀNG Thị Minh Thảo**, TRẦN Thị Thanh Thúy, 2001. *Cursoriness of Material Composition and Forming Polymetal - Copper Sulphide formation in Hoa Binh and neighbouring area*. Vietnam National University. University Contest of Student's Scientific Researches, 2001, Hanoi, Vietnam; Proceedings, Vol.6, p.126 (in Vietnamese).
4. **HOÀNG Minh Thảo**, ĐỖ Văn Chương, NGÔ-ĐỨC Thành, NGUYỄN Thùy Dương, DUƠNG Thế Hưng, 2005: *Promoting Geosciences in Vietnam through the World Wide Web*. European Geosciences Union. General Assembly, 24-29 April 2005, Vienna, Austria; Geophysical Research Abstracts, 7, 00730.
5. **HOANG, Thi Minh Thao**; LE, Thi Lai; Jörn KASBOHM, 2004: *UV-protection creams: first results for substitution of non-natural additives by clay minerals*. The Clay Minerals Society; Gorges, Clays, and Coulees - 41<sup>st</sup> Annual Meeting, June 19-24, 2004, Richland, USA; Abstracts, p.37.
6. **HOANG, Thi Minh Thao**; LE, Thi Lai; Jörn KASBOHM, 2004: *UV-protection creams: first results for substitution of non-natural additives by clay minerals*. Deutschen Mineralogischen Gesellschaft und der Deutschen Ton- und Tonmineralgruppe e.V.; DMG 2004 Tagung, Karlsruhe 19.-22. September 2004; Berichte der Deutschen Mineralogischen Ges., Beih. Z. Eur. J. Mineral. Vol. 16 (2004), No. 1, p.89.
7. **HOANG, Thi Minh Thao**; LE, Thi Lai; Jörn KASBOHM, 2005: *Some possibilities of substitution non-natural additives by clay minerals in UV protection creams*. Association Internationale Pour l'Etude des Argiles; The 13<sup>th</sup> International Clay Conference - Claysphere: past, present and future and 49<sup>th</sup> Annual Meeting of the Clay Science Society of Japan, August 21-27, 2005, Waseda University, Tokyo, Japan; Program with Abstracts, p. 56.
8. **HOANG, Thi Minh Thao**; LE, Thi Lai; Jörn KASBOHM, 2006: *Behaviour of clay minerals for UV-radiation and first result of interaction of clay minerals and bacteria*. Groupe Français des Argiles & The Clay Minerals Society. Bridging Clays - Joint Meeting of The Clay Minerals Society and the French Clay Group: 43<sup>rd</sup> Annual meeting of the CMS - 4<sup>ème</sup> Colloque du GFA, June 3-7, 2006, France; Program & Abstracts, p. 125